Bamboo for Gridshell Structures:
Design and Construction of Gridshell Structures using Indonesia Bamboo



By

Esti Asih Nurdiah

Submitted to the School of Architecture

In partial fulfilment of the requirements for the degree of

Doctor of Philosophy in Architecture

Supervisors:

Professor Wen-Shao Chang

Dr Tsung-Hsien Wang

The University of Sheffield

Faculty of Social Science

2024

Acknowledgement

Embarking on this PhD journey has been a long journey for me. I could not have completed it without guidance and help from these remarkable individuals. I am continually grateful to God for sending them my way, and I would like to express my gratitude to:

My supervisors, Prof. Wen-Shao Chang and Dr Tsung-Hsien Wang, for their guidance, inspiration, and support during my study.

My examiners, Dr Rodolfo Lorenzo, and Dr Tim Ireland, for their constructive feedback and inspiring discussion during the viva.

My sponsor, LPDP (Indonesia Endowment Funds for Education); without their funding support, I could not conduct and complete my PhD study.

Petra Christian University (PCU) in Indonesia as my home institution. I would like to thank Prof. Djwantoro Hardjito, the Rector of PCU, for his support and encouragement; Prof. Antoni, Dr Jimmy Chandra, and Dr Adi Santoso, for providing laboratories for conducting the material tests; Dr Rudy Setiawan, former Dean; Dr Rully Damayanti, current Dean of Faculty of Civil Engineering and Planning, and Dr Fenny Elsiana, Head of Department of Architecture for their support during my fieldwork. Additionally, I am grateful to my colleagues at PCU for their friendship and undying support: Prof. Lilianny Arifin, Bisatya Maer, and Altrerosje Asri. In loving memory of Maria Hidayatun, a mother figure to me. I am always grateful for her love and support.

My friends from Floor 9 Arts Tower: Esra Can, Choo Yoon Yi, Demet Yesiltepe, Deniz Kesichi, Ibrahim, Xiaolu Wang, Simone Ferris, Wanida Numsuk, Jie Xiong, Jin Cheng, Gao Yan, Aya Elghandour, Mahmoud, Melis Tekin, Maha Basha, Xiaozhi Yang, Xuezhu Zhai, Ayse Humeyra, Asma Rashid, Wadji and Dheena. Reena Sayani and Itzelle medina for always encouraging me.

My best friends who always support me from afar: Wellyn Migang, Erni Trifena, Anastasia Widiasih, and Dian Eka.

Peter Keogh, for his help with my English writing, and gave a lot of constructive feedback.

Lastly, my family, my wonderful and supportive sister, Desy, and my nephews, Joshua and Joseph.

Soli Deo gloria

Abstract

Bamboo is widely recognised as a sustainable material and has been used in construction for centuries. In Indonesia, bamboo is extensively utilised due to its abundance and suitability for the local climate. Gridshell structures, which consist of grids and lattices, are efficient for large-span buildings as they require less material compared to solid shells. Constructing gridshell structures using bamboo offers a sustainable construction practice. However, the use of bamboo for gridshells poses challenges due to its hollow tube structure, diaphragms, and variability in shape and material properties.

This study investigates the feasibility of using Indonesian bamboo for gridshell structures by examining material properties, analysing structural performance and behaviour, experimenting with construction methods, and exploring form-finding and structural optimisation. Material tests were conducted on three Indonesian bamboo species: Gigantochloa apus, Gigantochloa atter, and Dendrocalamus asper, to determine their properties for structural analysis. Finite Element Analysis (FEA) in Abaqus was employed for structural analysis, and construction methods were explored by building two full-scale gridshell models using both full-culm and split bamboo. Form-finding and optimisation, crucial for gridshell design, were conducted using Rhinoceros with Grasshopper, Kangaroo, and Karamba 3D plug-ins

The study produced a dataset of material properties for the selected bamboo species and examined their bending capabilities. The findings suggest that the selection of bamboo species is crucial for achieving desirable gridshell geometries, as not all species are suitable for bending-active gridshells. Structural analysis highlighted discrepancies between FEA simulations and load tests on physical models. The study also recommends suitable construction methods for bamboo gridshell structures based on their form—full-culm or split bamboo. Additionally, a framework for form-finding and optimisation specific to bamboo gridshell structures is proposed. This comprehensive understanding of the bamboo gridshell design process contributes to practical applications and enhances knowledge on the utilisation of bamboo for gridshell structures.

Keywords: bamboo gridshell, material properties, form-finding, optimisation, construction method.

Table of Contents

Acknowledgement iii
Abstract v
Table of Contents vii
List of Figures xii
List of Tables xviii
List of Nomenclature xix
CHAPTER 1 | INTRODUCTION 1
1.1. Research Background 1
1.2. Research Rationale 5
1.3. Research Question 6
1.4. Research Aims and Objectives 7
1.5. Thesis Structure 8
CHAPTER 2 | LITERATURE REVIEW 11
2.1. Bamboo as Building Material 11
2.1.1. Bamboo Plant and Species 11
2.1.2. Bamboo Morphology and Anatomy 13
2.1.3. Physical Properties of Bamboo Culms 16
2.1.4. Mechanical Properties 17
2.1.5. Bamboo as Sustainable Material 19
2.2. Gridshell Structures: Definition and Design Principles 20
2.2.1. The Definition of Gridshell Structures 20
2.2.2. History of Gridshell Structures 20
2.2.3. Classification of Gridshell Structures 22
2.2.4. Form-Finding Gridshell Geometry 23
2.2.5. Structural optimisation 25
2.2.6. Material Selection 26

2.3. The Construction of Gridshell Structures 29
2.3.1. Erection Methods of Gridshell Structures 30
2.3.2. Jointing and Nodal Connection 32
2.4. Summary 33
CHAPTER 3 | RESEARCH METHODOLOGY 35
3.1. Overview 35
3.2. Research Design 35
3.2.1. Research Framework 35
3.2.2. Research Constraint and Limitation 38
3.3. Summary 39
CHAPTER 4 | MATERIAL PROPERTIES OF INDONESIAN BAMBOO 41
4.1. Overview and Research Objectives 41
4.2. Research Method 42
4.2.1. Material Selection and Preparation 42
4.2.2. Compression Strength Parallel to the Fibre 44
4.2.3. Tension Strength Parallel to the Fibre 45
4.2.4. Shear Strength Parallel to the Fibre 46
4.2.5. Bending Strength and Stiffness Parallel to the Fibre 47
4.2.6. Tension Strength Perpendicular to the Fibre 49
4.2.7. Bending Strength Perpendicular to the Fibre 50
4.2.8. Moisture Content 52
4.2.9. Density 52
4.3. Material Tests Results 53
4.3.1. Compression Strength Parallel to the Fibre 53
4.3.2. Tension Strength Parallel to the Fibre 58
4.3.3. Shear Strength Parallel to the Fibre 64
4.3.4. Bending Strength and Stiffness Parallel to the Fibre 70

4.3.5. Tension Strength Perpendicular to the Fibre 76
4.3.6. Bending and Stiffness Perpendicular to the Fibre 81
4.4. Discussion 86
4.4.1. Material properties of Indonesian bamboo 86
4.4.2. Bending Capability 89
4.4.3. Utilisation and Implication for Gridshell Structures 93
4.5. Summary 95
CHAPTER 5 | STRUCTURAL ANALYSIS OF GRIDSHELL STRUCTURE 96
5.1. Overview and Research Objectives 97
5.2. Research Method 98
5.2.1. Gridshell Geometries and Meshes 99
5.2.2. Input Parameters 101
5.3. Results 106
5.3.1. FEA Results of Model 1: Full-Culm Bamboo 106
5.3.2. FEA Results of Model 2: Split Bamboo 113
5.4. Discussion 118
5.4.1. Comparison Study between FEA Results and Full-Scale Models 118
5.4.2. Implications on Gridshell Structure Design 123
5.5. Summary 124
CHAPTER 6 | CONSTRUCTION OF BAMBOO GRIDSHELL 125
6.1. Overview 125
6.2. Material and Methods 128
6.2.1. Material Selection and Preparation 129
6.2.2. Pre-Construction: Test on Bamboo's Depth of Curvature 130
6.2.3. Construction Part 1: Model-1 133
6.2.4. Construction Part 2: Model-2 134
6.2.5. Experimental Set-up for Load Test 135

6.3. Results of the Construction Process 136
6.3.1. Bending Test and Depth of Curvature 136
6.3.2. Construction of Gridshell Structure Model Using Full-culm Bamboo 137
6.3.3. Construction of Gridshell Structure Model Using Split bamboo 144
6.3.4. Load Testing of Gridshell Models 148
6.4. Discussion 152
6.4.1. Determining Construction Methods for Full-culm Bamboo Gridshell Structures 152
6.4.2. Critical Reflection on the Construction Process 156
6.5. Summary 158
CHAPTER 7 | PARAMETRIC MODELLING: FORM-FINDING AND OPTIMISATION OF BAMBOO GRIDSHELL STRUCTURE 161
7.1. Overview 161
7.2. Research Methods 162
7.2.1. Research Design and Material Selection 162
7.2.2. Initial Model Development 163
7.2.3. Bending-Active Form-Finding 163
7.2.4. Structural Analyses of Optimisation Modification Strategies 164
7.2.5. Optimisation Process 166
7.2.6. Input Parameters in Computational Simulations 166
7.3. Results 169
7.3.1. Form-Finding of Full-culm Bamboo 169
7.3.2. Effect of Modifications on Structural Performance of Full-Culm Bamboo Gridshell Models 171
7.3.3. Optimisation of Full-Culm Bamboo Gridshell Model 178
7.3.4. Form-Finding of Split Bamboo 182

7.3.5. Effect of Modifications on Structural Performance of Split Bamboo Gridshell Models 183
7.3.6. Optimisation of Split Bamboo Gridshell Model 189
7.4. Discussion 194
7.4.1. Form-finding of Bamboo Gridshell Structures 194
7.4.2. Optimisation Strategies of Bamboo Gridshell Structures 196
7.4.3. Bamboo Gridshell Structures: Computational Design and Construction Practices 198
7.4.4. Limitations of the Study and Future Applications 202
7.5. Summary 203
CHAPTER 8 | CONCLUSION: UNDERSTANDING BAMBOO GRIDSHELL STRUCTURES 205
8.1. Recapitulation of Research Objectives and Key Findings 205
8.1.1. Material Properties of Indonesian Bamboo Species 205
8.1.2. Structural Performance of Bamboo Gridshell Structures 207
8.1.3. Construction Methods and the Process of Erecting Gridshell Structures 208
8.1.4. Form-Finding and Optimisation Strategies 209
8.2. Recommendations for Future Research 211
REFERENCES 215

List of Figures

Figure 1-1. a. Tongkonan, vernacular houses of Toraja tribes; b. Uma, vernacular houses of West Sumbanese. 2
Figure 1-2. a - b. The OBI eco campus, located near Jatiluhur Dam in Jatiluhur, West Java Province. 3
Figure 1-3. a. Common bamboo grooves in Indonesia; b. Bamboo grooves as part of people activities; c. Bamboo shelter as a place for gathering 4
Figure 2-1. Bamboo forest distribution based on climate zone. 11
Figure 2-2. Map of bamboo species richness in Asia Pacific. 12
Figure 2-3. Distribution of bamboo genera in Indonesia. 13
Figure 2-4. Bamboo anatomy. 14
Figure 2-5. Bamboo culm structure in longitudinal section. 15
Figure 2-6. Bamboo culm wall cross section. 16
Figure 2-7. Examples of gridshell structures built within 1980s to 2020s. 22
Figure 2-8. Gridshell terminology described strained and unstrained gridshell. 23
Figure 2-9. a. COOP Distribution Centre in Switzerland, designed by Heinz Isler using the pneumatic model; b. Concept of a new train station in Stuttgart using the tension model; c. The form-finding process of Mannheim Multihalle using the hanging mode. 25
Figure 2-10. Structural optimisation strategies. 26
Figure 2-11, Plotted of building materials based on Ashby diagram and the ratio of strength to stiffness. 28
Figure 2-12. Study of elastica curves. 28
Figure 2-13. British National Museum; b. Savill Garden. 30
Figure 2-14. Gridshell erection methods. 30
Figure 2-15. a. The erection process of the Essen gridshell using a crane; b. The erection process of the German Pavilion using cables. 30
Figure 2-16. a. & b. Erection process of the Mannheim Multihalle using a jacket tower; c. Erection process of Weald & Downland using the PERI-UP scaffolding system. 31
Figure 2-17. a. Finger joint; b. construction of scarf joints. 32
Figure 2-18. Bamboo poles connection to create long members. 32
Figure 2-19. Example of nodal connections. 33
Figure 2-20. Parameters in bamboo gridshell design process. 34
Figure 3-1. Schematic illustrating the conceptual framework, showing the interdependent and role of parameters. 36
Figure 3-2. Research Framework 38
Figure 4-1. Bamboo poles for material tests 43
Figure 4-2. Full-culm bamboo showing the division of the culm into three parts: upper-middle-bottom, and the cutting position in node and internodes for each item test. 44
Figure 4-3. Set up of compression test 45
Figure 4-4. Specimen setting for tension parallel to the fibre. 46
Figure 4-5. Shear test set up; a. Shear plate; b. Specimen and shear plates on the testing machine 47
Figure 4-6. Test setup for bending parallel to the fibre 48

Figure 4-7. Bending parallel to the fibre test 48
Figure 4-8. Bending perpendicular to the fibre test setup and the measurements. 51
Figure 4-9. Failures in compression: a. Fibre buckling b. Fibre buckling in the inner wall c. Splitting. 53
Figure 4-10. Average compression strength parallel to the fibre with error bars standard deviation. 55
Figure 4-11. Examples of stress-strain curve taken from D. asper group specimens, upper sections. 57
Figure 4-12. Correlation between MOR in compression parallel to the fibre and moisture content. 57
Figure 4-13. Correlation between MOR in compression parallel to the fibre and density. 58
Figure 4-14. Specimen after trial tension test, 2 specimens failed at tabs. 59
Figure 4-15. a. Trial specimens with wood tabs; b. Trial specimens without wood tabs after the test; c. failure due to shear; d. Detail of failure at tabs; e. Details of failure due to shear. 59
Figure 4-16. Problems due to gripping mechanism: a. Crushing at grips; b. Specimen buckled; c. Specimen with thick width. 60
Figure 4-17. Graph summary of MOR in tension with error bars of standard deviation. 62
Figure 4-18. Stress-strain curve of tension test parallel to the fibre taken from Gigantochloa apus test group, upper part no. 1 to 10. 63
Figure 4-19. Failure mode in tension: a. splintering; b. Delamination; c. Trimmed tension and delamination. 64
Figure 4-20. Failures in shear parallel to the fibre test: a. failure at one shear plane, b. failure at two shear planes, c. failures in specimen with node and thick wall, d. characteristic of failure. 65
Figure 4-21. Cracking at specimens with thick walls. 65
Figure 4-22. Average shear strength parallel to the fibre with error bars of standard deviation. 66
Figure 4-23. Example of force-displacement curve, taken from G. atter specimen no. 1 to 4. 68
Figure 4-24. Correlation between MOR in shear parallel to the fibre and density .. 69
Figure 4-25. Correlation between MOR in shear parallel to the fibre and moisture content 69
Figure 4-26. Average bending strength parallel to the fibre with error bars of standard deviation. 71
Figure 4-27. Curve force and displacement of bending parallel to the fibre tests. .. 72
Figure 4-28. Failure in bending parallel to the fibre test bamboo species Gigantochloa apus. 73
Figure 4-29. Failure modes recorded in tests: a. Failure at the saddle, b. Compression, c. Culm collapse, d. Combination of bending mechanism 74
Figure 4-30. Fibre kinks in compression failure mode. 74
Figure 4-31. Correlation between MOR and Moisture Content in bending parallel to the fibre. 75
Figure 4-32. Correlation between MOR and density in bending parallel to the fibre. 76

Figure 4-33. Failures after the test, a. example of failure, b. Failure in symmetrical form, c. Failures in asymmetrical form. 77
Figure 4-34. Average tension strength perpendicular to the fibre with error bars of standard deviation. 78
Figure 4-35. Example of force-displacement curvature taken from D. asper upper section test group. 80
Figure 4-36. Correlation between MOR in tension perpendicular to the fibre and moisture content. 80
Figure 4-37. Correlation between MOR in tension perpendicular to the fibre and density. 81
Figure 4-38. Splitting behaviour due to bending perpendicular to the fibre; a. One splitting (S); b. Two splittings (EW); c. Splitting location between E/W & S. .82
Figure 4-39. Average of Bending strength perpendicular to the fibre with error bars of standard deviation. 83
Figure 4-40. Example of force-displacement curve taken from D. asper middle part group test. 85
Figure 4-41. Correlation between MOR in bending perpendicular to the fibre and moisture content. 85
Figure 4-42. Correlation between MOR in bending perpendicular to the fibre and fibre density. 86
Figure 4-43. Determination of radius of curvature. 92
Figure 4-44. Bending mechanism of hollow tube beam. 94
Figure 5-1. The generated models of Model-1 and Model-2 in Rhinoceros. 100
Figure 5-2. Bamboo three axes: Longitudinal, radial and tangential. 101
Figure 5-3. Deformed shape of Model 1 under gravity load. 107
Figure 5-4. Deformation and displacement resulting from load application based on scenario 1 on Model 1. 107
Figure 5-5. Stress distribution based on Scenario 1 loading on Model 1. 108
Figure 5-6. Deformed shape and displacement of Model 1 under load application based on Scenario 2. 109
Figure 5-7. Stress distribution under scenario 2 loading of Model 1. 109
Figure 5-8. Displacement of Model 1 under Scenario 3 load application. 110
Figure 5-9. Stress distribution under the application of Scenario 3. 111
Figure 5-10. Displacement of Model 1 under Scenario 4 loading. 111
Figure 5-11. Stress distribution under the application of Scenario 4, ...112
Figure 5-12. Deformed shape of Model 2 under gravity load. 113
Figure 5-13. Displacement of Model 2 under scenario 1. 114
Figure 5-14. Stress distribution on Model 2 under load scenario 1. 114
Figure 5-15. Displacement of Model 2 under load application based on Scenario 2. 115
Figure 5-16. Stress distribution under Scenario 2 load application. 115
Figure 5-17. Displacement of Model 2 under load application of Scenario 3. 116
Figure 5-18. Stress distribution based on Scenario 3. 116
Figure 5-19. Displacement of Model 2 under load application of Scenario 4. 117
Figure 5-20. Stress distribution based on Scenario 3. 117
Figure 5-21. Comparison of displacement obtained from FEA in Abaqus and load-tests on full-scale model based on loading Scenario 1 119

Figure 5-22. Comparison of displacement obtained from FEA in Abaqus and load-tests on full-scale model based on loading Scenario 2. 120
Figure 5-23. Comparison of displacement obtained from FEA in Abaqus and load-tests on full-scale model based on loading Scenario 3. 121
Figure 5-24. Comparison of displacement obtained from FEA in Abaqus and load-tests on full-scale model based on loading Scenario 4. 122
Figure 6-1. a. Cloudscape Pavilion inside China Academi of Art; b. Erection process of bamboo gridshell during the workshop by David Rockwood....126
Figure 6-2. Gymnasium building in Green School, a. View from the interior; b. Details of the jointing and connections; c. Layers of the gridshells; d. Combination of arches and gridshell. 127
Figure 6-3. Construction workflow of full-scale model and load tests. 128
Figure 6-4. Sectional area of the bamboo species selected for construction. 130
Figure 6-5. Materials for the construction: a. Bamboo Gigantochloa apus for Model 1; b. Bamboo Dendrocalamus asper for Model 2. 130
Figure 6-6. Illustration on bending method of bamboo culm using slicing method; b-d. Example of arches made using slicing method. 131
Figure 6-7. a. Example of failures due to breaking at slicing; b-c. Details showed the failure of slicing. 132
Figure 6-8. Illustration of bending bamboo experiment set to identify the depth of curvature. 132
Figure 6-9. Final design of Model 1 for full scale model. 134
Figure 6-10. Form Finding of Model 2 using split bamboo. 135
Figure 6-11. The characteristic of failures: a. Buckling, b. Stress concentration, c. Fibre shrinking after heating due to thermal loss. 137
Figure 6-12. a. Illustration of method in bending the bamboo poles; b. The first arch; c. The second arch; d. ground grid as guidelines. 139
Figure 6-13. a. Early construction stage of Model 1; b. Grids arrangement and axis. 139
Figure 6-14. a. The workers were completing Model-1; b. Raising the height by pulling the gridshell using a chain block; c. Heat application to add the curvature. 140
Figure 6-15. Jointing technique using internal union; a. The smaller bamboo tube was inserted; b. Two bamboo culms were connected; c. Position on other culms....141
Figure 6-16. a - b. Lengthen the member by overlapping. 141
Figure 6-17. Nodal connection using lashing join....142
Figure 6-18. a. Nuts and bolts connection at the perimeter; b. connection at the boundary; c. failure due to diametric compression; d. failure due to longitudinal splitting....143
Figure 6-19. a. Splitting methods using axe; b. Trimming the split bamboo....144
Figure 6-20. a. Detail connection using thin wire for split bamboo; b. Connection during erection process....145
Figure 6-21. a. Process of laying the members and forming the grids; b. Completion of the lattice....145
Figure 6-22. a. Erection process; b. Installation details of the chain blocks to the lattice; c. Shaping the form; d. Additional workers pushed the corner while the rachet strap was shortened. 146

Figure 6-23. a-b. Buckling at opening members; c. Installing the boundary beams; d. Completed structure. 147
Figure 6-24. a. Failure at the joineries between beams (1); b. Failure at joineries between beams (2); c. Cracking and splitting. 148
Figure 6-25. Initial gridshell shape before loading. 149
Figure 6-26. Displacement and deformation curve from the Scenario 1 loading applications. 149
Figure 6-27. Point loads and measurement Scenario 2. 150
Figure 6-28. Displacement of main curve due to Scenario 2 loading application. . 150
Figure 6-29. Point loads and Measurement Scenario 3. 151
Figure 6-30. Deformation of main curve due to Scenario 3. 151
Figure 6-31. Deformation of main curve due to Scenario 4. 152
Figure 6-32. Efforts in raising the full-culm gridshell curvature; a. Using chain blocks, b. The workers tried to push up the structure. 153
Figure 6-33. Testing on split bamboo showing a significant deformation in shape. 155
Figure 6-34. The utilisation of split bamboo; a. at The Arc, utilised in anticlastic curvature; b. in this study, utilised as synclastic curvature. 155
Figure 6-35. The non-uniform morphology of bamboo; a. from the longitudinal view, b. from the cross-sectional view. 157
Figure 7-1. Research workflow. 162
Figure 7-2. Examples of similar gridshell forms a. Woodome project; b. Toledo gridshell; c. Portalen Pavilion; d. Throndheim gridshell 163
Figure 7-3. Curvature analysis and form-finding of full-culm models. 170
Figure 7-4. Deformed shape due to mesh density modification on Model 1. 172
Figure 7-5. Effect of mesh density: a. Mesh density and displacement; b. Mesh density and total mass. 173
Figure 7-6. Shape deformation resulting from mesh configuration modification. 175
Figure 7-7. a. Effect of mesh configuration modification on utilisation factors; b. Effect of mesh configuration on displacement 176
Figure 7-8. Shape deformation due to modification in the number of bamboo grid layers. 177
Figure 7-9. Effect of sizing modification: a. on the displacement; b. on the total mass. 178
Figure 7-10. Baseline Model-1 for optimisation. 180
Figure 7-11. Optimisation of Model-1 181
Figure 7-12. a. Effect of mesh density and sizing optimisation on utilisation factors; b. Effect on displacement of Model-1 using full-culm bamboo G. apus. 181
Figure 7-13. Form-finding process of targeted geometry of Model-2 183
Figure 7-14. Results of mesh density modification on utilisation factors of Model 2. 184
Figure 7-15. Effect of mesh density on Model 2: a. Effect on the maximum displacement; b. Effect on the total mass. 185
Figure 7-16. Deformed shape and utilisation factors of mesh configuration modification. 186
Figure 7-17. a. Effect of mesh configuration modification on utilisation factors; b. Effect on displacement. 187
Figure 7-18. Deformed shape and utilisation factors due to sizing modifications 188

Figure 7-19. a. Effect of sizing modification on displacement; b. Effect on total mass. 189
Figure 7-20. Baseline Model-2 for optimisation. 190
Figure 7-21. a. Effect of optimisation by modifying mesh density and sizing on utilisation factors of Model-2 using Gigantochloa apus; b. Effect on displacement. 191
Figure 7-22. a. Effect of optimisation by modifying mesh density and sizing on utilisation factors of Model-2 using Gigantochloa atter; b. Effect on displacement. 192
Figure 7-23. a. Effect of optimisation by modifying mesh density and sizing on utilisation factors of Model-2 using Dendrocalamus asper; b. Effect on displacement. 192
Figure 7-24. Proposed optimised structure for Model-2 using spilt bamboo based on the material selection. 193
Figure 7-25. a. UNAM pavilion in Mexico (Lorenzo et al., 2017); b. ZBC Pavilion in Hong Kong (Crolla, 2017). 195
Figure 7-26. Grishell mesh at the Arc of Green School, configuring in quadrilateral 197
Figure 7-27. Profile section and layering options. 198
Figure 7-28. a Experiment in bending bamboo poles, b. Bending bamboo by torching. 199
Figure 7-29. a. Expected curvature during design process, b. Final gridshell geometries after investigating the depth of curvature. 200
Figure 7-30. a. Role of scale model as guideline for construction workers; b. Erection process of full-scale model. 202

List of Tables

Table 4-1. Test setup of tension strength perpendicular to the fibre 50
Table 4-2. Summary of compression test results of three species. 54
Table 4-3. Summary of compression test based on the position within the culms. 55
Table 4-4. Summary of the compression test results based on nodes and internodes. 56
Table 4-5. Summary of MOR tension parallel to the fibre of three bamboo species. 62
Table 4-6. Summary of MOR tension parallel to the fibre based on the position within the culms 63
Table 4-7. Summary of shear strength parallel to the fibre. 66
Table 4-8. Summary of shear strength based on the position within the culms. 67
Table 4-9. Summary of shear strength based on node and internode. 67
Table 4-10. Summary of bending parallel to the fibre test results. 70
Table 4-11. Summary of tension perpendicular to the fibre for each species. 78
Table 4-12. Summary of tension strength perpendicular to the fibre based on parts of the culms. 79
Table 4-13. Summary of bending strength and stiffness perpendicular to the fibre as per species. 83
Table 4-14. Summary of bending strength and stiffness perpendicular to the fibre as per sections of bamboo culms. 84
Table 4-15. Summary of average MOR based on the position within the culm of the three Indonesian bamboo species. 87
Table 4-16. The calculations of axial and flexural stiffness based on material test results. 90
Table 4-17. Study of Young's modulus and bending strength to the assessment on radius of curvature. 91
Table 4-18. Minimum radius of curvature full-culm bamboo based on bending parallel to the fibre tests. 92
Table 5-1. SI unit for the simulation 99
Table 5-2. Input material properties for Abaqus simulation. 103
Table 5-3. Input dimension of the profile. 103
Table 5-4. Point loads position on the models based on four scenarios. 105
Table 6-1. Point loads position on the full-scale models. 136
Table 6-2. Loads – Scenario 2 (in kg) 150
Table 6-3. Loads - Scenario 3 (in Kg) 151
Table 7-1. Input data of radii of curvature for Model-1 164
Table 7-2. Modification parameters on initial design. 165
Table 7-3. Input material properties. 168
Table 7-4. Input cross-section dimension for full-culm bamboo. 168
Table 7-5. Input cross-section dimension for split bamboo. 168
Table 7-6. Radii of curvature and height resulting from the form-finding process. 170

List of Nomenclature

A	Sectional area
a	Span from support to saddle point at four-point bending parallel to the fibre test
b	Specimen thickness
C_R	Redundancy factor
C_{DF}	Service class and load duration
C_T	Service temperature
COV	Coefficient of variation
Do	Outer diameter
D_i	Inner diameter
d	Hole diameter for pin apparatus at tension perpendicular to the fibre test
E	Young's modulus
E_m	Young's modulus in bending parallel to the fibre
$E_{m,90}$	Young's modulus in bending perpendicular to the fibre
EA	Axial Stiffness
E_mI_B	Flexural stiffness
EW	East – West axis
F	Force
F_{ult}	Ultimate force
f_c	Compression strength parallel to the fibre
$f_{t,0}$	Tension strength parallel to the fibre
f_V	Shear strength parallel to the fibre
$f_{m,0}$	Bending strength parallel to the fibre
$f_{t,90}$	Tension strength perpendicular to the fibre
FEA	Finite Element Analysis
$FS_{C/m}$	safety factors
G	Shear moduli
h	Neutral axis location
I_B	Moment of inertia
L	Length
$LVDT$	Linear variable differential transformer
MOR	Modulus of Rupture
MC	Moisture content
M_{ult}	Bending moment
m_o	Mass of oven-dry specimen
m_i	Mass of specimen test piece
NS	North – South axis
R	Radius of centreline
R_i	Radius of inner surface
r	Correlation coefficient
$StDev$	Standard deviation
V	Volume
v	Poisson's ratio
X_m	allowable member design capacity
δ	Wall thickness
ρ	Basic density
P_{test}	Specimen's density at the time of the test
P_{12}	The density at 12 % moisture content
Δ	Displacement

CHAPTER 1 | INTRODUCTION

1.1. Research Background

Construction industries have been responsible for contributing to the greenhouse gas emission in the cities for nearly 40 per cent (UN-Habitat, 2013, p. 145). There is an urgent need to implement sustainable construction practices, including the use of materials from renewable sources. The practices can be adopted as an approach to regenerative development without sacrificing natural resources for human activities and produce positive environmental, social, and economic impacts (Zea Escamilla, Habert, & Wohlmuth, 2016).

The utilisation of bamboo in the built environment aligns with the principles of sustainable development and construction, which has been a global issue. Bamboo is a renewable material that is easy to cultivate, matures rapidly, and can be harvested in three to five years (Chang et al., 2018a). As a building material, bamboo offers flexible and straightforward methods of application, whether utilised for structural or non-structural elements (Widyowijatnoko, Trautz, & Baier, 2012). As the awareness of sustainable development increases among the public, along with the desire to implement its principles, the potential for utilising bamboo as a building material is immense, including in Indonesia.

Historically, bamboo has been extensively used in construction for centuries and is integral to the daily lives of people in Indonesia. The historical application of this material can be traced back to traditional Indonesian houses. A study of vernacular *Tongkonan*[1] houses showed that bamboo was used for both the roof rafters and covering (Figure 1-1a). Short bamboo poles are 'sewn' using bamboo strips and then stacked into layers, forming a thick roof (Kis-Jovak, 1988). In the houses and barns of the *Batak Toba*[2], the flexibility of bamboo is utilised to create a curved roof (Schefold, Nas, & Domenig, 2004). The roof frame of *Uma*[3] is constructed from bamboo poles assembled on the ground before being erected on the house's core post (Nurdiah, Asri, & Hariyanto, 2015), as depicted in Figure 1-1b. These studies indicate that local people have employed bamboo by utilising the advantages of bamboo, namely its flexibility and length, to construct the roof in distinctive shapes.

[1] Tongkonan refers to the traditional house of the Toraja, an ethnic group originating from Central and South Sulawesi province.
[2] The Batak Toba is an ethnic group from the Lake Toba region in North Sumatera province.
[3] Uma is the term used for the traditional houses of the Sumbanese, an ethnic group originating from the island of Sumba in East Nusa Tenggara province.



Figure 1-1. a. Tongkonan, vernacular houses of Toraja tribes; b. Uma, vernacular houses of West Sumbanese.

Although the utilisation of bamboo in traditional houses was once a fundamental aspect of traditional construction practices, the rising influence of industrialised materials such as steel and concrete has diminished its importance. The term 'poor man's timber' is relevant among people in Indonesia when referring to bamboo. Bamboo is utilised primarily in rural areas and for small to medium buildings, such as cowhouses, small huts, fences, and non-permanent or replaceable structures. These trends have significantly impacted the perception of bamboo buildings and discouraged people from using bamboo in buildings. However, the development of bamboo architecture in some parts of Indonesia has shown promise recently, evidenced by the emergence of bamboo buildings and the growth in interest of young architects in exploring the material. In recent decades, the value of bamboo as a building material has been increasing. It has been employed for various functions and building typologies, including hotels, restaurants, and multi-function halls.

In recent designs, bamboo has been used for large building structures and has proven capable of enclosing large-span spaces. The Outward Bound Indonesia (OBI) Great Hall (Figure 1-2) uses three bamboo species: *bambu tali* (*Gigantochloa apus*); *bambu gombong* (*Gigantochloa pseudoarundinacea*); and *bambu petung* (*Dendrocalamus asper*). The application is in accordance with its diameter and role; for example, bambu petung has a bigger diameter used for columns, while other species with a smaller diameter are used for roof frames and rafters. The columns and frames are arranged in a circular configuration, thus creating an oval-shaped building (Muhsin et al., 2015). Green School in Bali uses bamboo as the primary material for all the buildings inside the campus area. Some of the buildings are enclosed large-span spaces and in circular forms, highlighting the flexibility of bamboo. In the latest development, during the G20 Summit in Bali in 2022, a bamboo dome was built as one of the venues.



Figure 1-2. a - b. The OBI eco campus, located near Jatiluhur Dam in Jatiluhur, West Java Province.

The examples illustrate that despite experiencing a decline in popularity compared to industrialised materials, bamboo is currently regaining momentum among the communities and local people in Indonesia. Moreover, in terms of locality, the incorporation of bamboo in Indonesian architecture can promote local wisdom and context, encouraging the usage of local material as a form of identity in this era of globalization (Lianto et al., 2019). These examples also illustrate the exploration of bamboo architecture in Indonesia, indicating a preference for spatial structures and the investigation of diverse forms, resulting in dynamic and organic shapes (Nurdiah, 2016).

Meanwhile, gridshell is one form of shell structure that consists of a grid arrangement. Since gridshells are constructed of grids or lattice, the structure uses less material than the solid shell structure (Saleh Tabari, Khojastehmehr, & Filz, 2022; Douthe, Caron, & Baverel, 2010). Furthermore, gridshell structures can be an effective design alternative, capable of meeting various design requirements. Gridshell elements, such as configuration, grids, and construction methods, can be modified as needed. In this context, engineers and architects can collaborate to devise shapes that are both aesthetically appealing and structurally efficient through computer-aided form-finding (Harris et al., 2003).

Exploring the potential of gridshell structures in Indonesia is a significant development, owing to the versatility of gridshell designs that can be adapted into a broad variety of organic shapes. The organic shapes have been commonly found in Indonesian dwellings and settlements, with traditional houses featuring roofs in various designs, including saddle, conical, and hip shapes. Consequently, the gridshell forms are likely to be readily accepted by local people, as they resonate with familiar architectural shapes.

From the cultural and climate standpoint, people in Indonesia engage in gathering as part of dynamic societal interactions, portraying a reciprocal relationship among individuals and groups (Lukman, 2015). As Indonesia is characterised by a hot and humid tropical climate, with high levels of solar radiation, precipitation and humidity, people prefer to seek shelter

under the shade, the significant role of which is reflected in the design of the roofs with long and wide eaves. Indeed, it is often stated that Indonesian architecture is predominantly roof architecture (Prijotomo, 2008). A gridshell structure can enclose a large space beneath the roof, providing a suitable place for people to gather and offering protection from solar radiation and heavy rain, which frequently occur in Indonesia during the rainy season. The geometry od gridshell can be designed with large openings to allow cross-ventilation within the building, which is suitable for the humid climate.



Figure 1-3. a. Common bamboo grooves in Indonesia; b. Bamboo grooves as part of people activities; c. Bamboo shelter as a place for gathering

Simultaneously, the use of bamboo in gridshell structures offers advantages for disaster mitigation. Given Indonesia's vulnerability to natural disasters, such as earthquakes, volcanic eruptions, floods, and landslides, there is a need for quickly constructed shelters capable of housing many individuals for mitigation purposes. Bamboo gridshells could serve as a viable disaster mitigation strategy in Indonesia.

Therefore, it can be concluded that the potential of bamboo gridshell structures in Indonesia is significant. In terms of material, bamboo is sustainable, renewable, locally abundant, and easy to cultivate across Indonesia. Moreover, utilising bamboo for gridshell structures can enhance material efficiency and sustainability, aligning with sustainable development goals. Gridshell forms, capable of being moulded into organic shapes, are likely to be embraced by local people due to their resemblance to traditional Indonesian architectural forms and structures. In terms of climate and culture, gridshell roofs can provide protection against excessive solar radiation and precipitation; they also offer shade for local community activities. Based on these considerations, this thesis explores the theme

of utilising Indonesian bamboo for gridshell structures which highlights its significant potential within the context of Indonesia.

1.2. Research Rationale

Research in gridshell structure has been increasing in recent decades, as shown by Dyvik, Manum, & Rønnquist (2021), and contributes to theoretical studies, structural analysis, form finding, and materials. However, among materials used for gridshell structures, research in gridshell bamboo is limited, and few published research studies can be found compared to timber, steel, and other composite materials.

Attempts to utilise bamboo for gridshell structures have been made for a long time. In 1976, AA (Associate Architect) School students and professors built a bamboo gridshell prototype in London, and in 1977, a project was led by Eda Schaur in India (Hernández, 2015, p. 30). In Japan, two concrete shell structures were built using bamboo gridshell as the formworks designed by Yoh+Architect. The projects were the Naiju Community Centre, built in 1994, and the Uchino Community Centre in 1995 (Chilton & Tang, 2017, pp. 103–106). Meanwhile, a bamboo gridshell with four supports was built at the University of Mexico, a project led by Oliva Salinas (García et al., 2015). Furthermore, in 2015, a large-span bamboo gridshell structure with a span of 32 metres was erected in Hong Kong, a project led by the Department of Architecture, Chinese University of Hong Kong (Crolla, 2018, 2017; Crolla & Fingrut, 2016). The project used computational form-finding and adapted local connection systems commonly used in scaffolding into the structure.

The construction of gridshell structures using Indonesian bamboo has also been undertaken in Indonesia, as evidenced by the construction of the Arc, a wide-span bamboo gridshell structure within the Green School campus in Bali. The Arc features arches made from *bambu petung* (*Dendrocalamus asper*), while the gridshells are stretched between the arches, made from split bamboo and assembled in an anticlastic shape. The building highlights the potential for Indonesian bamboo in gridshell design. However, the curvature of the arches was not achieved by the principle of active bending. While the gridshells made from split bamboo employed an active bending system. This raises questions regarding the impact on bending capacity of using split versus whole culm bamboo on the bending capacity of bamboo. Moreover, the nodal connections in the Arc use nuts and bolts, present potential issues under tension stress, meriting further investigation.

Therefore, although research in bamboo gridshell and constructing bamboo gridshell structures has been conducted and continuous to evolve recently, many questions have not been answered. Several studies were conducted based on computational simulations, while

others were based on experimental methods using physical modelling. Elnagar (2017) studied bamboo gridshell structures through computational modelling and simulation for his thesis and used laminated bamboo as the main material. Research on bamboo gridshell by Rockwood, (2015) was conducted through physical form-finding and empirical experiments which involved the construction of several gridshell models and proposed connections system. From Rockwood's research, we can learn the limitations of bamboo when utilised in a bending active system.

From the previous projects and research about bamboo gridshell, several questions need to be addressed for further implementation. Despite the common perception about bamboo – that bamboo is flexible and easy to bend – the question remains whether all bamboo species can be utilised for active bending gridshell structures. Since bamboo is a natural material, questions need to be asked about the potential deviation between the design of the gridshell structure and the built structure, and about ways to identify the deviation. Regarding the gridshell geometrics, we need to know whether the bamboo gridshell which uses and bending-active system can be constructed in accordance with the standard methods for elastic gridshell structures which use other materials. The identified gaps are the main focus of this research.

1.3. Research Question

The primary challenge in gridshell bamboo research is that bamboo has many variations in species and properties, which influence the gridshell design process and construction. Three issues need to be addressed in bamboo gridshell design: better understanding on the material properties of Indonesian bamboo; investigating whether the bamboo and their properties affect the structural performance; finding the construction method that is suitable for working with the material; designing methods and criteria to achieve optimum structure for bamboo gridshell. All these issues become the gap that will be addressed and discussed in this research. Therefore, the research question of this research is:

How is the feasibility of Indonesian bamboo in its utilisation for gridshell structure?

In order to address the issues, sub-research questions are as follows:

Question 1 – How do the material properties and bamboo morphology affect its bending capability for the utilisation in gridshell structure?

Question 2 – How do forms and forces affect the structural performance of gridshells constructed with Indonesian bamboo?

Question 3 – What are the most suitable construction methods for bamboo gridshell?

Through the research questions, the material properties of bamboo are explored and identified to understand the characteristics of bamboo and the effect of bamboo's properties on the whole gridshell design process. Even though research on the bamboo's material properties has been done extensively, comprehensive data on Indonesian bamboo properties is limited. Moreover, each bamboo species has different characteristics and properties that may not be suitable for a particular structure system, which creates a need for further studies to investigate the implementation of bamboo to the gridshell structure. Meanwhile, form-finding and optimisation are essential to gridshell structure design since the form cannot be separated from the structure. Research on form-finding and optimisation has been done through various methods, from physical modelling to computational modelling and numerical analysis. However, the form-finding and optimisation process of bamboo gridshell should be in accordance with the characteristics and properties of the bamboo used as the material. The construction of gridshell structure is also significant in determining whether the gridshell design is buildable and can resist loads, especially in bending active gridshell structures.

1.4. Research Aims and Objectives

This research aims to assess the feasibility of the utilisation of Indonesian bamboo in gridshell structures by determining the correlation between bamboo as the material, the form and forces of gridshell structures, and the construction method. This research consists of four main objectives, which are listed below.

Objective I: Identify the material properties of Indonesian bamboo

- To obtain data on the physical and mechanical properties of three Indonesia bamboo species.
- To examine the correlation between the material properties and the resulting bending capabilities of the bamboo species.
- To determine how these bending capabilities affect the bamboo utilisation in gridshell structures.

Objective II: Examine the structural morphology of bamboo gridshell using Indonesian bamboo

- To evaluate the structural performance of bamboo gridshells based on the material properties of Indonesian bamboo.

- To compare the results of computational simulations with the results of full-scale models of bamboo gridshell structures.

Objective III: Investigate the construction of bamboo gridshell

- To identify the suitable erection methods when bamboo is the material used for the lattice.
- To evaluate the impact of the construction methods on the structural integrity and durability of bamboo gridshell.

Objective IV: Investigate the form-finding and optimisation processes for bamboo gridshell.

- To investigate the form-finding of gridshell geometry considering the unique characteristics of bamboo.
- To assess the effect of optimisation strategies on the structural performance of gridshell models.
- To propose optimised structural models suitable for bamboo gridshells by considering utilisation factors, displacement, and material usage.

1.5. Thesis Structure

This thesis is divided into eight chapters as follows:

Chapter 1 presents the introduction to the research topic by describing the reasoning, research background, and research gap. This chapter presents the main and detailed research questions, which lead to the research's aims and objectives that form the overall research.

Chapter 2 reviews the relevant literature related to the research topic. The review focuses on the three main parts: material, form and forces, and construction. The material covers reviews on bamboo as a building material, which includes the anatomy, the physical and mechanical properties, and the sustainability of bamboo. The form and forces part reviews the literature related to gridshell structure from the definition, history, materials, form finding, and optimisation. Whilst the construction part reviews the construction methods for gridshell structures in general and the possibilities of construction methods for bamboo gridshell.

Chapter 3 presents the overall research methodology and the research framework used to assess the feasibility of utilising Indonesian bamboo for gridshell structures. The chapter

outlines the main research parameters and their relation to the research question and objectives. This chapter also outlines the methods for the achievement of each objective.

Chapter 4 presents the material properties of bamboo. This chapter reports and discusses the results of the material properties of three selected Indonesia bamboo, namely *Gigantochloa apus, Gigantochloa atter,* and *Dendrocalamus asper*. The first part of the chapter describes the detailed methods for the material test in accordance with ISO 22157:2019. The second part discussed the results and the correlation between physical and mechanical properties. The material properties investigated in this project include mechanical properties parallel to the fibre (compression, tension, shear, and bending), and perpendicular to the fibre (bending and tension).

Chapter 5 presents the structural analysis of two gridshell models using full-culm and split bamboo under applied loads. The structural analysis is done through finite elemen analysis (FEA), carried out in commercial software Abaqus. Results from Chapter 4 become the input parameter for material properties and dimensions. The discussion highlights the effectiveness of FEA by comparison with load tests on physical model.

Chapter 6 describes the construction of two full-scale models as part of the investigation of suitable construction methods for bamboo gridshell. The first part describes the construction process, from investigating the curvature depth and assembly stage to the erection process of two models using full-culm and split bamboo. The second part describes the load tests on the full-scale models.

Chapter 7 describes the utilisation of parametric design tools for form-finding and optimisation of bamboo gridshell. In this chapter, the form-finding process considers the data obtained from the previous chapter regarding the minimum curvature of bamboo. The process is carried out in Rhinoceros using plug-ins Grasshopper and Kangaroo for the form-finding., while the structural performance is analysed using plug-in Karamba3D. A series of optimisations are performed in this chapter to understand how the structure behaves under the optimisation strategies.

Chapter 8 summarises and concludes the key findings from the research related to the research questions. This chapter also proposes the potential research topics in the future related to the outcomes.

CHAPTER 2 | LITERATURE REVIEW

2.1. Bamboo as Building Material

2.1.1. Bamboo Plant and Species

Carl von Linne introduced the term "bamboo" in 1753 to describe a plant similar to grass (Minke, 2016, p. 9). Bamboo is a giant grass that belongs to the grass family Poaceae, subfamily Bambusoideae, comprising about 119 genera and more than 1482 species (Clark, Londoño, & Ruiz-Sanchez, 2015). It can be classified as a woody and herbaceous plant, similar to trees and grasses (Nath, Lal, & Das, 2015). The diverse bamboo family can be divided into three tribes: *Arundinarieae* (temperate woody bamboo), *Bambuseae* (tropical woody bamboo), and *Olyreae* (herbaceous bamboo) (Clark, Londoño, & Ruiz-Sanchez, 2015).

Bamboo grows in both tropical and subtropical regions within the latitudinal range of 46°N to 47°S worldwide, with the exception of Europe, and spans from sea level to an altitude of approximately 4,000 m (Minke, 2016; Lobovikov, Schoene, & Yping, 2012; Scurlock, Dayton, & Hames, 2000). It thrives naturally in tropical and subtropical climates, covering a total area of 38,000 million hectares, equivalent to 3.2% of the total global forest area. Asia stands as the primary source of bamboo, contributing 65% of the world's total resources, while Central and South America account for 28%, and Africa for 7% (Correal, 2016). Bamboo distribution based on the climate region can be seen in Figure 2-1.

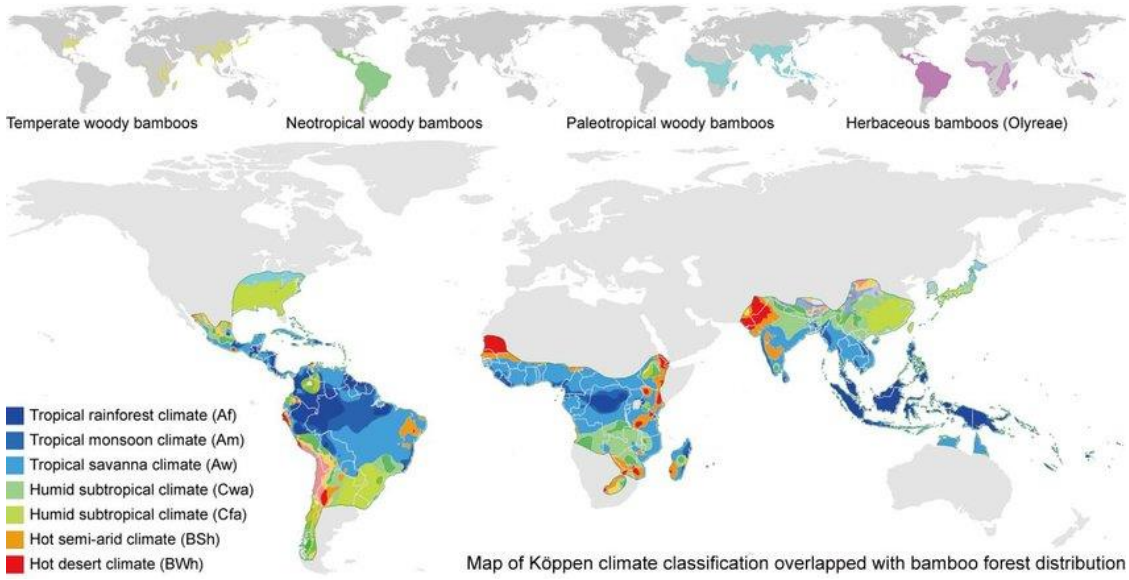


Figure 2-1. Bamboo forest distribution based on climate zone.
(Huang, Sun, & Musso, 2017)

In the Asia Pacific region, China has the highest number of total bamboo species, which is around 626 number of species. At the same time, the second is India, with 102 species, and the third is Japan, with 84 species (Bystriakova et al., 2003, p. 10). The map of potential species richness can be seen in Figure 2-2. Research on bamboo species in Indonesia is ongoing, and a number of newly identified species might be found in the future, including endemic species. Based on the recent research, the number of bamboo species identified in Indonesia is 175 species from 24 genera (Ervianti, Widjaja, & Sedayu, 2018). The identification shows different results than the number of bamboo species in Indonesia reported by Bystriakova et al. (2003), which mentioned only 56 occurring species in Indonesia. The difference can be due to the limitation based on the bamboo type included in the list.

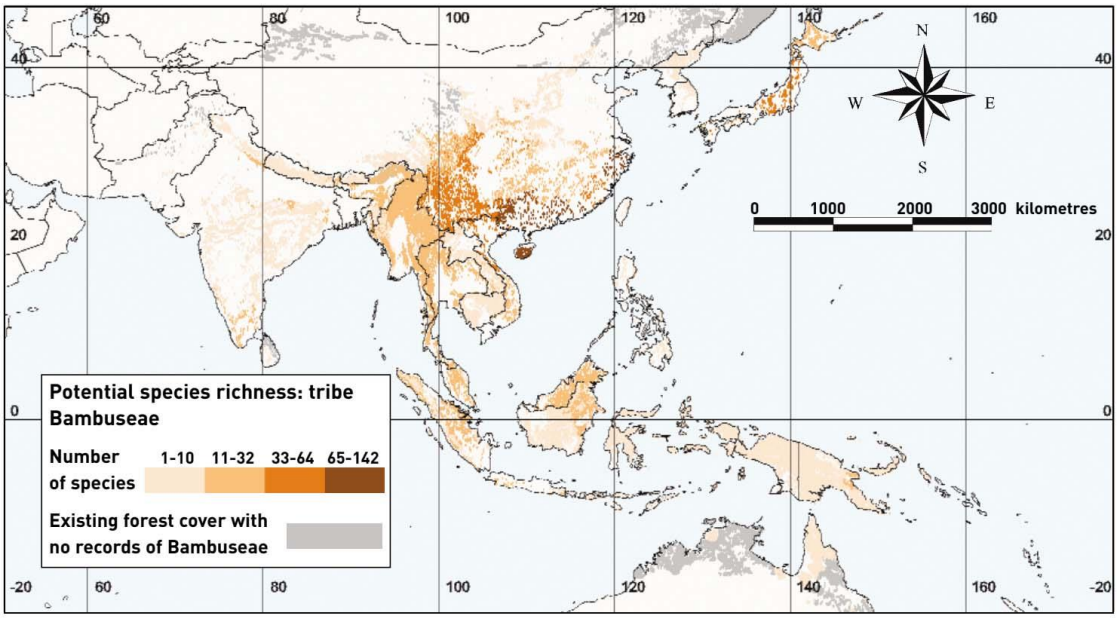


Figure 2-2. Map of bamboo species richness in Asia Pacific.
(Bystriakova et al., 2003)

According to the study conducted by Widjaja (2000), the distribution of bamboo genera in Indonesia exhibited disparities between the western and eastern regions of the country. Genera *Bambusa, Gigantochloa,* and *Dendrocalamus*, characterised by relatively thick walls and medium to large diameters, predominantly flourish in the western part of Indonesia. Conversely, Genera *Schizorachyum, Dinochloa, Nastus,* and *Racemobambos*, featuring thin walls and smaller diameters, are commonly found in the eastern part. Among the variety of species, there are five species that can be found within the Indonesian Archipelago, spanning from Sumatera to Papua: *Bambusa blumeana, Bambusa vulgaris, Dendrocalamus asper, Gigantochloa asper, Gigantochloa atter,* and *Schizotachyum brachycladum.*

Damayanto & Fefirenta (2021) conducted a study to identify the distribution of bamboo genera. The study revealed and uneven distribution of 24 bamboo genera across 12 regions in Indonesia, which can be seen in Figure 2-3. It classified the growth as either wild or cultivated and categorised the origin as native, introduced, or endemic. Only four genera, namely *Bambusa, Dendrocalamus, Gigantochloa,* and *Schizotachyum*, were found to be distributed across all regions. The study summarises and provides comprehensive information concerning the distribution of bamboo genera, thereby providing beneficial in the identification of local bamboo and the determination of suitable bamboo species for construction purposes.

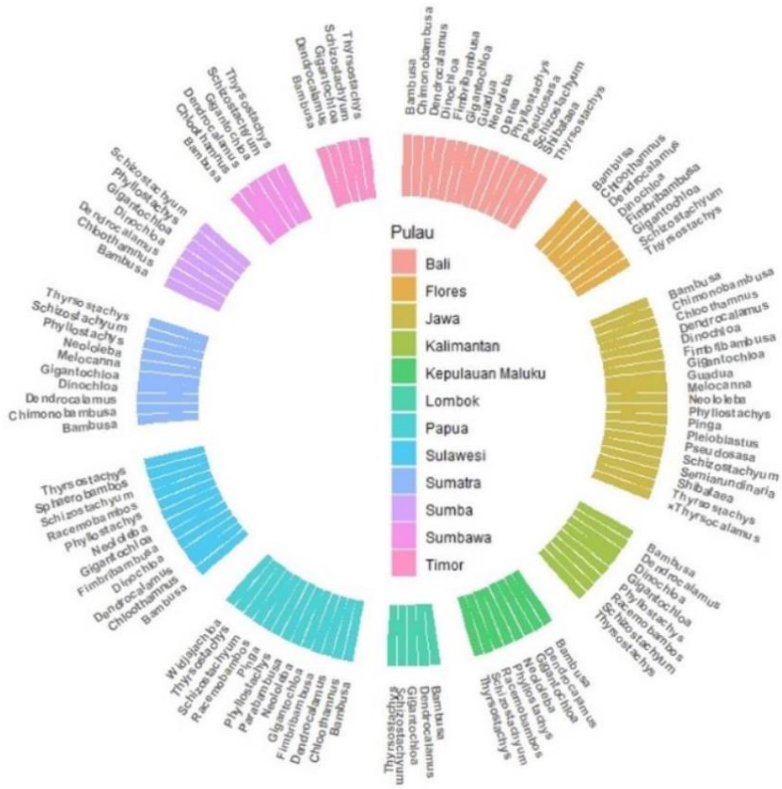


Figure 2-3. Distribution of bamboo genera in Indonesia.
(Damayanto & Fefirenta, 2021)

2.1.2. Bamboo Morphology and Anatomy

Section of bamboo plants can be categorised into belowground and aboveground parts (Figure 2-4). The belowground part of bamboo comprises rhizomes, which can be classified into two types: Sympodial and monopodial (Banik, 2015, p. 45). The monopodial rhizome, or *leptomorph*, has a long, thin, and relatively uniform form. It grows horizontally in linear directions and produces single shoots at regular intervals. Monopodial bamboo is referred to as 'running bamboo' and typically thrives in temperate climate regions, displaying invasive tendencies. The sympodial rhizome, or *pachymorph*, grows and forms compact

clumps; its short and thick roots produce axillary buds into stems, hence the term 'clumping bamboo'. This type predominates in tropical regions and is considered more productive and non-invasive (Goh, Yap, & Tong, 2020). The majority of bamboo in Indonesia is the clumping type (Widyowijatnoko, Trautz, & Baier, 2012; INBAR, 2005). Due to the characteristic of the sympodial rhizome, bamboo grows in clumps and frequently in very dense formations. Consequently, some of them do not grow in a perfectly straight culm but tend to be bent or curved (Widyowijatnoko, Trautz, & Baier, 2012).

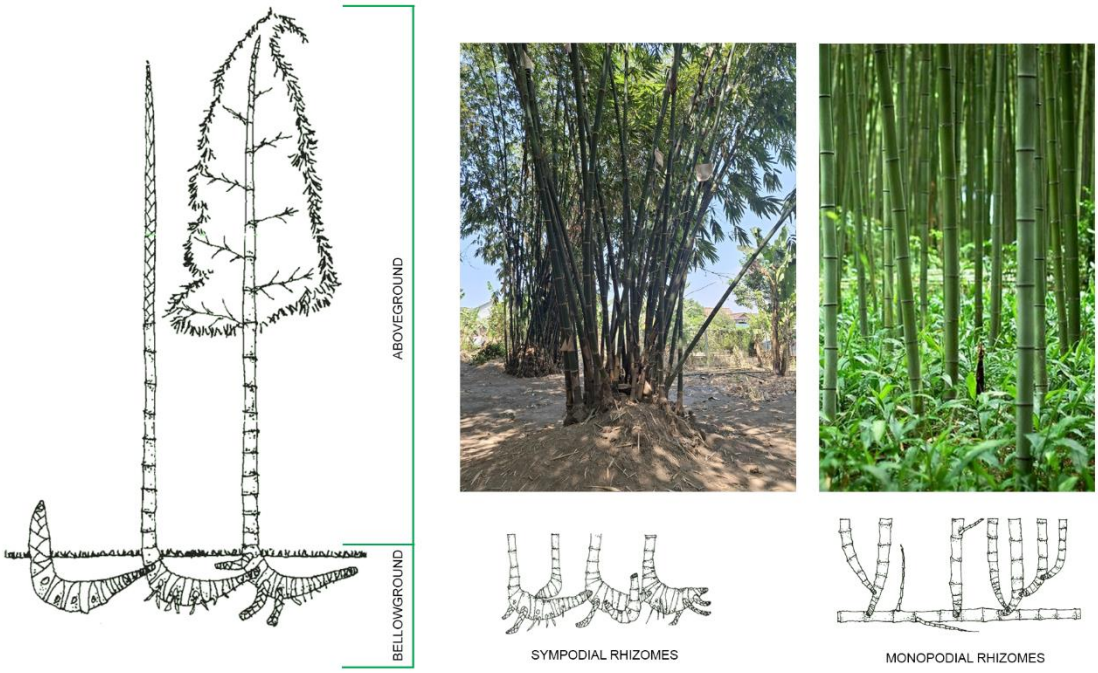


Figure 2-4. Bamboo anatomy.
(Minke, 2016, p. 12)

The aboveground part is the culm, which is hollow, segmented into nodes and internodes, and tapered. The growth of the culm is from the buds, and it can grow rapidly, around 20 cm to 100 cm per day, reaching a full height of 15-30 m within a year, depending on the species (Rockwood, 2015). The culm gradually develops in strength and manages to reach optimal mechanical properties within 3-5 years, a period that varies depending on the species, and starts to deteriorate and collapse in around ten years (Sharma et al., 2015). Bamboo possesses a hierarchical gradient structure, consisting of macroscopic gradient structures in culm diameter, wall thickness, and internode length, and microscopic gradient structures in the distribution of the bundle sheath (Amada et al., 1996).

Bamboo culm has the characterisation of a hollow tube, segmented, and has spaces separated by nodes (Liese & Tang, 2015, p. 227). The node is a circular disc within the hollow tube formed a diaphragm, called septa, which divides the culm into several internodes. The

culm structure is illustrated in Figure 2-5. The nodes serves a function in preventing axial cracking and bending buckling (Gangwar & Schillinger, 2019; Amada et al., 1996). The distance between nodes is shorter at the bottom part of the culm and gets wider in proportional dimension when reaching the upper part (Rockwood, 2015). The culm is taper and not perfectly uniform in size from the bottom to the top, with the bottom part having a larger diameter and thicker wall. Meanwhile, the wall becomes thinner and the diameter smaller at the upper part, but the fibre density increases (Liese & Tang, 2015, p. 228). These characteristics indicate that bamboo is a functionally graded material (Amada et al., 1996).

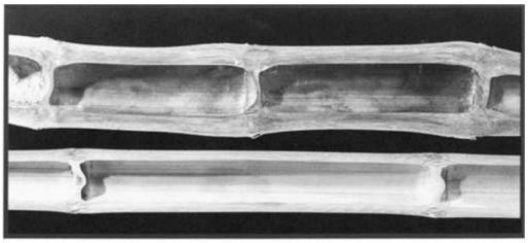


Figure 2-5. Bamboo culm structure in longitudinal section. (Liese & Tang, 2015)

The culm wall comprises fibres and matrix with a composition of about 50% parenchyma cells, 40% fibres, and 10% vascular bundles, as depicted in the cross-section (Figure 2-6); the vascular bundles in dark colour are assembled with fibres and parenchyma (Liese & Tang, 2015). Parenchyma cells refer to the ground tissues, predominantly thin cell walls interconnected with the vascular bundles (Grosser & Liese, 1971). Parenchyma cells are smaller at the outer portion of the culm and grow larger and longer as they approach the centre. Parenchyma plays a crucial role in the culm's life, particularly in storing and managing starch (Liese & Tang, 2015, pp. 229–230). The fibres are long, slenderr, and frequently forked extremities. They contribute to and influence the culm's flexibility and the appearance of its fractures after breaking (Liese & Tang, 2015, pp. 230–234). The vascular bundle is composed of two metaxylem vessel, fibres, and metaphloem sieve tubes with companion cells (Liese & Tang, 2015, p. 234). The principal axis of vascular bundles is parallel to the stem's longitudinal orientation, distinguishing the character of the bamboo's cross-section (Gangwar & Schillinger, 2019). The outer part of the culm, called the cortex, protects from mechanical wounding and retains moisture content during the living period; it consists of compact fibre bundles and thick wall. Meanwhile, the inner part, called the lacuna, is composed of parenchyma cells and usually exhibits variation among species (Liese & Tang, 2015, p. 235).

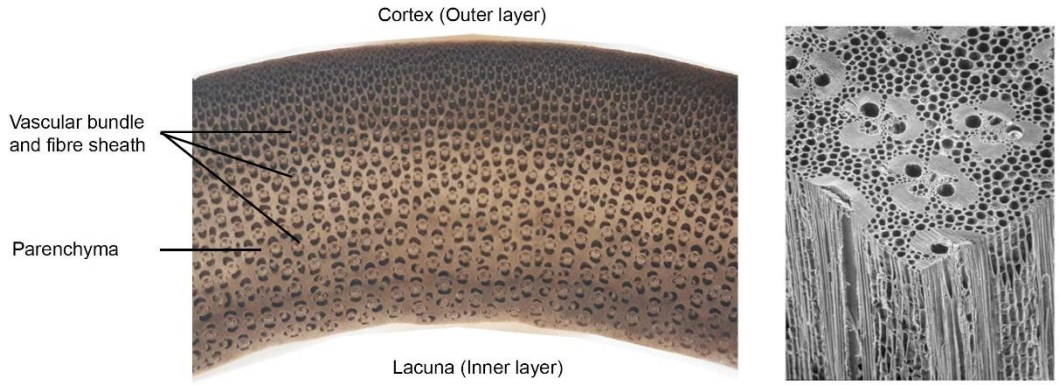


Figure 2-6. Bamboo culm wall cross section.
(Liese & Tang, 2015, p. 235)

Studies on bamboo anatomy, macroscopic and microscopic, of Indonesian bamboo have been done by Maulana et al. (2022), who identified the anatomical characteristics of four bamboo species in Java, Indonesia, which were *Dendrocalamus asper, Dendrocalamus giganteus, Bambusa vulgaris* var*. vulgaris,* and *Bambusa vulgaris* var. *striata*. The research identified the composition, types, and characteristics of the cells. From the findings, the vascular bundles of *D. asper* and *B. vulgaris* are categorised as type IV, while *D. giganteus* and *B. vulgaris* are type III. Moreover, *Dendrocalamus* has a longer fibre length than *Bambusa*.

2.1.3. Physical Properties of Bamboo Culms

Physical properties refer to the substance that can be observed physically in bamboo culms, such as moisture content, fibre saturation point and shrinkage, and density of fibres. Bamboo is a hygroscopic material; therefore, it is sensitive to the humidity change in the environment by absorbing or desorbing moisture until it reaches a state of equilibrium with the surrounding climate conditions (Liese & Tang, 2015; Husain et al., 2007). The strength and durability of bamboo as a building material are highly affected by moisture content, where freshly harvested bamboo has lower strength than bamboo culm that has been dried. Moreover, moisture content also influences the dimensional stability, flexural strength, and creep effect of bamboo culm (Correal, 2016).

Fibre saturation point (FSP) is the condition when the cell walls are fully saturated, but no free water inside the cell cavities (Liese & Tang, 2015; Husain et al., 2007). FSP is generally between 20% to 30% and varies within bamboo culm and species (Correal, 2016). After some time, bamboo reaches a certain level of moisture content regarding the relative

humidity in the environment. The condition is called equilibrium moisture content (EMC), which also affects its dimensional volume (Husain et al., 2007). Bamboo tends to shrink in radial directions more than in tangential directions, and the shrinkage pattern influences the dimensional stability of bamboo culms (Anokye et al., 2014).

Bamboo density ranges from approximately 0.4 to 0.9 gr/cm^3, where the density increases from the lacuna to the cortex and from the bottom to the upper part (Liese & Tang, 2015). Based on Lo, Cui, & Leung (2004), the density correlates with the strength properties of bamboo. However, Lo stated that even though fibre density can be an indicator, the strength capacity of bamboo culms is dependent on the wall thickness. Research on bamboo bending capacity shows a weak to moderate correlation between flexural properties and density (Nurmadina, Nugroho, & Bahtiar, 2017). This indicates that bamboo strength and density might have a strong correlation in some properties, but less correlated with others.

2.1.4. Mechanical Properties

Mechanical properties are attributed to the structural capabilities of bamboo that include the compressive and tensile strength, modulus of elasticity (MOE), modulus of rupture (MOR), flexural strength and shear strength (Goh, Yap, & Tong, 2020). The taper form of the culm shows that bamboo has naturally adapted to lateral loads, such as wind load and gravitational load (Goh, Yap, & Tong, 2020). The cross-section of bamboo with hollow-tube form shows high efficiency compared to the massive section of timber beam (van der Lugt, van den Dobbelsteen & Janssen, 2006).

Bamboo has high tensile strength, which, according to Patil & Mutkekar (2014), the ultimate tensile strength of some bamboo species varies from 140N/mm^2 to 208N/mm^2 and bamboo can resist tension better than compression. The tensile strength is related to fibre density. As a result, the highest tensile strength corresponds to the external wall area with the highest fibre densities; meanwhile, the lowest strength corresponds to the inner wall area, and the area between has intermediate strength (Tan et al., 2011). Within the bamboo culm, the lowest tensile strength is recorded at the nodes compared to the internodes. Bamboo also has weak tensile resistance perpendicular to the fibres, while at the transverse direction, the lignin matrix acts to resist the tension force (Goh, Yap, & Tong, 2020).

Moisture content influences the compressive strength and structural failures due to compression load. Research by Awalluddin et al. (2017) found that the compressive strength of all bamboo increased when the moisture content decreased. During the compression test on bamboo in wet conditions (high moisture content), bamboo was likely to fail at the end-bearing mode. In contrast, in dry conditions (low moisture content), the frequent failure that

occurred was the splitting mode or cracks along the fibre (Goh, Yap, & Tong, 2020). Further, the relation between fibre density and compressive strength is evident. Within the culm, bamboo is weak to buckling when a compression load is applied, with cracks along the longitudinal fibre. This is due to the characteristic of bamboo as a fibrous material. In addition, with an increase in outer diameter, the compressive strength decreases significantly; thus, the strength at the top section is considered to be higher than the base section (Lo, Cui & Leung, 2004).

The MOE or young's modulus of bamboo can be described as "a measure of the stiffness of the bamboo matrix and its resistance to elastic deformation" (Javadian et al., 2019). Thus, MOE affects the flexibility of bamboo. Patil & Mutkekar (2014) claimed that bamboo with a higher MOE is of higher quality and is suitable as a building material in earthquake prone areas. MOE has a close relation with density and age. According to Nordahlia et al. (2012), MOE increased along with age due to the hardening process of culm walls as the density of fibres in the walls becomes thicker with age. However, the increasing of culm diameter affects the decreasing of the average MOE. This is due to the fibre density becoming reduced, and the lignin content increasing when culm diameter increases (Javadian et al., 2019).

Transverse material properties address the mechanical properties perpendicular to the fibre. As bamboo is an orthotropic material, its mechanical properties differ between parallel and perpendicular directions. Moreover, bamboo is considered weak in tangential tensile stress (Arce-Villalobos, 1993), and splitting along the fibre is a common failure in bamboo culms that cause the collapse of bamboo structure (Janssen, 1981). However, the mechanical properties perpendicular to the fibre are less explored due to the nature of failures and the complexity of the tests. Bamboo has an uneven round shape, causing a complication in controlling the eccentricities within the wall thickness (Arce-Villalobos, 1993). Test methods to obtain mechanical properties perpendicular to the fibre were proposed by Sharma, Harries, & Ghavami (2013) and Mitch (2009), investigating the tensile perpendicular fiber and diametric compression, which were adopted in BS ISO 22157:2019 as tension and bending strength perpendicular to the fibre.

Sharma et al. (2013) conducted edge-bearing tests on two bamboo species: *Bambusa stenostachya* and *Phyllostachys aurea* and noted different trends in the strength distribution along the culm. While the modulus of rupture increased along the wall thickness for the thin-wall species (*P. aurea*), the thick-wall species (*B. stenostachya*) did not show the same trend. The test also investigated the flexural behaviour at positive (North-South/NS) and negative (East-West/EW) directions and found that the modulus of rupture in the NS direction was greater. The test results of two bamboo were significantly low. *B. stenostachya* MOR in NS

direction (f_{NS}) was 11.5 Mpa and in ES (f_{ES}) direction was 6.5 Mpa, while for *P. aurea*, f_{NS} was 5.8 Mpa and f_{ES} was 3.3 Mpa. His study of transverse mechanical properties of *P. nigra* carried out through edge bearing test showed result of 11.1 – 12.5 Mpa.

After exploring several test methods, Mitch (2009) developed a split-pin test to investigate splitting capacity and tensile behaviour perpendicular to the fibre. The split test reduced the complexities and eccentricities by using full culm specimens instead of partial culm as the previous method. The results also showed poor properties with failure stress 1.004 – 1.065 Mpa. Akinbade et al. (2021) developed a framework and investigated the required computational tools for investigating the mechanical properties of bamboo culm.

2.1.5. Bamboo as Sustainable Material

The construction sector has contributed significantly to global carbon dioxide (CO_2) emissions. The use of green materials as a replacement or alternative to industrialised materials is thus needed (Goh, Yap, & Tong, 2020). The sustainability aspects of bamboo have been researched, and the findings have shown the immense capability of bamboo in sequestering carbon, reducing CO_2 emission, and conserving energy (Chang et al., 2018; van der Lugt, van den Dobbelsteen & Janssen, 2006). Zea Escamilla, Habert, & Wohlmuth (2016) set out how bamboo can reduce CO_2 emissions in two ways: captured during the plantation period and stored in buildings; and avoided electricity generation when using material by-products.

Bamboo also provides benefits to the environment and plays a vital role in land maintenance. The bamboo ecosystem is a place for animals to live (Lobovikov, Schoene, & Yping, 2012). Planted bamboo on degraded soil can help rehabilitate the land (Sharma, Wahono, & Baral, 2018; Nath, Lal, & Das, 2015). Furthermore, bamboo does not require high investments and maintenance: a bamboo plantation is easy to establish and returns faster revenue since the harvesting period is short compared to timber. Those benefits are suitable to the situation in Indonesia, where degraded land is estimated to account for 24 million hectares or 13% of the Indonesian landmass (Sharma, Wahono & Baral, 2018).

The fast-growing characteristic of bamboo can be the prominent value compare to wood or timber products. By evidencing a short rotation age, the bamboo growth accretion rate is higher than timber and can be harvested in 3 to 5 years (Chang et al., 2018). It matures rapidly which makes bamboo an important replacement material to wood regarding the supply and demand issues of wood (Li, Yuan & Guan, 2016). In summary, the sustainability of bamboo is evident because of its role in carbon sequestration, the positive impact on land maintenance, and the fast-growth characteristic.

2.2. Gridshell Structures: Definition and Design Principles

2.2.1. The Definition of Gridshell Structures

A shell is a structure capable of spanning over a large distance and covering space in the form of a relatively thin layer. A shell structure is described as "*a three-dimensional structure that resists applied loads through its inherent shape*" (Harris & Roynon, 2008). It is defined as a spatial structure with a curved surface, single or double-curved (Naicu, Harris, & Williams, 2014) and a type of form-active structure that is capable of transferring the imposed loads through its shape (Rockwood, 2015, p. 26). The characteristic of a shell structure is that it has a very thin surface and geometrical anisotropy which demonstrates the load-transfer behaviour, such as membrane action, bending and shear (Adriaenssens et al., 2014, p. 45). In terms of surface ratio, according to (Tang, 2015), theoretically, axial and shear in-plane forces are found in a perfect shell; thus, the structure can achieve a slenderness ratio of 1:500 or more.

A direct definition of gridshell is a shell with holes or a subtractive pattern of holes in the surface (Chilton & Tang, 2017, p. 1; Rockwood, 2015, p. 26). It is also referred as 'lattice shell' or 'reticulated shell' which can be defined as a double-curvature shell built of grids, instead of the usual solid surface (Naicu, Harris, & Williams, 2014). The structure is considered as effective because the gridshell needs fewer materials than a solid surface and is capable of enveloping a large span space (Douthe, Baverel, & Caron, 2006). Based on the definitions, it can be said that gridshell has the characteristic of a solid shell structure; however, the forces and loads are transferred through lattice or grid configuration.

2.2.2. History of Gridshell Structures

The history of gridshell structures can be dated to Vladimir Shukhov's research on lattice structures in the 1890s, years before the computational design was introduced. Shukhov designed three types of lattice structures, which were suspension, vaulted and rigid spatial shell, presented at the All-Russian Industrial Art Exhibition in 1896 (Edemskaya & Agkathidis, 2016). However, the term 'gridshell' was first mentioned by Frei Otto during his investigation of light-wieght shell structures in the late 1950s. During his study, Otto used an inverse hanging chain and found that when an equal mesh square grid was deformed into rhombi, it could be formed into a double-curved surface; he described the structure as '*gitterschale*' (Liddell, 2015). His first experiment on gridshell was the Essen project in 1962, which functioned as a German pavilion (Tang, 2013). Later, in the 1970s, Frei Otto's research

attracted the architect of the Mannheim project, Carl Mutschler & Partners, and they decided to collaborate with Frei Otto in designing the project which resulted in the first large scale timber gridshell structure built in Mannheim, Germany, in 1975 (Liddell, 2015).

Several gridshell structures have been built from the 1960s to nowadays, and a review was done by Peloux (2017, pp. 22–43), which showed the distribution of elastic gridshell based on the material and the span within the time frame. Even though several gridshell structure was built within 1960s to 18970s, Peloux recorded a 'dry period' to describe the lack of elastic gridshell built for 25 years after Mannheim Multihalle. However, in 1994 and 1995, two concrete shells were built in Fukuoka, Japan, using split bamboo as the formwork (Chilton & Tang, 2017). Interestingly, the bamboo was weaved into a basket-like, and from the documented images, the formwork was constructed as elastic gridshells. The gridshell structure returned in the late 1990s with some prominent structures, such as the Japan Pavilion for expo 2000, designed by Shigeru Ban, in Hannover, Weald and Downland in 2002, and Saville Garden in 2006.

Bamboo gridshell structures were not new and had been recorded since the 1970s by the Institute of Light Surface Structures (IL), Stuttgart University (Oliva Salinas, Mendoza, & Meza, 2018). IL published two projects carried out by the Architectural Associate (AA) students in London, and Eda Schaur in Ahmedabad, built gridshell prototypes using bamboo with a very small diameter. (Hernández, 2015, p. 30). However, bamboo gridshell was also less developed and constructed for a long period. In the 2010s, the utilisation of bamboo in gridshell structures started to be explored as the demand for sustainable materials and construction became a recent issue. In 2011, at National Autonomous University, a large gridshell structure was built by students under the lead of Professor Oliva Salinas. And in 2015, a prominent large-scale bamboo gridshell, ZBC Pavilion, was built in Hong Kong. Designed by a Chinese University of Hong Kong (CUHK) team, the structure was constructed based on traditional bamboo construction for scaffolding in Hong Kong (Crolla, 2017). The latest gridshell bamboo is The Arc in Bali, which was completed in 2021.

Gridshell structures have been built since 1960s in various forms, using timber, steel, composite materials, and others, including bamboo, which shown in Figure 2-7.

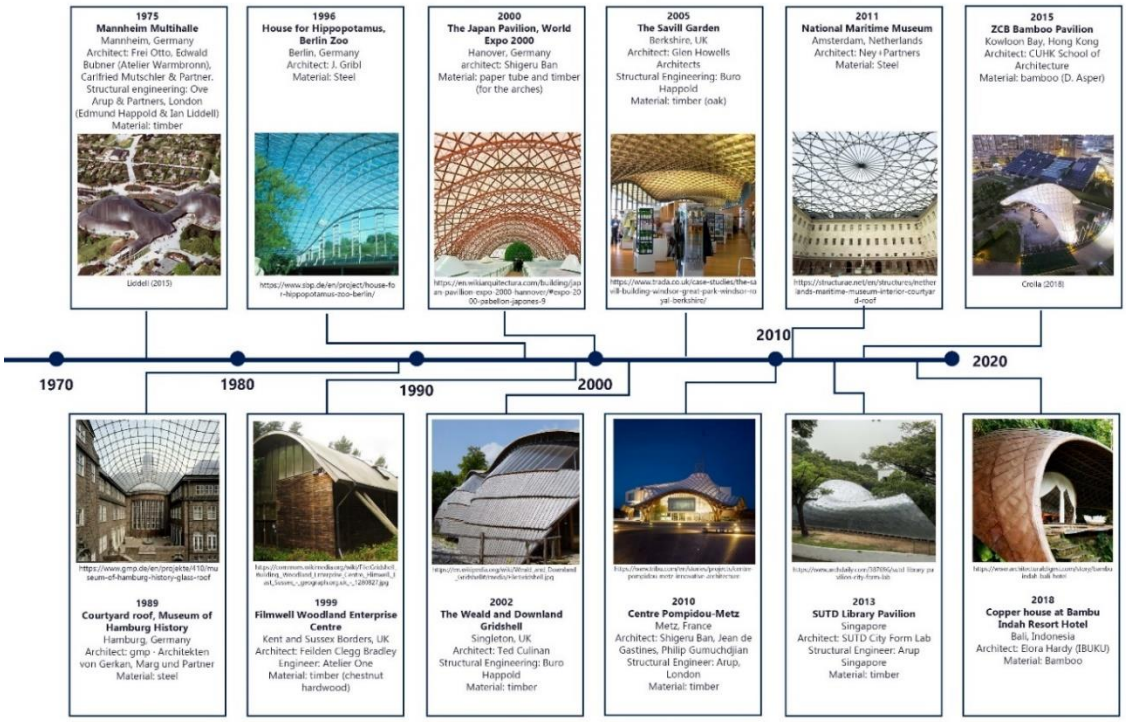


Figure 2-7. Examples of gridshell structures built within 1980s to 2020s.

2.2.3. Classification of Gridshell Structures

Based on construction methods, gridshell structures can be classified into unstrained and strained gridshells (Figure 2-8). Unstrained gridshells are built from prefabricated nodes and members, which means that the lattices or members are pre-produced in curved forms, or the curvature is developed through nodes while the members may remain straight (Rombouts, Schevenels, et al., 2019; Adriaenssens et al., 2014, p. 91). The material for unstrained gridshell structures is usually steel or curved laminated wood. This method is useful for freeform gridshell structures and is driven by the mixture of several considerations, including aesthetic, form, physical and constructional considerations (Adriaenssens et al., 2014, p. 92). Unstrained gridshell, also called a reticulated shell or rigid gridshell, refers to a gridshell structures that are not formed and constructed through an active bending process (Dyvik, Manum, & Rønnquist, 2021; Peloux, 2017). Since the form is achieved by assembling straight or pre-bending members, the nodal connections need to be specifically designed (Rombouts, Lombaert et al., 2019).

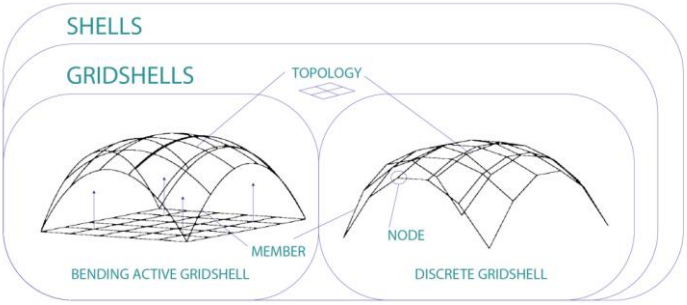


Figure 2-8. Gridshell terminology described strained and unstrained gridshell. (Dyvik, Manum, & Rønnquist, 2021)

Strained gridshell produce the form by assembling the initial flat grid consisting of continuous members, which is then lifted up until the designated form is achieved. It can be constructed on-site without pre-produced curved members and connectors (Rombouts, Lombaert et al., 2019). Mannheim Multihalle and other timber gridshell are the examples of strained gridshell. The curve is shaped by actively bending the members; thus, the structural elements also can be called as active bending (Adriaenssens et al., 2014). Active bending is 'systemised elastic deformation' through bending the members and appears as a simple method to produce curved elements (Lienhard et al., 2013). Gridshells built through this method also can be called 'elastic gridshells' which refers to the materiality and construction process. Elastic gridshells consist of straight continuous members that are arranged into grids and layers, and then the grids are bent gradually into the final shape (Dyvik, Manum, & Rønnquist, 2021; Peloux, 2017; Hernández, Baverel, & Gengnagel, 2013).

Furthermore, elastic gridshell can be categorised as regular and irregular gridshell, which refer to the construction and erection methods. Regular gridshell means that the gridshell is erecting from the initially flat grid, which is in a regular form of equal mesh size, into the designated form. Thus, the nodal connection should ensure movement to allow deformation during the form-finding process. In comparison, irregular elastic gridshell means that the construction process was done by individually bending the members. The advantage of the process is the members can be formed to follow the forces flow; however, the construction process consumes more time than regular gridshell (Rombouts, Lombaert, et al., 2019; Hernández, 2015).

2.2.4. Form-Finding Gridshell Geometry

The definition of form-finding can be described as "*a forward process in which parameters are explicitly or directly controlled to find an optimal geometry of structure which is in static equilibrium with a design loading*" (Adriaenssens et al., 2014, p. 2). For structures where the forms are highly influenced by forces, form-finding is a crucial stage in the design process.

According to Li (2018), the term was initially used to describe the method of creating the equilibrium forms of 'force-active' structural systems subject to certain limits. However, 'force-passive' structural systems can utilise the final equilibrium forms with few adjusted settings. Thus, a 'force-passive' structural system can also use the form-finding term to describe the form generating process. Another definition of form-finding from Douthe, Baverel & Caron (2006) described the process of form-finding as an exploration for stable and aesthetic forms of shell structure. Based on those definitions, it can be concluded that form-finding is a process to find a stable and equilibrium form of shell structure with controlled parameters.

Before computational methods existed, the form-finding process of shell structure used physical models. The use of physical models is believed to provide similar indications on how the larger version of structures would behave, even though many types of structures cannot be simply scaled up and behave similarly at full size (Adriaenssens et al., 2014, p. 34). Li (2018) classified physical model methods of form-finding shell structures according to the manufacturing methods into three categories: hanging models; tension models; and pneumatic models. Pneumatic models use a membrane which is blown up to a particular shape as a mould, to represent an equilibrium state under pressure loads. Tension models use a soap film or gauze to find the equilibrium shape within the pre-set boundaries of a minimal surface, representing the equilibrium state with internal stress. The hanging model characterises an equilibrium state of a force-active structure under gravity. Hanging model is self-forming, and the self-weight and loads are transferred purely in tension. However, the pure compression model occurs when the model is turned upside down (Li, 2018, pp. 62, 95–97).

Hanging models using chains have been used frequently in the design and study of shell structures since the masonry vaults and domes era. Firstly practised by Robert Hooke, it conveys the idea that when the chain is hanging, it acts in pure tension; then when the hanging shape is inverted, it obtains the equivalent arch that acts in pure compression. Thus, the shape is funicular geometry formed due to its self-weight or by loading a certain weight (Adriaenssens et al., 2014, pp. 7–8). Frei Otto used hanging chain models during the form-finding of Mannheim Multihalle (Figure 2-9) to find the initial form. The comprehensive process was described by Liddell (2015), namely that besides using model, the form was also calculated numerically using force densities.

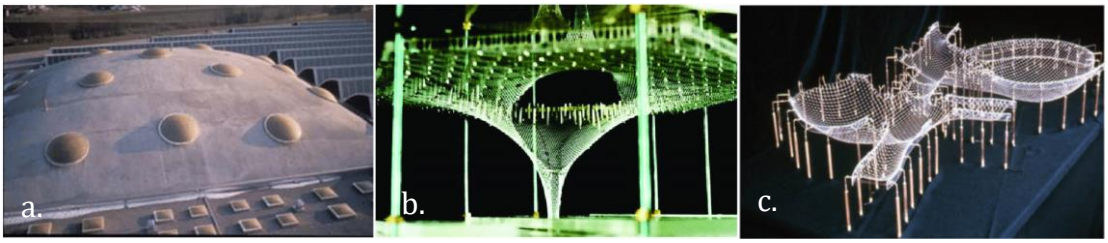


Figure 2-9. a. COOP Distribution Centre in Switzerland, designed by Heinz Isler using the pneumatic model; b. Concept of a new train station in Stuttgart using the tension model; c. The form-finding process of Mannheim Multihalle using the hanging mode.
a & b.Li (2018, p. 96) and Liddell (2015)

Therefore, the hanging model is only the first approach in form-finding because it represents the simple compression stress. In contrast, for a gridshell structure, the state of stresses is the combination of bending, compressive, and tensile stresses (Douthe, Baverel & Caron, 2006).

Nowadays, numerical analysis methods rely on computational simulation and have been studied using various methods. Based on Adriaenssens et al. (2014, pp. 115–116) and Li (2018, p. 63), the methods can be classified into three groups/families: (1) stiffness matrix methods, using the standard elastic and geometric stiffness matrices; (2) geometric stiffness methods, which are material independent, only considering geometric stiffness; (3) dynamic equilibrium methods, solving dynamic equilibrium problems to achieve a steady-state solution equal to the static solution of static equilibrium. Veenendaal and Block compared the three methods and suggested that the procedure in form-finding should consist of four elements: (1) a discretisation to define initial geometry; (2) a data structure that records the form, connectivity of the discrete elements, and forces; (3) equilibrium equations that identify the relation of internal and external forces; and (4) an integration scheme that shows how to solve the equilibrium quotation (Adriaenssens et al., 2014, p. 116).

2.2.5. Structural optimisation

Besides form-finding, structural optimisation becomes the next step that is necessary for gridshell design. Structural optimisation refers to an inverse process to obtain the geometry of the structure in which parameters are indirectly optimised. The objectives are to minimise the material and weight of the structure, minimise the deflection or dynamic vibration of the structure, and maximise the stiffness by reducing the structural compliance, thus achieving efficiency in the structure (Adriaenssens et al., 2014, p. 3). Structural optimisation, as depicted in Figure 2-10, can be categorised into three groups: topology

optimisation, size optimisation, and shape optimisation (Seifi, 2019; Li, 2018; Christensen, Gladwell, & Klarbring, 2009). Topology optimisation means that the optimal design of structure form will be achieved by adding or removing the elements (bar/beam) between predefined nodes. For size optimisation, the optimal design will be obtained by changing the size of the structure elements, for example, changing the sectional area of trusses members or plate thickness (Seifi, 2019). Shape optimisation means changing or modifying the geometry to obtain the optimal design, which includes the geometry contour and boundaries (Christensen, Gladwell, & Klarbring, 2009).

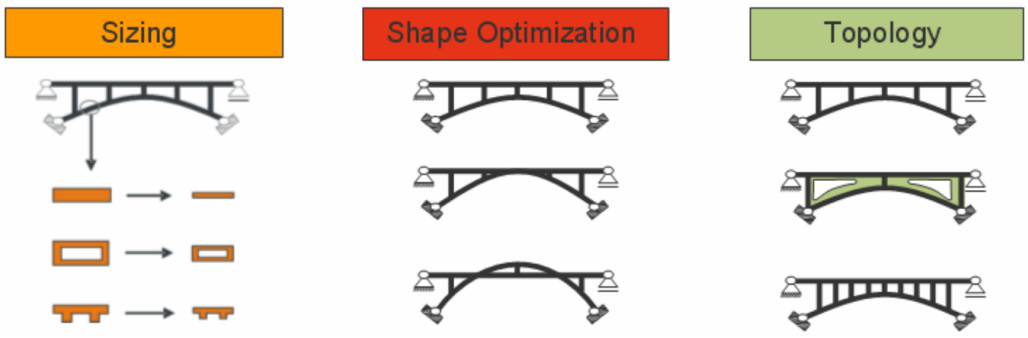


Figure 2-10. Structural optimisation strategies.
(Li, 2018, p. 69)

2.2.6. Material Selection

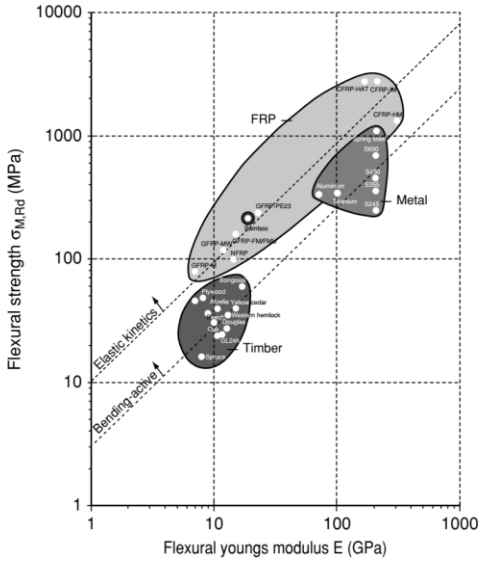
In an elastic gridshell with an active bending structure system, bending the material is the strategy to define the form (Lienhard & Knippers, 2013). Therefore, material selection is crucial, and specific criteria are needed in selecting suitable materials. Material with high-breaking strain and sufficient stiffness is needed to guarantee the structure is able to bear loads and residual stresses (Kotelnikova-Weiler et al., 2013; Lienhard et al., 2013). Besides that, other factors also determine the suitability of materials for gridshell structures. As reviewed by Hernández (2015), selecting materials for gridshell structures should consider the ratio of Young's modulus to the strength, the axial and bending stiffness of the profiles, and the long-term behaviour. From Hernández's studies, the ratio of Young's modulus to strength (E/f_m) influences the stress utilisation and the radius of curvature that the materials can reach. At the same time, the selection of cross-section or profiles, including layering the grid members, influence the stiffness and utilisation factors of materials. Meanwhile, the long-term behaviour, such as creep and relaxation, need to be considered and can influence the final geometry of gridshell.

Study on elastic gridshell by Hernández (2015), refer to Euler-Bernoulli beam theory and define that the minimum radius of curvature (ρ_{min}) can be calculated from the Young's modulus (E) and the design strength (σ_d) of the material, as stated in equation 2-1. Where the profile is easier to bend when the ratio of Young's modulus to strength is lower. Furthermore, Hernández recorded that the minimum radius of curvature for bamboo is 66 - 85•z, where z is half of the profile's section height.

$$\rho_{min} = \frac{E}{\sigma_d}.z \qquad 2\text{-}1$$

Various material selections exist for gridshell structures, from timber, steel, aluminium, and composite materials. Several studies have identified and listed material selection for existing gridshell structures (Collins & Cosgrove, 2016; Hernández, 2015; Quinn & Gengnagel, 2014). Timber lath has been used extensively for elastic gridshell. At the same time, in recent decades, composite materials based on fibre-reinforced polymers, such as GFRP (glass fibre-reinforced polymers), NFRP (natural glass fibre-reinforced polymers), and CFRP (Carbon fibre-reinforced polymers) have been greatly interest with some prominent examples, such as Soliday Pavilion and Creteil Cathedral, both in France.

Material selection based on the flexural strength and flexural Young's modulus has been plotted by Lienhard based on Ashby (1999), as shown in Figure 2-11, which displays the categorisation of building materials. Materials suitable for active bending structures propose a ratio of flexural strength and Young's modulus (σ_m/E) >2.5. Meanwhile, elastic kinetic systems need to consider fatigue control and limit the allowable elastic stress; thus, a ratio of σ_m/E >2.5 is used (Lienhard et al., 2013). Bamboo, timber, and reed have been used extensively for active bending structures in vernacular architecture and traditional construction practices (Chilton & Tang, 2017; Lienhard et al., 2013). Bamboo application in active bending form and structure is versatile and can be utilised as full-culm, laths, and composite (Seixas et al., 2021).



Type: metals	Flexural strength $\sigma_{M,Rd}$ (MPa)	Flexural youngs modulus E (GPa)	Ratio
S245	245	210	1.17
S355	355	210	1.69
S450	450	210	2.14
S690	690	210	3.29
Spring steel	1100	210	5.24
Titanium	340	102	3.33
Aluminum	330	70	4.71
Timber			
Spruce	16	8	2
Pine	24	11	2.18
Douglas	30	12	2.5
Western hemlock	35	13	2.69
Yellow Cedar	40	15	2.67
Oak	30	10	3
Beech	35	10	3.5
Afzelia	40	11	3.64
Bongossi	60	17	3.53
GL24h	24	11.6	2.07
GL28h	28	12.6	2.22
GL32h	32	13.7	2.34
GL36h	36	14.7	2.45
Plywood F25	25	5.5	4.54
Plywood F40	40	6.0	6.67
Plywood F50	50	7.0	7.14
Plywood F60	60	9.0	6.67
Bamboo	213	19.13	11.13
FRP*			
CRFP-HAT	2800	165	16.97
CRFP-IM	2800	210	13.33
CRFP-HM	1350	300	4.5
P E 23	300	23	13.04
GRFP-M	80	7	11.43
GRFP-MW	120	12	10
GRFP-FM/FMU	160	15	10.67

Figure 2-11, Plotted of building materials based on Ashby diagram and the ratio of strength to stiffness.
(Lienhard et al., 2013)

Regarding the design strategy and understanding the scalability of the structures, the dimension scale and curvature of active bending structures can be studied through elastica arch, which shows the elastic deformation curve of the beam after the buckling (Lienhard & Knippers, 2013). The design strategy can be implemented in the form-finding process of active bending structures by seeking the radius of curvature of the materials. However, the value differs amongst bamboo species, and further investigation is needed to determine the values.

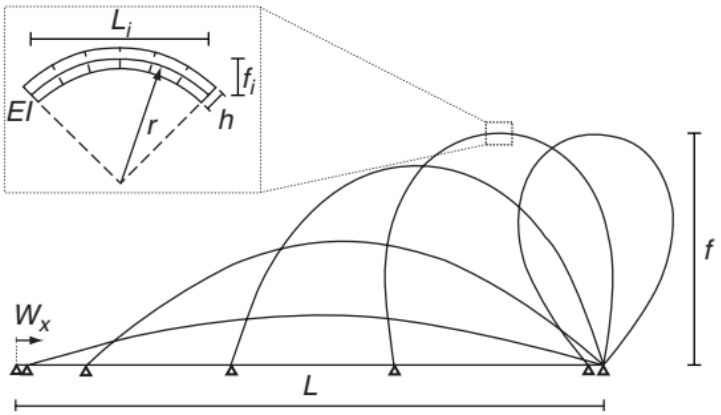


Figure 2-12. Study of elastica curves.
(Lienhard & Knippers, 2013)

Several case studies of active bending structures used the elastica curves principle to obtain the radius of curvature and use the information in the form-finding process (Figure 2-12). The radius of curvature data is mostly obtained by conducting empirical tests. Seixas et al. (2021) implemented the elastic curves principle in the form-finding of a bamboo pantograph structure using full-culm bamboo. The radius of curvature was obtained from empirical tests, and the results were used to determine the arches' curvature. The arches were formed by actively bending bamboo culm and bundled several culms into one arch. Suzuki, Slabbinck, & Knippers (2020) utilised bamboo slats (or split bamboo) to construct an active bending structure using computational form-finding. Before the form-finding, they did several tests to determine the radius of curvature. Interestingly, they used the form of lath bamboo curvature as a module and designed a radial repetition as the 'grid' in Grasshopper with plug-in ElastiSpace. As a result, the grid form was determined from the curvature radius.

From the literature, several problems arise from the utilisation of full-culm bamboo in active bending structures due to material limitations. Longitudinal splitting frequently occurs, and one of the causes is due to connection design. Thus, suitable connections should be developed (Seixas et al., 2017). Meanwhile, even though bamboo slats are more flexible than full-culm bamboo, utilising bamboo slats in form-finding in the computational design is difficult for at least two reasons: the non-linear characteristic caused by the composite structures and the distribution of nodes which affects the bending (Yang & Xu, 2021).

2.3. The Construction of Gridshell Structures

As reviewed in Section 2.2.3., gridshell structures can be categorised into two structural systems based on the bending process and the construction methods, which are unstrained and strained gridshell (Rombouts, Schevenels, et al., 2019, p. 3). Unstrained gridshell is formed by the configuration of straight members or fabricated bending members assembled on site. The courtyard glass roof of British National Museum is one example of an unstrained gridshell structure (Figure 2-13a). Meanwhile, a strained gridshell is formed by bending initially straight members into curvature on the construction site. Thus, the strained gridshell uses an active bending system, and is called an elastic gridshell. Many prominent gridshell structures have been built using the active bending principle, for example, the main building's roof of Savill Garden (Figure 2-13b) and a gridshell structure in Weald and Downland Living Museum.



Figure 2-13. British National Museum; b. Savill Garden.

2.3.1. Erection Methods of Gridshell Structures

As reviewed in Section 2.2.3., the basic principle in constructing an elastic gridshell structure is actively bending the members. The regular gridshell is erected by giving shaping from a flat grid on the ground, while the irregular gridshell is by bending the members individually. Several methods have been explored since regular gridshells need to be erected from flat grids. Three methods have been tested and employed to build notable gridshell structures: lift-up, push-up, and ease down, and the new proposed method is inflated or pneumatic (Quinn, Gengnagel, & Bletzinger, 2016; Quinn & Gengnagel, 2014), shown in Figure 2-14. The lift-up or pull-up method involves assembling the flat grid on the ground and then lifting the grid, and the elevating tools are varied from cranes or cables (Liuti & Pugnale, 2015). The Essen project and the German Pavilion at the 1967 Expo in Montreal used this method (Figure 2-15). This method offers speed in construction, but several disadvantages may occur. The cables might introduce loads and create stress concentrations on the nodes (Quinn & Gengnagel, 2014).

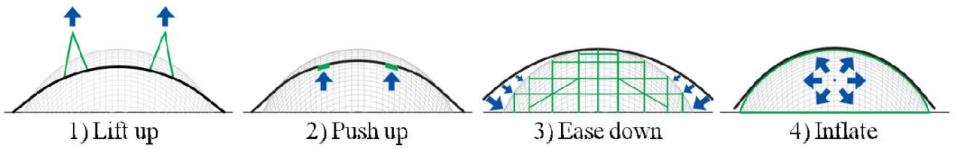


Figure 2-14. Gridshell erection methods.
(Quinn, Gengnagel, & Williams, 2015)

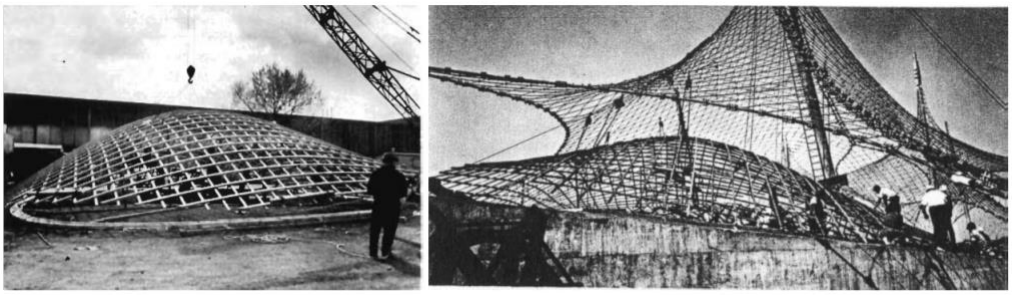


Figure 2-15. a. The erection process of the Essen gridshell using a crane; b. The erection process of the German Pavilion using cables.
(Quinn & Gengnagel, 2014)

The push-up method uses a static formwork or jacket tower to push the grids gradually (Liuti & Pugnale, 2015). Mannheim Multihalle was erected using this method (Figure 2-16a and Figure 2-16b). Even though the first plan involved using cranes and cables, this was changed to the push-up method because the nodes needed to be supported in the correct position during the process (Liddell, 2015). The ease-down method requires scaffoldings to support the grids. The basic principle is to erect and place the grids on top of the scaffolding and then let the laths bend down into the expected forms (Quinn & Gengnagel, 2014). Weald & Downland (Figure 2-16c) and Savill Garden used this method to construct the structure (Harris & Roynon, 2008; Harris et al., 2003).

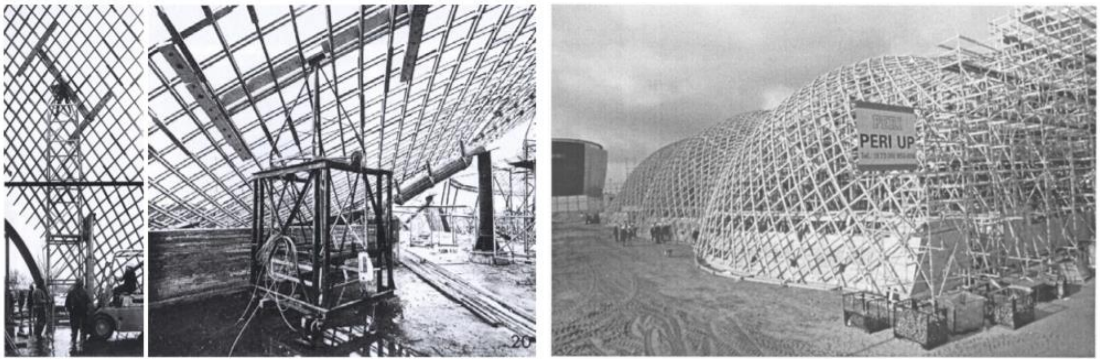


Figure 2-16. a. & b. Erection process of the Mannheim Multihalle using a jacket tower; c. Erection process of Weald & Downland using the PERI-UP scaffolding system.
a. & b. (Quinn & Gengnagel, 2014); b. (Harris et al., 2003)

The inflate concept uses a pneumatic formwork placed beneath the grids, then air is pumped into the formwork, and as a result, the grids are inflated (Quinn & Gengnagel, 2014). Pneumatic membrane has been used as formwork for concrete shell structure for a long time and uses less material and labour than conventional formwork (Kromoser & Huber, 2016). The inflate method for elastic gridshell is relatively new, but prototypes were successfully erected using pneumatic formwork (Quinn & Gengnagel, 2018; Liuti & Pugnale, 2015), showing its feasibility for gridshell structure.

The effectiveness of four known methods in erecting gridshell structures for bamboo gridshell is unknown. Very few records on constructing bamboo gridshell have been published. As a reference, the ZBC Pavilion was constructed using full-culm bamboo, and the erection method was by individually bending the culms. All process was done manually and relied on the skill of the workers (Crolla, 2018).

2.3.2. Jointing and Nodal Connection

Since gridshell consist of continuous members, one of the problems is how to join the material to ensure that the members are long enough and have sufficient length to construct the whole lattice. Learning from the construction of the Weald and Downland gridshell, the engineers designed finger joints and scarf joints to produce continuous members (Harris et al., 2003). These types of jointing are possible for materials that have a rectangular and solid cross-section such as laminated timber laths (Figure 2-17). However, raw bamboo poles evidence round and hollow sections with irregular dimensions. Furthermore, there are nodes and internodes within the culms, and the culm itself exhibit a tapered form. The study and design of a raw bamboo gridshell by CUHK (Figure 2-18) used lashing joints and coded the position to minimise misplacement (Crolla, 2017). Similarly, Rockwood (2015) also used lashing joints in his study. Designing the correct jointing based on the characteristics of bamboo as a natural material is important. Even though lashing the joint can reduce the risk of cracking, the practical method, the suitable rod materials, and the structural behaviour within the jointing have not been studied intensively.



Figure 2-17. a. Finger joint; b. construction of scarf joints.
(Harris et al., 2003, pp. 437–438)

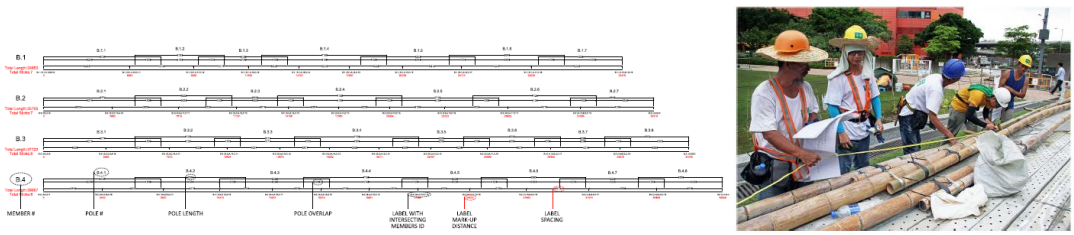


Figure 2-18. Bamboo poles connection to create long members.
Source: (Crolla, 2017)

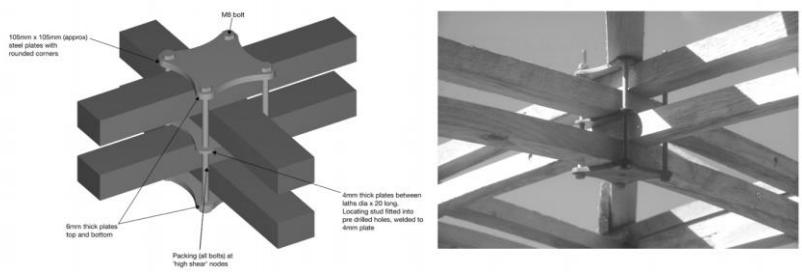


Figure 2-19. Example of nodal connections. (Harris et al., 2003)

The design of the nodal connection (Figure 2-19) significantly affects the success of the construction process, and a gridshell structure might consist of large numbers of nodes. Since in strained gridshells the structures are formed from flat grids, when the grids are erected, the nodes must accommodate any movements involved such as rotation and torsion. Moreover, in double-layer gridshells, some sliding of the layers might happen due to differences in curvature between the layers (Chilton & Tang, 2017; Harris et al., 2003, 2004). Once the desired form has been achieved, a connection needs to be added to clamp the grid layers to limit further movement (Chilton & Tang, 2017). In the case of a double-layer system, the nodes also play a role in transmitting shear between the parallel layers and form a composite section effectively (Chilton & Tang, 2017; Harris et al., 2004). A comparison study, which included the list of nodal connection designs used in several gridshell buildings, has been carried out by Quinn & Gengnagel (2014). Meanwhile, experiments on gridshell bamboo conducted by Rockwood found that during erection process, the bamboo poles had a tendency to fail in bending or buckling which typically occurred at the gridshell nodes (Rockwood, 2015, p. 52). Consequently, designing the nodes and connectors for gridshell bamboo not only has to consider the movements involved or whether it is a double-layer but also needs to tackle the buckling problem.

2.4. Summary

To summarise, the design process of elastic gridshell structures shall consider the material used for the grid members, the form and forces of the structure, and the suitable construction methods to build the structure. The three aspects are related and interdependent (Figure 2-20). Bamboo, as the material, has a particular anatomy, physical properties and mechanical properties that will influence the design of forms and the structural behaviour. It also affects how the structure will be constructed and the details, such as the jointing and connection. Form and forces relate to the structural morphology. In gridshell structures, the forms and forces cannot be separated since the forces will affect the

forms and vice-versa. The structural morphology and the material, therefore, highly influence the consideration of construction methods, and finding suitable construction methods is one of the key successes in building a gridshell structure.

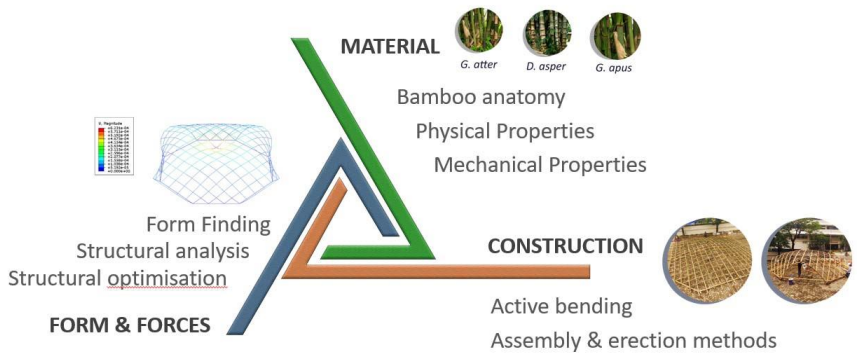


Figure 2-20. Parameters in bamboo gridshell design process.

CHAPTER 3 | RESEARCH METHODOLOGY

3.1. Overview

The design process for gridshell structures is fundamentally complex, requiring a proper collaboration between the architect who designs the form, and the engineer who devises the structural elements. In this context, the roles of architect and engineer are indistinguishable (Harris, 2011). Macdonald (2001) articulately stated that in the architecture of spatial structures, the structure is the architecture, and at the same time, the architecture is the structure. This interdependence highlights the integral synergy between architectural concepts and engineering practicality.

As previously discussed in the literature review and summarised in Section 2.4, designing a gridshell structure requires careful consideration of the material selection, structural morphology, and construction methods. Every material has distinct characteristics, properties, and limitations which can influence the gridshell's geometry and structural performance. Material selection also determines the construction methods. For example, gridshell made from steel is suitable for prefabrication, while timber gridshell might be more suitable for bending-active techniques. The interconnection between these factors is bidirectional. Optimal structural morphology can be achieved with specific materials and construction methods. At the same time, the selection of suitable erection methods for gridshell structures depends on the form and material of the gridshell. In summary, these parameters are interrelated and holistically approached to comprehensively understand the design process of gridshell structures.

The interdependence of these parameters guided the research through a comprehensive exploration of the use of Indonesian bamboo in gridshell structures, from the material selection and structural design phases to the construction methods, thereby providing a holistic view of the process and its design outcomes.

3.2. Research Design

3.2.1. Research Framework

Following the research questions, this research aimed to understand the utilisation of bamboo for gridshell structures, especially Indonesian bamboo. More particularly, bamboo gridshell structures intended to be erected based on the bending-active principle. To achieve

the aims, the research was carried out using a scientific approach, the epistemological stance of which was objectivist. Objectivists believe that '*meaning and therefore meaningful reality, exist as such apart from the operation of consciousness*' (Crotty, 1998, p. 8). The theoretical perspective reflects the nature of the research questions. The research strategy adopted the bottom-up approach, meaning that the design was built from known components to produce a complex design (Terpenny, Nnaji, & Bøhn, 1998). Therefore, this study investigated each aspect of gridshell design and then discussed the interconnection between these aspects to gain a comprehensive understanding of Indonesian bamboo utilisation in gridshell structures.

In the light of the findings from the literature review, this study was designed to assess the feasibility of utilising Indonesian bamboo for gridshell structures by investigating the three design parameters: material, structural morphology, and construction. The investigation delved into these three parameters to obtain the critical factors regarding bamboo utilisation for gridshell structures. Subsequently, the key findings from each parameter were applied and experimented with in the form-finding and optimisation process. The position and interconnection of each parameter are illustrated in Figure 3-1, which shows the conceptual framework and highlights the interdependence of these parameters. The research focused on these three design parameters along with form-finding and optimisation, leading to the formulation of four specific objectives, as described in Section 1.4.

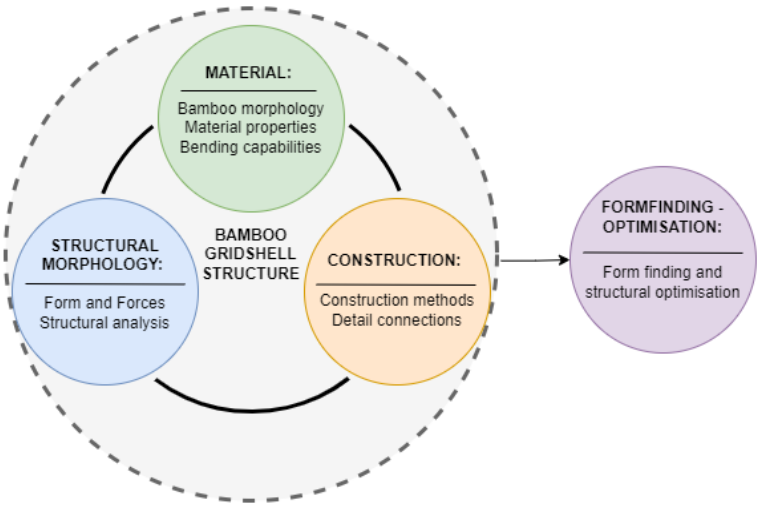


Figure 3-1. Schematic illustrating the conceptual framework, showing the interdependent and role of parameters.

The formulation of the four specific objectives into research framework is illustrated in Figure 3-2. Objective I, represented the material aspect, aimed to study the characteristics of Indonesian bamboo and determine its material properties. Therefore, the study was conducted through experimental research method. A series of material tests were carried out in compliance with ISO 22157:2019, which allowed for the gathering data on the physical and mechanical properties of bamboo. These tests produced a comprehensive set of data, which was subsequently analysed using statistical analysis to ensure a reliable interpretation. Meanwhile, the bamboo species selected for the experiments were chosen based on their diameter and widespread availability across Indonesia, ensuring that the findings would be applicable to a variety of regions. This approach aimed to reflect the diversity of bamboo resources within Indonesia and support future utilisation in construction projects.

Objective II was dedicated to discuss the structural morphology aspect of the structures where the form and forces were inseparable. Objective II focused on the investigation of the structural morphology by conducting a structural analysis of the gridshell models using finite element analysis (FEA). The results from FEA were compared with the outcomes of experimental tests performed on full-scale models, providing a basis for cross-validation. This comparison allowed for the identification of the discrepancies between computational simulation and full-scale model experimentation results.

Objective III was to review suitable construction methods to erect the structures. This part was conducted through experimental research methods by constructing two full-scale models. The models were erected to test the suitable methods and the impact of bamboo as the chosen building material for gridshell structures. The study involved evaluating the extent to which the material profile and depth of curvature influenced the erection methods, and vice versa. In this section, analysis and discussion were conducted through observations of the construction process.

Objective IV focused on the form finding and optimisation of bamboo gridshell structures by considering the results from Objectives I to III. The form-finding process took into account the bending capability of bamboo, based on the data obtained from the material tests and construction process. The optimisation considered the data taken from the structural analysis and incorporated the material properties during the iterative optimisation process. Objective IV employed computational simulations to examine the form-finding, structural analysis, and optimisation, ultimately proposing and efficient design process for bamboo gridshell structures.

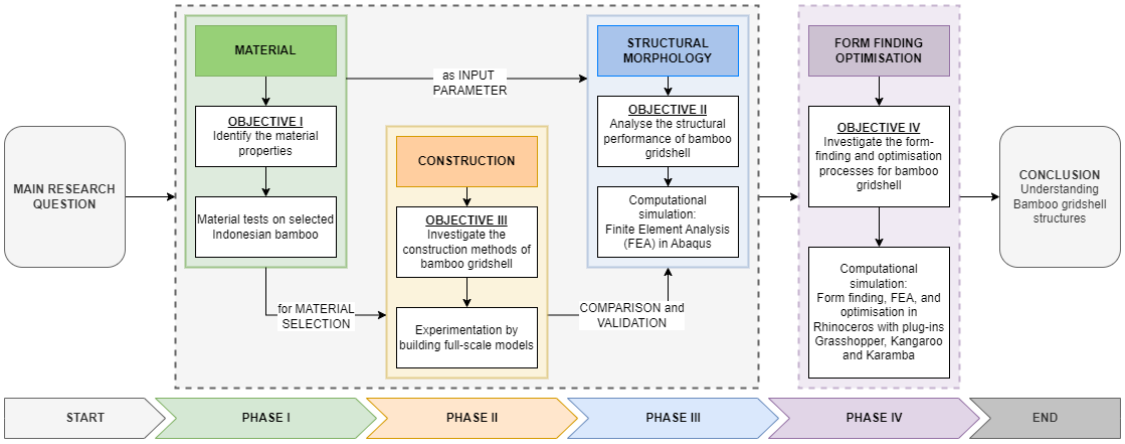


Figure 3-2. Research Framework

The workflow of the objectives was not necessarily in sequential order. The fundamental requirement was that objective I needed to be completed before performing the subsequent phases. The first phase was essential because, to perform structural analysis and conduct the construction, understanding of the characteristics of bamboo as the material and obtaining the material properties data are required. Meanwhile, to carry out the form-finding and optimisation, which reflects the design process of bamboo gridshell structures, findings from all three parameters were needed. Therefore, Objective I had to be completed first, and Objective IV could only be performed after the completion of Objective I to III.

Consequently, Objective II and III could be done simultaneously or in any order, with a condition both objectives were completed between the Objective I and IV. In this study, Objective III was commenced after the completion of Objective I, as the material testing and construction of full-scale models were conducted at Petra Christian University in Indonesia. Furthermore, given the COVID-19 pandemic, conducting Objective III immediately after Objective I in Indonesia minimised the need for international travel, which was complicated and uncertain due to the pandemic. Thus, the research workflow was executed as depicted in Figure 3-2.

3.2.2. Research Constraint and Limitation

This research focused on the assessment of Indonesian bamboo for gridshell structures; therefore, the material selection was limited to specific species of bamboo available in Indonesia. To ensure that the selected bamboo can represent all bamboo species available in Indonesia, the bamboo species were chosen based on their diameter and widespread availability across different regions in Indonesia.

The bamboo culms were purchased from local bamboo suppliers; thus, the availability and selection were following their existing control measures. The variability in material might affected the consistency of the results. Additionally, environment factors and different harvesting practices could influence the material properties, potentially limiting the generalisation of the findings. These constraints and limitations highlight the need for cautious interpretation of the results.

3.3. Summary

This chapter presents an overview of the research methods employed and the interrelationships between each objective in addressing the research questions. The methodology was developed based on insights gained from a literature review, which underlined the critical importance of material properties, structural morphology, and construction methods in the design of bamboo gridshell structures. Consequently, each objective was crafted to focus on a specific aspect, thereby enabling a more targeted investigation.

These objectives were interconnected, providing a holistic discussion that seeks to explain the feasibility of using Indonesian bamboo for gridshell structures and the design processes. Both experimental methods and computational simulations were employed to address the needs of each objective and to achieve the expected outcomes.

The focus of the research was limited to the bamboo species available in Indonesia. The selection of bamboo species was based on its availability across Indonesia. The variability of planting location, handling methods, and quality control become constraints and limitations that might influence the generalisation and interpretation of the results.

CHAPTER 4 | MATERIAL PROPERTIES OF INDONESIAN BAMBOO

4.1. Overview and Research Objectives

The literature review states that Indonesia has 175 species from 24 genera, and these genera are not evenly distributed across the country. *Bambusa, Gigantochloa,* and *Dendrocalamus* are common genera in the western part, whereas *Schizotachyum, Dinochloa, Nastus,* and *Racemobambos* are predominant in the eastern region (Ervianti, Widjaja, & Sedayu, 2018; Widjaja, 2000). Among these genera, *Bambusa*, *Dendrocalamus*, *Gigantochloa*, and *Schizotachyum* are found across all region (Damayanto & Fefirenta, 2021). Notably, species such as *Bambusa blumeana, Bambusa vulgaris, Dendrocalamus asper, Gigantochloa atter,* and *Schizotachyum brachycladum* are species that can be found almost in every part of Indonesia (Widjaja, 2000).

Bamboo is a functionally graded material with complex variations in the vascular bundles and fibres, leading to diverse material characteristics throughout the culm wall (Gangwar & Schillinger, 2019; Harries et al., 2017). Given the variability of these properties, this research necessitates the measurement of material properties to assess whether the bamboo species under study can withstand loads and is suitable for gridshell structures.

Studies on the material properties of Indonesian bamboo, as highlighted in the literature review, encompasses various species and mechanical properties, including compressive, tensile, and bending strengths. A study by Handana et al. (2020), investigating the compression and tension properties of bamboo from the species collected from three different regions in Indonesia, indicated variability in strength values. These findings suggest that environmental factors, such as soil conditions, precipitation, and fertilisation may influence the anatomical structure of bamboo, thereby impacting its strength and structural capacity.

Therefore, this chapter discusses the material properties of Indonesian bamboo that are needed for bamboo gridshell structures in this research. Objectives in this chapter are states as follows:

- To obtain data on the physical and mechanical properties of three Indonesia bamboo species.
- To examine the correlation between the material properties and the resulting bending capabilities of the bamboo species.

- To determine how these bending capabilities affect the bamboo utilisation in gridshell structures.

4.2. Research Method

The material tests were performed in Indonesia, utilising two laboratories owned by Petra Christian University: the Laboratory of Concrete and Building Materials and the Laboratory of Structures. The tests were conducted in accordance with ISO 22157:2019 "The Determination of the physical and mechanical properties of bamboo culms". The current standard testing methods for bamboo frequently adopt material testing approaches used for timber, such as ASTM D143, "Standard test methods for small clear specimens of timber", which can be served as a guideline for compressive, tensile, and shear tests. The use of ASTM standards is not specifically tailored to bamboo, the analytical approaches used for timber, given both are natural materials, can potentially be applied to bamboo. Furthermore, considering that bamboo is composite material, flexural tests such as ASTM D7264: "Standard test method for flexural properties of polymer matrix composite materials" can also be employed.

Among various standards, ISO 22157:2019 represents a standard that is specifically designed applicable to bamboo materials. Therefore, this study employed this standard test method to assess the material properties. The material properties investigated in this study included physical properties, such as density and moisture content, and mechanical properties parallel and perpendicular to the fibres. Mechanical properties parallel to the fibres included compression, tension, shear, and bending, while mechanical properties perpendicular to the fibres consisted of bending and tension.

4.2.1. Material Selection and Preparation

Material selection was based on the bamboo genera and species that can be found in all regions of Indonesia, the availability in the market, and the variability in dimension and wall thickness. Therefore, three Indonesian bamboo species were selected for this study, namely *Gigantochloa apus, Gigantochloa atter,* and *Dendrocalamus asper*. Although *G. apus* was not specifically mentioned as a species found in all regions, *Gigantochloa* was one of four genera noted as being evenly distributed across all regions. The selection of these three bamboo species represented the categorisation of small, medium, and large diameters. *Gigantochloa apus*, known by the local name as *bambu tali* or *apus*, has a smaller diameter, approximately 4-7 centimetres, and medium wall thickness. *Gigantochloa atter* has a medium diameter,

approximately 6-10 centimetres, and thin wall thickness. Meanwhile, *Dendrocalamus asper*, known as *bambu petung* or *betung*, has the largest diameter, approximately 10-15 centimetres, and a thick culm wall.

All three bamboo species have been commonly used for construction purposes in Indonesia. *G. apus* is known to be flexible, and local people use it for flag poles due to its flexibility. In buildings, *G. apus* can be used as poles for smaller structures and as long rafters. The utilisation of *G. atter* is relatively similar to that of *G. apus*, as this bamboo has similar features and can be used as poles and floors. Since *G. atter* has thin culm wall, it is mostly used as split bamboo for flat flooring or handicrafts. Meanwhile, *D. asper*, known as giant bamboo, has been extensively used for columns and beams in buildings. Its large diameter and thick wall made *D. asper* perfectly suited for axial compression columns. This bamboo is also known for its strength and high durability due to the thickness of its stem wall.

The bamboo culms used for the material tests were purchased from Sahabat Bambu, a local bamboo supplier. The bamboos were harvested from Magelang, a regency in Central Java surrounded by mountains, some of which are active volcanos, and forests. This location boasts fertile soil with high water content. The selected culms were chosen from three to four years old bamboo regarding the optimum age for harvesting. The culms were preserved by immersion in a boron solution for a minimum of two weeks to prevent fungus and termite attack. After preservation, the culms were air-dried for two weeks before being transported to the laboratory. Upon arrival at the laboratory, the culms were stored in a shaded area (Figure 4-1) and air-dried for a minimum of two weeks before being cut into specimens.



Figure 4-1. Bamboo poles for material tests

The specimens were collected from 20 bamboo poles of each species. The bamboo poles were approximately six metres in length, based on the specific length that could be provided by the seller[4]. As the bamboo poles were obtained from local suppliers, there was no information regarding the position of the poles within the whole plants. Following the tests method referenced in ISO 22157:2019, the poles were divided into three sections: upper, middle, and bottom, and cut into approximately two metres in length (Figure 4-2). Samples of each test were collected from these sections and cut according to the test standard procedures.

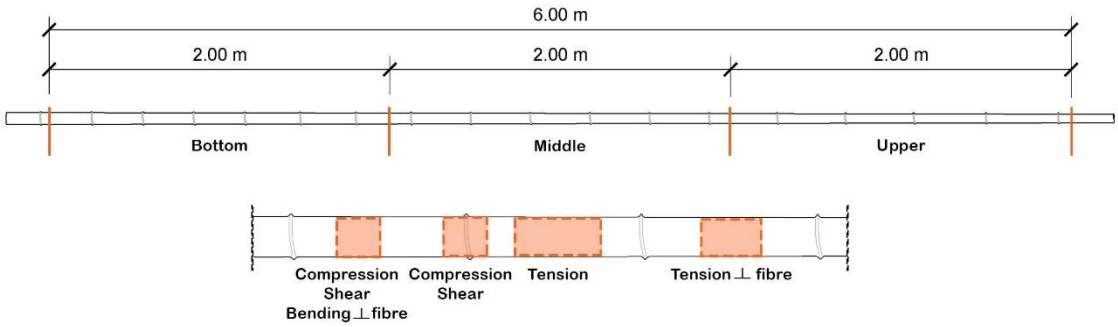


Figure 4-2. Full-culm bamboo showing the division of the culm into three parts: upper-middle-bottom, and the cutting position in node and internodes for each item test.

4.2.2. Compression Strength Parallel to the Fibre

Specimens for compression parallel to the fibre test were taken from the internode and node, taken from the bottom, middle and upper sections of the culm. Following the standard reference, the length of the specimen was lesser than the outer diameter. The specimens were measured using a digital calliper, taking measurements on the outer diameter (D_o), inner diameter (D_i), length (L), and wall thickness (δ). The measurements of diameter were taken as average from two measurement axes.

Compression tests for *G. apus* and *G. atter* were carried out using a JTM universal testing machine (UTM) with a load capacity of 30 Ton, while for *D. asper*, the compression tests were performed using a CONTROL compression machine with a capacity of 3,000 kN. The test for *D. asper* could not be performed using the same machine because its ultimate load exceeded 30T, which was beyond the capacity of the JTM machine. Load cell and linear variable differential transformer (LVDT) were installed in the machine to obtain force and

[4] The bamboo was transported using a truck which required the poles to be cut into six metres length to be fit with the container and meet the local transportation regulations.

displacement data (Figure 4-3). The speed on JTM machine was set to 0.01 mm/s, while in CONTROL machine, a load rate was used.



Figure 4-3. Set up of compression test

Compression strength (f_c) was calculated according to equation 4-1 and considering the section area as a hollow circular tube.

$$f_c = \frac{F_{ult}}{A} = \frac{4F_{ult}}{\pi({D_o}^2 - D_i^2)} \qquad 4\text{-}1$$

4.2.3. Tension Strength Parallel to the Fibre

Specimens for tension parallel to the fibre were prepared from internode part, cut from the bottom, middle, and upper sections of the culm. The specimens were cut radially from the culm; thus, the specimen width was the same as the wall thickness (δ). Specimen thickness (b) should equal one-half of the wall thickness or less but should not exceed 20 mm. "Tabs" made from softwood were added to the two ends of specimens to protect them from the machine's gripping mechanism (Figure 4-4). The test was conducted using JTM universal testing machine with a load capacity of 30 Ton with a speed of 0.01mm/s. The force was recorded from the machine, while an LVDT was used to record the displacement.

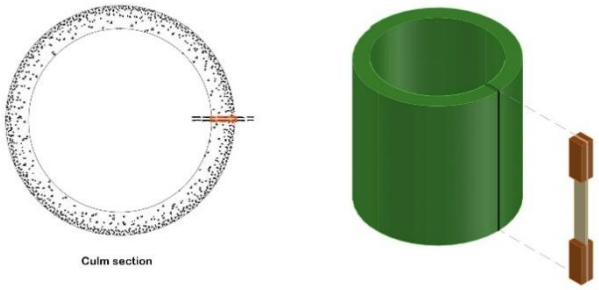


Figure 4-4. Specimen setting for tension parallel to the fibre.

Data taken for calculating the tension strength parallel to the fibre ($f_{t,0}$) was obtained using equation 4-2, where the strength was calculated by dividing ultimate force (F_{ult}) by the sectional area of the specimens. The sectional area was calculated from the specimen width, which is equal to wall thickness (δ) and the specimen thickness (b).

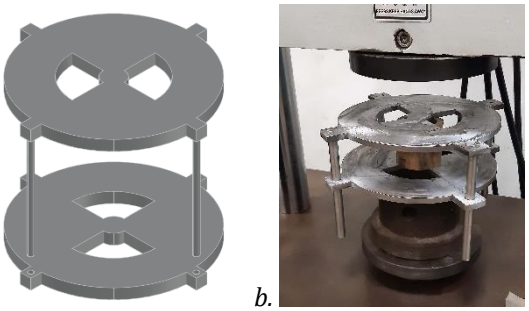
$$f_{t,0} = \frac{F_{ult}}{A_g} \qquad 4\text{-}2$$

Where:

$$A_g = \delta \times b \qquad 4\text{-}3$$

4.2.4. Shear Strength Parallel to the Fibre

Specimens were taken from internodes and nodes part of the culm. The specimens were cut under the condition where the length or specimens' height should be lesser than the outer diameter ($L<D$). Measurements were taken of the specimens' dimension, including outer diameter (D), inner diameter (D_i), and length (L). After the tests were performed, the wall thickness (δ) was measured at the four shear planes, and the failed locations were recorded. Specimens were measured using digital callipers with a precision of 0.01 mm. As shown in Figure 4-5a, pairs of shear plates were prepared with four interlocks to ensure the shear planes were align during the set up and the test. The test setup is depicted in Figure 4-5b. The test speed was set to 0.01 mm/s, and the force and displacement data were taken from the machine crosshead readings.



a. *b.*

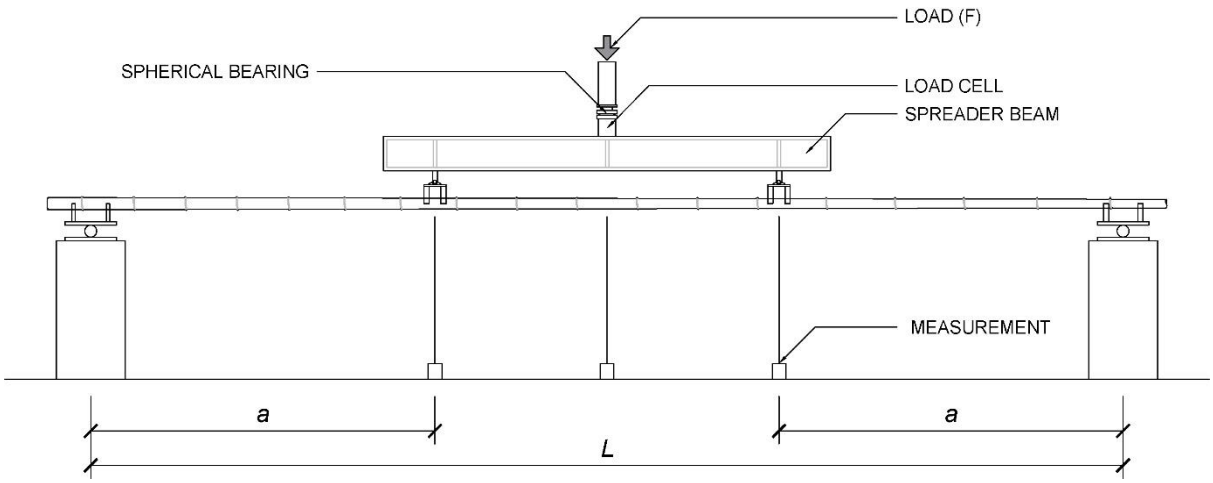
Figure 4-5. Shear test set up; a. Shear plate; b. Specimen and shear plates on the testing machine

The formula for calculating the shear strength parallel to the fibre (f_v) was according to equation 4-4, where the ultimate force was divided by the sum of shear planes, measured from the wall thickness (δ) and specimen length (L).

$$fv = \frac{Fult}{\sum(\delta \times L)} \qquad 4\text{-}4$$

4.2.5. Bending Strength and Stiffness Parallel to the Fibre

Bending parallel to the fibre test was conducted based on the four-point flexural test, as stated in the standard reference. A bamboo culm was positioned on two posts with a clear span, and a spreader beam was installed to distribute the point loads on the culm. The load was applied gradually using an Enerpac hydraulic jack, and a load cell was installed under the jack to record the force (F). A spherical bearing was placed between the hydraulic jack stroke and load cell to ensure the load was applied perpendicular to the beam. The span for *D.* asper was set differently from *G. apus* and *G. atter.* Initially, all bamboo was set to have the same condition with a span of 6.00 m. However, the trial test revealed that *G. apus* and *G. atter* experienced larger displacements more than 20 cm, while the hydraulic jack stroke length capacity was limited to a maximum of 20 cm. Therefore, the span for *G. apus* and *G. atter* was shortened to 3.60 m. Displacement (Δ) was measured using LVDT and laser meter at three locations: centre and under two points of the spreader beam. The test setup can be seen in Figure 4-6 and Figure 4-7.



	G. apus	G. atter	D. asper
L:	3.60 m	3.60 m	6.00 m
a:	1.20 m	1.20 m	2.00 m

Figure 4-6. Test setup for bending parallel to the fibre



Figure 4-7. Bending parallel to the fibre test

After the test, the bamboo poles were cut near the breaking point to accurately measure the diameter (D_o), inner diameter (D_i), and wall thickness (δ). Measurements were also taken at the two saddle points and the supports. Following these measurements, the small specimens were further cut, weighed, and placed in the oven for a minimum of 24 hours to determine the moisture content (MC) and density (ρ). The calculation for the bending moment (M_{ult}), bending strength parallel to the fibre ($f_{m,0}$), and tangent bending stiffness ($E_{m.}I_B$) were carried out according to equations 4-5, 4-6, and 4-8 respectively.

$$M_{ult} = \frac{F_{ult} \times a}{2} \quad 4\text{-}5$$

$$f_{m,0} = \frac{M_{ult} \times D}{2 \times I_B} \quad 4\text{-}6$$

$$I_B = \frac{\pi}{64} \times \left(D_0^4 - D_i^4\right) \quad 4\text{-}7$$

$$E_m = \frac{4(F_{60} - F_{20}) \cdot a(3L^2 - 4a^2)}{3\pi(\Delta_{60} - \Delta_{20}) \cdot [D^4 - (D - 2\delta)^4]} \quad 4\text{-}8$$

4.2.6. Tension Strength Perpendicular to the Fibre

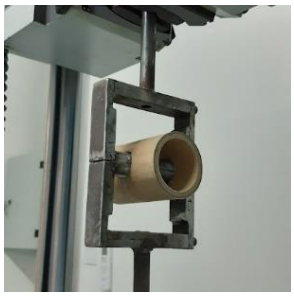
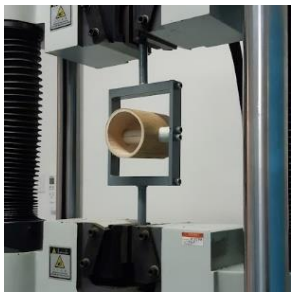
Specimens were taken from the internode part of 20 bamboo culms from each species. The specimens were prepared by drilling a hole through the culm in one pass. The hole diameter (d) for each bamboo was set to fall between *0.25D* and *0.50D*, as specified in

Table 4-1, which illustrate the test setup of tension strength perpendicular to the fibre. The length (L) was equal to the outer diameter (D_o) plus the hole diameter, calculated as $L = D_o + d$. A split-pin apparatus was prepared in accordance with ISO 22157:2019 and based on references (Sharma, Harries, & Ghavami, 2013; Mitch, 2009). The pin, with a diameter of at least *0.95d,* was inserted into the hole. Three split-pin apparatuses were prepared to accommodate the variations in the average diameter of each species. Specimens were positioned in the middle of the split-pin apparatus, with the axis position perpendicular to the machine's movement. The apparatus applied tension by pulling the specimens in opposite directions with a speed rate of 0.01 mm/s. The tests were performed using universal testing machine JTM with a capacity of 30 ton. Measurement taken before the tests included outer diameter (D_o), inner diameter (D_i), wall thickness (δ), and length (L). The force and displacement were recorded from the crosshead movement.

The tension strength perpendicular to the fibre ($f_{t,90}$) was calculated using the equation 4-9. Initially, 180 specimens were prepared from the three species. However, four specimens exhibited visible cracking prior to testing and were therefore excluded from the group.

$$f_{t,90} = \frac{F_{ult}}{2\delta(L - d)} \quad 4\text{-}9$$

Table 4-1. Test setup of tension strength perpendicular to the fibre

	G. apus	G. atter	D. asper
Test set up			
Hole diameter (d)	26 mm	30 mm	50 mm

4.2.7. Bending Strength Perpendicular to the Fibre

Specimens for bending perpendicular to the fibre test were taken from the internode part. Following the standard reference, specimens were cut with lengths less than the outer diameter, and the variation in diameter should not exceed 0.05 D from the specimen length. All specimens were marked and measured based on four quadrants: North-South (NS) and East-West (EW). The measurements consisted of lengths (L), outer diameter (D_o), inner diameter (D_i), and wall thickness (δ). D_o and D_i were taken as average diameters measured from the NS and EW axes. From these measurements, the radius of the centreline (R) was determined as $R = 0.5(D-\delta)$, and the radius of the inner surface (R_i) was calculated as $Ri = 0.5(D-2\delta)$. An estimation of neutral axis location (h) was estimated using equation 4-10.

$$h = R - \frac{\delta}{ln\left(\frac{2R+\delta}{2R-\delta}\right)} \qquad 4\text{-}10$$

During the test, specimens were loaded across the diameter with load points designated at N and S points. Two bearing strips were placed perpendicular to the machine head movement along the NS axis to ensure the specimen stayed in position and the load was spread evenly (Figure 4-8). The machine speed was set to 0.01 mm/s to meet the time requirement. However, specimens with thin walls need higher speed during the test than thick-wall specimens. Otherwise, the machine would fail to read the load and automatically stop after 20 seconds. Therefore, the test speed ranged from of 0.01 mm/s to 0.05 mm/s. Load (F_{ult}) and vertical displacement (Δ_v) were recorded from the machine crosshead.

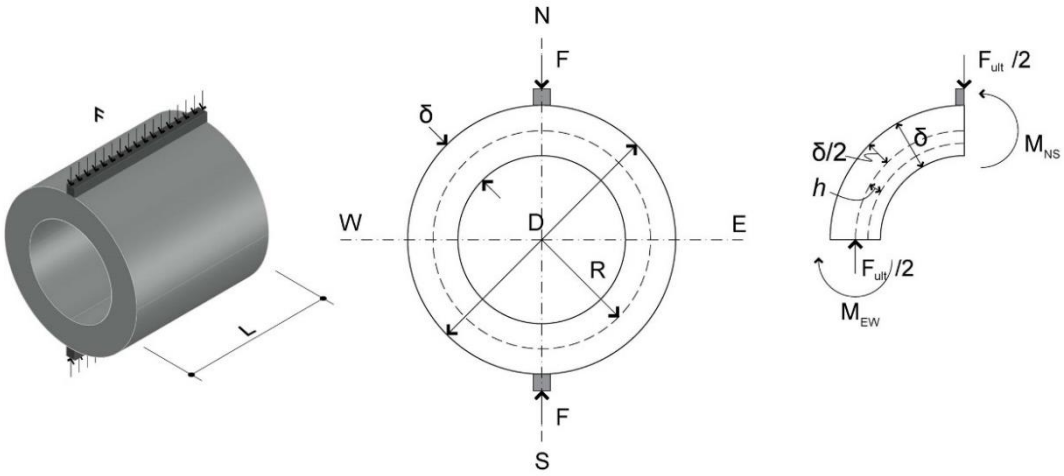


Figure 4-8. Bending perpendicular to the fibre test setup and the measurements.

Formula to calculate bending strength/modulus of rupture NS quadrant.

$$f_{m,90,NS} = \frac{MNS}{L\delta h}\frac{(R - Ri - h)}{Ri} \quad 4\text{-}11$$

Where,

$$M_{ult,NS} = \left(F_{ult} x \frac{R}{\pi}\right)\left[1 - \left(\frac{\delta^2}{12R^2}\right)\right] \quad 4\text{-}12$$

Formula to calculate bending strength/modulus of rupture EW quadrant.

$$f_{m,90,ew} = \frac{M_{EW}}{L\delta h}\frac{(R - R_i - h)}{R_i} \quad 4\text{-}13$$

Where,

$$M_{ult,EW} = -\left(F_{ult} \times \frac{R}{\pi}\right)\left[1 - \left(\frac{\delta^2}{12R^2}\right)\right] + \frac{F_{ult}R}{2} \quad 4\text{-}14$$

Calculation of circumferential modulus of elasticity:

$$E_{m,90} = \frac{3D^2(F_{60} - F_{20})}{2L\delta^2(\Delta_{60} - \Delta_{20})}\left(\frac{\pi k_1}{4} - \frac{2k_2^2}{\pi}\right) \quad 4\text{-}15$$

Where:

K1 = mode 1 critical stress intensity factor

$$k_1 \approx 1 + 7.6\frac{\delta^2}{D^2} \quad \text{4-16}$$

K2 = mode 2 critical stress intensity factor

$$k_2 = 1 - \frac{\delta^2}{3D^2} \quad \text{4-17}$$

4.2.8. Moisture Content

The determination of Moisture Content (MC) was conducted using the drying oven method. Specimens were weighed immediately after the test to obtain their initial mass (m_i). Subsequently, the specimens were placed in the drying oven at a temperature of 103±2°C for a minimal of 24 hours. After the specified duration, the specimens were weighed again to determine the oven-dry mass (m_0). The moisture content was calculated using equation 4-18.

$$MC = \left(\frac{m_i - m_0}{m_0}\right) \times 100 \quad \text{4-18}$$

4.2.9. Density

The data for the determination of fibre density was collected after the conducting the tests, with all specimens being measured and weighed. Measurements on the specimens' dimensions were taken to determine the specimen volume (V). Meanwhile, the specimens were weighed immediately after the tests to obtain the mass of the test piece (m_e). The data of the mass of the test piece and volume were used to determine the specimen's density during the time of test (ρ_{test}), in accordance with equation 4-19. Afterwards, the specimens were placed in a drying oven for a minimum of 24 hours at a temperature maintained between 103°C and 108°C. After the drying process, the specimens were weighed to determine the dry mass of the test piece (m_i). Utilising these measurements, the fibre basic density (ρ) was performed according to equation 4-21. Additionally, the density at 12% moisture content (ρ_{12}) was determined using equation 4-21.

$$\rho_{test} = \frac{m_i}{V} \quad \text{4-19}$$

$$\rho_{12} = \rho_{test}\left[\frac{1{,}12}{1+MC}\right] \quad 4\text{-}20$$

$$\rho = \frac{m_0}{V_0} \quad 4\text{-}21$$

4.3. Material Tests Results

4.3.1. Compression Strength Parallel to the Fibre

This section presents the results of the compression tests parallel to the fibre of three Indonesian bamboo species: *Gigantochloa apus, Gigantochloa atter, and Dendrocalamus asper*. The compression tests revealed several failure characteristics, mainly fibre buckling and splitting, as illustrated in Figure 4-9. In some specimens, the fibres inside the bamboo wall became densified and buckled in both the inner and outer walls (Figure 4-9a). Another common failure mode was buckling specifically in the inner walls (Figure 4-9b), where the inner wall fibres became densified and buckled inward. This inner wall buckling was observed in all specimens. Additionally, a combination of fibre buckling and splitting was found in some specimens, as shown in Figure 4-9a and Figure 4-9b. The observation during the compression tests revealed a distinct failure process in the bamboo specimens. When the compression load was applied, the bamboo wall initially densified. As the load increased, the wall began to buckle, and afterwards, the buckling led to the eventual splitting of bamboo fibres.

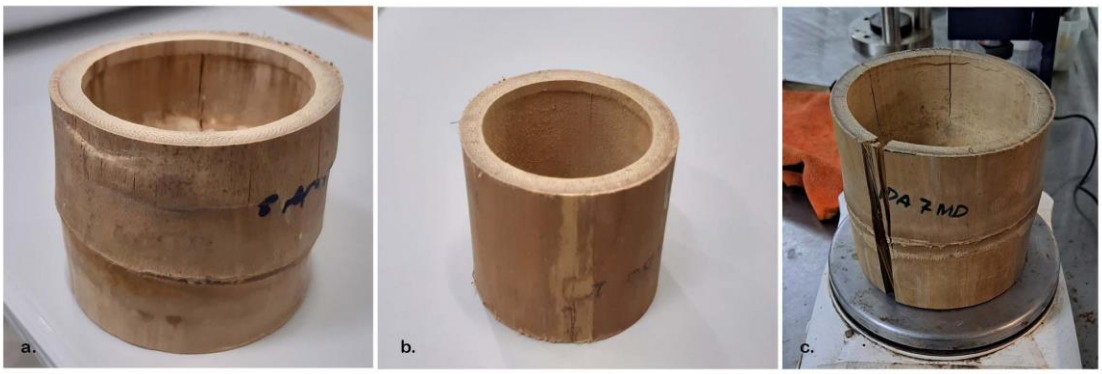


Figure 4-9. Failures in compression: a. Fibre buckling b. Fibre buckling in the inner wall c. Splitting.

A summary of compression strength parallel to the fibre is presented in Table 4-2. The data highlight the differences in the specimen dimensions and mechanical properties among the species. *Gigantochloa apus* exhibited an outer diameter (D_o) ranging from 49.70 mm to

77.25 mm, averaging 63.17 mm. The wall thickness (δ) varied from 4.25 mm to 14.35 mm, with an average of 8.16 mm. Its compression strength (f_c) averaged at 43.04 N/mm^2, with the highest coefficient of variation among the species at 20.13%, which indicates significant strength variability.

Specimens of *Gigantochloa atter* possess larger diameter than *G. apus*, ranging from 49.70 mm to 77.25 mm. The average diameter was 63.17 mm. Despite exhibit larger diameter, the wall thickness was similar to *G. apus*, between 5.48 mm to 14.19 mm, averaging 7.81 mm. Thus, *G. atter* possessed walls that were proportionally thin relative to its cross-sectional diameter. The compression strength of the G. atter ranged from 30.76 N/mm^2 to 69.44 N/mm^2, with the average of 48.24 N/mm^2.

As the largest species, *Dendrocalamus asper* had diameter ranging from 121.64 mm to 157.56 mm and wall thicknesses from 7.38 mm to 18.79 mm, with an average of 12.35 mm. *D. asper* exhibited highest compression strength, with an average value of 53.32 N/mm^2, ranging from 37.80 N/mm^2 to 67.52 N/mm^2. The ultimate force reached a maximum of 422.10 kN, with the lowest loading during the test recorded at 140.30 kN. The coefficient of variation was the lowest among the species, at 11.21%, indicating that the compression strength of *D. asper* varied the least. The results also demonstrated that *D. asper* performed best in withstanding compression.

Table 4-2. Summary of compression test results of three species.

Specimen		***n***	***D_o*** *(mm)*	***δ*** *(mm)*	***F_{ult}*** *(kN)*	***fc*** *(N/mm^2)*	***MC*** *(%)*	***ρ*** *(kg/m^3)*
G. apus	min	120	49.70	4.25	31.46	28.97	10.76%	462.61
	max		77.25	14.35	85.88	80.68	39.79%	897.64
	$\bar{x}$		63.17	8.16	57.92	43.04	20.08%	701.70
	Stdev		5.66	2.14	11.69	8.67	5.50%	108.38
	Cov (%)		8.96	26.28	20.18	20.13	27.39	15.44
G. atter	min	120	76.57	5.48	45.52	30.76	11.32%	421.00
	max		105.55	14.19	143.08	69.44	14.51%	896.60
	$\bar{x}$		89.94	7.81	95.44	48.24	13.47%	643.70
	Stdev		6.99	1.78	20.09	8.61	0.60%	105.79
	Cov (%)		7.77	22.74	21.05	17.84	4.45	16.43
D. asper	min	61	121.64	7.38	140.30	37.80	9.78%	480.34
	max		157.56	18.79	422.10	67.52	13.84%	878.24
	$\bar{x}$		141.32	12.35	266.93	53.32	12.05%	678.97
	Stdev		8.91	2.21	60.22	5.98	0.76%	79.19
	Cov (%)		6.30	17.87	22.56	11.21	6.31	11.66

The graph with error bars illustrating the average compression strength parallel to the fibre (Figure 4-10) indicates that *Gigantochloa apus* exhibited the highest standard deviation (StDev = 8.67). This suggesting significant variation in strength among the

specimens. The variability in strength was paralleled with the fluctuation in moisture content, which were more pronounced in *G. apus* than in other species. The disparities arose because the tests were not conducted simultaneously; there were intervals between the testing of each group, with *G. apus* being the first batch. The bamboo culms used for *G. apus* were delivered to the laboratory approximately two weeks prior to testing. As a result, some of these culms were not adequately dried and exhibited higher moisture content.

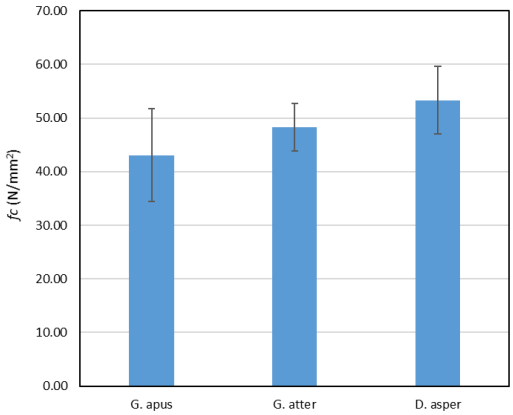


Figure 4-10. Average compression strength parallel to the fibre with error bars standard deviation.

Based on the position within the culms, *G. apus* and *G. atter* exhibited similar trend; their strength increased from the bottom towards the upper section. The compression strength of *G. apus* increased from 40.38 N/mm^2 at the bottom to 41.72 N/mm^2 in the middle, reaching 47.01 N/mm^2 at the upper section. Similarly, *G. atter*, the strength increased from 45.49 N/mm^2 at the bottom to 48.73 N/mm^2 in the middle and peaked at 50.49 N/mm^2 at the upper section. In contrast, *D. asper* showed different pattern; the compression strength varied less with position within the culm. The strength slightly increased from 53 N/mm^2 at the bottom to 53.82 N/mm^2 in the middle, but then slightly decreased to 53.16 N/mm^2 at the upper section.

Table 4-3. Summary of compression test based on the position within the culms.

Specimen		***n***	***D*** *(mm)*	***δ*** *(mm)*	***fc***		
					mean *(N/mm²)*	***Stdev***	***COV***
G. apus	Upper	40	58.68	6.38	47.01	10.35	22.03
	Middle	40	65.43	7.86	41.72	6.47	15.51
	Bottom	40	65.41	10.24	40.38	7.41	18.34
G. atter	Upper	40	87.34	6.67	50.49	8.47	16.78
	Middle	40	90.96	7.40	48.73	8.08	16.58
	Bottom	40	91.53	9.36	45.49	8.70	19.13
D. asper	Upper	21	135.81	10.90	53.16	5.74	10.80
	Middle	20	140.20	12.26	53.82	5.85	10.87
	Bottom	20	148.23	13.95	53.00	6.59	12.44

The influence of node and internode on compression strength is detailed in Table 4-4. Based on the test results of all specimens, internodes consistently exhibit higher compression strength compared to nodes. Specifically, in *G. apus*, compression strength at the node measured 42.46 N/mm^2, while at the internode it increased to 43.62 N/mm^2. Similarly, *G. atter* displayed a node compression strength of 47.46 N/mm^2, contrasting with 49.01 N/mm^2 at the internode. Likewise, in *D. asper*, compression strength at the node was 52.42 N/mm^2, whereas at the internode it rose to 54.25 N/mm^2.

These findings highlight the significant role of internodes in strengthening compression strength across all three bamboo species. Moreover, the phenomenon indicated that the structural composition and arrangement of fibres within internodes contribute substantially to the material capability in withstand compressive stress.

Table 4-4. Summary of the compression test results based on nodes and internodes.

Specimen		***n***	***D*** *(mm)*	***δ*** *(mm)*	***fc*** ***mean*** *(N/mm2)*	***Stdev***	***COV***
G. apus	Node	60	63.28	8.75	42.46	7.88	18.56
	Internode	60	63.06	7.58	43.62	9.42	21.58
G. atter	Node	60	89.98	8.05	47.46	7.78	16.40
	Internode	60	89.90	7.58	49.01	9.28	18.93
D. asper	Node	31	142.03	12.50	52.42	4.21	8.03
	Internode	30	140.59	12.19	54.25	7.33	13.52

The stress-strain curve for compression, presented in Figure 4-11, displayed characteristics typical of ductile materials. In the case of the tested bamboo specimens, the stress increased to a peak after the initial application of compressive load, indicating the maximum load the material could withstand. However, after reaching the peak, the stress decreased gradually. This behaviour showed the characteristic of ductile failure where the material continues to deform under constant or decreasing load. The gradual decrease suggests that the bamboo fibres were progressively buckling and failing. Interestingly, in some instances, the stress slightly increased again before ultimately failing. This behaviour was particularly evident in the graphs of specimens from the *D. asper* test group, specifically for the Upper 1 internode and Upper 13 internode in Figure 4-11. These specimens showed a noticeable rise in stress after initial decline post reaching the peak, indicating a secondary load-bearing capacity before complete failure. Such characteristics highlight the inherent variability and resilience of bamboo as natural composite material.

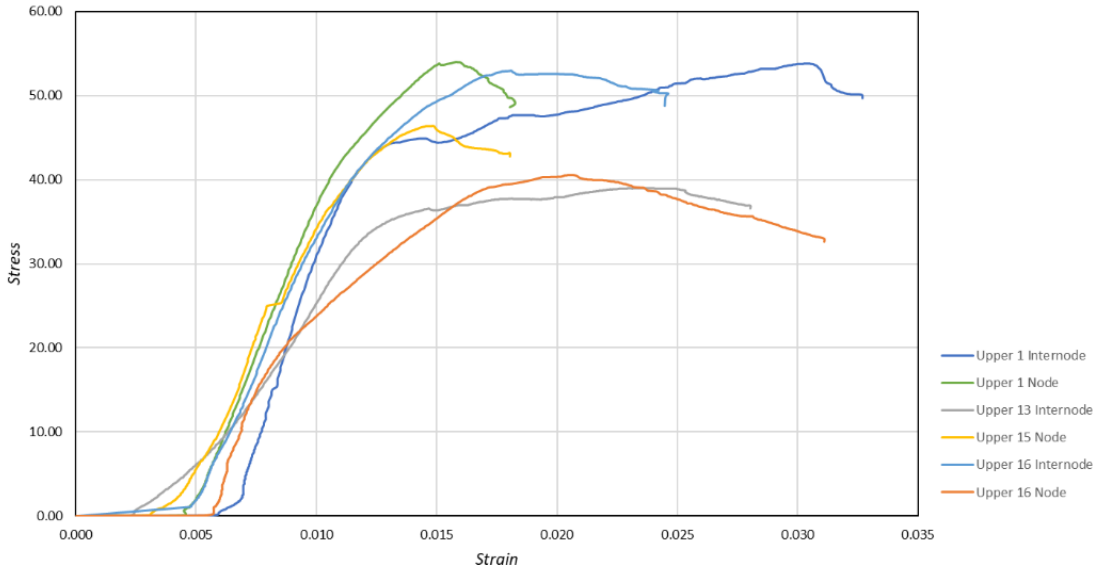


Figure 4-11. Examples of stress-strain curve taken from D. asper group specimens, upper sections.

Regression analysis was performed to determine the correlation between mechanical properties and physical properties. The analysis revealed that compression strength (f_c) and moisture content (*MC*) had a negative correlation (Figure 4-12), indicating that compression strength increased as moisture content decreased. The Pearson correlation coefficient for all species was above 0.30 ($r > 0.30$), with values of 0.40 for *G. apus*, 0.66 for *G. atter*, and 0.33 for *D. asper*. Therefore, *G. apus* and *D. asper* exhibited a moderate correlation, while *G. atter* showed a strong correlation. Additionally, compression strength was positively correlated with density (Figure 4-13). The *r-values* indicated moderate to strong correlations, with values of 0.46 for *G. apus*, 0.58 for *G. atter*, and 0.53 for *D. asper*.

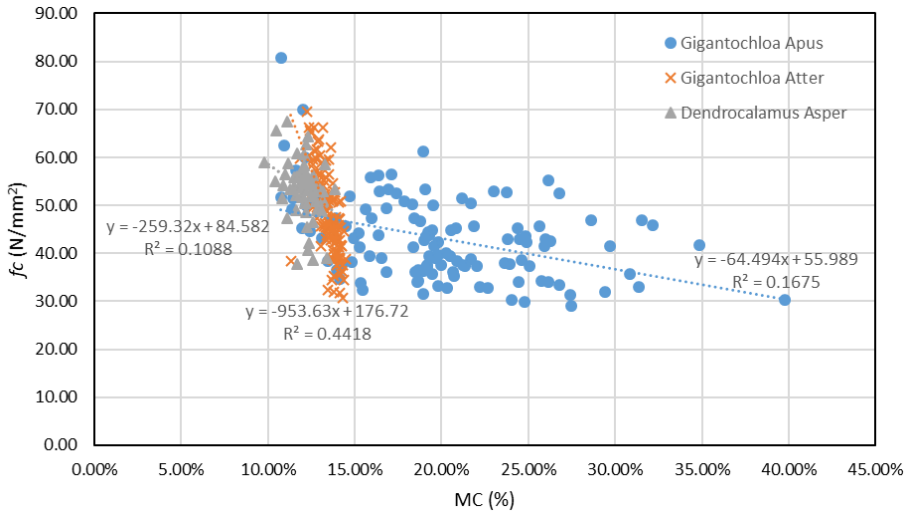


Figure 4-12. Correlation between MOR in compression parallel to the fibre and moisture content.

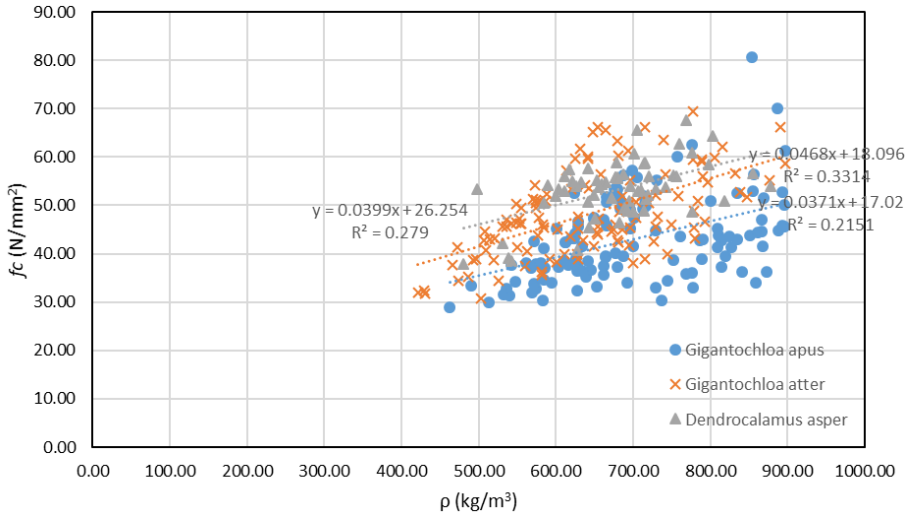


Figure 4-13. Correlation between MOR in compression parallel to the fibre and density.

The compression test results indicated that bamboo exhibited reasonable performance in resisting compressive stress, with *D. asper* showing the highest strength among the tested species. Under the compression stress, bamboo behaved as a ductile material, continuing to deform as the fibres gradually buckled and failed. In relation to its physical properties, compression strength was higher in the upper sections compared to the bottom sections. This variation was associated with the fibre density, which is greater in the upper sections of bamboo culms. Furthermore, bamboo demonstrated the increasing compression strength as the moisture content decreased.

4.3.2. Tension Strength Parallel to the Fibre

Conducting the tensile test on bamboo presented significant challenges due to issues with the machine grips. Given that the bamboo wall comprised parenchyma and fibre bundles, the specimens were relatively soft. Consequently, the machine grips frequently crushed the specimens, resulting in failure not due to tension but due to damage at the tabs. ISO 22157:2019 recommended the addition of 'tabs' made from softwood to protect the specimens from the grips; however, this measure did not entirely resolve the problems.

Prior to performing the tensile tests, several trial tests adhering to ISO 22157:2019 were conducted. The results, depicted in Figure 4-14, indicated that one specimen failed at the gauge length, two specimens failed at the tabs, and one specimen failed at both the gauge length and the tabs. The high incidence of specimens breaking outside the gauge length could have compromised the validity and accuracy of the data. Therefore, in an effort to determine the optimal design for the specimens, additional trial tests were conducted with

modifications to the specimen's shape. These trials aimed to identify and adjust the aspects that could be refined to achieve the best possible design for accurate tensile testing



Figure 4-14. Specimen after trial tension test, 2 specimens failed at tabs.

In the next trials, the specimens were shaped into a dog bone configuration to protect and expand the tabs. They were then divided into two groups: specimens with additional wood tabs and those without (see Figure 4-15a and Figure 4-15b). The tests were performed under the same conditions, including speed. Post-testing analysis revealed that the predominant mode of failure was shear rather than tension. In many cases, the fibres within the tension area, or gauge length, remained intact, while those at the tabs exhibited characteristic signs of shear failure, even with the additional wood tabs. This observation was consistent across both groups, as evidenced by Figure 4-15c to Figure 4-15e. Although some specimens failed in the tension area, the occurrence of shear failure was more evident.

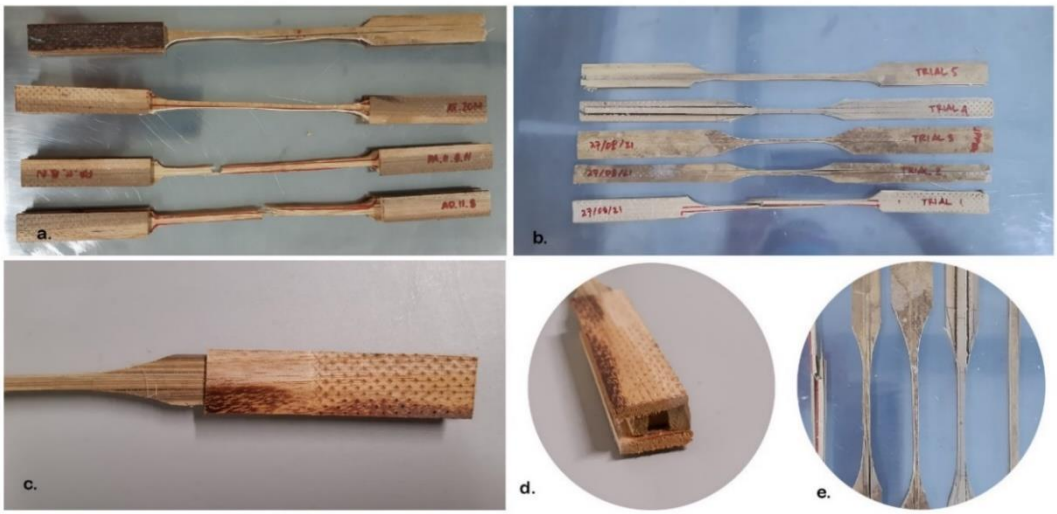


Figure 4-15. a. Trial specimens with wood tabs; b. Trial specimens without wood tabs after the test; c. failure due to shear; d. Detail of failure at tabs; e. Details of failure due to shear.

The second experiment involved the addition of wood tabs to the gripping machine. Specimens in this group did not exhibit shear failure; however, issues with the gripping mechanism and tabs were detected. The grips applied excessive force when pulling the specimen, resulting in crushing and damage (Figure 4-16a). Furthermore, the adjustment of grip force during specimen installation between grips should be conducted carefully. The grips tended to exert excessive force, causing compression, buckling, deformation, and damage to the specimen (Figure 4-16b).

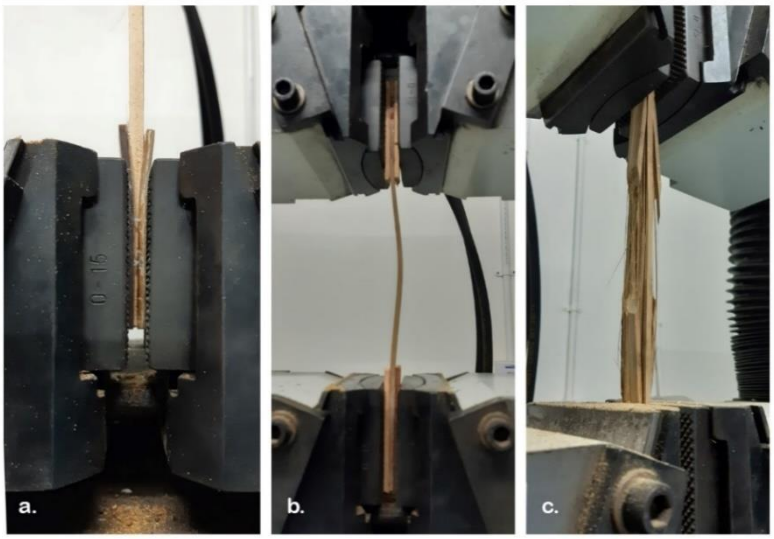


Figure 4-16. Problems due to gripping mechanism: a. Crushing at grips; b. Specimen buckled; c. Specimen with thick width.

After conducting trial tests and comparing the results, it was proven that shaping the specimens according to ISO standards was the optimal solution, as this shape minimised the possibility of shear failure. However, several adjustments were necessary. The ISO standard specifies that the thickness (b) should be less than half of the wall thickness (δ) and less than 20 mm ($b<(\delta/2)<20\ mm$). The trial tests, however, revealed that the width needed to be thin enough to avoid being crushed by the machine grips, as shown in Figure 4-16c. The specimen in the figure was from *D. asper*, which had a wall thickness of approximately 16 mm; thus, the specimen was cut with thickness of 8 mm, which complies with the ISO standard. However, during testing, the machine grips gradually increased the force, consequently crushing the specimen at the tabs before fibre at the gauge length break. Despite the addition of wood tabs, the relatively soft bamboo fibres could not withstand the force from the grips. After several trials, it was found that a safe thickness for the specimens was less than 4 mm.

Therefore, the specimen width for tension parallel to the fibre, as outlined by the ISO standard, might not be applicable for all machine grip mechanisms. A thinner width proved to provide optimal results for the test. The fibres at the gauge length would fail first before the machine's gripping mechanism could crush the specimen at the tabs. This adjustment allows the specimen to fail due to tension rather than experiencing failure at the tabs.

Another issue encountered while following the ISO standard was related to the quality and performance of the tabs, particularly the glue. Several trials failed due to problems with the glue. In the first trial, the wood tabs were glued using polyvinyl acetate adhesive and left for at least two days before testing, allowing sufficient time for the glue to dry. However, slips frequently occurred and were detected on the force-displacement curve. Further investigation revealed that the glue often came off and peeled from the specimens. Consequently, the second trial used epoxy glue, a combination of resin and hardener. This glue required a longer drying time but less effective result. Although the specimens were air-dried for more than three days, some still peeled off from the tabs during testing.

The third experiment used a combination of clear-casting resin and catalyst, which showed better performance. This adhesive required at least 24 hours to dry, but for optimal performance, the specimens were air-dried for at least two days. This approach significantly reduced the occurrence of tab failures, as resin effectively addressed the peeling issue. Moreover, the application of resin not only strengthened the tabs but also permitted the fibre to stretch at the gauge length.

The entire process with the trial tests revealed that performing tension tests based on ISO standards required several adjustments. While some issues may be attributed to the machine settings, the problems related to the specimen's width and tabs could occur in any setup. Therefore, learning from the trial tests performed, this study could suggest practical adjustments for the ISO standards.

Test results from a total of 60 specimens of *G. apus*, 51 specimens of *G. atter*, and 58 specimens of *D. asper*, illustrated in Figure 4-17 and detailed in Table 4-5, highlighted the remarkable tensile strength parallel to the fibre. Among the tested species, *G. apus* exhibited the highest average Modulus of Rupture (*MOR*) in tension, measuring 284.33 N/mm^2. In contrast, *G. atter* displayed an average MOR in tension of 263.24 N/mm^2, accompanied by a coefficient of variation of 21.45%, the most strength varied among the species studied. Conversely, *D. asper* demonstrated the lowest average MOR in tension, recorded at 232.81 N/mm^2, with a variation of 20.17%. Despite *G. apus* having the smallest diameter, it showcased the highest MOR in tension within the culm. These findings underscore the

impressive mechanical properties of bamboo, with G. apus showed highest tensile strength among other tested species.

Table 4-5. Summary of MOR tension parallel to the fibre of three bamboo species.

Specimen		***n***	***δ*** *(mm)*	***F_{ult}*** *(kN)*	***f_t*** *(N/mm²)*
G. apus		60			
	Min		4.70	3.10	176.38
	Max		11.90	9.89	367.44
	Mean		6.79	5.27	284.33
	Stdev		1.63	1.36	45.70
	COV		23.97	25.74	16.07
G. atter		51			
	Min		5.06	2.02	147.86
	Max		12.60	12.66	370.93
	Mean		7.41	5.26	263.24
	Stdev		1.86	2.56	56.46
	COV		25.12	48.79	21.45
D. asper		58			
	Min		8.60	6.01	127.51
	Max		19.36	17.94	349.61
	Mean		13.08	10.65	232.81
	Stdev		2.86	2.78	46.95
	COV		21.90	26.07	20.17

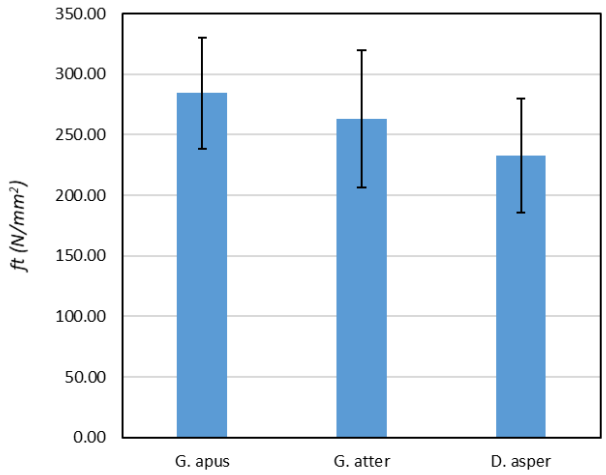


Figure 4-17. Graph summary of MOR in tension with error bars of standard deviation.

The summary of tension strength based on the position within the culm showed a consistent trend of increasing strength from the bottom to the upper sections across all three bamboo species. In *G. apus* test group, the MOR in tension rose from 255.69 N/mm² at the bottom to 307.67 N/mm² at the upper sections. Similarly, *G. atter* exhibited an increase from 242.52 N/mm² at the bottom to 279.67 N/mm² at the upper sections. Meanwhile, *D. asper* demonstrated an elevation from 218.80 N/mm² at the bottom to 240.35 N/mm² at the upper sections. The findings indicated that the tensile strength parallel to the fibre of

bamboo exhibited a consistent pattern of improved tensile strength towards the upper sections of the culms.

Table 4-6. Summary of MOR tension parallel to the fibre based on the position within the culms

					ft		
		n	***δ*** *(mm)*	***F_{ult}*** *(kN)*	***mean*** *(N/mm²)*	***stdev***	***cov*** *(%)*
G. apus	Upper	20	5.30	4.32	307.67	31.87	10.36
	Middle	20	6.66	4.96	289.61	48.24	16.66
	Bottom	20	8.42	6.52	255.69	40.95	16.02
G. atter	Upper	17	5.93	3.84	279.67	62.67	22.41
	Middle	18	7.17	4.54	267.05	44.87	16.80
	Bottom	16	9.17	7.16	242.52	58.66	24.19
D. asper	Upper	20	10.46	8.74	240.35	48.51	20.18
	Middle	19	12.67	10.79	238.89	47.68	19.96
	Bottom	19	16.24	12.52	218.80	43.75	19.99

The stress-strain curve depicted in Figure 4-18 suggests that bamboo exhibits brittle behaviour under tension stress, characterised by a rapid increase in stress followed by a sudden decline. This brittle behaviour is shown in the graph where the stress curve fails abruptly once its ultimate strength was surpassed. Further insight into the failure modes observed in the tests is provided in Figure 4-19, which illustrates the occurrence of splintering tension (a), delamination (b), and trimmed tension with delamination (c). It was observed during the tests that splintering and delamination phenomena occurred when the bonding between fibre bundles deteriorates, leading to fractures within the specimens.

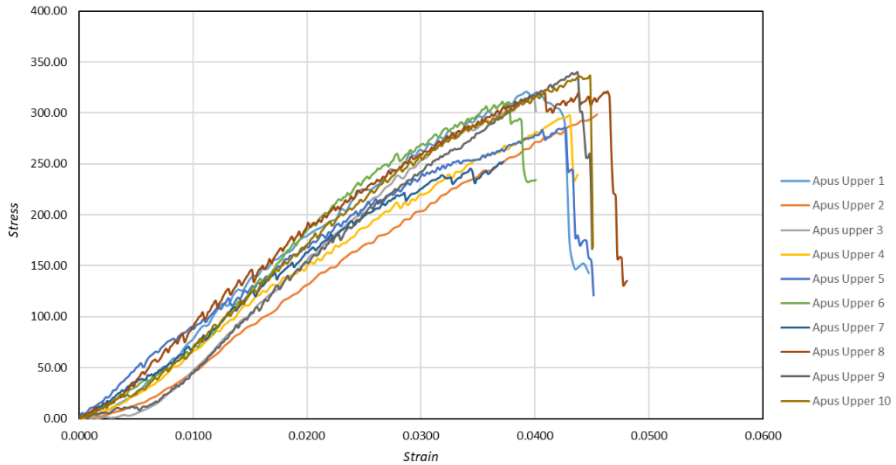


Figure 4-18. Stress-strain curve of tension test parallel to the fibre taken from Gigantochloa apus test group, upper part no. 1 to 10.

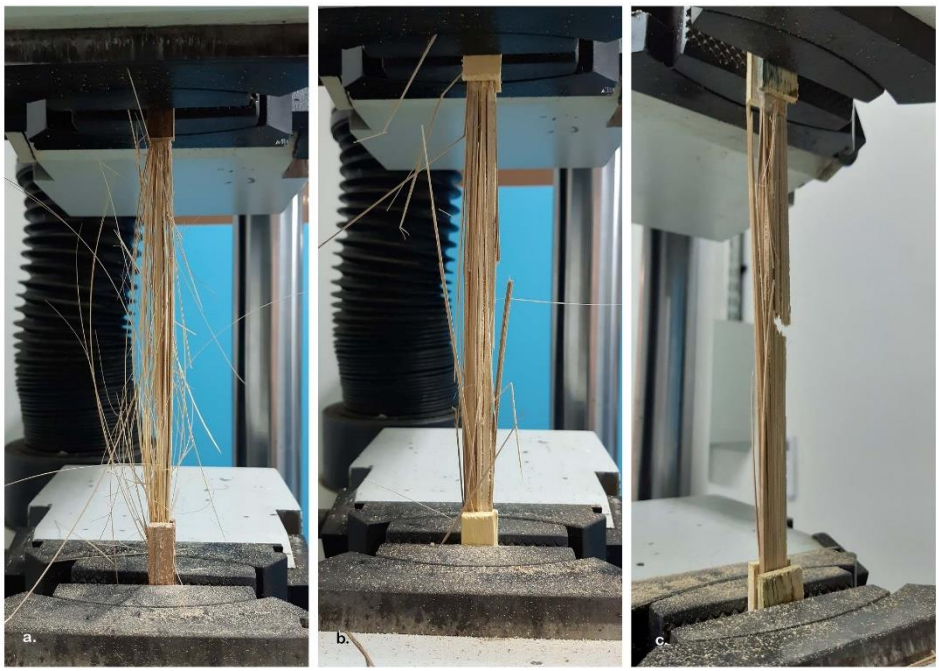


Figure 4-19. Failure mode in tension: a. splintering; b. Delamination; c. Trimmed tension and delamination.

The correlation between physical and mechanical properties in tension could not be established in this study due to limitations in the test material. When the tensile tests were performed, the specimens damaged and splintered, resulting in the loss of significant amounts of material. The fragmentation made it difficult to accurately measure and weight the remaining portion of the specimens. This situation preventing the determination of their density and moisture content. Consequently, the necessary data to analyse the relationship between the physical and mechanical properties was unavailable.

The findings from the tensile tests highlighted the excellent performance of bamboo in withstanding tensile stress. However, the tests also revealed the brittle nature of bamboo, with predominant failure modes including splintering, delamination, and trimming. This suggests that the fibre bonding in bamboo culms is weaker than their inherent strength.

4.3.3. Shear Strength Parallel to the Fibre

The specimens subjected to shear tests exhibited failure predominantly at the shear planes, as depicted in Figure 4-20. The majority of specimens experiencing failure in single shear plane, followed by instances of failure in two and three planes. Particularly, within the batch of G. apus specimens, one specimen simultaneously failed across four shear planes, and two specimens failed outside the four planes. The observed failures were attributed to cracking along the fibres, as illustrated in Figure 4-20d, indicating that the fibre's bonding was weak

in withstanding shear forces. Moreover, specimens taken from nodes also exhibited a similar failure mode, as depicted in Figure 4-20c, highlighting the consistent weakness of nodes in resisting shear forces.



Figure 4-20. Failures in shear parallel to the fibre test: a. failure at one shear plane, b. failure at two shear planes, c. failures in specimen with node and thick wall, d. characteristic of failure.

The observed failures also indicated that specimens with thick walls developed cracks outside the shear planes, as shown in Figure 4-21. Two specimens from the *G. apus* test group exhibited cracking outside the shear planes. Whereas specimens from other groups mostly failed at the designated shear planes. Conversely, specimens with medium and thin walls did not display this behaviour and all failures occurred in the shear planes.

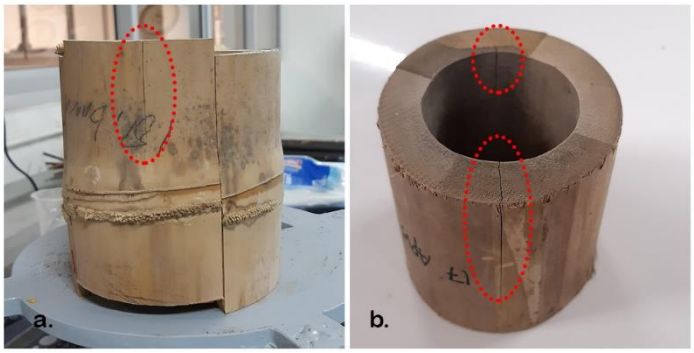


Figure 4-21. Cracking at specimens with thick walls.

The summary presented in Table 4-7 highlights the significantly low shear strength parallel to the fibre (f_v). The average MOR for G. apus was recorded at 10.46 N/mm^2, slightly higher than G. atter with an average of 10.63 N/mm^2, while D. asper exhibited the lowest strength, averaging at 9.95 N/mm^2. Figure 4-22 illustrates a summary of the average MOR in shear alongside the standard deviations. From the graph, G. apus displayed a higher standard deviation (*StDev*), which recording at 2.18 N/mm^2, and coefficient of variation (*COV*) of 21.23%. The results showed higher variability of strength properties, which indicated potential inconsistency. On the other hand, D. asper exhibited a lower standard

deviation at 2.11 N/mm² but the higher standard deviation of 21.23%. This suggested that despite possessing lowest average shear strength, its high variability in StDev and COV suggested less reliable performance, which might necessitate additional safety considerations on its utilisation in construction. G. atter demonstrated the lowest standard deviation at 1.99 N/mm² alongside a COV of 18.77%. Similar to the other two, G. atter also showed a tendency to be inconsistent.

Table 4-7. Summary of shear strength parallel to the fibre.

Specimens	***n***		***D*** *(mm)*	***δ*** *(mm)*	f_v *(N/mm²)*	***MC*** *(%)*	***ρ*** *(kg/m³)*
G. apus	*116*	Max	49.12	4.40	5.42	12.72%	474.26
		Min	74.00	13.44	17.52	22.21%	933.53
		$\bar{x}$	63.85	7.49	10.46	16.56%	687.48
		StDev	5.31	1.90	2.18	2.19%	114.13
		COV (%)	8.31	25.44	20.89	13.20	16.60
G. atter	*120*	Max	76.20	5.21	6.14	10.76%	423.40
		Min	107.50	12.11	16.08	14.44%	938.44
		$\bar{x}$	89.94	7.53	10.62	13.42%	651.44
		StDev	7.06	1.60	1.99	0.59%	116.05
		COV (%)	7.85	21.23	18.77	4.42	17.81
D. asper	*50*	Max	106.87	9.71	5.21	11.83%	481.63
		Min	141.82	22.92	14.15	13.97%	871.60
4		$\bar{x}$	125.71	14.06	9.95	13.05%	674.21
		StDev	7.61	2.82	2.11	0.50%	96.51
		COV (%)	6.06	20.08	21.23	3.86	14.31

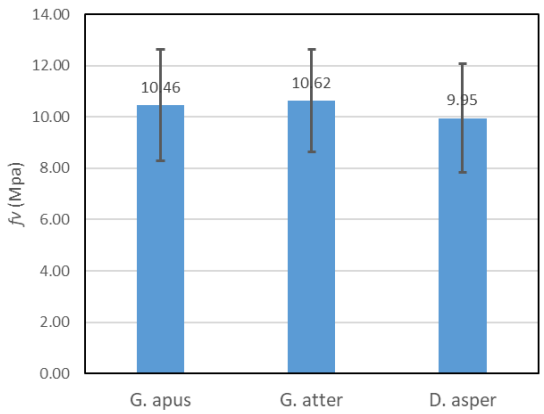


Figure 4-22. Average shear strength parallel to the fibre with error bars of standard deviation.

Regarding the position along the bamboo culms, all bamboo species showed a similar trend (Table 4-8). Shear strength tended to decrease from the upper to the bottom sections, indicating that position within the culm affects the strength of bamboo. G. apus exhibited the highest shear strength at the upper section with a MOR of 10.97 N/mm², which decreased to 9.75 N/mm² at the bottom section. Similarly, the shear strength of G. atter was 11.20 N/mm² at the upper section and decreased to 10.07 N/mm² at the bottom. D. asper showed the lowest average shear strength, with 10.37 N/mm²a at the upper and 9.59 N/mm² at the bottom section.

Table 4-8. Summary of shear strength based on the position within the culms.

Specimen		*n*	*D* (mm)	*δ* (mm)	*fv* (N/mm2)
G. apus **($\bar{x}$)**	Upper	38	59.48	5.78	10.97
	Middle	40	65.25	7.29	10.66
	Bottom	38	66.74	9.41	9.75
G. atter **($\bar{x}$)**	Upper	40	87.28	6.45	11.20
	Middle	40	91.00	7.21	10.60
	Bottom	40	91.54	8.93	10.07
D. asper **($\bar{x}$)**	Upper	17	120.08	11.39	10.37
	Middle	16	126.47	13.92	9.89
	Bottom	17	130.64	16.87	9.59

The tests were performed to specimens taken from nodes and internodes parts to investigate the effects of these features on the shear strength. The results, presented in Table 4-9, showed the average MOR, calculated from all nodes and internodes of the culms, disregarding their specific position within the culms. The nodes in *G. apus* exhibited a slightly lower MOR compared to the internodes, with an average MOR of 9.92 N/mm^2 at the nodes and 10.99 N/mm^2 at the internodes. Conversely, both *G. atter* and *D. asper* showed slightly higher MOR at the nodes than at the internodes. However, the differences in MOR between nodes and internodes for all species were insignificant. As shown in the average MOR presented in Table 4.9, the difference in shear strength between nodes and internodes was only 1.07 N/mm^2 for *G. apus*, 0.28 N/mm^2 for *G. atter*, and 0.09 N/mm^2 for *D. asper*. These results indicate that the presence of nodes and internodes has minimal significance in affecting the shear strength of bamboo culms.

Table 4-9. Summary of shear strength based on node and internode.

Specimen		***n***	***D*** (mm)	***δ*** (mm)	***fv*** $\bar{x}$ (N/mm^2)	*StDev*	*COV* (%)
G. apus	Internode	59	63.47	7.14	10.99	2.24	20.40
	Node	57	64.24	7.84	9.92	2.00	20.19
G. atter	Internode	60	90.01	7.24	10.48	2.02	19.32
	Node	60	89.88	7.82	10.77	1.97	18.29
D. asper	Internode	27	126.95	14.05	9.91	1.88	19.01
	Node	23	124.27	14.08	10.00	2.40	23.97

Examples of the force-displacement curves is shown in Figure 4-23. As can be seen from the graphs, the load increased gradually until reaching the peak or maximum load, at which point the specimens broke abruptly. This behaviour was similar to the tension tests, indicating the characteristic of brittle material. The phenomenon also suggested that bamboo culms could experience sudden failure under shear stress. The immediate collapse is critical considerations for structural applications, as suggests that bamboo may not

provide sufficient warning before failure, posing potential risks to the integrity and safety of structures using bamboo as a primary material.

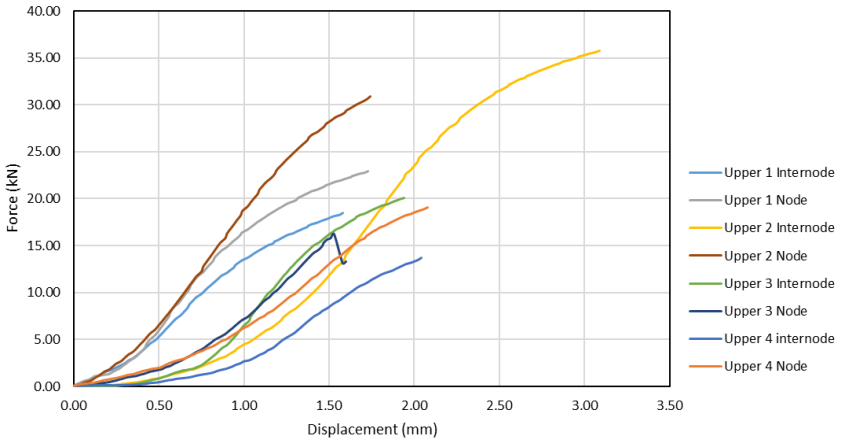


Figure 4-23. Example of force-displacement curve, taken from G. atter specimen no. 1 to 4.

The regression analysis was performed to investigate the correlation between the MOR in shear and density, as well as between MOR and moisture content (*MC*). The scatter plots for these analyses are presented in Figure 4-24 and Figure 4-25. The regression analysis between MOR and density across the selected species revealed a positive correlation; however, the analysis of R-square and p-value indicated that density is not always a strong predictor for the MOR. The analysis for *G. apus* showed an R-square of 0.0112, which is relatively low, and a p-value for the density variable of 0.25895, above the 0.05 threshold. These indicate that there is no statistically significant relationship between MOR and density for *G. apus*. Similarly, for *D. asper*, the R-square was 0.1498, and the p-value for the density variable was 0.05484, slightly above the threshold, suggesting that the relationship was less significant. However, *G. atter* showed different results, with an R-square of 0.2705 and a p-value for the density variable of 0.006259, indicating a relatively significant relationship between MOR and density.

The regression analysis on the correlation between MOR and MC also showed similar trends. For *G. apus*, the extremely low R-square value of 0.000138 indicates a very low correlation. Moreover, the p-value for the MC variable was 0.90391, which is far above the threshold. *D. asper* showed a similarly low R-square of 0.0577 and a p-value for the MC variable of 0.092792. Meanwhile, for *G. atter*, the R-square was 0.10804, indicating a relatively low correlation. However, the p-value for the MC variable was 0.000246989, which is far below the threshold, indicating a statistically significant relationship between MC and MOR. These analysis results indicate that MC is not a strong predictor of MOR for both *G.*

apus and *D. asper*. Conversely, *G. atter* showed a significant correlation, although the R-square value indicates that the correlation only explains a small portion of the variability.

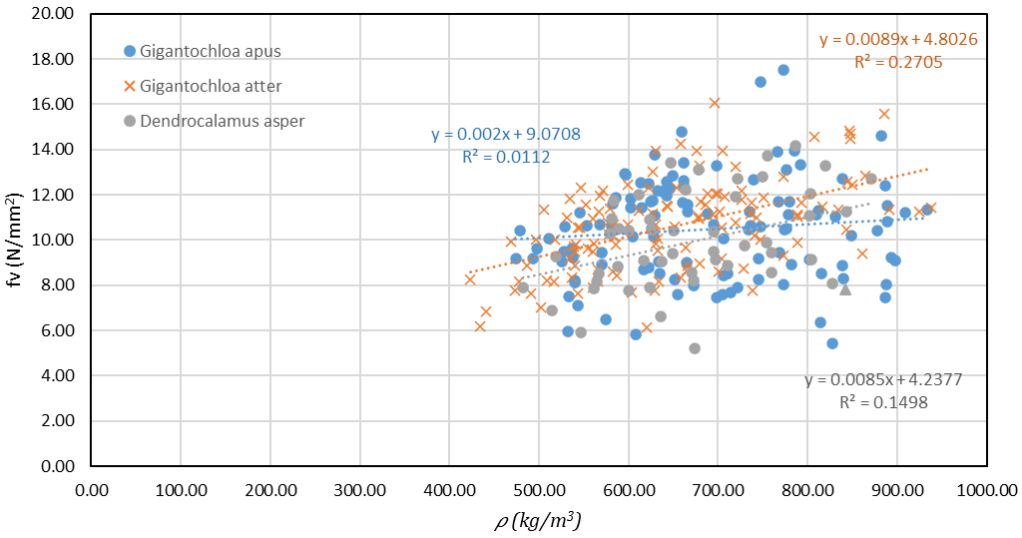


Figure 4-24. Correlation between MOR in shear parallel to the fibre and density

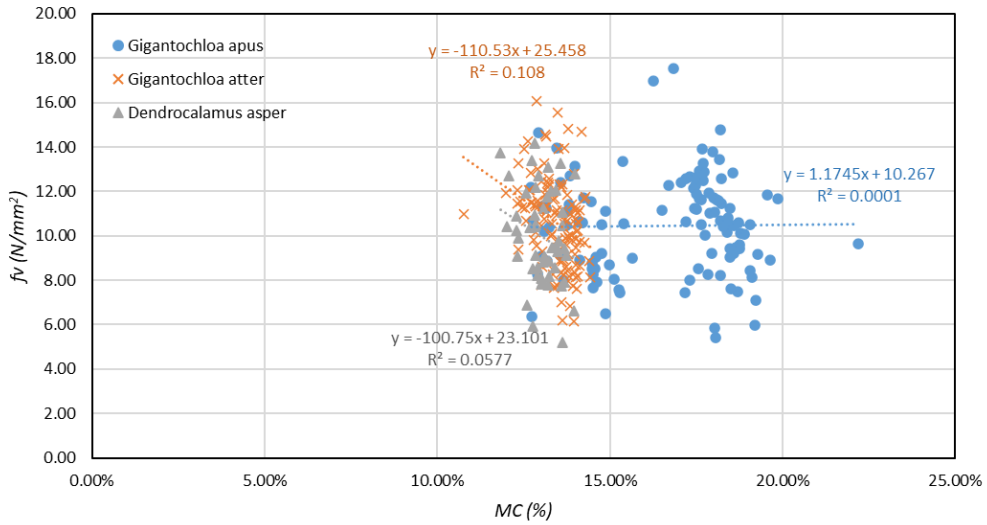


Figure 4-25. Correlation between MOR in shear parallel to the fibre and moisture content

The test results indicated that the overall shear strength parallel to the fibre of bamboo culms was moderately low across the three studied species. *G. atter* exhibited the highest MOR in shear, while *D. asper* had the lowest. Analysis based on the section within the culm showed that the upper sections had slightly higher MOR compared to the lower sections, although the difference was minimal. Additionally, the comparison between nodes and internodes revealed no significant difference in shear strength, suggesting that the presence of nodes and internodes did not notably affect the shear strength. Force and displacement curves indicated that in withstanding shear, bamboo behaves as a brittle material with failure typically occurring as sudden splitting. Regression analysis to examine the

correlation between physical and mechanical properties revealed inconsistent behaviour among the species. *G. apus* and *D. asper* showed insignificant correlations between MOR in shear and their physical properties, whereas *G. atter* demonstrated a statistically significant relationship.

4.3.4. Bending Strength and Stiffness Parallel to the Fibre

The summary of bending parallel to the fibre test results is presented in Table 4-10. *G. apus* exhibited the highest strength, with an average modulus of rupture (*MOR*) in bending (f_m) of 71.02 N/mm^2, a maximum of 100.80 N/mm^2, and a minimum of 47.04 N/mm^2. *G. atter* demonstrated a greater variation in the MOR compared to the other two species, with a minimum MOR of 42.69 N/mm^2, a maximum of 106.00 N/mm^2, and an average of 62.79 N/mm^2. *D. asper* had the lowest results, with an average MOR of 57.16 N/mm^2, a minimum of 42.75 N/mm^2, and a maximum of 78.02 N/mm^2.

The results indicated that, despite having the smallest outer dimensions among the studied species, *G. apus* demonstrated superior performance in resisting bending stress parallel to the fibres. Conversely, *D. asper*, with its larger outer diameter, exhibited the lowest strength in bending. These findings suggest that *G. apus* has greater potential for use in gridshell structures. *G. apus* can withstand higher bending stresses and support heavier loads compared to the other species studied. Such excellent performance characteristics are essential and well-suited for the requirements of gridshell structures.

Table 4-10. Summary of bending parallel to the fibre test results.

Specimen		***Δ*** *(mm)*	$f_{m,o}$ *N/mm²*	$E_{m,0}$ *N/mm²*	$E_m.I_B$ *Nmm²*	M_{ult} *Nmm*	***MC*** *(%)*	***ρ*** *(kg/m2)*
G. apus	Min	77.00	47.04	16,275.87	1.82E+10	1,360,200	11.46%	505.87
	Max	161.00	100.80	29,194.56	3.23E+10	2,520,000	13.76%	808.05
	$\bar{x}$	129.29	71.02	22,277.00	2.56E+10	2,085,428	12.24%	688.47
	Stdev	27.18	17.67	5,003.04	5.21E+09	433,480	0.93%	115.12
	COV (%)	21.03	24.88	22.46	20.34	20.79	7.62	16.72
G. atter	Min	67.00	42.69	17,892.05	2.99E+10	1,680,000	13.41%	549.84
	Max	237.00	106.00	31,244.71	5.58E+10	3,960,000	25.95%	824.49
	$\bar{x}$	117.25	62.79	21,886.66	4.04E+10	2,580,000	18.39%	706.68
	Stdev	52.33	21.45	4,634.34	9.92E+09	897,997	4.46%	88.26
	COV (%)	44.63	34.16	21.17	24.56	34.81	24.23	12.49
D. asper	Min	126.09	42.75	18,426.45	1.30E+11	4,800,000	25.48%	543.91
	Max	140.04	78.02	23,495.00	2.59E+11	12,000,000	38.22%	816.38
	$\bar{x}$	134.23	57.16	21,223.34	2.06E+11	8,300,000	32.49%	729.78
	Stdev	5.47	12.88	2,145.68	4.57E+10	2,579,147	4.86%	102.78
	COV (%)	4.08	22.53	10.11	22.17	31.07	14.97	12.49

The average MOR with error bars of standard deviation depicted in Figure 4-26 showed a high deviation of MOR within the species. G. apus had a coefficient of variation (COV) of 24.88% and a standard deviation (StDev) of 17.67, and G. atter had a COV of 34.16 and StDev

of 21.45, while D. asper had a COV of 22.53% and StDev of 12.88. These results implied a significant variability in the bending strength within each species. This variability could implicate bamboo utilisation for bending-active system such as gridshell structures. High variability of strength could lead to unpredictable behaviour under load, potentially compromising the structural integrity and reliability of the gridshell structures. Therefore, careful selection and testing of bamboo as gridshell members are crucial to ensure its performance.

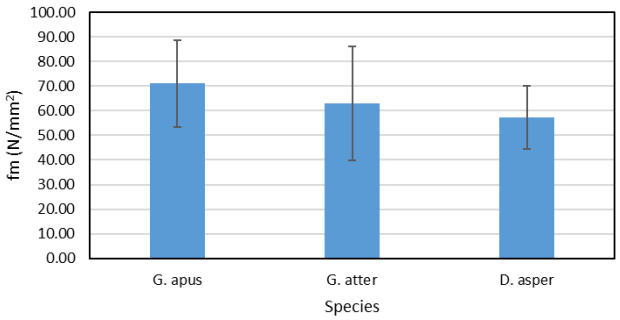


Figure 4-26. Average bending strength parallel to the fibre with error bars of standard deviation.

The plotted data of force and displacement, as illustrated in Figure 4-27 and extracted from measurements at the midpoint, revealed two distinct tendencies in bamboo behaviour under bending. Some specimens exhibited short plastic deformation before failure, indicating a combination of elastic and plastic behaviour in the bamboo culm. In such instances, as the load increases, the culm reaches its yield point, transitioning into plastic deformation, enabling the bamboo to undergo some degree of ductile behaviour before eventual failure. However, other specimens displayed characteristics of a brittle material, with a sudden drop in force without significant plastic deformation.

These observations implied the main issue of bamboo utilisation in general structures, which related to variability and uncertainty behaviour. Regarding the variability, in one batch of bamboo, some culms might inhibit a characteristic of short plastic deformation, while some other might be brittle. Meanwhile, brittle failure poses challenges for predicting failure and necessitates additional safety measures in structural design to mitigate the sudden failure. Regarding bamboo utilisation for gridshell structures, brittle modes can complicate the assembly and bending process in form-finding of gridshell structures. If the members were suddenly break, it would affect the whole assembled members and its structural integrity.

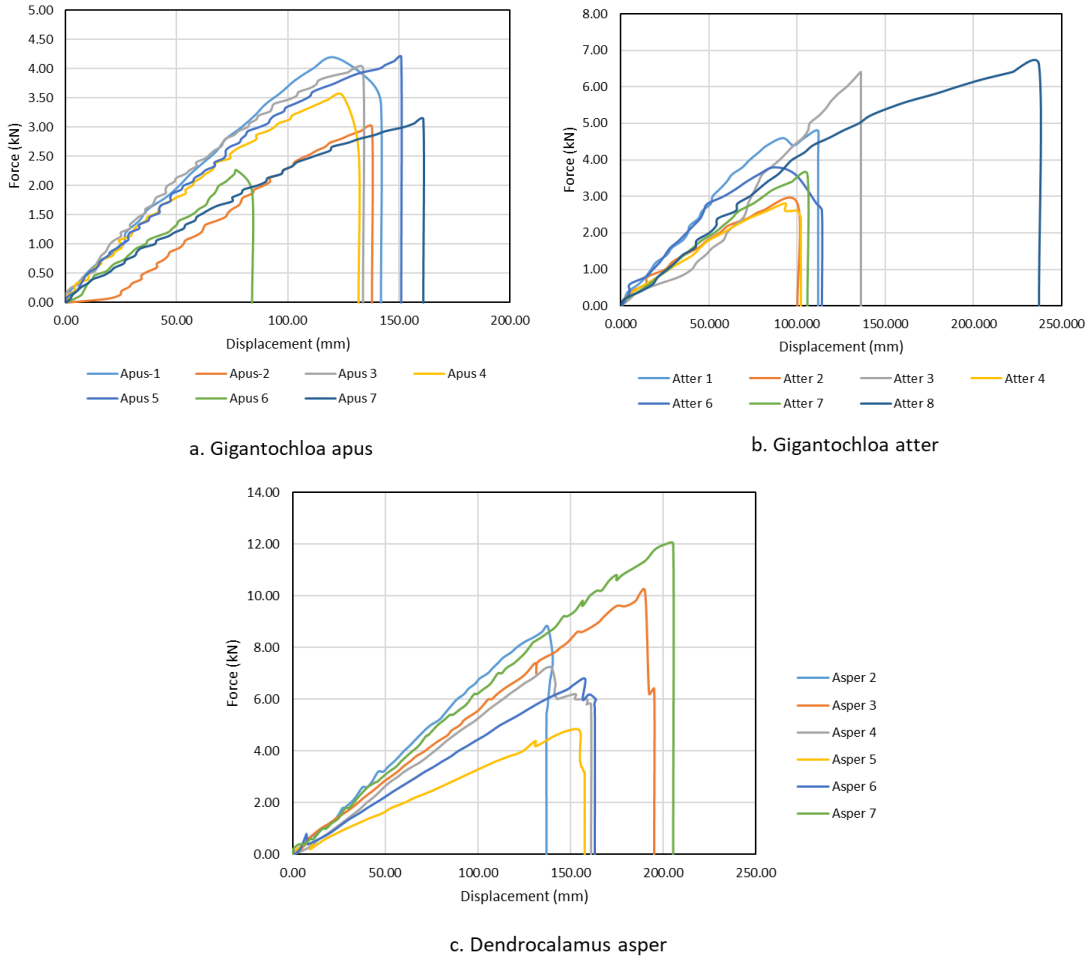


Figure 4-27. Curve force and displacement of bending parallel to the fibre tests.

The force-displacement curves not only revealed the mechanical behaviour under bending stress but also offered information on the displacement. Upon examining the displacement data, notable trends emerge: both *G. apus* and *G. atter* exhibited pronounced displacement, indicative of their ability to bend and deform significantly. This is reflected in the displacement values detailed in Table 4.10, which highlight the notably large and narrow displacement observed in *G. apus* and *G. atter* specimens, respectively. In contrast, *D. asper* specimens displayed relatively stable displacement characteristics. Understanding these displacement patterns is crucial, especially in the context of utilising bamboo for gridshell structures.

Observing Figure 4-27, it is clear that bamboo can bend significantly to a certain extent before breaking. Specimens from the test groups *G. apus* and *G. atter* were each cut to lengths of 3.60 metres, resulting in average displacements of 12.93 cm and 11.73 cm, respectively. Meanwhile, the D. asper specimens, which were 6 metres in length, could deform to an average of 13.42 cm. This data can be utilised to predict the radii of curvature of bamboo culms, a topic explored further in Section 4.4.2.

Although bamboo can bend significantly, it has limitations and will fail when reaching its allowable strength. Referring to Trujillo, Jangra, & Gibson (2017), the failures observed in bending parallel to the fibre tests in this study can be categorised as failure under the saddle, compression, culm collapse, and a combination of bending mechanisms. An example of failure during the bending tests is depicted in Figure 4-28 showing the bamboo culm species *Gigantochloa apus* collapsed after testing.



Figure 4-28. Failure in bending parallel to the fibre test bamboo species Gigantochloa apus.

Failure under the saddle, particularly near the upper section, was the most frequent failure observed in this study. This type of failure occurred due to stress concentration at the load application point, where the culms were crushed under the saddle, as depicted in Figure 4-29a. Failure in compression mode can be seen in Figure 4-29b, showing culm kinks and fibre crushing on the topside. Fibre kinking is visible in Figure 4-30 where the fibres twisted within the bamboo culm. Culm collapse failure mode is shown in Figure 4-29c, where the culm failed due to a loss of its transverse properties, causing splitting and buckling.

In addition to single-mode failures, several specimens exhibited failures resulting from a combination of bending mechanisms. For instance, specimen Asper-7 experienced failure due to a combination of shear and compression forces. The shear failure was characterised by long splitting in the shear area between fibres (Figure 4-29d). Simultaneously, the compression failure manifested as culm kinks in the compressed area and long splitting in the shear area along the bamboo culm. This specimen underwent a sudden collapse without experiencing a plastic deformation phase. This observation suggests the presence of complex stresses within the bamboo culm.



Figure 4-29. Failure modes recorded in tests: a. Failure at the saddle, b. Compression, c. Culm collapse, d. Combination of bending mechanism



Figure 4-30. Fibre kinks in compression failure mode.

Notably, compression was the predominant failure mode observed in *D. asper* specimens, as evidenced by the example depicted in Figure 4-29b. The occurrence of compression failure in *D. asper* might be attributed to the large diameter and thick wall which cause the culm kinks. Conversely, in *G. apus* specimens, culm collapse was the most common mode of failure, as illustrated in Figure 4-28and Figure 4-29b. This collapse phenomenon may be associated with the smaller diameter of *G. apus* culms, which are more susceptible to

buckling under bending loads. These differences in failure modes highlight the intricate interaction between morphology and mechanical behaviour of bamboo culm. Therefore, it could be a consideration for the process of selecting bamboo species in structural design and analysis.

Analysis on the correlation between physical properties and bending strength parallel to the fibre was performed to assess whether the moisture content and density statistically influenced the bending strength. However, given the limited sample size, the analysis posed challenges. The scatter plot (Figure 4-31) depicting the correlation between MOR and MC exhibited varying degrees of negative correlation across the studied bamboo species. *G. apus* and *D. asper*, with low R-square values of 0.0143 and 0.0604 respectively, indicated relatively weak negative correlations. Conversely, *G. atter* demonstrated a strong negative correlation with an R-square of 0.6508. Since all correlations showed negative values, this implies an inverse relationship between MOR and MC; where MC was high, MOR tended to be low.

Meanwhile, the correlation between MOR and density showed positive relationship, as depicted in Figure 4-32. *G. apus* showed the strongest relationship with R-square of 0,8703 indicating that density is a significant predictor of MOR in bending. *G. atter* also exhibited a positive correlation with slightly weaker R-square of 0.7155. *D. asper* showed a lower positive correlation with R-square of 0.248. These results suggested that MC and density may have a role in influencing the bending strength parallel to the fibre. However, considering the tests involved a small number of specimens, further investigation with a larger dataset is needed to provide more robust data.

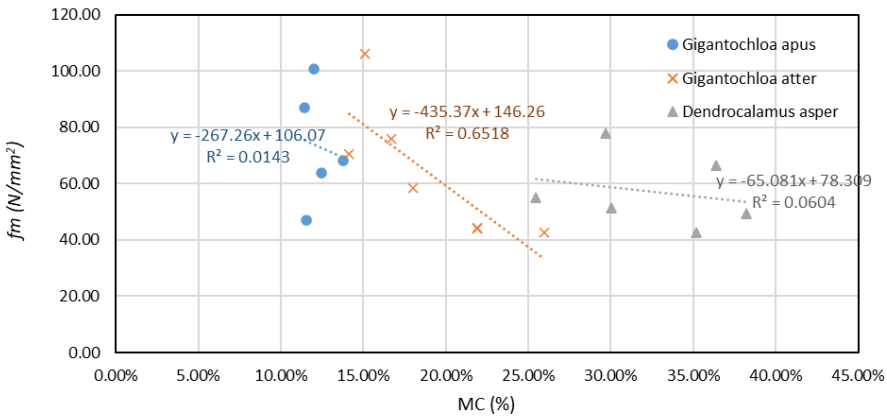


Figure 4-31. Correlation between MOR and Moisture Content in bending parallel to the fibre.

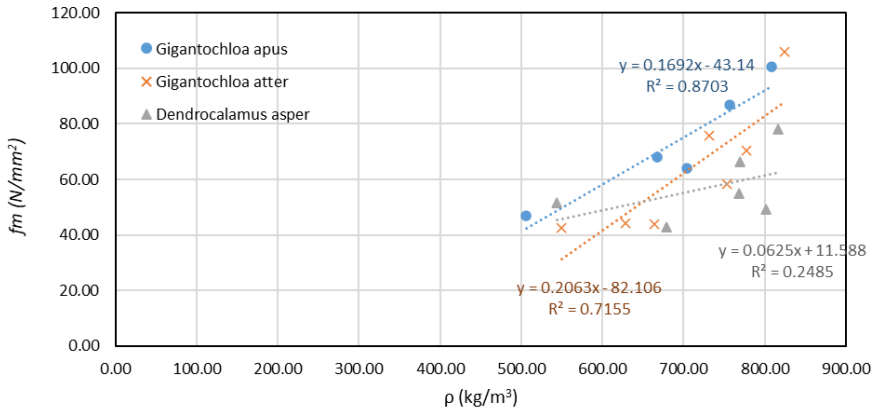


Figure 4-32. Correlation between MOR and density in bending parallel to the fibre.

The bending parallel to fibre test results demonstrated the excellent strength properties of bamboo in resisting bending stress. However, the force-displacement curves revealed variability in the behaviour of bamboo culms under bending. Some culms exhibited a short plastic deformation period, while others failed suddenly, behaving such as brittle material. This variability underscored the uncertainty in using bamboo for structural applications. The failure modes identified in this study indicated complex stress mechanisms during bending, involving compression, tension, shear, and stresses perpendicular to the fibre. Furthermore, bamboo morphology played a significant role in its ability to withstand bending stress. Regression analysis showed a negative correlation between MOR and MC, and a positive correlation between MOR and density. The results varied by species: *G. atter* showed that MC and density could be predictor for MOR, whereas *G. apus* and *D. asper* did not follow this pattern. These findings suggested that the correlation between these variables is species-dependent. However, due to the small number of specimens tested, further studies with larger sample sizes are necessary to validate these results.

4.3.5. Tension Strength Perpendicular to the Fibre

Conducting tension perpendicular to the fibre using split-pins was complicated and required an apparatus with precise dimensions and positioning. Additionally, the apparatus should be easy to disassemble and reassemble. Furthermore, the pin diameter should be proportional to the culms' diameter. Therefore, to accommodate the varying diameters of the bamboo culms, three split-pin apparatuses were prepared. Ensuring the specimens hanging on the pin were positioned perpendicular to the machine's movement was also challenging. The specimens' positions were carefully observed and measured before conducting the test. Another challenge was drilling the holes for the pin apparatus.

Following Mitch (2009) suggestion, the holes were drilled in one step using a hole saw, and the specimens were clamped on the drill table to ensure the hole's linearity.

Initially, a total of 180 specimens were prepared for the tests. However, after the inspection prior to the test, some specimens exhibited visible cracks or damage. Those specimens were omitted from the tests, resulting in fewer number of specimens. Ultimately, 179 specimens taken from the internode parts of the culms were tested. The observed failures after the split-pin test primarily involved fibre splitting, with examples of failures shown in Figure 4-33. Splitting occurred on one side or both sides, as shown in Figure 4-33c. Most failures resulted in symmetrical splitting, as shown in Figure 4-33b, although some specimens exhibited asymmetrical splitting, as illustrated in Figure 4-33c.

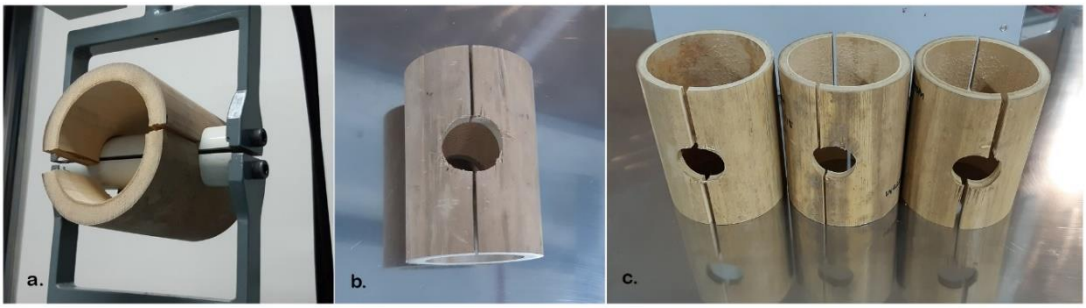


Figure 4-33. Failures after the test, a. example of failure, b. Failure in symmetrical form, c. Failures in asymmetrical form.

The test results presented in Table 4-11 revealed that the MOR for tension perpendicular to the fibre ($f_{t,90}$) was extremely low across all tested bamboo species. *G. apus* exhibited the highest result, with and average value of 2.04 N/mm^2, while *G. atter* showed slightly lower value of 1.64 N/mm^2. *D. asper* displayed the lowest MOR, with and average of 1.32 N/mm^2. These results indicate a consistent trend of decreased strength in tension perpendicular to the fibre among the studied species.

Compared to the study conducted by Mitch (2009), the test results in this study were higher. Mitch conducted the split-pin tests on *Bambusa stenostachya* and found the MOR to range between 1.004 and 1.161 N/mm^2. However, despite this study showed slight increase in strength, the overall performance of bamboo culms in resisting tensile stress perpendicular to the fibre remains poor. The exceptionally low MOR observed in tension perpendicular to the fibre highlights a potential significant weakness in bamboo' structural integrity. Bamboo components are critical when subjected to forces acting perpendicular to their fibre orientation.

Table 4-11. Summary of tension perpendicular to the fibre for each species.

Specimen	*n*	*D* (mm)	*δ* (mm)	*Fult* (kN)	*ft,90* (N/mm^2)
G.apus	58				
min		50.65	4.60	0.48	0.62
max		70.35	7.39	2.30	3.44
$\bar{x}$		62.73	5.82	1.50	2.05
SD		4.52	0.67	0.40	0.51
COV		7.20	11.59	26.69	25.05
G. atter	60				
min		74.75	5.25	0.68	0.79
max		104.14	13.57	5.48	2.32
$\bar{x}$		88.93	7.34	2.16	1.64
SD		7.14	1.79	0.87	0.40
COV		8.03	24.40	40.12	24.64
D. asper	61				
min		112.98	11.19	1.73	0.51
max		145.83	119.10	8.34	1.99
$\bar{x}$		127.42	42.42	4.37	1.32
SD		8.06	41.26	1.22	0.35
COV		6.32	97.27	28.03	26.08

A summary of the average tension strength perpendicular to the fibre, along with error bars depicting the standard deviation, is presented in Figure 4-34. The standard deviation values were 0.51 for *G. apus*, 0.40 for *G. atter*, and 0.35 for *D. asper*. Meanwhile, the variation in tension strength among specimens was considerable, with *G. apus* exhibiting a variation of 25.05%, *G. atter* 24.64%, and *D. asper* 26.08%. The standard deviation and coefficients of variation percentage highlight the significant variability in strength properties observed across the specimens. The high levels of variation may be attributed to inherent differences in bamboo culms, including variations in growth patterns, density, and structural composition.

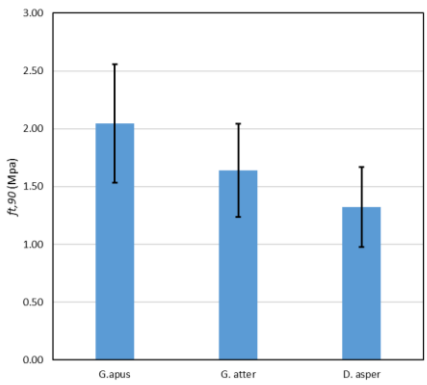


Figure 4-34. Average tension strength perpendicular to the fibre with error bars of standard deviation.

Further investigation into the distribution of strength within bamboo culms, as depicted in Table 4-12, presented the average MOR at the upper, middle, and bottom sections of bamboo culm. While differences between each section were less significant, noteworthy trends emerged within specific species. In both *G. apus* and *D. asper*, a subtle increase in

strength was observed from the bottom to the upper segment. On the other hand, *G. atter* exhibited a different pattern, with the highest strength recorded at the bottom section, while the middle and upper sections displayed similar strength levels.

Despite the variation among the species, no statistically significant differences were identified in strength distribution across the culm segments. However, the coefficient of variation of all species was ranged between 20.44% and 28.88%, indicating high variability within the data set.

Table 4-12. Summary of tension strength perpendicular to the fibre based on parts of the culms.

Specimens	***n***	***D (mm)***	***δ (mm)***	***F_{ult} (kN)***	***ft,90 (N/mm²)***		
					$\bar{x}$	***SD***	***COV***
G. apus ($\bar{x}$)							
Upper	19	60.93	5.40	2.05	2.05	0.54	26.46
Middle	20	64.43	6.21	1.63	2.04	0.50	24.31
Bottom	19	66.14	7.62	1.98	2.01	0.41	20.44
G. atter ($\bar{x}$)							
Upper	20	86.52	6.20	1.67	1.57	0.45	28.88
Middle	20	89.69	6.96	1.95	1.57	0.38	24.03
Bottom	20	90.59	8.87	2.85	1.78	0.36	20.16
D. asper ($\bar{x}$)							
Upper	20	123.88	100.69	4.03	1.41	0.33	23.40
Middle	21	127.23	12.80	4.18	1.30	0.37	28.60
Bottom	20	131.17	15.25	4.89	1.27	0.33	26.35

The force-displacement curve illustrated in Figure 4-35 exhibit behaviour similar to the behaviour observed in tension parallel to the fibre, which was the characteristic of brittle material. It can be seen in the graph that, during the tests, the force abruptly decreased upon reaching the ultimate value, followed by rapid damage and fracture of the specimens. This brittle behaviour highlights the structural vulnerability of bamboo when subjected to tensile forces, regardless the orientation. The sudden drop in force following peak load indicated a lack of ductility, emphasising that bamboo structures have a tendency of sudden failure under tension.

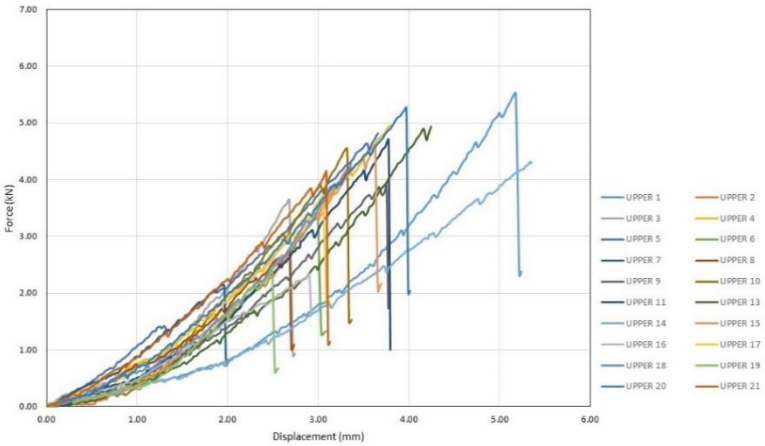


Figure 4-35. Example of force-displacement curvature taken from D. asper upper section test group.

Regression analysis was conducted to explore the relationship between modulus of rupture (*MOR*) in tension perpendicular to the fibre and moisture content (*MC*) and density (δ). The correlation between MOR and MC is illustrated in Figure 4-36, revealed a significant negative correlation across all species, with p-values less than 0.05, where the p-values was 0.009 for *G. apus*, 0.008 for *G. atter*, and 0.0015 for *D. asper*. This negative correlation suggests that as moisture content decreases, the tension strength perpendicular to the fibre of the bamboo culms tends to increase. Conversely, the correlation between strength and density, illustrated in Figure 4.30, exhibited a positive trend. However, the p-values for all species were more than 0.05, where the p-value was 0.349 for *G. apus*, 0.139 for *G. atter*, and 0.235 for *D. asper*. These findings imply that there is no significant correlation between tension strength perpendicular to the fibre and fibre density. Despite the positive trend, the lack of statistical significance suggests that other factors may contribute to bamboo strength beyond density alone.

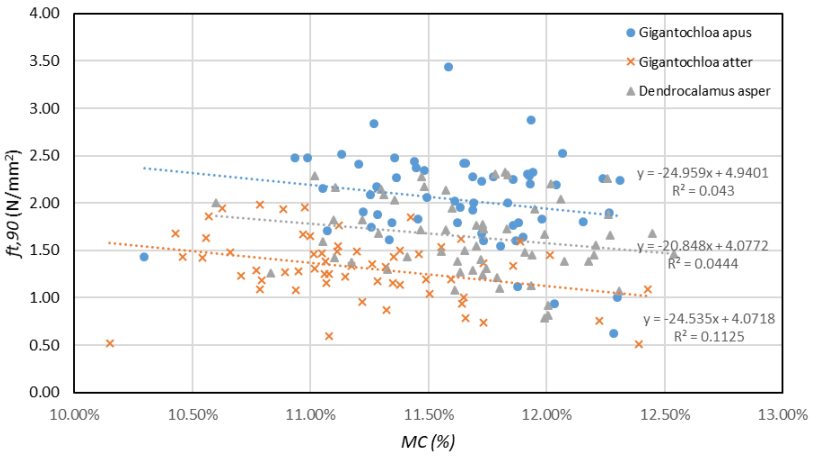


Figure 4-36. Correlation between MOR in tension perpendicular to the fibre and moisture content.

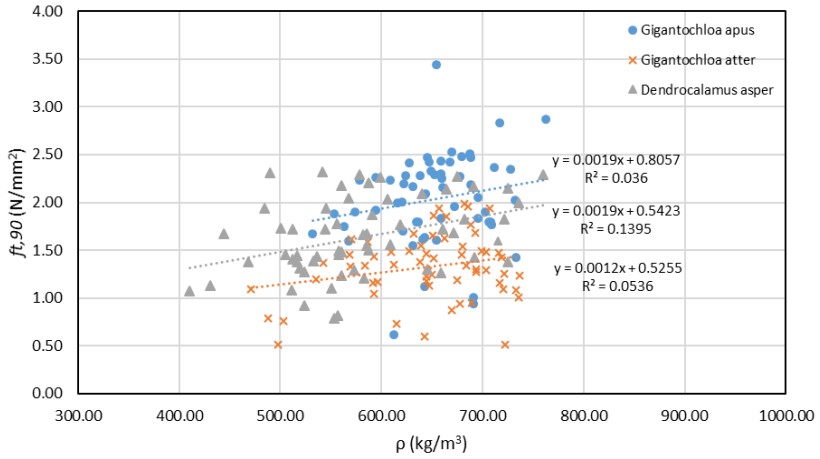


Figure 4-37. Correlation between MOR in tension perpendicular to the fibre and density.

In summary, the tests results showed the poor performance of bamboo culms in withstanding tension perpendicular to the fibre. The low MOR demonstrated extremely low values compared to other strength properties, including strength parallel to the fibre, such as compression, tension, shear, and bending. The tendency for sudden splitting highlights the critical vulnerability of bamboo culms when subjected to forces beyond their ultimate strength.

4.3.6. Bending and Stiffness Perpendicular to the Fibre

The bending perpendicular to the fibre test, also known as the edge bearing test, was particularly challenging to perform. The test revealed the softness of bamboo, which adversely affected the performance of the testing machine. Throughout the tests, there were some instances where the machine failed to register the force while the specimens were already compressed. Conversely, increasing the machine speed led to the rapid failure of the specimens. This issue was particularly prevalent when testing specimens with thin walls and larger diameters. *G. atter*, characterised by thin walls, exhibited a relatively large ratio between outer diameter and wall thickness. In contrast, all specimens from *D. asper*, which featured thicker walls, were successfully tested, producing obtainable data

The characteristic of failure in bending perpendicular to the fibre tests was splitting, which occurred mainly in the NS and EW directions (Figure 4-38a). However, some specimens split not at the four quadrants but between two quadrants, as seen in Figure 4-38c, where the specimen failure location was between the East-West and South quadrants. Additionally, some specimens split at two quadrants, as observed in Figure 4-38b, where the specimen split occurred both at the west and east positions. Meanwhile, bamboo with a

larger diameter but thin wall was softer and did not easily break during compression. In Figure 4-38d., the specimen was significantly compressed into an oval shape before failing.

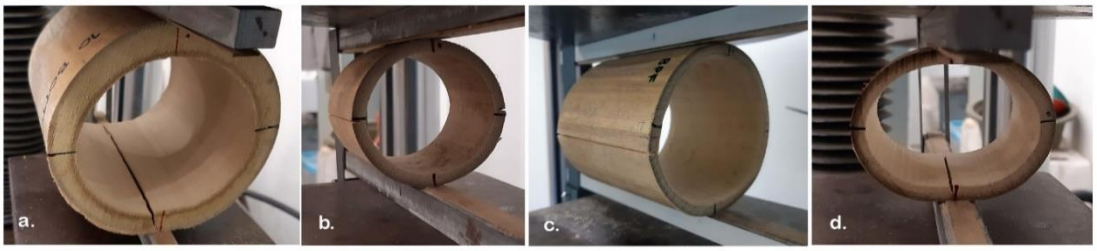


Figure 4-38. Splitting behaviour due to bending perpendicular to the fibre; a. One splitting (S); b. Two splittings (EW); c. Splitting location between E/W & S.

The average MOR in bending perpendicular to the fibre of all specimens is presented in Table 4-13. The test results indicated low MOR, signifying the low performance of transverse mechanical properties in bamboo culms (Table 4-13). Generally, MOR at the NS direction ($f_{m,90,NS}$) exhibited higher values compared to the EW direction ($f_{m,90,EW}$), a trend consistent with previous research by Sharma, Harries, & Ghavami (2013). Among the three species, *G. apus* demonstrated the highest MOR in the NS direction, with an average value of 16.13 N/mm^2, followed by *D. asper* with an average of 12.77 N/mm^2, and *G. atter* with an average of 12.59 N/mm^2. MOR in the EW direction was significantly lower, almost half of the MOR in the NS direction, where *G. apus* recorded 8.88 N/mm^2, G. atter recorded 6.97 N/mm^2, and D. asper recorded 7.03 N/mm^2.

Young's modulus in the transverse direction ($E_{m,90}$) was also notably low, with *D. asper* exhibiting the highest elastic modulus at an average of 1,375.62 N/mm^2, followed by *G. apus* at 1,303.22 N/mm^2 and *G. atter* with the lowest average of 1,088.99 N/mm^2. These results were consistent with the observed behaviour of specimens from the *G. atter* test group, which were softer and exhibited significant deformation under compression. However, *G. apus* displayed the highest variation, with a coefficient of variation (COV) of 35.26%, while D. asper exhibited the lowest variation at 23.37%.

Table 4-13. Summary of bending strength and stiffness perpendicular to the fibre as per species.

Specimen	n	D (mm)	δ (mm)	$M_{ult,NS}$ (Nmm)	$f_{m,90,NS}$ (N/mm²)	$M_{ult,EW}$ (Nmm)	$f_{m,90,EW}$ (N/mm²)	$E_{m,90}$ (N/mm²)
G. apus	59							
Min		48.73	4.48	3,183.46	7.29	1,833.73	3.97	496.65
Max		72.24	11.64	18,523.35	26.52	11,123.21	14.67	2,453.38
$\bar{x}$		**63.11**	**6.91**	**6,635.63**	**16.06**	**3,850.49**	**8.84**	**1,303.22**
SD		5.45	1.59	3,004.52	4.06	1,791.40	2.25	459.55
COV (%)		8.63	22.99	45.28	25.26	46.52	D, 25.47	35.26
G. atter	57							
Min		71.94	4.72	2,885.07	6.75	1,651.95	3.72	424.47
Max		105.23	12.53	21,244.26	18.84	12,234.43	10.45	1,990.13
$\bar{x}$		**89.58**	**7.52**	**8,861.61**	**12.59**	**5,098.09**	**6.97**	**1,088.99**
SD		7.01	1.58	3,722.86	2.95	2,155.82	1.64	331.16
COV (%)		7.83	21.01	42.01	23.43	42.29	23.53	30.41
D. asper	60							
Min		108.85	9.50	10,843.69	7.50	6,224.58	4.16	780.33
Max		144.50	21.31	91,304.25	18.73	53,851.52	10.32	2,011.25
$\bar{x}$		**127.24**	**13.89**	**43,373.00**	**12.77**	**25,135.13**	**7.03**	**1,375.62**
SD		8.52	2.88	17,224.54	2.67	10,130.00	1.48	321.54
COV (%)		6.70	20.74	39.71	20.88	40.30	21.09	23.37

The summary of average bending strength perpendicular to the fibre ($f_{m,90}$) in the NS and EW directions, including error bars representing the standard deviation, is presented in Figure 4-39. Bamboo *G. apus* exhibited the highest variation, with a coefficient of variation of 25.17%. In comparison, *D. asper* demonstrated the lowest variation, with a coefficient of variation of 20.91%. Thus, although *G. apus* had a higher MOR, the variation in strength among the specimens was the greatest.

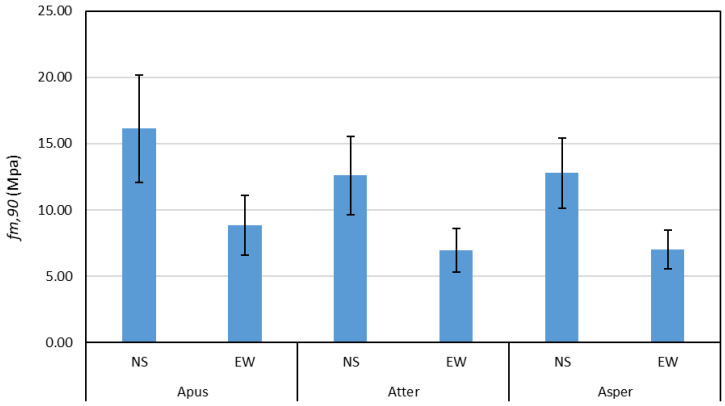


Figure 4-39. Average of Bending strength perpendicular to the fibre with error bars of standard deviation.

Previous findings by Sharma, Harries, & Ghavami (2013) identified differing trends regarding the relationship between wall thickness and bending perpendicular to the fibre test results. While their findings indicated that the MOR tended to increase align with wall thickness, their study on *B. stenostachya* did not corroborate this trend, suggesting different behaviours between thin-walled and thick-walled bamboo.

The tests conducted in this study, as presented in Table 4-14, showed a tendency for the MOR to increase from the bottom to the upper parts of the bamboo culms. Both *G. apus* and *D. asper* exhibited the lowest MOR at the bottom, with significant increases towards the upper sections. Specifically, the MOR for the bottom part of *G. apus* culms in the two directions were $f_{m,90,NS}$ = 14.75 N/mm^2 and $f_{m,90,EW}$ = 8.07 N/mm^2, while at the upper parts, the values increased to $f_{m,90,NS}$ = 18.70 N/mm^2 and $f_{m,90,EW}$ = 10.32 N/mm^2. For *D. asper*, the MOR at the bottom parts were $f_{m,90,NS}$ = 11.70 N/mm^2 and $f_{m,90,EW}$ = 6.41 N/mm^2, and at the upper parts were $f_{m,90,NS}$ = 14.01 N/mm^2 and $f_{m,90,EW}$ = 7.73 N/mm^2. Conversely, *G. atter* demonstrated a different tendency, with the MOR increasing from the bottom to the middle part, but slightly decreasing towards the upper part. Based on the findings, there was no clear and consistent correlation between wall thickness and the bending strength perpendicular to the fibre.

Table 4-14. Summary of bending strength and stiffness perpendicular to the fibre as per sections of bamboo culms.

Specimen	D (mm)	δ (mm)	Ro/δ	$Fult$ (N)	$M_{ult,NS}$ (Nmm)	$f_{m,90,NS}$ (N/mm^2)	$M_{ult,EW}$ (Nmm)	$f_{m,90,EW}$ (N/mm^2)	$E_{m,90}$ (N/mm^2)
***G. apus* ($\bar{x}$)**									
Upper	59.25	5.51	5.54	538.50	4,576.03	18.70	2,634.37	10.32	1,462.73
Middle	64.46	6.80	4.95	676.00	6,179.55	14.95	3,569.83	8.23	1,157.73
Bottom	65.54	8.38	4.16	1,039.50	9,172.38	14.75	5,358.41	8.07	1,297.17
***G. atter* ($\bar{x}$)**									
Upper	87.41	6.43	6.97	513.89	6,609.20	13.04	3,790.71	7.23	1,130.23
Middle	90.47	7.22	6.34	677.37	8,987.66	13.49	5,160.73	7.47	1,161.56
Bottom	90.68	8.80	5.34	830.50	10,769.05	11.33	6,215.22	6.25	982.94
***D. asper* ($\bar{x}$)**									
Upper	120.94	11.12	5.49	1,618.50	28,098.48	14.01	16,178.17	7.73	1,433.90
Middle	128.37	13.94	4.67	2,351.50	42,478.43	12.61	24,571.39	6.93	1,448.05
Bottom	132.40	16.63	4.06	3,277.00	59,542.08	11.71	34,655.82	6.41	1,244.89

The force-displacement curve in Figure 4-40 illustrates that bamboo culms exhibit a notable elastic characteristic when subjected to diametric compression. The material undergoes substantial deformation, with some specimens were capable of reaching displacement of over 5 mm before failing. However, despite the high deformability, the graph indicated the typical of brittle materials. This suggested that while bamboo could deform significantly under diametric compression, the bamboo culms breaking suddenly once the peak force is reached. This combination of high deformability and sudden failure highlights the complicated mechanical behaviour of bamboo.

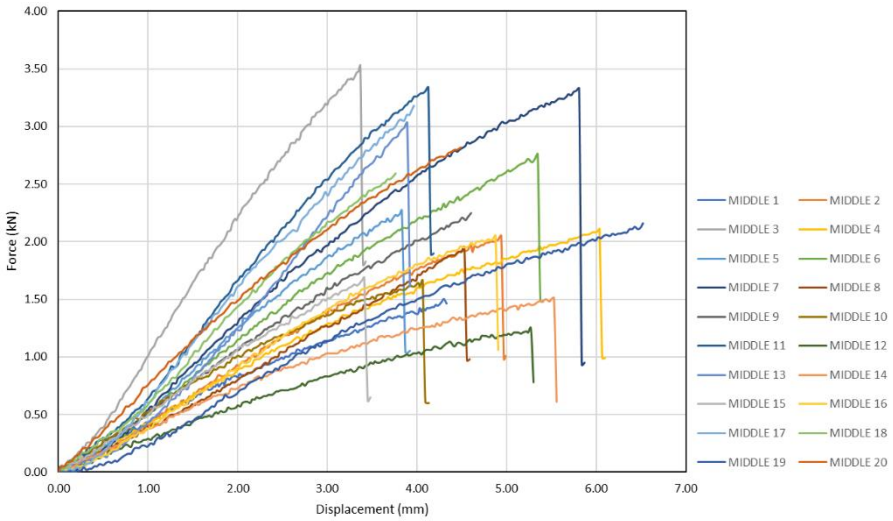


Figure 4-40. Example of force-displacement curve taken from D. asper middle part group test.

Regression analysis to examine the correlation between the MOR in bending perpendicular to the fibre and moisture content revealed a negative revealed a negative correlation, with all p-values <0.05 (Figure 4-41). This indicated a statistically significant relationship between strength and moisture content, despite the weak correlation as suggested by the R^2 values. Therefore, the regression analysis suggested that as the moisture content decreases, the bending strength perpendicular to the fibre increases.

On the other hand, the correlation analysis between the strength and fibre density showed positive correlation. However, the p-values varied across species: 0.0037 for *G. apus*, 0.834 for *G. atter*, and 0.111 for *D. asper*. These differences suggested that the correlation between bending strength perpendicular to the fibre was inconsistent across all species.

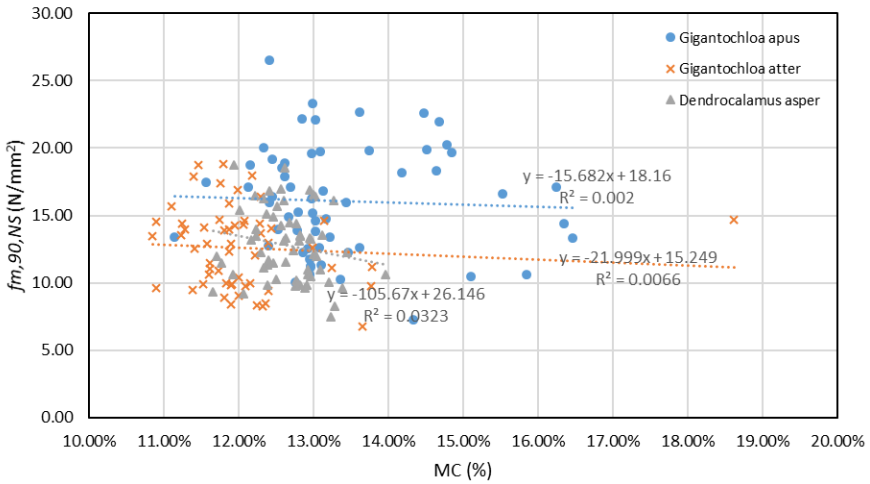


Figure 4-41. Correlation between MOR in bending perpendicular to the fibre and moisture content.

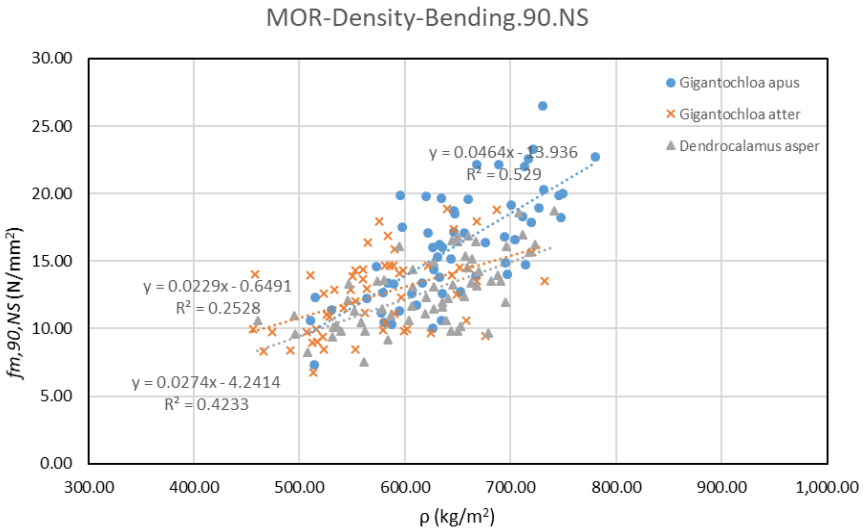


Figure 4-42. Correlation between MOR in bending perpendicular to the fibre and fibre density.

To summarise, the bending perpendicular to the fibre test revealed the inherent weakness of bamboo in withstanding stress perpendicular to the fibre. Among the three species tested, *G. apus* exhibited the highest strength, while *G. atter* had the lowest. For *G. apus* and *D. asper*, the strength increased progressively from the bottom to the upper sections of the culms. In contrast, *G. atter* showed a significant increase in strength from the bottom to the middle sections, but a slight decrease from the middle to the upper sections.

4.4. Discussion

4.4.1. Material properties of Indonesian bamboo

As discussed in the literature review, bamboo is an anisotropic material, which means bamboo has different properties in different directions within the culm. The results of the material tests using samples from 20 culms of three Indonesian bamboo species, summarised in Table 4-15, confirm the anisotropic nature of bamboo. The average Modulus of Rupture (MOR) of compression parallel to the fibre (f_C) ranged from 43.04 N/mm² to 53.32 N/mm², indicating that bamboo has adequate compression strength parallel to the fibre. Additionally, the average MOR in tension parallel to the fibre (f_t) was significantly high compared to other strength properties, ranging from 232.81 N/mm² to 284.33 N/mm². However, the MOR in shear parallel to the fibre (f_V) was relatively low, with values averaging between 9.95 N/mm² and 10.62 N/mm². The results show that bamboo has excellent strength parallel to the fibre, with the exception of shear strength.

Despite promising strength parallel to the fibre, bamboo exhibits significantly lower strength properties in transverse directions which indicates a key limitation. The results of

bending tests perpendicular to the fibre showed moderate strength with the average MOR in North-South direction ($f_{m,90,NS}$) in the range of 12.59 N/mm² to 16.06 N/mm², and in East-West direction ($f_{m,90,EW}$) even lower, between 6.97 N/mm² and 8.84 N/mm². Meanwhile, the tension tests perpendicular to the fibre ($f_{t,90}$) indicated extremely low resistance, with the average MOR ranging from 1.32 N/mm² to 2.05 N/mm².

Table 4-15. Summary of average MOR based on the position within the culm of the three Indonesian bamboo species.

Species	Position	Parallel to the fibre				Perpendicular to the fibre		
		f_c	f_t	fv	f_m	$f_{t,90}$	$f_{m,90,NS}$	$f_{m,90,EW}$
		N/mm²	N/mm²	N/mm²	N/mm²	N/mm²	N/mm²	N/mm²
G. apus ($\bar{x}$)	Upper	47.01	307.67	10.97		2.05	18.62	10.28
	Middle	41.72	289.61	10.66		2.04	14.95	8.23
	Bottom	40.38	255.69	9.75		2.01	14.75	8.07
	Means ($\bar{x}$)	**43.04**	**284.33**	**10.46**	**71.02**	**2.05**	**16.06**	**8.84**
G. atter ($\bar{x}$)	Upper	50.49	279.67	11.20		1.57	13.04	7.23
	Middle	48.73	267.05	10.60		1.57	13.49	7.47
	Bottom	45.49	242.52	10.07		1.78	11.33	6.25
	Means ($\bar{x}$)	**48.24**	**263.24**	**10.62**	**62.79**	**1.64**	**12.59**	**6.97**
D. asper ($\bar{x}$)	Upper	53.16	240.35	10.37		1.41	14.01	7.73
	Middle	53.82	238.89	9.89		1.30	12.61	6.93
	Bottom	53.00	218.80	9.59		1.27	11.71	6.41
	Means ($\bar{x}$)	**53.32**	**232.81**	**9.95**	**57.16**	**1.32**	**12.77**	**7.03**

The material test findings demonstrate that bamboo is suitable for load-bearing structural elements, such as columns and arches. However, it is crucial to consider the risk of buckling, particularly with slender bamboo culms which are more prone to buckling under the compression than the thicker culms. The diameter of the bamboo significantly influences its structural performance under the compression stress. For instance, with diameter ranging from 80 mm to 200 mm, *D. asper* exhibits higher compression strength and thus has better resistance to buckling. Conversely, *G. apus*, with its smaller diameter ranging from 40 mm to 80 mm, is more susceptible to buckling under the compression. These characteristics should be carefully considered, especially when employing bamboo in bending-active structures.

Furthermore, results presented in Table 4-15 indicate that bamboo is potentially robust in withstanding tensile stress parallel to the fibre. However, it is important to note that tensile strength is reduced significantly at the nodes, which can lead to structural vulnerabilities. Moreover, based on the tensile test findings, some of specimens were failed

due to shear stress (see Section 4.2.3 and Figure 4-15). This phenomenon was attributed to the moderately low shear strength of bamboo. For structural application, the limitation on shear resistance significantly impacts the design of connection and joinery systems. In some cases, the bamboo fibre at connections failed due to splitting at bolted areas, necessitating modifications and reinforcements to enhance the structural integrity.

It is also important to highlight that strength perpendicular to the fibre is considerably low, supporting findings from previous published studies (Sharma, Harries, & Ghavami, 2013; Mitch, 2009; Arce-Villalobos, 1993). This characteristic creates challenges in structures built using bending-active techniques, where materials are expected to withstand stresses from multiple directions. The inherent weakness perpendicular to the fibre could lead to fractures or deformations both during the bending process and when the structure is subject to loads.

As a final point, the material test results and analysis of all properties indicate that bamboo is a functionally graded material. This is evident from the differences in mechanical properties from the bottom to the upper section of the culms, as well as in fibre density (ρ) and moisture content (MC). Mechanical properties parallel to the fibre, such as compression and tension, exhibit significant differences in strength between top-middle-bottom sections. Meanwhile, strength properties perpendicular to the fibre show less significant disparities. However, it is worth noting that significant variations of the mechanical properties were observed within the entire culm, highlighting the unpredictable nature of bamboo as a construction material.

A whole culm bamboo can reach heights of over 10 metres when growing, with some species growing to more than 20 metres in length. Therefore, when harvested, a whole bamboo culm can be cut into two to five sections, depending on the desired length or other considerations, such as transportation and preservation needs. For example, bamboo culms commonly sold in Java Island, Indonesia, range from four to six metres, tailored to fit transportation methods such as truck length. In this condition, the tip of one bamboo pole can potentially serve as the base of another, and vice versa. This poses a challenge in accurately identifying the right section within the culms and determining the material properties.

This study also addresses the challenges encountered during the identification process in the sample preparation stage. The bamboo supplier in Indonesia did not usually identify and provide a record about the exact position of culms within the whole bamboo plants, complicating the identification of specific sections within the culm for the material tests. Consequently, the identification was based on characteristics observed within individual

poles, leading to potential misclassification of top to bottom parts. Addressing these identification challenges is crucial for the utilisation of bamboo in construction and preliminary determination of the material properties.

To mitigate these challenges, the implementation of robust identification and standardization processes for bamboo culm is suggested. Simple measures, such as documenting and identifying the position of bamboo poles within the whole culms, can improve accuracy in early identification of the properties. Furthermore, considering harvesting age and timing is advisable, as bamboo exhibits optimal properties when harvested between three to five years. By improving identification practices, the bamboo can enhance the utilisation of bamboo in construction in general.

4.4.2. Bending Capability

Bamboo is commonly perceived as a flexible material since during the growth period, bamboo has to withstand and bend with the wind. However, bamboo's bending capacities are varied and influenced by several key factors, including species and its morphology, material properties, diameter and wall thickness, moisture content, and culm orientation. Some species feature smaller diameter and slender poles, which enhances the flexibility. In contrast, other species may possess larger diameters and thicker walls, contributing to greater stiffness.

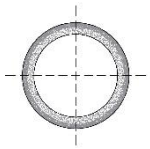
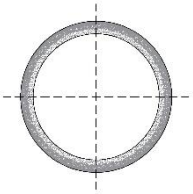
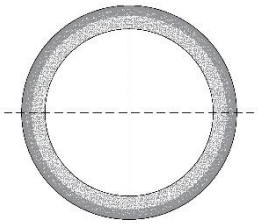
In the context of bending-active structure, such as gridshells, bamboo is manipulated into curved forms, and thus necessitates a thorough understanding of the relationship between its sectional properties and material characteristics. As stated by Hernández (2015), the sectional profile significantly affects the form-finding process and structural integrity of elastic gridshells. The study suggested that both axial stiffness (*EA*) and Flexural stiffness (*EI*) are crucial in selecting appropriate bamboo sections for gridshell applications.

Evaluation of the axial stiffness indicates the capacity of material to resist axial loads. A higher axial stiffness basically implies that the material can support greater loads with minimal deformation, thus maintaining the structural integrity of gridshells. The calculation demonstrates that *Dendrocalamus asper* exhibits the highest axial stiffness, indicating its excellent performance in load-bearing elements. On the other hand, *Gigantochloa apus* displays the lowest stiffness, suggesting that the bamboo species is less suitable for structural elements under high compression (see Table 4-16).

Flexural stiffness indicates resistance to bending; however, at the same time, the value also indicates the material's flexibility to bending. Flexural stiffness is directly linked to the moment of inertia (I_B) which for bamboo can be calculated as per equation 4-7. Therefore,

the diameter of bamboo holds a crucial role in determining the stiffness. Based on the calculation in Table 4-10. *D. asper*, with the larger diameter, possesses the highest flexural stiffness, indicating that the culms are stiffer compared to *G. apus* and *G. atter*. However, although the high flexural stiffness is advantageous for gridshell durability, it reduces the flexibility of bamboo to be formed into curvature.

Table 4-16. The calculations of axial and flexural stiffness based on material test results.

	Gigantochloa apus	**Gigantochloa atter**	**Dendrocalamus asper**
Sectional profile			
EA	2.28E+09	4.41E+09	5.01E+10
EI	2.56E+10	3.93E+10	2.06E+11

Therefore, while the assessment of axial stiffness demonstrates the suitability of materials for gridshell structures, evaluations of flexural stiffness might contradict its suitability. To achieve optimal gridshell performance, materials need to exhibit both effective axial and flexural stiffness while maintaining sufficient flexibility for the form-finding process. Identifying an appropriate sectional form could enhance performance and highlight the balance requirement in material selection for gridshell structures.

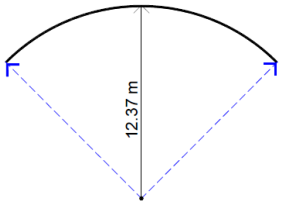
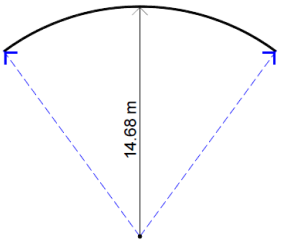
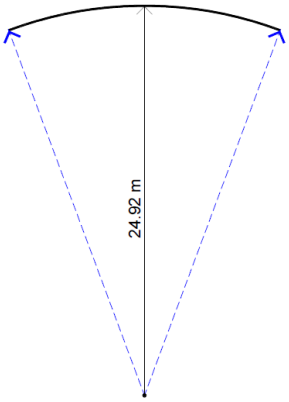
In addition to the evaluation of bending capabilities by means of the assessment of axial and flexural stiffness, determining the radius of the curvature is also a significant assessment method. However, the inherent variability in flexibility among bamboo species poses a challenge in determining the radius of curvature. One method used to assess the radius of curvature is by examining the ratio between Young's modulus (E) and bending strength (f_m).

The Young's modulus and bending strength can be used to assess the suitability of material such bamboo for bending-active structures. Examining the ratio between Young's modulus and bending strength provides critical assessment on the capabilities of material to deform into bending-active structures. While this suggests a degree of flexibility, the ratio primarily reflects the stiffness (E) relative to its strength (f_m). Therefore, even though higher ratio indicates that the material capable to undergo significant elastic deformation before reaching its ultimate strength, its application for bending-active principles resulting in

lower curvature or higher radius of curvature. Meanwhile, lower ratio indicates a significantly lower stiffness compared to bending strength, allowing for greater deformation under load. This also indicates that the materials are capable for creating deeper curvature with smaller radii of curvature.

As presented in Table 4-17, *D. asper* exhibits and Young's modulus of 21,223.34 N/mm^2 and bending strength of 57.16 N/mm^2, resulting in the ratio of approximately 371.29. Meanwhile, *G. apus* with Young's modulus of 22,277 N/mm^2 and bending strength of 71.02 N/mm^2 exhibits the ratio of approximately 313.67. In between, G. atter with Young's modulus of 20,549.80 N/mm^2 and bending strength of 63.09 N/mm^2 results in the ratio of 325.71.

Table 4-17. Study of Young's modulus and bending strength to the assessment on radius of curvature.

	Gigantochloa apus	**Gigantochloa atter**	**Dendrocalamus asper**
Ratio of E/ f_m	$\frac{E}{f_m} = \frac{22{,}277.00}{71.02} = 313.67$	$\frac{E}{f_m} = \frac{20{,}549.80}{63.09} = 325.71$	$\frac{E}{f_m} = \frac{21{,}223.34}{57.16} = 371.29$
Prediction of radii of curvature $R = \frac{E}{f_m} \cdot \frac{D}{2}$			
	12.27 m	14.68 m	24.92 m

Using the ratio of Young's modulus and bending strength along with the average diameter of bamboo culm, we can predict the radius of the curvature. This prediction is an essential measure for preliminary design process of structures using bending-active principle. By employing the formula as per equation 2.4 and average outer diameter of bamboo, the approximately the radii of curvature of the studied bamboo presented was obtained.

Displacement data obtained from the bending test parallel to the fibre also can provide valuable information for predicting the radii of curvature of bamboo culm. Tests on bending parallel to the fibre (see Table 4-10) measured and recorded the displacements (Δ) of the three bamboo species used in this research. The displacement was used as the height (h) of

curvature, while the span (L) was the distance between the supports (Figure 4-43). To calculate the minimum radius of curvature, equation 4-22. was used, where the height was determined from the average displacement ($h = \Delta$). The calculation and displacement data, length, and radius of curvature can be seen in Table 4-18.

$$r = \frac{4h^2 + L^2}{8h} \qquad 4\text{-}22$$

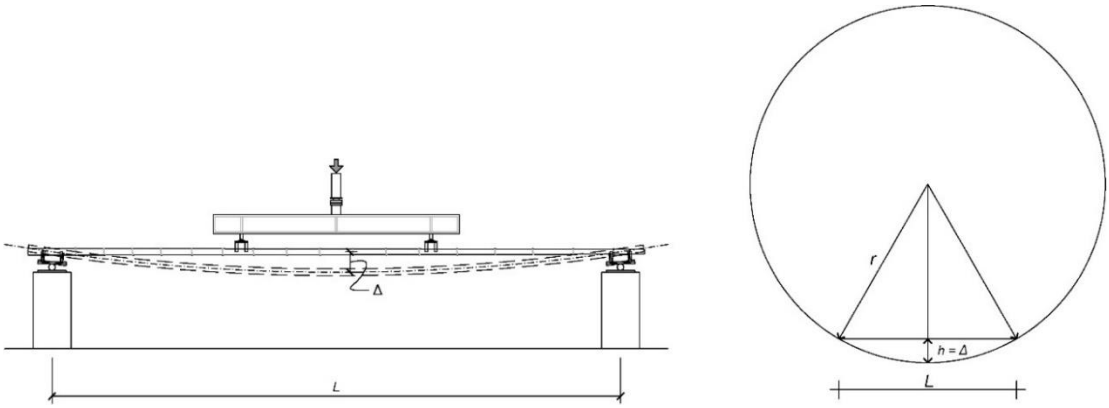


Figure 4-43. Determination of radius of curvature.

Table 4-18. Minimum radius of curvature full-culm bamboo based on bending parallel to the fibre tests.

Species	L (cm)	Δ (cm)		r (cm)
G. apus	360	*Min*	7.70	2,107.75
		Max	16.10	1,014.26
		Ave	12.93	**1,259.37**
G. atter	360	*Min*	6.70	2,421.26
		Max	23.70	695.39
		Ave	11.73	**1,386.94**
D. asper	600	*Min*	13.78	3,272.49
		Max	20.54	2,201.12
		Ave	16.43	**2,747.11**

As presented in Table 4-17 and Table 4-18, the results obtained from the ratio of Young's modulus and bending strength showed similar trends, particularly evident with *G. apus*, which exhibited very close results. The predicted radii of curvature from the ratio were 12.27 m, while the average from the displacement data was 12.93 m. Similarly, for *G. atter*, the difference was not substantial, with a predicted ratio resulting in 14.68 m, while the average from displacement data was 13.87 m. *D. asper* showed slightly larger discrepancies, with a predicted ratio average of 24.95 m, compared to the average of 27.47 m from the tests. However, since the displacement data indicated a range between 22.01 m and 32.72 m, the results from the prediction fell within this range.

Moreover, both prediction and test data reveal that *G. apus* is capable of achieving the smallest radii of curvature, indicating the capability of the bamboo to bend more deeply than the other two studied species. Meanwhile, *D. asper* exhibits significantly high radii of curvature, suggesting that this species is only capable of creating very narrow curvature. Therefore, the use of *D. asper* for gridshell applications as full-culm bamboo should be carefully considered.

However, it is important to note that while both methods –predicting radii of curvature through the ratio of Young's modulus to bending strength and using displacement data– provide valuable insights, they also have inherent limitations. Predictions based on the ratio of Young's modulus to bending strength are challenged by the significant variability in the modulus of elasticity and the outer dimensions of bamboo. Consequently, average values may not accurately represent the entire population. Nevertheless, this method is straightforward and suitable for preliminary design phases.

Conversely, predictions derived from displacement data tend to be more accurate as they reflect the actual behaviour of the material under load. However, these results are susceptible to the specific conditions and setup of the tests. Moreover, the results are specific to the tested bamboo, which may not perfectly replicate the real conditions or bamboo sources under different circumstances. Therefore, to achieve more precise and reliable data, further comprehensive analyses are recommended. Advanced methods such as finite element analysis (FEA) and other relevant computational techniques should be employed to enhance the accuracy of the predictions.

In summary, the versatility of bamboo in bending-active structures arises from its inherent properties. The analysis revealed that while all bamboo species have relatively similar Young's modulus, the diameter plays a crucial role in determining their suitability for application in gridshell structures using bending-active principles. From the discussion on axial and flexural stiffness, as well as the prediction of radii of curvature, the results suggest that *G. apus* demonstrates promising performance for applications as full-culm bamboo in gridshell structures.

4.4.3. Utilisation and Implication for Gridshell Structures

When bamboo is subjected to bending, a bamboo culm experiences a combination of tensile, compressive, and shear stresses, as illustrates in Figure 4-44. The upper layer of the culm is under tension; in this case, the high tensile strength is advantageous. Conversely, the lower fibres are under compression, where the material is more prone to buckling. The neutral zone in the middle layer experiences significant shear stress. This shear stress can lead to

failures such as radial cracking and splitting, due to bamboo's inherently low shear strength. These mechanical behaviours are essential considerations for bending-active gridshell structures.

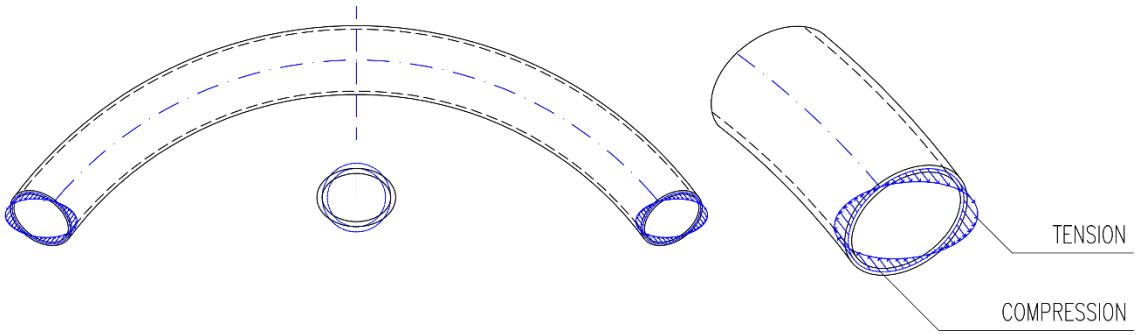


Figure 4-44. Bending mechanism of hollow tube beam.

As reported in Section 4.3.4, failures during bending tests are often due to buckling, fibre kinking, stress concentrations at the saddle point, and splitting due to shear stress. The buckling and fibre kinking occurred in the layer that suffer the compressive stress. It seems the tension layer can withstand the bending process, while the compression layer fails. Observations from the tests showed that tension layer of the culms mostly remained intact. In addition, buckling tendencies are more pronounced in slender bamboo poles, such as G. apus. Therefore, application for bending-active structures must consider preventing buckling in the compressed area.

Shear stress is critical factor that need to be considered during bending process because it influences the deformation and failure behaviour. Failure in resisting shear can triggered radial cracking, splitting and fibre delamination. Failure in shear can lead to the sudden collapse, which also recorded during the shear tests and bending tests.

In addition to the axial stresses experienced during bending, circumferential stresses also play a crucial role. As the bamboo culm is bent, its sectional profile undergoes significant deformation. This deformation occurs not only along the longitudinal axis of the bamboo but also around its circumference. The outer fibres of the bamboo culm experience stretching, while the inner fibres undergo compression. These circumferential stresses act perpendicular to the longitudinal axis of the bamboo and contribute to its overall bending behaviour. However, these stresses can also lead to radial cracking and splitting, particularly in sections where the material's properties perpendicular to the fibres are weak.

Bamboo's weaknesses, such as splitting and buckling, present significant challenges for its use in gridshell structures. Splitting often occurs at nodes or defects due to stress concentrations and the material's low shear strength perpendicular to the fibres. This weakness necessitates careful design and planning for the depth of curvature when

designing gridshell structures. Additionally, it is necessary to design joints and connections carefully to prevent structural failures due to shear stress. Buckling is another critical concern, especially for slender bamboo species like *Gigantochloa apus*, which are more prone to instability under compressive loads. Design strategies, such as increasing the diameter or using thicker-walled bamboo, can help mitigate this issue. Furthermore, the natural variability in bamboo's mechanical properties requires thorough testing and conservative design approaches to ensure the safety and reliability of gridshell structures.

4.5. Summary

This chapter presented the results of material tests conducted on three Indonesian bamboo species, with samples taken from 20 culms of each species. The findings reveal that bamboo exhibits excellent structural performance in terms of strength parallel to the fibre, with the exception of shear strength, which is significantly lower. Conversely, bamboo shows low performance in terms of strength perpendicular to the fibre.

The results and discussions highlight that for the application of bamboo in active bending gridshell structures, it is essential to consider the variation in strength in different directions, particularly the compression strength during the bending process. The tests indicated that while bamboo can effectively withstand tensile stresses, it is more prone to failure in compression, which can lead to buckling and fibre kinking.

Additionally, the shear strength, especially in the middle layer during bending, poses a limitation due to its low value. Therefore, careful consideration must be given to the design and implementation of bending methods to achieve an optimum radius of curvature. This is crucial for ensuring the structural integrity and performance of active bending gridshell.

In conclusion, the successful utilisation of bamboo in gridshell structures depends on addressing its anisotropic properties. Effective strategies must be developed to optimise the bending process, considering the material's strengths and weaknesses to maximise its potential in sustainable architectural applications.

CHAPTER 5 | STRUCTURAL ANALYSIS OF GRIDSHELL STRUCTURE

5.1. Overview and Research Objectives

Structural analysis is an essential component of numerical analysis for gridshell structures, providing insight into how the structure resist and respond to loads. In gridshell design, where geometry is closely related to the load-bearing behaviour, numerical analysis can perform as models for simulations and predictions of the structural performance, such as stress distribution, deformation, and displacement. The analysis on the structural performance provides critical feedback for the design process, eventually, influencing the structural design and performance, and the following stages, such as form-finding and optimisation.

Finite Element Analysis (FEA) is a commonly used method in the numerical analysis fo shell structures. FEA offers various types of analyses needed for gridshell design, including stress distribution, deformation, and displacement. It examines structural capacity and performance under applied loads. Numerous software options are available for FEA, such as Abaqus, ANSYS, and SAP 200. By using FEA in gridshell design process, the material capacity and the structural performance can be thoroughly studied.

Utilising bamboo as a material for gridshell structures presents complexities and challenges in numerical analysis. Findings of Chapter 4, which discussed the material tests, highlighted the variations in strength within bamboo culms, including significant differences in strength parallel and perpendicular to the fibre. Whilst the axial strength components in bamboo culm are moderately high, the strength components perpendicular to the fibre are notably low. Additionally, variations in dimensions and wall thickness pose challenges for numerical analysis. Therefore, numerical analysis of bamboo structures often needs validation through empirical load tests on full-scale models to confirm the capacity of bamboo in withstanding loads.

This chapter aims to numerically analyse the use of bamboo in gridshell structures in two forms: full-culm bamboo and split bamboo. The numerical analysis predicts shape deformation, displacement values, and stress distribution. The deformed shape and displacements from the structural analysis was compared with the results from the empirical load tests.

The objectives of this chapter are defined as follows:

- To evaluate the structural performance of bamboo gridshells based on the material properties of Indonesian bamboo.
- To compare the results of computational simulations with the results of full-scale models of bamboo gridshells.

5.2. Research Method

This study aimed to assess the structural performance of bamboo gridshell structures by investigating the forces involved, as well as the resulting displacement and deformation from the applied loads. The structural analysis results were then compared to the measurements obtained from load tests performed on full-scale models (further described in Chapter 6) for validation purposes. This comparison was essential to identify discrepancies between the theoretical models and real-world behaviour, thereby enhancing the predictability of the models. To achieve these objectives, the structural analysis was conducted using finite element analysis (FEA).

FEA was performed using the commercial software Abaqus to analyse the structural performance of the bamboo gridshells. Abaqus was selected for its advanced capabilities and suitability for complex structural analyses. The software can define and simulate complex material behaviours, making it ideal for accommodating the anisotropic properties of bamboo. Abaqus also offers a wide range of element types, including beam, shell, and solid elements, which are essential for accurately modelling the bamboo gridshell structures. Additionally, Abaqus can model complex assemblies with interacting components, a crucial feature for simulating the intricate connections in bamboo gridshells.

The FEA was conducted on two bamboo gridshell models, based on the geometries and details of the full-scale models described in Chapter 6. The first model utilised full-culm bamboo, while the second used split bamboo. These models were initially recreated in Rhinoceros using the Grasshopper and Kangaroo plug-ins. After modelling, they were exported as 3D models to Abaqus for structural analysis.

It is important to note that Abaqus is a unitless platform, meaning it neither determines nor requires specific units for its input parameters. To ensure accuracy and consistency in the simulation, all units were standardised according to the SI unit system. The units used were metres for length and dimensions, Newton for force, kg for mass, N/m^2 for stress, and kg/m^3 for density, as presented in Table 5-1.

Table 5-1. SI unit for the simulation

Quantity	SI unit
Length/dimension	m
Force/Load	N
Mass	kg
Stress	N/m^2
Density	kg/m^3

5.2.1. Gridshell Geometries and Meshes

The basic gridshell geometry chosen for the structural analysis was using a synclastic shell geometry, characterised by its double-curvature and dome-like shape. This basic geometry was selected due to its effective load distribution properties, which would allow further investigation to evaluate the performance of bamboo. This geometry also consisted of uniform curvature configuration, which simplified the analysis and ensured a robust structural performance, making it ideal for studying the behaviour under various loading conditions.

Furthermore, this geometry facilitated direct comparison and validation with full-scale models built during the construction stage. By aligning the analytical model closely with the physical structure, a comprehensive understanding and identification of any discrepancies can be obtained, allowing a comparison between theoretical predictions and real-world behaviour. This approach also could provide information to improve the bamboo gridshell structure design process.

Before conducting the FEA in Abaqus, two gridshell models were created in the CAD software Rhinoceros using the plug-ins Grasshopper and Kangaroo as illustrates in Figure 5-1. The first model (M-1) was a bamboo gridshell structure constructed with full-culm bamboo, as described in Chapter 6. This structure had a span of 10.80 metres by 10.80 metres, a mesh size of 0.60 metres by 0.60 metres, and reached a final height of 1.13 metres after relaxation. The boundary conditions were octagonal, and the mesh configuration was square without bracing. The model was developed in Rhinoceros by assembling members into grids on the ground and setting the boundary conditions. The curvature was generated by applying force at the centre point; this force was controlled in Grasshopper by adjusting the force vector to achieve the desired height. Using the solver Kangaroo, the form-finding process continued until the model entered the relaxation stage and achieved the designated form and expected height.

The remodelling of the second model (M-2) was conducted using a slightly different process from the first. The second model was constructed using split bamboo, and the erection process began by assembling flat grids on the ground, pulling the grid upwards using chain blocks, and then pushing the corners inward. Given that M- 2 was constructed

using split bamboo, its dimensions were smaller, with a span of 8.40 metres by 8.40 metres, a mesh size of 0.60 metres by 0.60 metres, and a final apex height of 2.35 metres. In Rhinoceros, the form-finding process started by constructing grids with the same mesh size and setting an octagonal boundary condition. Anchors were made movable with a slide bar to control the distance. To inflate the grids and create the curvature, a force load was induced at the centre point. The form-finding began by moving the anchors inward by a distance of 1.40 metres and adjusting the force vector until the model achieved the expected form and height. The models were exported as *.iges files, which were compatible with Abaqus.

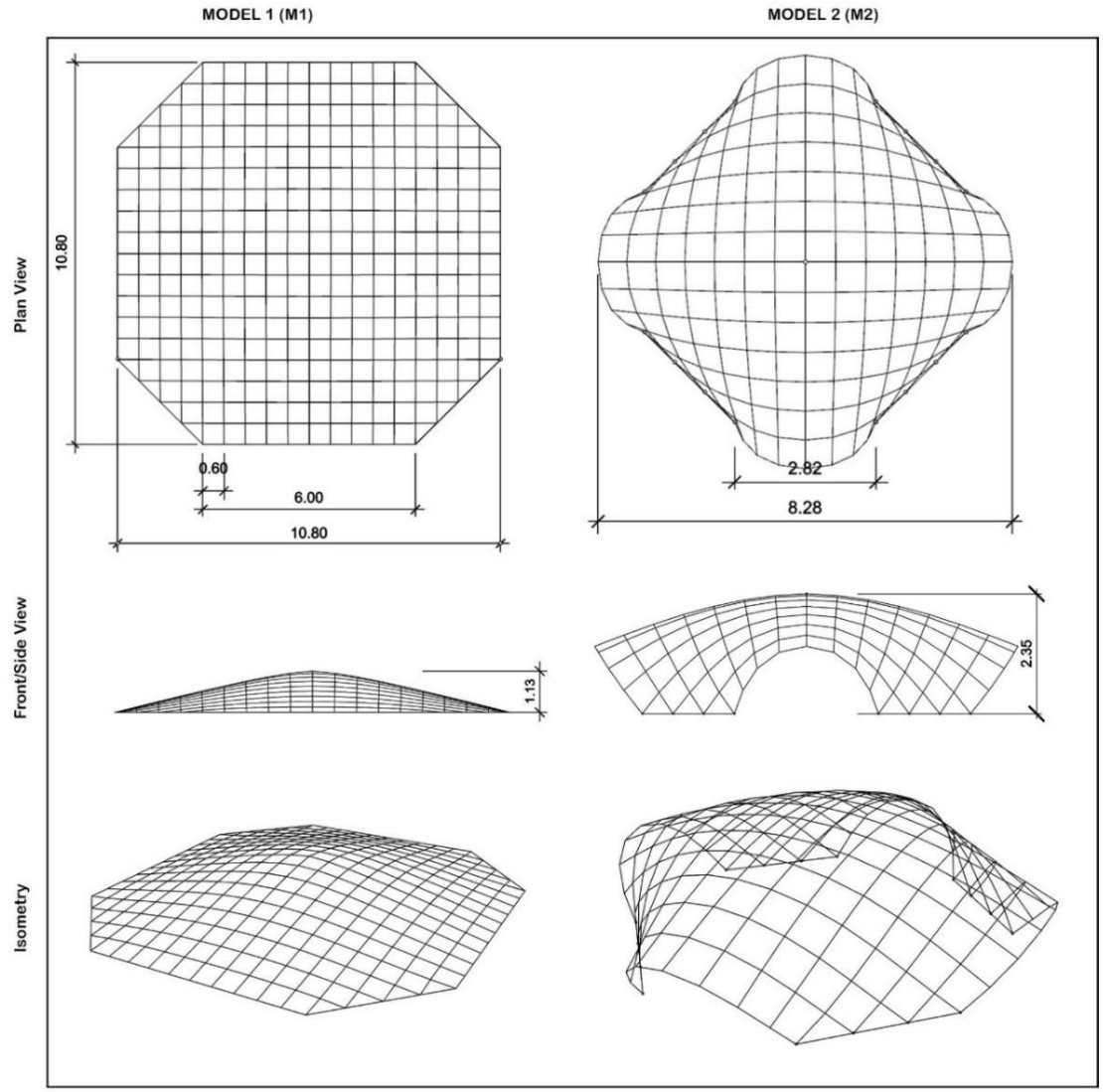


Figure 5-1. The generated models of Model-1 and Model-2 in Rhinoceros.

5.2.2. Input Parameters

The models were imported into Abaqus as parts, and the subsequent process involved determining their properties. Consistent with the full-scale models in Chapter 6, *Gigantochloa apus* was used as the input material for Model-1 (M-1), while *D. asper* was employed for Model-2 (M-2) in the structural analysis. Given that bamboo is an anisotropic material, it exhibits a variety of mechanical properties along its longitudinal-L, radial-R, and tangential-T axes, as illustrated in Figure 5-2. The mechanical properties along the longitudinal axis are determined based on properties parallel to the fibre. In wood, the radial axis corresponds to the growth ring direction, while the tangential axis is perpendicular to the fibre direction. In this simulation, the mechanical properties of bamboo in the longitudinal direction were derived from properties along the fibre. Regarding the radial and tangential directions, bamboo was simplified to be transversely isotropic; thus, the properties along the radial and tangential axes were assumed to be equal and maintained the same value.

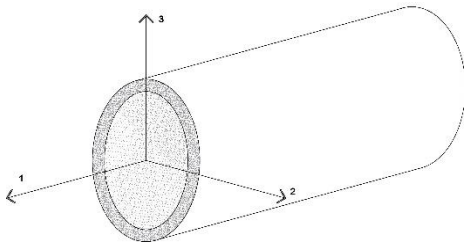


Figure 5-2. Bamboo three axes: Longitudinal, radial and tangential.

The input parameters for material in Abaqus utilised engineering constants, which were expressed in the software as detailed in Equation 5-1. E_1, E_2, and E_3 represented Young's modulus in three directions, while v_{12}, v_{13}, and v_{23} denoted Poisson's ratios, and G_{12}, G_{13}, and G_{23} stood for the shear moduli.

$$\begin{Bmatrix} \varepsilon_{11} \\ \varepsilon_{22} \\ \varepsilon_{33} \\ \gamma_{12} \\ \gamma_{13} \\ \gamma_{23} \end{Bmatrix} = \begin{bmatrix} 1/E_1 & -v_{21}/E_2 & -v_{31}/E_3 & 0 & 0 & 0 \\ -v_{12}/E_1 & 1/E_2 & -v_{32}/E_3 & 0 & 0 & 0 \\ -v_{13}/E_1 & -v_{23}/E_2 & 1/E_3 & 0 & 0 & 0 \\ 0 & 0 & 0 & 1/G_{12} & 0 & 0 \\ 0 & 0 & 0 & 0 & 1/G_{13} & 0 \\ 0 & 0 & 0 & 0 & 0 & 1/G_{23} \end{bmatrix} \begin{Bmatrix} \sigma_{11} \\ \sigma_{22} \\ \sigma_{33} \\ \sigma_{12} \\ \sigma_{13} \\ \sigma_{23} \end{Bmatrix} \quad 5\text{-}1$$

The input material properties of bamboo used findings from the material tests conducted in Chapter 4. Young's modulus in the axial or longitudinal direction (E_1) utilised data obtained from the bending parallel to the fibre test (E_m). Meanwhile, Young's modulus in the

radial and tangential directions (E_2, E_3) was determined based on the results of bending perpendicular to the fibre ($E_{m,90}$). The Poisson's ratio of bamboo varied within the culms, influenced by ages, growth, and radial direction. A study on Moso bamboo found the range from 0.180 to 0.334 (Lu et al., 2022). Unfortunately, the tests to determine the Poisson's ratio could not be carried out due to equipment limitations in the laboratory. Furthermore, data or literature on the Poisson's ratio of *Gigantochloa apus* and *Dendrocalamus asper* were not available. Therefore, the Poisson's ratio for simulation in the structural analysis was assumed to be 0.3. The shear moduli (G) were calculated based on Equation 5-2.

$$G = \frac{E}{2(1+v)} \qquad 5\text{-}2$$

Given the high variability in the material properties of bamboo, it is crucial to determine the characteristic values that can reliably represent the material properties used for the simulation. Using the average value is not advisable because bamboo properties are significantly affected by various factors such as age, nutritional growth, and treatment. The properties also vary within single culm, as presented in Chapter 4. Moreover, in one batch of bamboo culms, predicting the uniformity is difficult.

Unfortunately, there are no existing building standards or SNI (*Standar Nasional Indonesia*/Indonesian National Standard) specifically dedicated to bamboo construction in Indonesia. Therefore, this study determined the material properties in accordance with ISO 22156:2021, which provides guidelines for bamboo structures, bamboo culms, and structural design. The choice of this standard as reference was due to its comprehensive guidance on adjusting bamboo material properties while considering factors such as safety, utilisation, and other relevant factors. These factors needed to be addressed in response to the high variability of material properties, as well as the uncertain characteristics and limitations discussed in Section 4.2.5 and Section 4.4.1. Thus, ISO 22156:2021 was utilised for determining the input material properties in Abaqus.

According to the ISO standard, the capacity of bamboo should consider the possibility of longitudinal splitting, as bamboo is prone to this issue. Splitting can occur due to the changes of moisture content in the environment, posing a significant risk to structural integrity. Consequently, the bending capacity was adjusted by accounting for factors such as redundancy factor (C_R), service class and load duration (C_{DF}), service temperature (C_T), and safety factors ($FS_{C/m}$). The allowable member design capacity (X_m) was determined following equation 5.3.

$$X_i = X_{ik} \times C_R \times C_{DF} \times C_T \times (1/FS_c) \quad 5\text{-}3$$

Young's modulus in bending (E_m and $E_{m,90}$), used as input parameter in Abaqus, was calculated from the 5th percentile characteristic value with 75% confidence ($E_{0,05,\ 0,75}$) to accommodate bamboo's susceptibility to splitting. The redundancy factor (C_R) was assumed to be 0.90, as the structures were single layer gridshells with non-redundant members or components. Service class and load duration were assumed as 0.55 for permanent and long-term applied load for service class 2. The service temperature (C_T) was assumed to be one, as it was presumed that the structure would not be exposed to heat over 38°C. The safety factors component ($FS_{C/m}$) was assumed to be 2, which applies to bending. Input material properties for structural analysis are presented in Table 5-2.

Table 5-2. Input material properties for Abaqus simulation.

Species	E_1 (N/m²)	E_2=E_3 (N/m²)	ν_{12} = ν_{13} = ν_{23}	G_{12}= G_{13} (N/m²)	G_{23} (N/m²)	ρ (kg/m³)
G. apus	3.41E+09	1.32E+08	0.3	1.31E+09	5.09E+07	679.75
D. asper	4.24E+09	2.03E+08	0.3	1.63E+09	7.82E+07	664.37

The determination of the sectional profile or cross-sectional dimensions was in accordance with ISO 22156:2021, which recommends using the minimum culm outer diameter (D) and wall thickness (δ) when the diameter variation along the length exceeds 10%. The dimensions for full-culm bamboo were derived from a dataset of *G. apus* obtained from material tests. In contrast, the dimensions for split bamboo were assumed based on the splitting cross-sectional area of *D. asper* bamboo. The specific dimensions are presented in Table 5-3.

Table 5-3. Input dimension of the profile.

Species	**Full-culm**			**Split**	
	D (m)	*r (m)*	*δ (m)*	*Width (m)*	*Height (m)*
G. apus	0.04872	0.02436	0.00425	-	-
D. asper	-	-	-	0.0600	0.0148

After assigning the material properties and profiles, the beam orientation was set to ensure that the cross-sections of the members were aligned correctly. The models were then assembled, and other parameters were determined accordingly.

Pin joints are used in the simulation to mimic the actual behaviour of bamboo structures where elements are typically tied or bolted, allowing rotational flexibility. Connectors were

set to 'join' with constraints in three degrees of freedom (DOF): U1, U2, and U3. The connectors were assumed to be fixed in translation but allowed rotational movement.

The boundary conditions for M-1 were set with the perimeter beams and configured in octagonal shapes. In Abaqus, the boundary conditions were assumed to be fixed supports, by constraining all rotational and translational degree of freedom in x, y, z directions. This setup ensured that the structure was fully restrained at the supports, preventing any movement or rotation. The boundary conditions were applied at points along the perimeter beams.

In contrast, M-2 featured a different configuration, as presented in Figure 5-1, where the synclastic gridshell structure had four openings and four anchors. The boundary conditions for M-2 were set at the points along the anchor lines, which were assumed to be fixed supports. Similar to M-1, the rotational and translational degrees of freedom in the x, y, and z directions were constrained, ensuring full restraint at the anchor points.

The loading system was imposed in two types: gravitational and point loads. The gravitational load was represented by the self-weight of the material, achieved by inputting the density (ρ) into the input material, as listed in Table 5-2. This gravity load was set in Abaqus to assess the effect of the material's weight on the deformation.

Point loads were applied to the structures according to four scenarios presented in

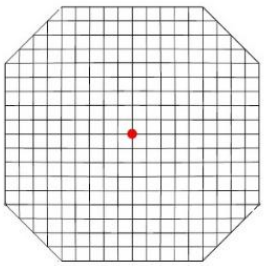
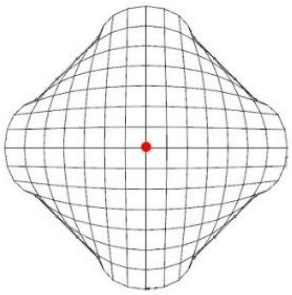
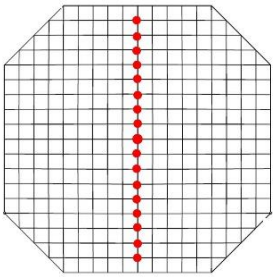
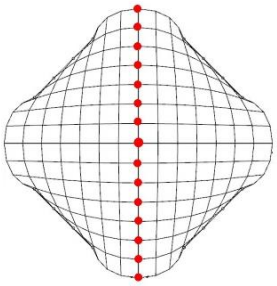
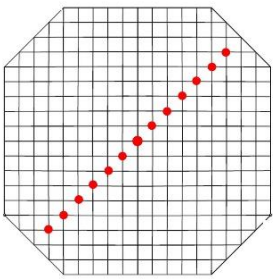
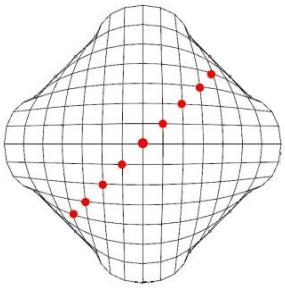
Table 5-4. The first scenario involved a single concentrated load placed at the apex, simulating a point load directly at the top of the structure. The second scenario applied several concentrated loads along the centre line of the structures, mimicking a uniform load distribution along the central axis. The third scenario positioned concentrated loads along the diagonal line, representing diagonal loading conditions. Lastly, the fourth scenario involved an asymmetric load, placed at an off-centre position within the structures to simulate uneven loading conditions.

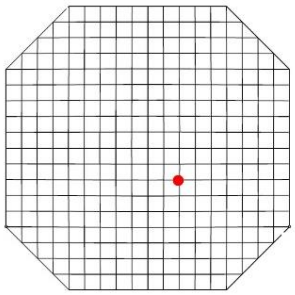
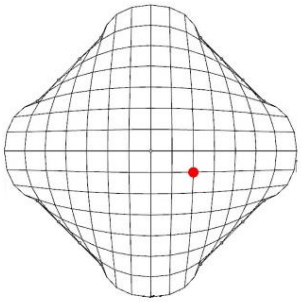
These loading scenarios were designed to represent possible real-world loading conditions, with point load locations at the centre, symmetrical, and asymmetrical positions. These scenarios provided a comprehensive assessment of the structural performance under various loading conditions. The magnitude of the point loads, specified in Table 5-4, was determined based on the loads applied to the full-scale models during the construction stage. as detailed in Table 6-1. By imposing the same magnitude, the results of this FEA could be validated against the load tests conducted on the full-scale models.

The loading conditions in the simulations excluded roofing and wind loads to focus on examining the effect of the material on deformation. These conditions are also relevant to

the full-scale models, as they were constructed without roofing. Consequently, it was assumed that wind load would have a negligible influence on the models.

Table 5-4. Point loads position on the models based on four scenarios.

Scenario	Position/Loads	Model 1 (N)		Model 2 (N)	
1	Centre point (apex)				
	Load	No	in N	No	in N
		1	196	1	40
		2	392	2	120
		3	588	3	200
2	Centre line				
	Load on each point	No	in N	No	in N
		1	40	1	40
		2	80	2	80
		3	120	3	120
3	Diagonal line				
	Load on each point	No	in N	No	in N
		1	40	1	40
		2	80	2	80
		3	120	3	120

4	Asymmetric					
	Load	No	in N		No	in N
		1	196		1	40
		2	392		2	120
		3	588		3	200

5.3. Results

In this section, the results of the finite element analysis (FEA) conducted on two bamboo gridshell models, namely Model-1 using full-culm bamboo and Model-2 using split bamboo, are presented. The FEA aimed to assess the structural performance of these models under four scenarios loading conditions. The results include stress distribution, displacement patterns, and deformation characteristic observed in response to applied loads. The subsections are divided into full-culm and split bamboo to gain deeper insight and understanding into the behaviour and performance of bamboo gridshell structures.

5.3.1. FEA Results of Model 1: Full-Culm Bamboo

The structural system supports various loads including self-weight, wind loads, and other external forces. In this chapter, simulations were conducted with exclusion of the roofing and wind loads to isolate the influence of material properties on deformation characteristics. External loads were applied in four distinct scenarios to analyse structural behaviour under different loading conditions and to identify critical points based on deformation patterns, displacements, and stress distributions.

Figure 5.3 illustrates the deformed shape of Model 1 under the influence of gravity load alone. Without additional external loads, the material exhibited deformation resulting in a maximum displacement of 1.028 cm. Analysis of the deformed shape indicated a slight curvature increase at the centre, with more significant deformation observed near the boundary conditions.

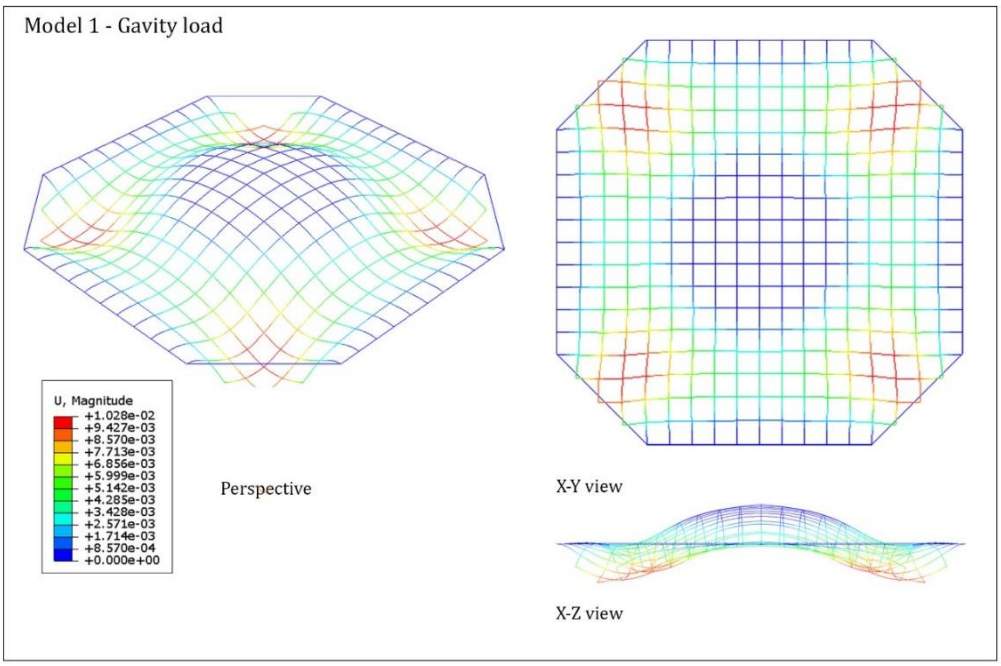


Figure 5-3. Deformed shape of Model 1 under gravity load.

Figure 5-4 illustrates the deformed shape and displacement of Model 1 under load scenario 1. The image shows that the displacement due to gravity load exceeded that resulting from the initial loading step (Load 1). Gravity load induced significant displacement near the boundary condition, with the maximum displacement observed near the four corners, reaching 1.052 cm. The simulation recorded this as the highest displacement. The introduction of the first additional load did not significantly contribute to displacement, but gravity exerted a substantial load on the structure.

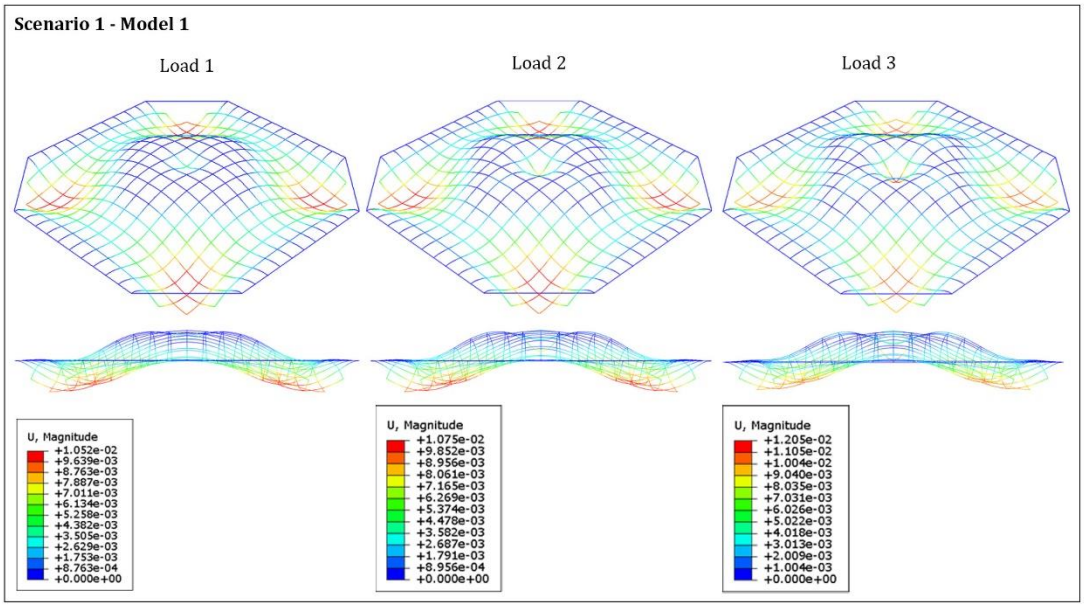


Figure 5-4. Deformation and displacement resulting from load application based on scenario 1 on Model 1.

After applying the second and third loading steps, the deformed shape exhibited greater displacement at the loading points. The maximum displacements for the second and third loading steps were recorded as 1.075 cm and 1.205 cm, respectively. At this stage, the highest displacement was no longer caused by gravity load alone; instead, the external loads induced greater displacement in the structure.

Figure 5-5 shows the stress distribution of Model 1 under both gravity load and an external load applied at the centre of the gridshell. Different stress concentrations in the members were observed across the three loading applications. During the first application (Load 1), the gravity load was more dominant, causing stress concentration near the boundary conditions. However, during the second (Load 2) and third (Load 3) applications, several members experienced higher stress levels. Two curvature lines along the centre in the X and Y directions exhibited the highest stress due to deformation, which consequently affected other grid members.

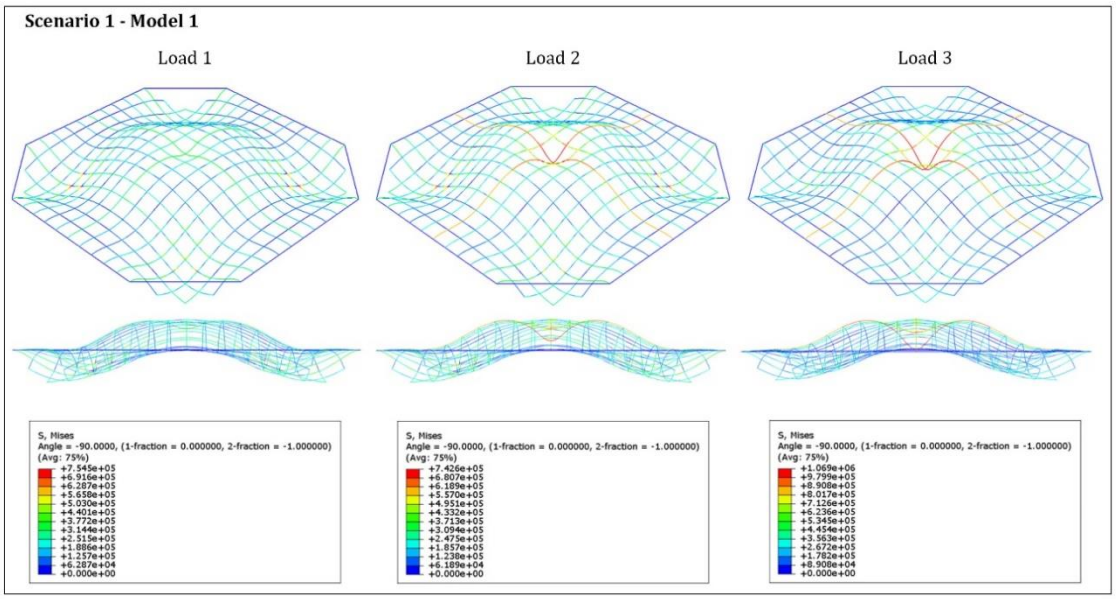


Figure 5-5. Stress distribution based on Scenario 1 loading on Model 1.

Applying an external load along the centre line (Scenario 2) resulted in major displacement on the side of the structure, as shown in Figure 5-6. The maximum displacements for Load 1, Load 2, and Load 3 were 1.56 cm, 2.73 cm, and 3.09 cm, respectively. These displacements did not occur at the centre of curvature but near the boundary. During the application of Load 1, the displacement due to gravity load was prominent. However, as the loads increased, the mesh behaved like a woven structure, reducing the displacement induced by the gravity load.

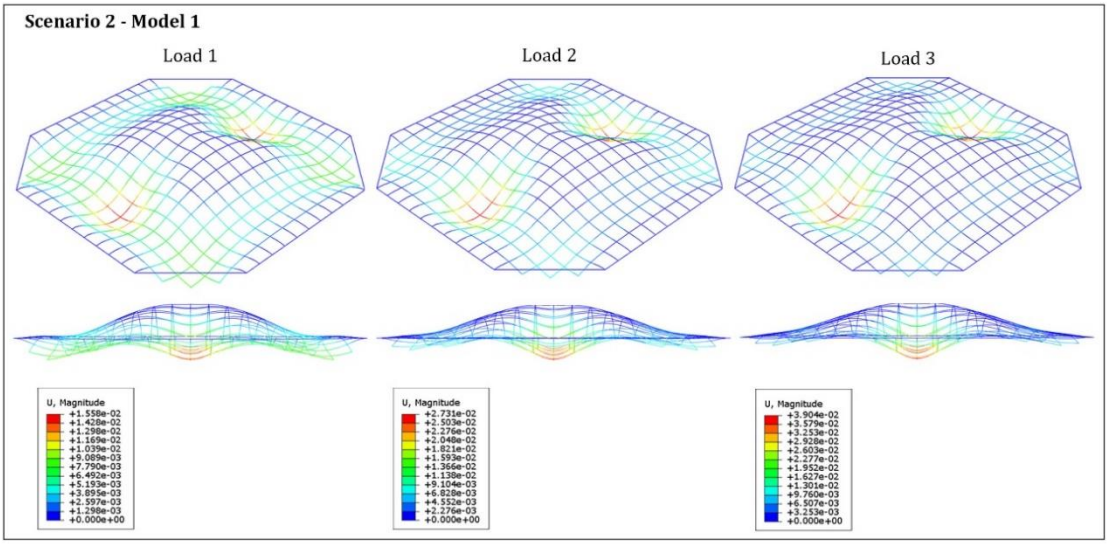


Figure 5-6. Deformed shape and displacement of Model 1 under load application based on Scenario 2.

Observing the stress distribution in Figure 5-7, it depicted stress concentration on the members where the loads were applied and on those boundary conditions. This stress concentration indicated that these areas are critical points that withstand the highest forces from the applied loads. Those members likely experience higher level of deformation and potential structural fatigue. In contrast, the members oriented perpendicular to the direction of the load application experienced the lowest stress concentration. This suggested that these perpendicular members contribute to the overall stability of the structure by distributing the load more evenly.

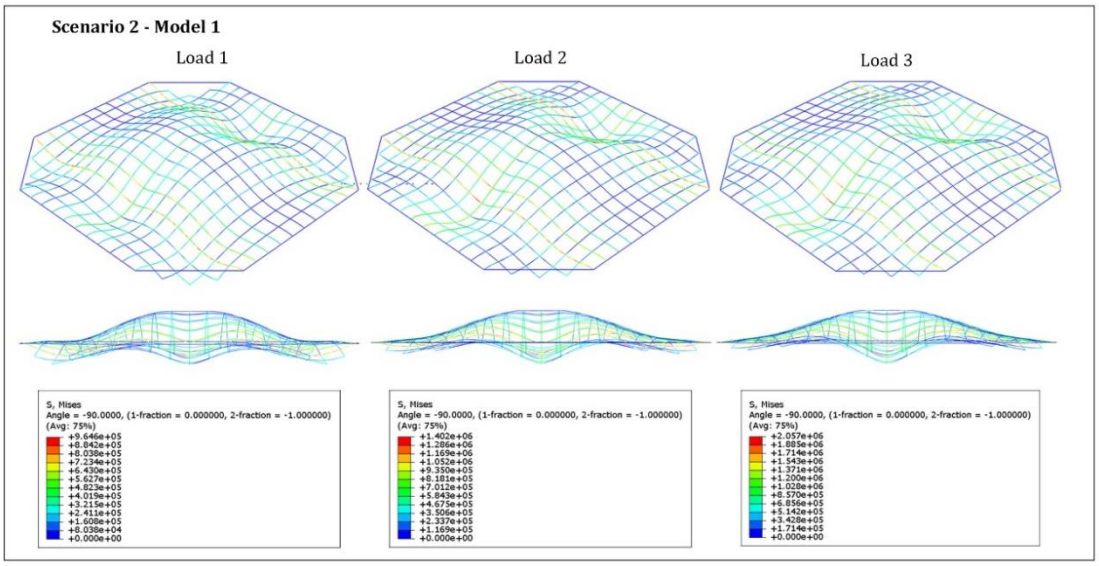


Figure 5-7. Stress distribution under scenario 2 loading of Model 1.

Applying diagonal loads (Scenario 3) to the gridshell models resulted in behaviour similar to Scenario 2, with major displacements occurring not at the centre of curvature but at both sides near the corners or boundary (Figure 5.8). However, the displacements observed in Scenario 3 were higher than those in the previous scenario. Under the first loading (Load 1), the maximum displacement reached 3.33 cm, while the second (Load 2) and third (Load 3) loadings resulted in maximum displacements of 5.73 cm and 8.13 cm, respectively. The maximum displacement due to gravity load was also observed at the same locations. Thus, the addition of external loads in these positions induced greater overall displacement, highlighting the compounded effect of gravitational and diagonal loads on the structure.

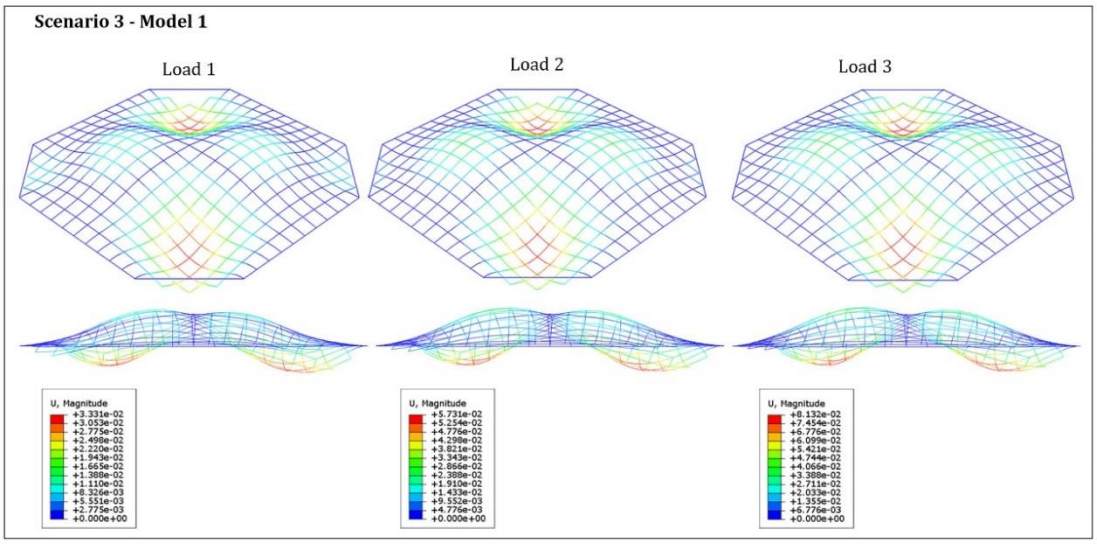


Figure 5-8. Displacement of Model 1 under Scenario 3 load application.

From the stress distribution depicted in Figure 5-9, it was observed that high stress levels were concentrated around the diagonal lines, where the loads were applied. This indicated that this area was particularly vulnerable to the applied diagonal loads. During the applications of Load 2 and Load 3, significant stress was also observed at the central point of the gridshell, even though the major displacements did not occur at this location. This phenomenon suggests that the centre of the structure plays a crucial role in transferring and distributing the applied loads, thus experiencing higher stress levels despite lesser visible deformation. While the major deformation and stress occurred around the loading points, the members oriented in the opposite direction exhibited minimal deformation.

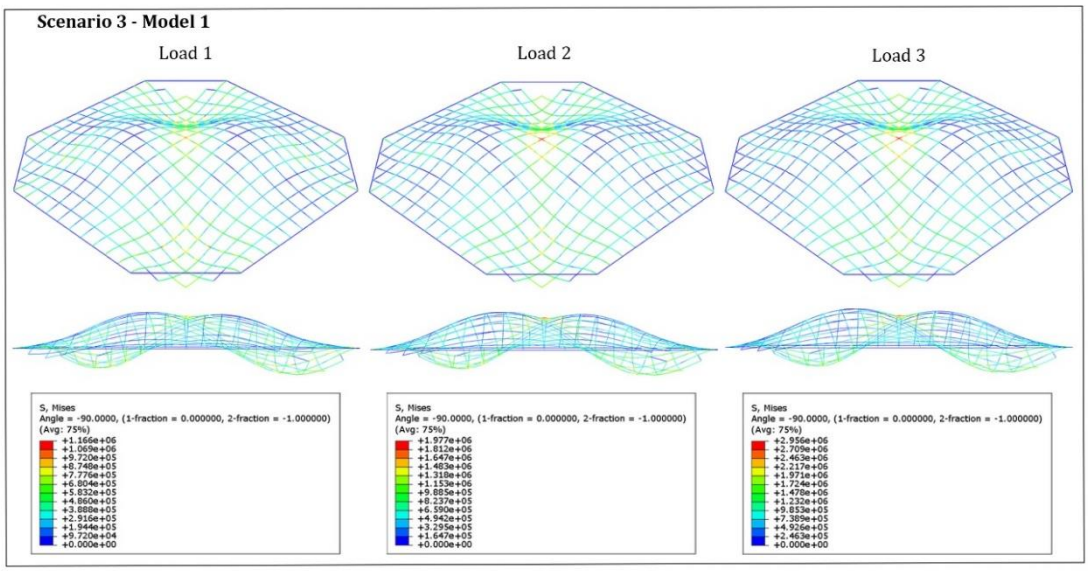


Figure 5-9. Stress distribution under the application of Scenario 3.

Under the application of external load at an asymmetric position, significant displacement in Model 1 was observed specifically at the point of load application. This behaviour was consistent with that observed in Scenario 3, where the application of loads in non-central locations induced substantial displacements in the structure. In this case, the application of external loads resulted in progressively higher displacements: for Load 1, the maximum displacement reached 1.41 cm, for Load 2, it increased to 2.81 cm, and for Load 3, it further escalated to 4.17 cm (Figure 5-10). These findings indicated that the asymmetrically applied loads have a pronounced impact on the structural integrity, causing notable deformations.

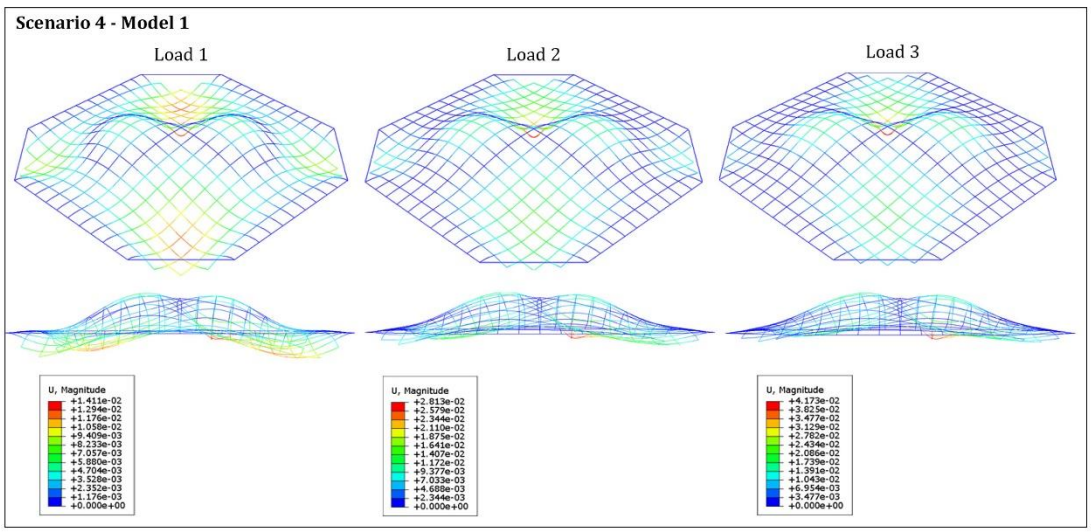


Figure 5-10. Displacement of Model 1 under Scenario 4 loading.

From the stress distribution shown in Figure 5.11, it is evident that the stress was primarily concentrated at the loading point. Additionally, there was a notable concentration of stress in the areas surrounding the loading point, while other regions of the structure experienced significantly lower stress levels. During the application of Load 1, the influence of the gravity load was clearly visible throughout the model, contributing to the overall stress distribution. However, with the application of Load 2 and Load 3, the stress became increasingly concentrated around the loading point. This indicated that as the external loads increased, the stress distribution shifted more towards the area of load application, reducing the stress impact on the other parts of the structure.

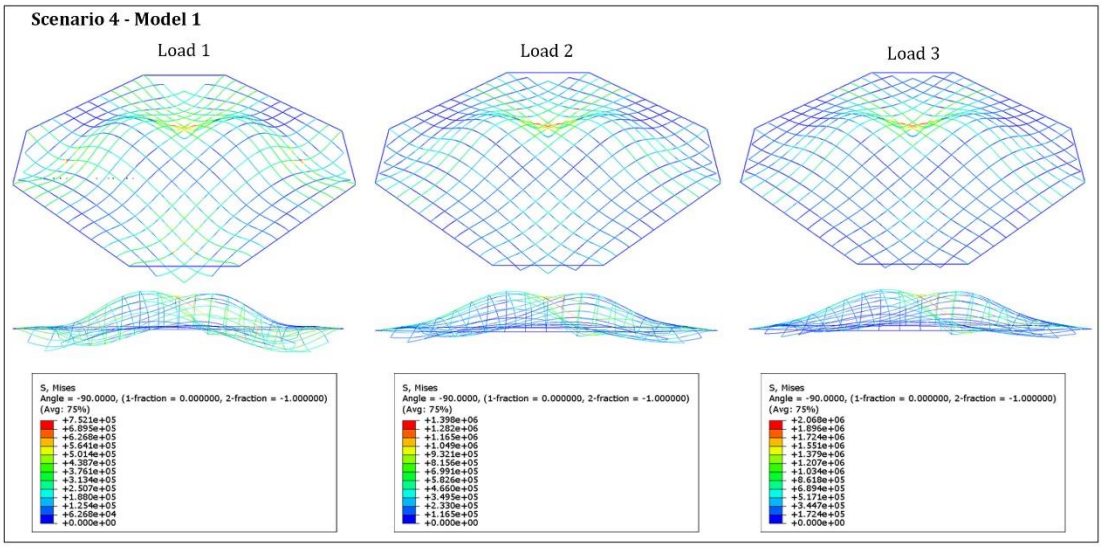


Figure 5-11. Stress distribution under the application of Scenario 4,

Structural analysis of full-culm bamboo gridshell using FEA in Abaqus revealed how different loading scenarios impact the models. These simulations, which excluded roofing and wind loads to isolate the material effects, demonstrated significant displacements primarily near boundary conditions under gravity load. External loads introduced in different scenarios further intensified deformations and stress concentrations, particularly at load application points. Stress distributions illustrated varying impacts on different sections of the structure, with perpendicular members showing lower stress levels. These findings underscored the importance of considering load magnitudes and positions in structural analysis, as higher loads at specific points can lead to localised stress concentrations, potentially resulting in structural vulnerabilities. Strategic load management is essential in design to mitigate stress concentrations and enhance overall stability of bamboo gridshell structures.

5.3.2. FEA Results of Model 2: Split Bamboo

Similar to simulations conducted on full-culm gridshell models, simulations on split bamboo excluded the roof and wind structures to isolate the material's impact on structural performance. External loads were applied following the same methodology as in Model-1. Figure 5-12 illustrates the deformed shape of Model 2 under gravity load, showing a maximum displacement of 4.15 cm at the apex area. The entire mesh exhibited deformation, with a slight elevation observed at the centre point. The gravity load was applied based on the input density of the bamboo split, highlighting its influence on the gridshell geometry.

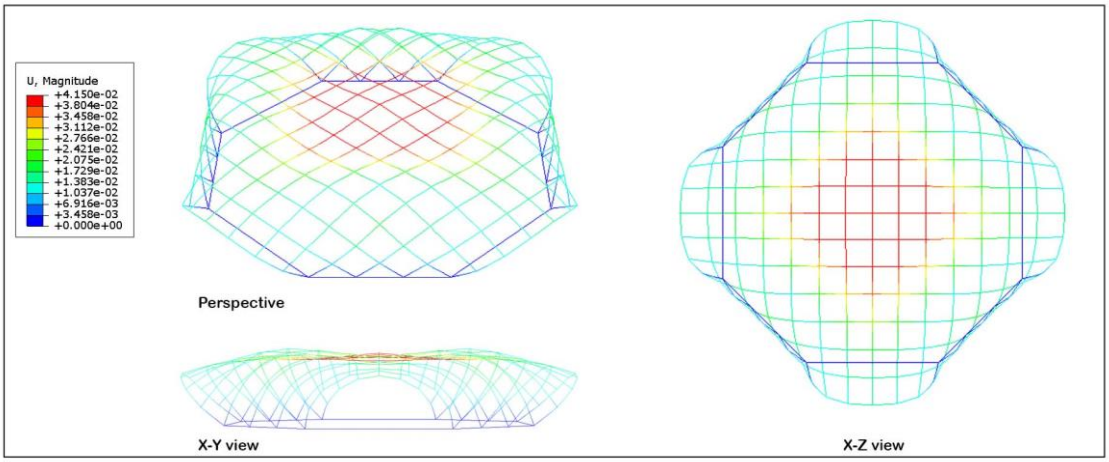


Figure 5-12. Deformed shape of Model 2 under gravity load.

Load application at the centre of gridshell model resulted in significant changes in deformed shape. Displacement observed under the first load application (Load 1) was measured at 4.84 cm, indicating a moderate effect on the structure. However, with the application of Load 2 and Load 3, displacements increased to 6.40 cm and 8.03 cm, respectively. These higher displacements visibly altered the deformed shape particularly at the loading point, as depicted in Figure 5-13. The deformed shape illustrated the structural response to increased loading.

Analysis of stress distribution revealed relatively even stress distribution across the gridshell model, with notable concentration observed at nodes. Interestingly, unlike Model-1, where grid members along the centre line experienced higher stress, in Model-2, these members exhibited lower stress levels. Conversely, grid members at the four sides of the structure displayed higher stress concentrations, indicating varying load distribution patterns compared to the previous model.

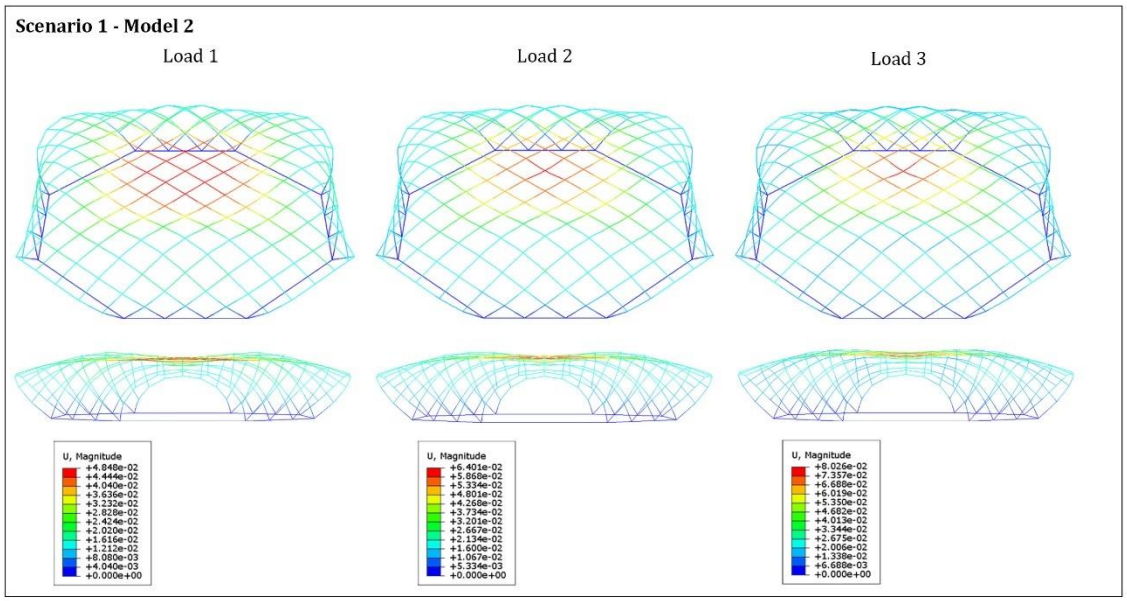


Figure 5-13. Displacement of Model 2 under scenario 1.

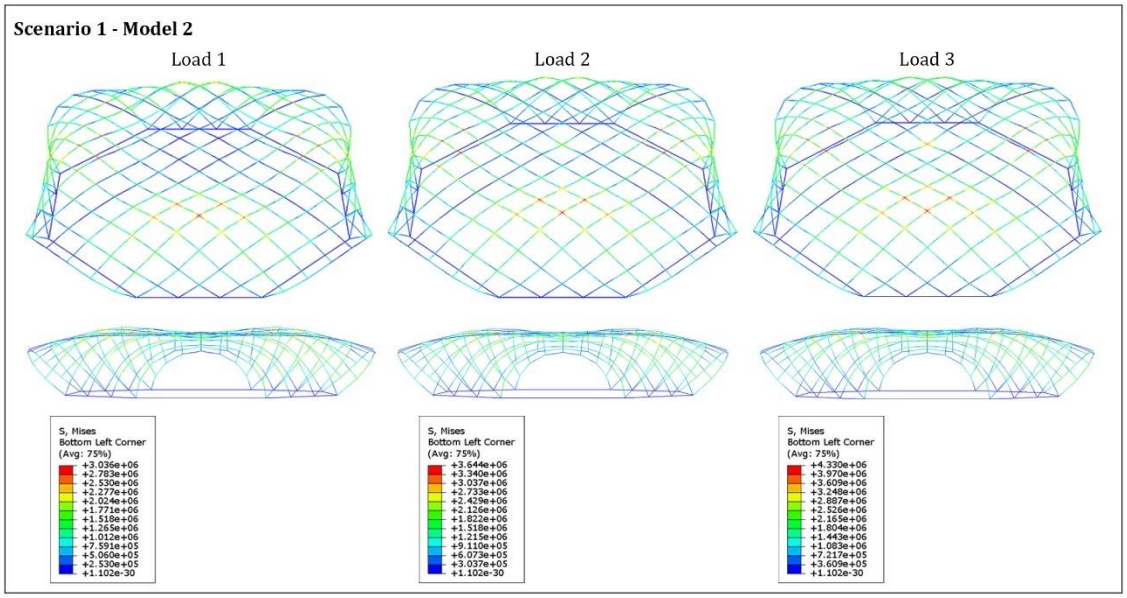


Figure 5-14. Stress distribution on Model 2 under load scenario 1.

Load application along the centre line (Scenario 2) resulted in significant displacement, as depicted in Figure 5-15. The first load (Load 1) induced a maximum displacement of 8.99 cm, demonstrating notable structural response. Subsequently, Load 2 increased the displacement to 13.85 cm, and Load 3 escalated it further to 18.70 cm. The deformed shape analysis indicated a slight elevation in curvature at the centre point, with decreasing deformation towards the perimeter, illustrating the structural response to increasing loads.

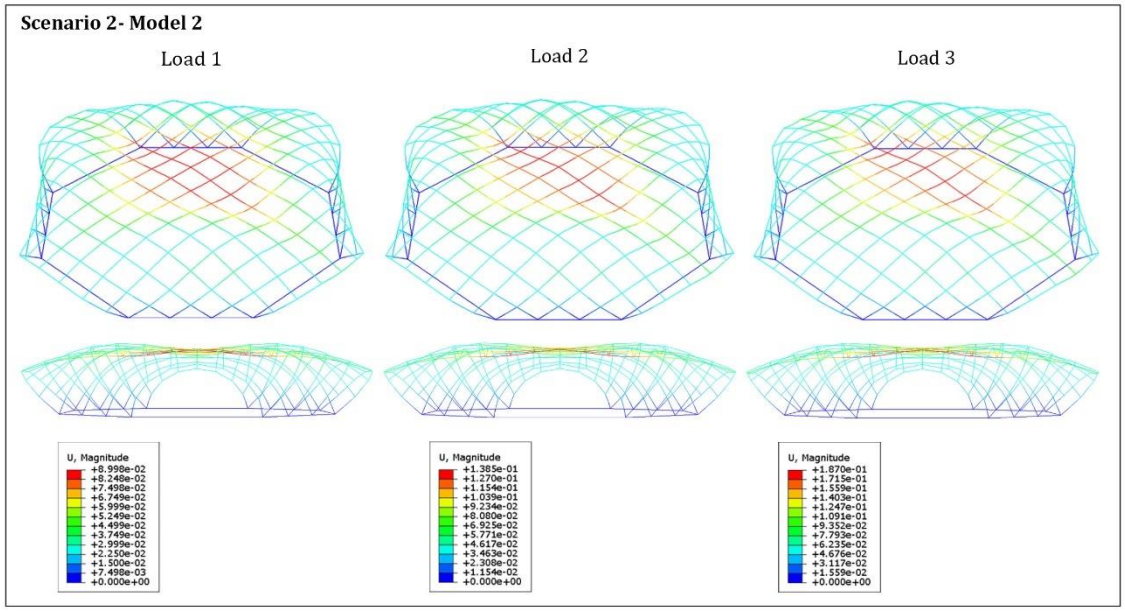


Figure 5-15. Displacement of Model 2 under load application based on Scenario 2.

Stress distribution, as illustrated in Figure 5-16, revealed localised stress concentrations in the four directions where the curvature lines intersected the anchors. These areas exhibited higher stress levels due to the concentrated load paths. In contrast, members along the centre line showed lower stress levels, suggesting they were effectively distributing the applied loads.

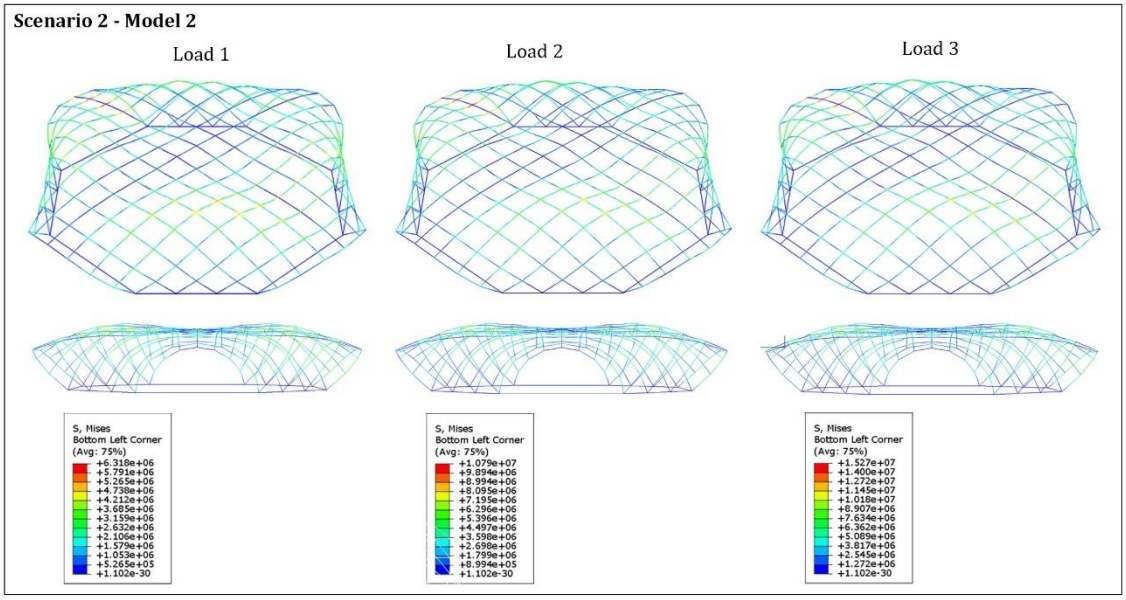


Figure 5-16. Stress distribution under Scenario 2 load application.

Load application along the diagonal line (Scenario 3) resulted in significant displacements, as observed in Figure 5-17. During the first load application, the maximum

displacement measured 6.70 cm, which increased to 9.25 cm during the second application, and further to 11.81 cm during the third application. The deformed shape analysis revealed a curvature that initially rose slightly at the centre point and then tapered downward towards both sides along the diagonal line, illustrating the gridshell response to the applied loads. Analysis of the stress distribution, depicted in Figure 5-18, highlighted areas of high stress concentration at nodal connections where point loads were applied. These areas experienced higher stress levels due to the direct load transfer through the gridshell structure.

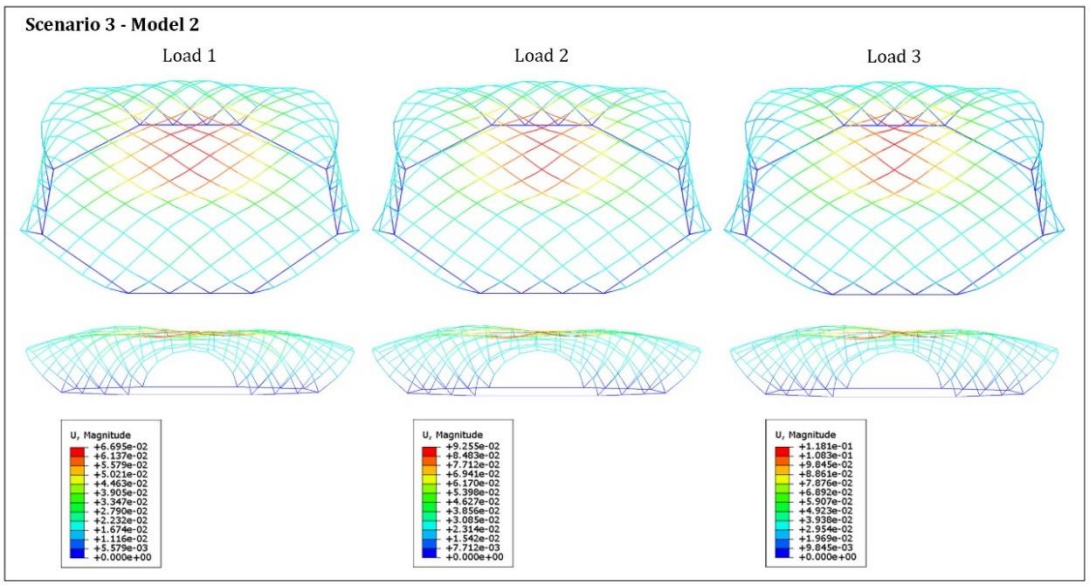


Figure 5-17. Displacement of Model 2 under load application of Scenario 3.

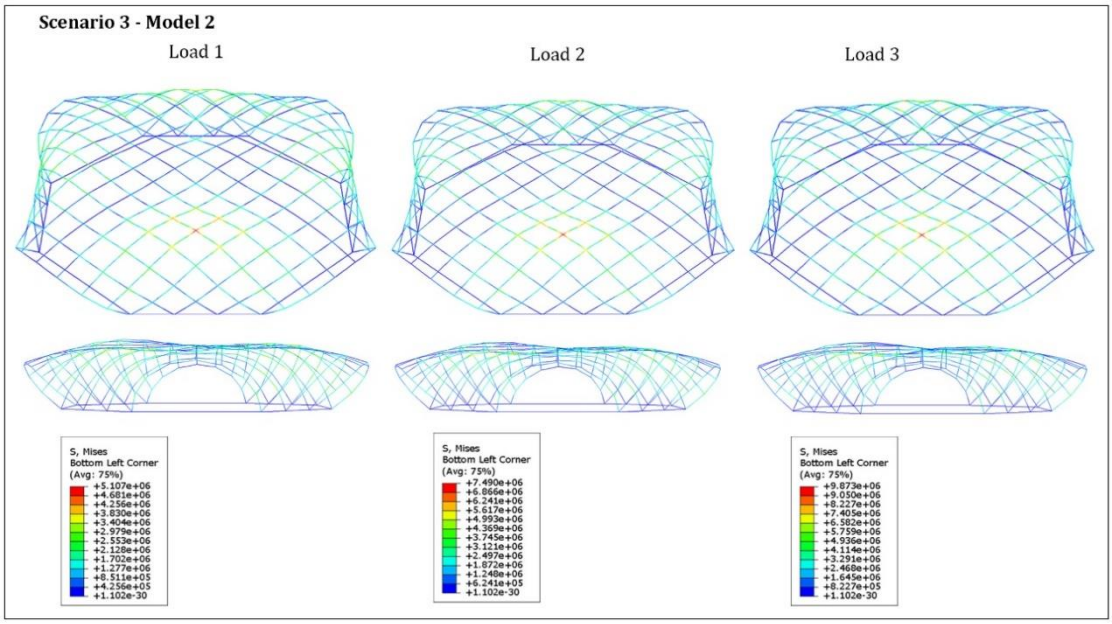


Figure 5-18. Stress distribution based on Scenario 3.

The application of a point load at an asymmetrical position (Scenario 4) resulted in uneven deformation across the structure, with maximum displacements concentrated around the loading location, as shown in Figure 5.19. Following the first load application, the maximum displacement measured 4.67 cm, which increased to 5.96 cm during the second application, and further to 7.69 cm during the third application. This progressive increase in displacement illustrated the cumulative effect of applied loads on the structural integrity of the gridshell model.

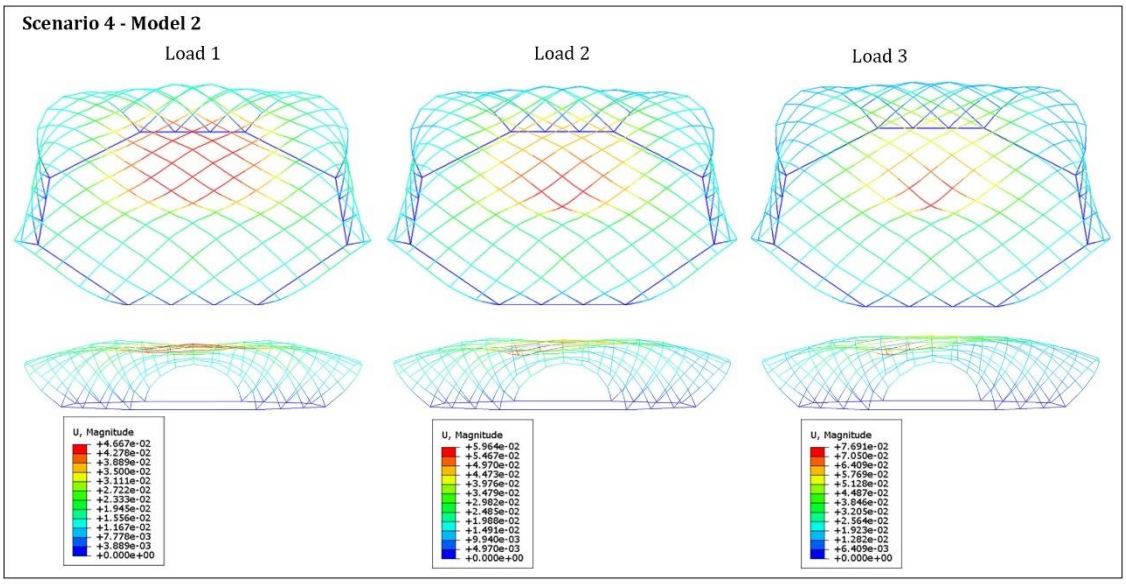


Figure 5-19. Displacement of Model 2 under load application of Scenario 4.

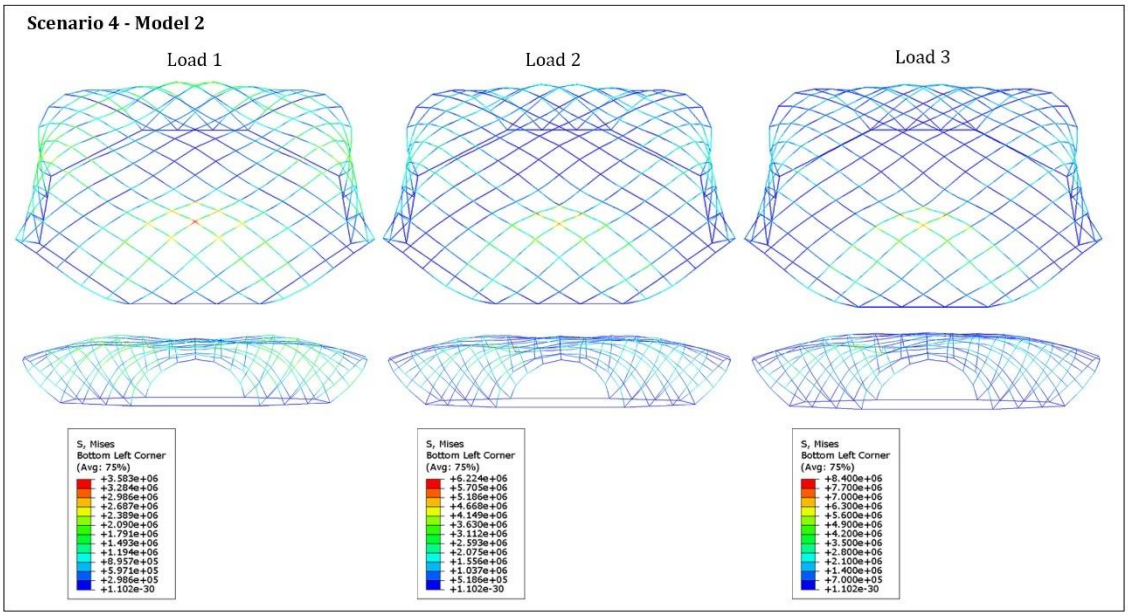


Figure 5-20. Stress distribution based on Scenario 3.

Stress analysis revealed significant concentration around the loading position, indicating localised stress points where the applied load was directly transferred through the structure (Figure 5-20). These areas experienced heightened stress levels due to the concentrated load, highlighting critical points in the structure that may require reinforcement or design optimization to mitigate potential structural vulnerabilities. High concentrations of stress was spotted at nodal connections and area near the point load, along with significantly deformed shape.

The simulations, excluding roof and wind structures to isolate material effects, demonstrated significant displacements primarily near boundary conditions under gravity load. External loads intensified deformations, with stress distributions showing varying impacts on different sections of the structure. In Scenario 2, load application along the centre line induced substantial displacements, reaching 18.70 cm under Load 3, with stress concentrations observed at nodes and higher stresses at the perimeter compared to the centre line. Similarly, diagonal load applications resulted in maximum displacements of 11.81 cm under Load 3, with stress concentrations observed at nodal. Conversely, point load applications at asymmetrical positions caused uneven deformations, with maximum displacements of 7.69 cm under Load 3 and stress concentrations observed mainly around the loading position.

5.4. Discussion

5.4.1. Comparative Study between FEA Results and Full-Scale Models

The structural analysis in this chapter involved simulating load applications to the gridshell models, while Chapter 6 details the load tests conducted during the construction phase. This section presents a comparative study focusing on the structural displacements od bamboo gridshell models analysed through FEA in Abaqus, compared with empirical data obtained from load tests conducted during construction, as detailed in Section 6.3.4. Model-1 experienced collapse and damage after the second load application, preventing further analysis. Consequently, the comparisons are based exclusively on the results from Model-2.

According to the load application based on the four scenarios (Table 5.4), the initial loading was applied at the apex or centre of the gridshell. Both Finite Element Analysis (FEA) and load tests recorded significant displacements around the loading position. Figure 5-21 presents a comparison of displacement data extracted from Abaqus simulations and physical measurements on a full-scale model.

The figure illustrates similar deformation patterns derived from the displacement data. The gridshell structure exhibited gradual deformation with notable displacement at the centre point, corresponding to the loading position. Displacements increased with the magnitude of loading, showing consistent patterns between FEA and load-test results, albeit with slight differences during the first loading application.

The curves resulting from FEA simulations for the first loading application showed relatively smooth curvature, whereas in the load tests, the curve exhibited a sharper peak at the loading point. For the second and third loading applications, both curves depicted significant displacement with a sharper peak at the loading point. Notably, the curves from the load test data had a more pronounced pointing shape compared to FEA data. This comparison in Figure 5-21 highlights that loading at the centre position induces pointed and sharp curvatures in both FEA and load-test scenarios.

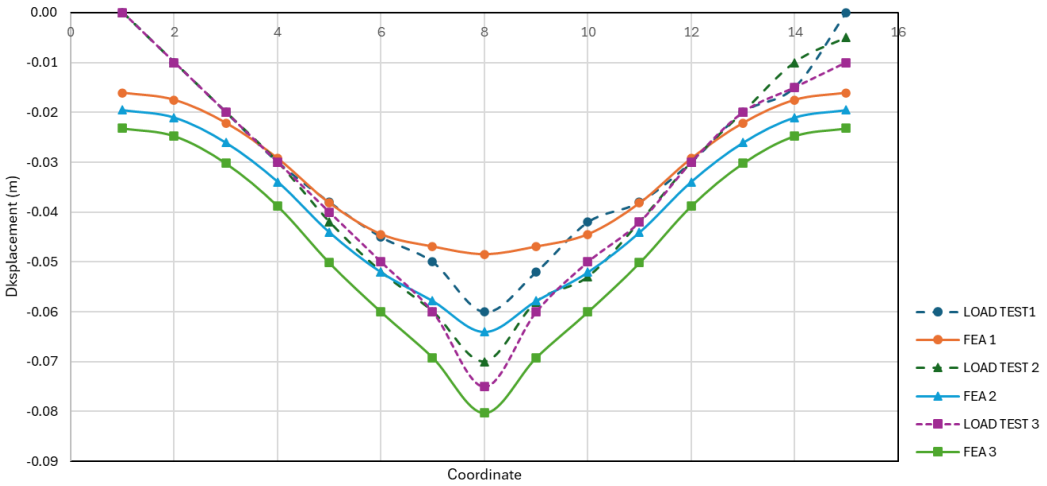


Figure 5-21. Comparison of displacement obtained from FEA in Abaqus and load-tests on full-scale model based on loading Scenario 1

In terms of displacement values, the data from load tests generally showed slightly smaller displacements compared to FEA, except for the maximum displacements during the first and second loading applications. Specifically, during the first loading application, the maximum displacement recorded from load tests was approximately 0.06 m, whereas FEA results indicated 0.048 m. Similarly, for the second loading application, load test measurements recorded 0.07 m compared to FEA's 0.064 m. During the third loading application, the maximum displacement from load tests was 0.075 m, slightly less than FEA's 0.08 m. These results indicate minor discrepancies between load test data and FEA predictions.

Scenario 2 involved hanging loads along the centre line in three stages of loading applications. Figure 5-22 presents deformation and displacement data from both FEA and load tests. The curve in the figure illustrates uneven displacement in the load test results, characterised by irregular peaks and troughs, whereas the FEA curve shows a smoother and more symmetrical curvature. The FEA curve indicates gradual displacement towards the centre area, with a slight elevation at the central node resulting in a small increment at the centre point.

Although the curves from the load test exhibit bumps and unevenness, the general patterns are broadly similar to those observed in FEA. As the gridshell gradually deformed, nodes at the centre and near-centre displayed similar displacements and tended towards flattening.

Upon evaluating the displacement data, overall measurements from the load tests consistently showed significantly smaller values compared to FEA results. Maximum displacements recorded from the load tests during the first to third loading applications were approximately 0.040 m, 0.060 m, and 0.080 m, respectively. In contrast, FEA predicted displacements of 0.089 m, 0.137 m, and 0.185 m for the same loading stages. These discrepancies highlight substantial differences between FEA predictions and actual load test outcomes.

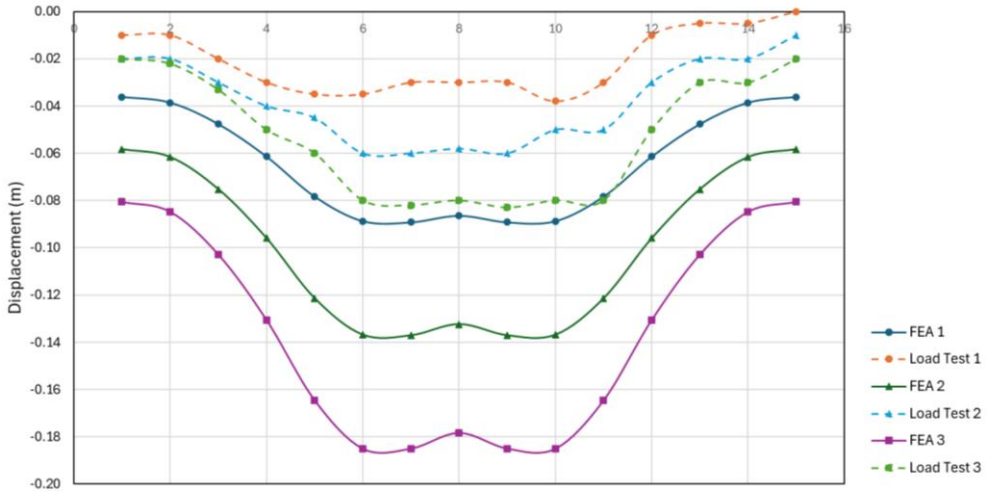


Figure 5-22. Comparison of displacement obtained from FEA in Abaqus and load-tests on full-scale model based on loading Scenario 2.

The load application along the diagonal line in Scenario 3 resulted in different deformation shapes between FEA and load tests, as depicted in Figure 5-23. The curvature shapes in the load test data were uneven and jagged, with pronounced displacement on one side and less deformation on the other. In contrast, FEA resulted in smooth and symmetric

curvature. These discrepancies indicate differences between computational simulation and physical construction. Computational models provide perfect geometry and conditions, whereas achieving such perfection in real construction is challenging, leading to inevitable discrepancies.

Examining the displacement data, overall results from the load tests showed lower displacements compared to FEA. However, the maximum nodal displacements recorded during the load tests were higher, measuring approximately 0.080 m, 0.100 m, and 0.110 m for the first to third load applications, respectively. In comparison, FEA data recorded maximum displacements of 0.064 m, 0.088 m, and 0.112 m for the corresponding applications.

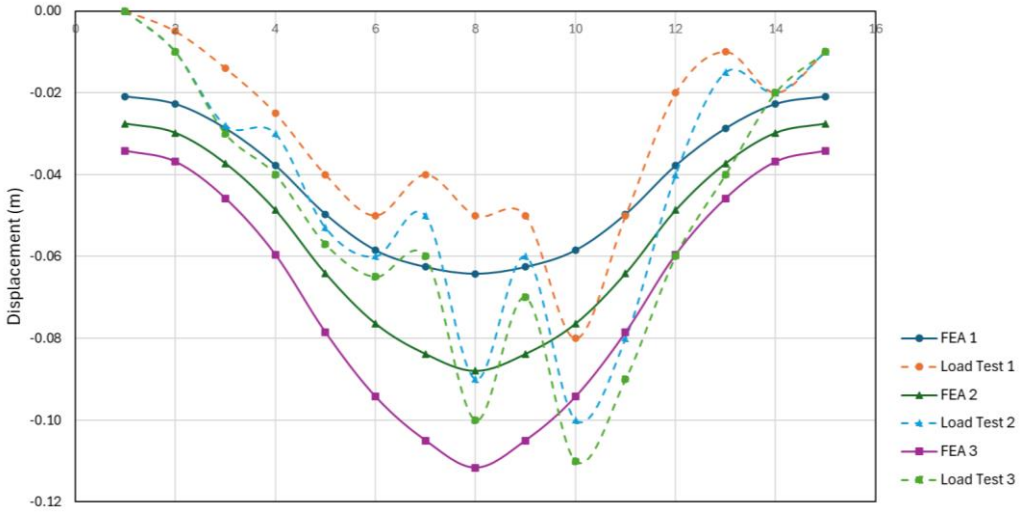


Figure 5-23. Comparison of displacement obtained from FEA in Abaqus and load-tests on full-scale model based on loading Scenario 3.

Load application at the asymmetrical position resulted in an asymmetrical displacement curve, as illustrated in Figure 5.24. The displacement curves from the load tests showed uneven patterns, with higher displacements observed on one side of the gridshell, particularly near the loading point. However, the overall patterns were relatively similar to those observed in FEA. The FEA curves exhibited smooth and consistent patterns, with higher displacements concentrated near the loading position. It is also noteworthy that the perimeter areas far from the loading point exhibited less deformation compared to the areas closer to the loading.

Overall, the displacement values from the load tests were smaller than those from FEA, with maximum displacements recorded from the first to third loading applications approximately at 0.045 m, 0.042 m, and 0.050 m, respectively. In comparison, FEA results showed displacements of 0.035 m, 0.051 m, and 0.059 m for the same loading stages.

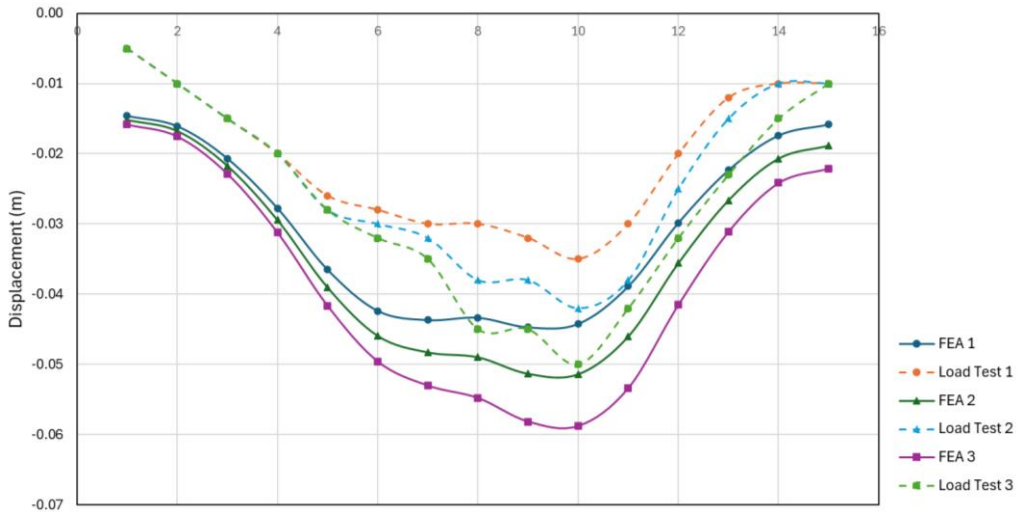


Figure 5-24. Comparison of displacement obtained from FEA in Abaqus and load-tests on full-scale model based on loading Scenario 4.

The comparative study on the displacement results from FEA and load test data reveals significant insights into the displacement patterns, shapes, and the effects of load magnitude, highlighting discrepancies between FEA and load test data. The displacement patterns generated from FEA data exhibit smoother and more measurable shapes that follow the load pattern. For instance, if the load position is symmetrical relative to the gridshell geometry, the displacement pattern is also symmetrical. In contrast, the curves from load test data result in uneven and jagged shapes. However, despite differences in the overall shape, the displacement patterns between FEA and load tests show similarities. Of the four load scenarios in load tests, three exhibited patterns similar to FEA results.

The spatial distribution of displacement between FEA and load tests indicates higher displacement near the loading points, demonstrating similarities in general spatial deformation. However, FEA often predicts more uniform deformation across the structure compared to the localised effects observed in load tests.

These results highlight the differences between computational models and real-world construction. Computational models are calculated under perfect conditions using algorithms, resulting in deformation that follows precise calculations. In real-world construction, various factors influence structural performance and stability. For example, the final geometry resulting from form-finding may not be built with accurate measurements, leading to misalignment of some members and positions, which can affect the overall stress distribution within the structure. These disparities suggest that while FEA can accurately predict overall trends, it may not fully capture the nuances and irregularities present in physical structures.

Regarding the effect of load magnitude on deformation, load test results generally showed smaller displacements compared to FEA predictions. However, there were instances where maximum displacements recorded during load tests exceeded those predicted by FEA, particularly in Scenario 3. This indicates potential underestimation in FEA models or overestimation in assumptions of structural rigidity. Environmental factors during construction could also contribute to these discrepancies. The full-scale models were constructed during the monsoon season with high precipitation in outdoor spaces. Rainfall occurred almost daily, and on the fifth day of construction, extremely heavy rainfall caused temporary floods around the neighbourhood and construction site. Considering bamboo is a hygroscopic material whose strength properties are affected by moisture content, weather conditions during construction might affect the material's strength properties. Regardless of the main cause, it is crucial to ensure the safety of the structure in FEA so that displacement in real-world construction is less than in FEA, ensuring its safety.

The discrepancies between FEA and load tests underscore the importance of validating FEA models with empirical data from load tests. The calibration process can enhance FEA accuracy in predicting real-world structural behaviour, particularly in determining suitable input parameters for the simulation, such as material properties. Accurate predictions of structural performance are crucial for ensuring structural safety.

In conclusion, although FEA has proven to be a reliable tool for analysing bamboo gridshell structures, its utilisation should be critically evaluated and validated against empirical data. This approach can mitigate potential safety issues arising from the unpredictability of bamboo. An integrated approach enhances the accuracy of structural predictions and supports decision-making in the design process.

5.4.2. Implications on Gridshell Structure Design

Findings from the comparative study between FEA and full-scale models suggest the importance of incorporating safety margins in the FEA to accommodate variations in material properties. Bamboo's anisotropic nature and sensitivity to environmental changes pose significant implications for its behaviour in gridshell structures. Adjusting material properties in FEA simulations based on international standards for bamboo structures is critical for accurately predicting structural performance. However, the observed discrepancies between simulation results and empirical load tests highlight the need for further refinement in incorporating material properties and accounting for environmental effects in design processes.

To enhance the structural performance and resilience of bamboo gridshell structures, design optimisation strategies must be employed. Refining boundary conditions, incorporating structural bracing, and optimising load distribution mechanisms are essential for mitigating deformation and stress concentrations. Iterative design processes and sensitivity analyses play a vital role in identifying optimal design configurations that balance structural efficiency with material limitations.

Moreover, achieving precise geometries in real-world construction is challenging compared to ideal conditions in FEA models. This study revealed that load tests on physical models often have uneven displacement curves, which might result from imperfections in the construction process. Improved construction practices and quality control are crucial for the successful construction of safe structures.

Environmental factors, such as weather conditions and moisture content, significantly impact the behaviour and durability of bamboo gridshell structures. Strategies for mitigating environmental effects through appropriate material treatment, construction practices, and maintenance protocols are essential for ensuring long-term structural integrity and sustainability. Considering these factors in design processes is crucial for achieving resilient and environmentally conscious structural solutions.

5.5. Summary

This chapter presents a detailed structural analysis of bamboo gridshell models using Finite Element Analysis (FEA) in Abaqus, focusing on both full-culm and split bamboo materials. The chapter examines deformation and stress distribution under various load scenarios, highlighting discrepancies between computational simulations and empirical load tests on full-scale model.

A comparative study of the split bamboo gridshell structure between the FEA model and the physical model revealed discrepancies between the results. However, despite these discrepancies, the overall performance showed similarities. The FEA models appeared more polished, while the physical models were more uneven and varied. These differences indicate several factors that influenced the results, such as environmental conditions, construction accuracy, and FEA input parameters.

Overall, this chapter demonstrates the effectiveness of FEA in analysing bamboo gridshells while emphasising the importance of empirical validation and practical considerations in achieving safe and reliable designs.

CHAPTER 6 | CONSTRUCTION OF BAMBOO GRIDSHELL

6.1. Overview

The construction phase, particularly the erection method, is crucial in determining whether a conceptual design of a gridshell structure can be realised. The erection process of elastic gridshell structures can be challenging and complex due to the need to assemble long members intertwined into a spatial structure. While unstrained gridshells, such as those made from steel, can be fabricated and assembled relatively straightforwardly, strained or elastic gridshells using bending-active members require complex methods to achieve their designated forms.

In general, erection methods for gridshell structures can be classified into lift-up, push-up, ease-down, and inflated (see Section 2.3.1). However, references to erection methods for bamboo gridshells are limited, despite several notable examples of bamboo gridshell structures having been built to date.

The ZCB Pavilion in Hong Kong is a prominent example of a bamboo gridshell in recent years. Designed and constructed by a team from the Department of Architecture at CUHK in 2015, the building represents a large-span, non-permanent gridshell structure entirely built from bamboo culms. The construction process involved lifting the members on top of bamboo scaffolding, manually bending them on site, and tying them to maintain the form. It was reported that several errors, amendments, and corrections occurred on site due to interconnection problems, installation errors, annotation errors, and the bamboo's bending behaviour (Crolla, 2017, 2018; Crolla & Fingrut, 2016).

The Cloudscape Pavilion in Hangzhou, China, is another non-permanent bamboo gridshell, designed as a free-form gridshell built using a combination of strained and unstrained methods. Several members were bent before assembling using hot bending methods; however, no details were provided regarding the methods, such as the heating techniques and how the local craftsmanship bent the members. The pre-bent members were assembled with other members on site using scaffolding (Huang & Zhou, 2018). The record did not mention the diameter of the bamboo poles and the species; however, images showed that the bamboo had a very small diameter (Figure 6-1a).

Rockwood (2015) explored the construction through experimental methods by building several scaled models of bamboo gridshells, investigating the connections, assembly, and erection methods. The experiment used *Phyllostachys vivax*, with an outside diameter of 2.5

cm to 4 cm and a wall thickness of 3 mm to 5 mm. The erection methods involved manually bending and pushing up the straight members (Figure 6-1b). Rockwood used both full-culm bamboo and split bamboo. Rockwood's experiment demonstrated various construction methods and connector systems; however, further investigation is needed into the gridshell's load-bearing capacity and the feasibility of implementing these methods for larger span structures.



Figure 6-1. a. Cloudscape Pavilion inside China Academi of Art; b. Erection process of bamboo gridshell during the workshop by David Rockwood.
Source: (Huang & Zhou, 2018; Rockwood, 2015)

A notable example of a permanent gridshell building is The Arc, a gymnasium hall located within the Green School campus (Figure 6-2). The structure consists of arches, with gridshell structures made from split bamboo laid between the arches, creating membrane-like surfaces. The anticlastic shell form was intended to optimise bamboo's tension properties, as the tensile strength of bamboo fibres is significantly higher than their compression strength. The arches use full-culm bamboo, while the gridshells use split bamboo formed into double layers. The connections are fixed using small nuts and bolts. Unfortunately, there is no published record on the construction methods, particularly how the gridshells were laid between the arches.

Compared to the construction and erection methods of timber gridshells, literature and information regarding bamboo gridshells are not as extensive as other materials such as timber and steel. Some factors remain unanswered; for instance, bamboo's hollow, node-and-internode-composed nature may influence the bending methods and the depth of curvature. Based on Rockwood's experiments (2015), it was recognised that buckling and splitting were significant challenges in achieving desirable curvature. Numerous bamboo poles snap and break during the bending process.



Figure 6-2. Gymnasium building in Green School, a. View from the interior; b. Details of the jointing and connections; c. Layers of the gridshells; d. Combination of arches and gridshell.

Meanwhile, during the construction of the ZCB Pavilion, one major challenge was due to the varied properties of bamboo, which led to many corrections and modifications on site (Crolla, 2017). Additionally, realising a gridshell structure from computational design into construction is challenging. These issues raise questions on how to construct a bamboo gridshell, whether the erection methods for timber gridshells are suitable for bamboo gridshells, and whether gridshell designs can be directly realised in construction.

Based on these considerations, this chapter focuses on the following objectives:

- To identify the suitable erection methods when bamboo is the material used for the lattice.
- To evaluate the impact of the construction methods on the structural integrity and durability of bamboo gridshell.

Therefore, to achieve these objectives, experiments in this study were carried out by building full-scale models of bamboo gridshells and conducting load tests.

6.2. Material and Methods

The experimental research method achieved its objectives by constructing physical models of bamboo gridshells. The construction process took place within the Petra Christian University campus in Surabaya, Indonesia. Initially, there were plans to hold a workshop involving student participation. However, due to the COVID-19 pandemic and associated restrictions in 2021, the construction was carried out by hiring construction workers. Five construction workers were hired from Sahabat Bambu, a community-based enterprise that provides services such as bamboo supply, preservation, construction, and conservation. Although the workers had extensive experience in bamboo construction based on local craftsmanship, it was their first time constructing a bamboo gridshell and employing the bending-active principle.

The entire construction phase comprised pre-construction, construction, and load tests, which the workflow was as depicted in Figure 6-3. The pre-construction stage was a continuation of the form-finding process outlined in Chapter 5 and the experimental phase aimed to determine the maximum depth of curvature achievable by the culms. This process was iterative, with form-finding informing the design and tests providing information on the maximum curvature, which then influenced revisions to the design. Tests on the depth of curvature also aimed to investigate potential failures and characteristics of failures, particularly when heat was applied during the bending process. Data from the pre-construction phase were used to determine the final forms and identify suitable erection methods for the two models.



Figure 6-3. Construction workflow of full-scale model and load tests.

During the construction phase, two bamboo gridshells were erected, with one structure utilising full-culm bamboo while the other used split bamboo. The construction stage aimed to investigate suitable erection methods and identify any arising problems. In the final stage, load tests were conducted by imposing loads on the full-scale models to assess the structures' ability to withstand loads.

6.2.1. Material Selection and Preparation

Model-1 utilised the full-culm bamboo with *Gigantochloa apus* as the chosen species, with diameters ranging between 4 cm to 8 cm and an age of 3-4 years. The decision was based on the findings outlined in Chapter 4. The bending test results, cross-sectional analyses and curvature assessment indicated that *G. apus* demonstrate superior performance characteristics for bending-active structures compared to the other two species investigated. The choice of *G. apus* provided an opportunity to explore its potential suitability for larger span gridshell structures and aligning with the research objective of assessing the viability of Indonesian bamboo. This is particularly relevant as many tropical Indonesian bamboo species exhibit moderately large diameter, offering potential advantages over smaller-diameter alternatives.

The bamboo culms used for Model-1 were freshly harvested from Magelang, Central Java, and transported to the construction location in Surabaya within two weeks of harvesting (Figure 6-4 and Figure 6-5a). The length of each culm was approximately 6 meters, adhering to transportation regulations and logistics constraints. Upon arrival at the construction site, the bamboo culms were stacked and propped up to prevent direct contact with the ground. This precautionary measure aimed to mitigate exposure to soil moisture, particularly rainwater, given that construction took place during the heavy monsoon season.

Model-2 utilised split bamboo taken from *Dendrocalamus asper* (Figure 6-4 and Figure 6-5b) with a diameter between 9 cm to 15 cm and an age of 3-4 years. *D. asper* features a thick wall measuring between 8 mm to 20 mm, ensuring that the strips are sufficiently thick. The entire culms of *D. asper* were manually broken into long pieces and subsequently cleaned into strips, as the laboratory had limited cutting equipment available. These culms originated from the same batch as the culms used for material test specimens, which had undergone treatment with Borax Boric acid solution and had been stored in the laboratory for at least eight months, ensuring they were in a dry condition.

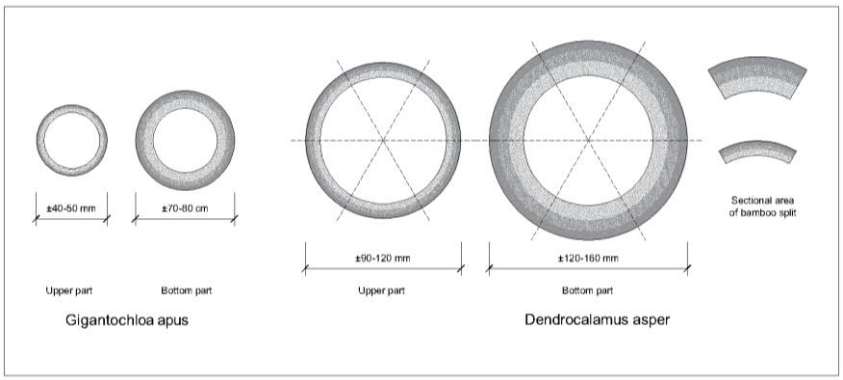


Figure 6-4. Sectional area of the bamboo species selected for construction.



Figure 6-5. Materials for the construction: a. Bamboo Gigantochloa apus for Model 1; b. Bamboo Dendrocalamus asper for Model 2.

6.2.2. Pre-Construction: Test on Bamboo's Depth of Curvature

Before constructing the full-scale models, it was essential to test the depth of curvature a bamboo culm can achieve. Although the material test of bending perpendicular to the fibres had provided the bending strength and information regarding maximum deflection, the methods used to bend the bamboo could affect the depth of curvature. Methods for bending bamboo culms commonly used in Indonesia can be categorised as heating and slicing. Heating methods utilise heat sources, which can be applied through boiling, steaming, or using fire. Applying heat to a bamboo culm can soften the fibres, allowing them to be bent. The slicing technique involves cutting half of a bamboo pole in a V-shape and then gluing it to reconnect the poles (Figure 6-6). This method is straightforward and has been a common practice in Indonesia. The majority of bamboo arches in prominent buildings, including those in Bali and other parts of Indonesia, were formed by slicing the bamboo culms.

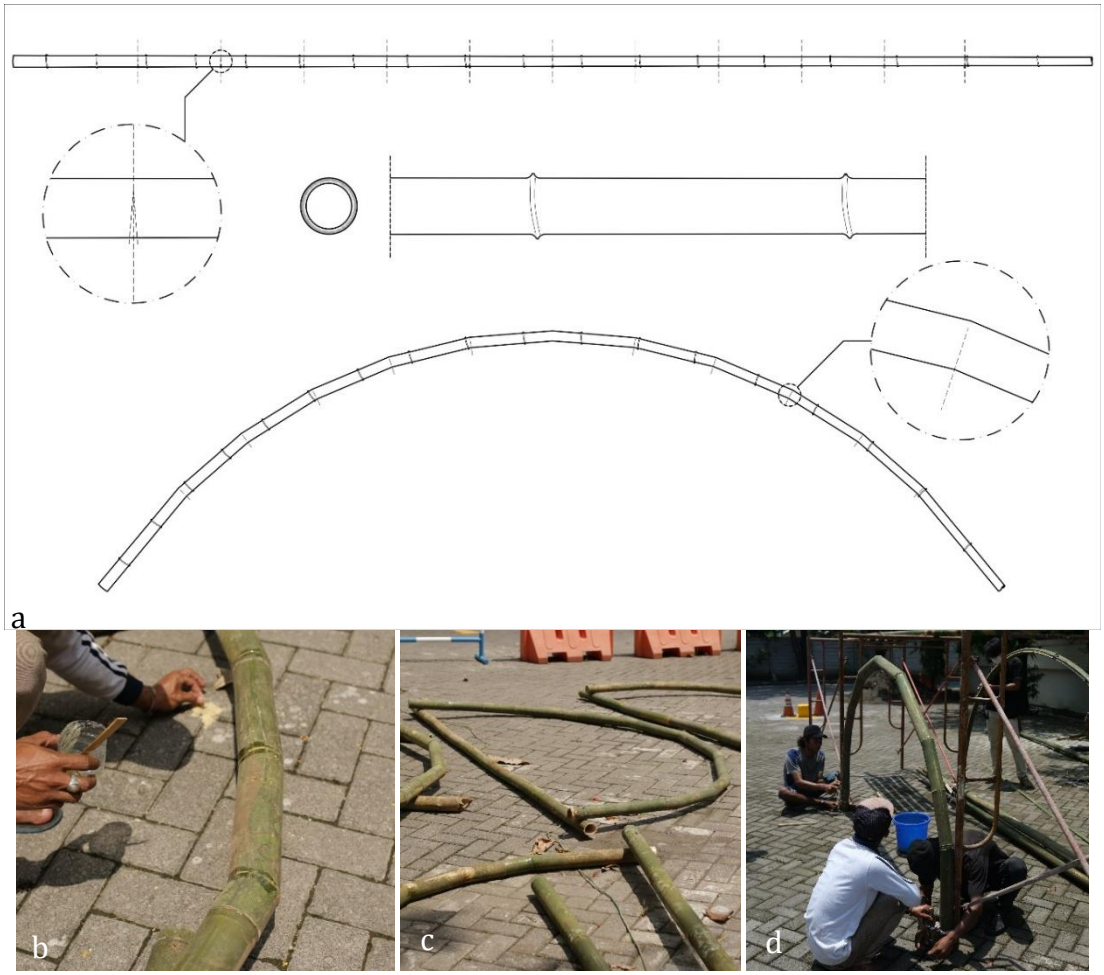


Figure 6-6. Illustration on bending method of bamboo culm using slicing method; b-d. Example of arches made using slicing method.

The slicing technique produced a non-smooth curve. Although considered uncomplicated and convenient, this method can reduce the strength of the bamboo because slicing cuts through the continuity of the fibres, leaving only a small strip to bear the loads. Furthermore, the deeper the required curvature of the arches, the shorter the slicing distance must be. Consequently, slicing significantly reduces the strength capacity of the bamboo culms, rendering the structure prone to collapse. Additionally, the strength of the glue and the quality of the craftsmanship also play critical roles in determining the load-bearing capacity of the arches. In some instances, a structure may collapse suddenly due to failures at the slicing points (Figure 6-7).



Figure 6-7. a. Example of failures due to breaking at slicing; b-c. Details showed the failure of slicing.

The slicing technique was not utilised in this research; instead, the bamboo culms were manually bent to align with the research objectives of employing bending-active principles for bamboo gridshell structures. In this experiment, the heating method using fire was applied. A bamboo pole, approximately 6.00 metres in length, was positioned atop two scaffolds, and a rope was attached at the pole's centre. The rope was secured in such a way that it could be shortened by twisting a small blade located in the middle. Ratchet straps were used instead of ropes (Figure 6-8). A gas torch was employed to soften the bamboo's fibres, making the pole more pliable and enhancing the depth of the curve. Water was regularly applied with a cloth to prevent the culm from overheating.

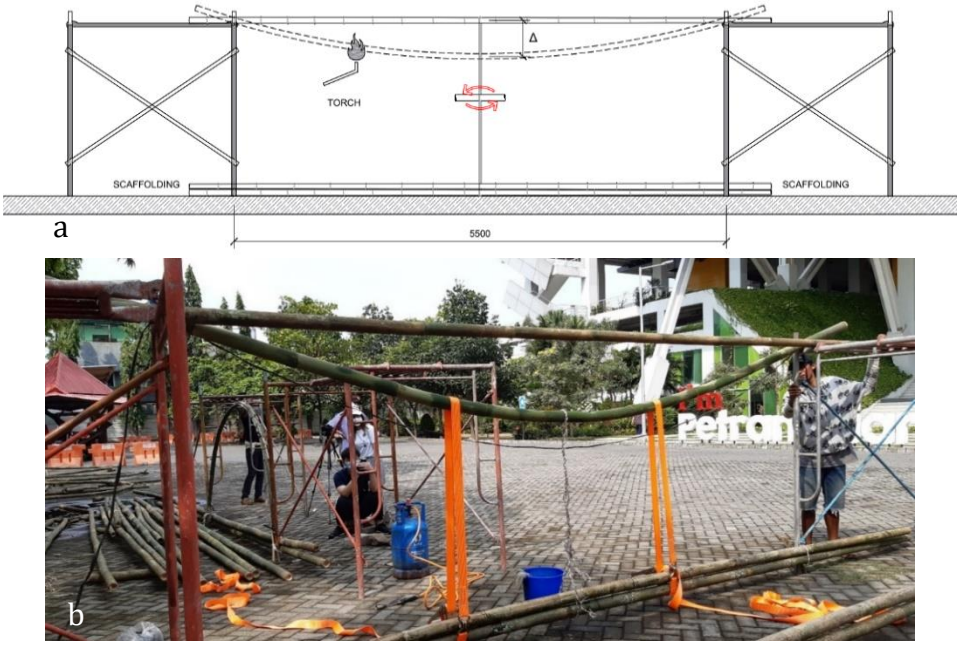


Figure 6-8. Illustration of bending bamboo experiment set to identify the depth of curvature.

Besides gathering data on the depth of curvature, the test was crucial to determine the bending and erection methods for the entire structure. An additional experiment was

conducted by placing a bamboo pole atop scaffolding, then bending it by tying the two ends and progressively shortening the rope. This method was anticipated to function similarly to the erection process of timber gridshells, wherein a timber gridshell is formed by either pulling up or easing down from a flat grid. However, the results from this experiment indicated that the method was both ineffective and hazardous. The bamboo culm proved difficult to bend, being both hard and tough. While it was feasible to pull down individual bamboo poles, pulling up or easing down became exceedingly difficult and burdensome once the poles were interconnected into a flat lattice. Furthermore, the bamboo pole tended to swing back towards its original form, posing significant risks to the workers; there was a potential for injuries or accidents if the bamboo reverted to its natural shape. During one of the experiments, the bamboo poles swung back and nearly caused injury to the workers. Consequently, any bending method adopted should carefully consider these safety concerns.

6.2.3. Construction Part 1: Model-1

The modelling was undertaken in Rhinoceros using the Grasshopper plug-in, as detailed in Chapter 5. The initial design conceptualised a synclastic gridshell achieved by pushing the four corners until the maximum curvature was attained. However, the experiments on the depth of curvature, as discussed in Section 6.2.2, highlighted significant challenges. It was difficult to bend the bamboo using the intended method, as bamboo, particularly Gigantochloa apus with diameters ranging from 4 to 8 cm, was tough and exhibited a low radius of curvature. Furthermore, during bending attempts, the bamboo tended to spring back to its original form, posing a risk of injury to the workers. Given these safety concerns, the complexities of bending bamboo, and the most appropriate construction methodology, it was decided to erect the structure by laying and bending the bamboo into arches individually.

Results from the depth of curvature tests also necessitated adjustments to the design. The initial dimensions proved unsuitable for construction using full-culm bamboo, as it produced a lesser depth of curvature. Consequently, constructing a gridshell of small dimensions would not achieve significant curvature. Therefore, in this experiment, the dimensions and form of Model-1 were modified from the initial design of 8.40 x 8.40 m to 10.80 x 10.80 m in order to raise the apex's height. The perimeter was redefined into an octagonal shape, acting as boundary conditions.

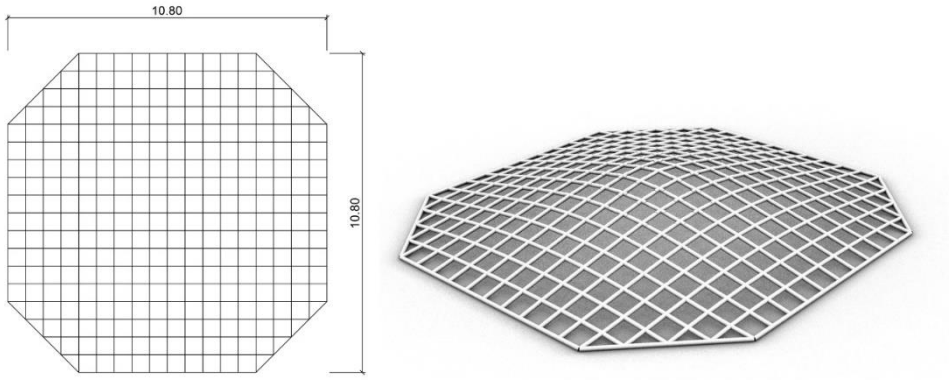


Figure 6-9. Final design of Model 1 for full scale model.

Prior to construction, a 1:50 scaled model was constructed to aid the understanding of the grid configuration and arrangement for the construction workers. After a discussion with the construction workers, we deliberated on potential and safe methods for erecting the gridshell, taking into account the insights gained from the experiments on determining the depth of curvature and bending bamboo poles. It was determined to erect two main arches initially and then gradually lay down the remaining arches until the grid structure was formed. The arches were then securely fastened to the boundary.

6.2.4. Construction Part 2: Model-2

The form finding process for Model-2 was conducted in Rhinoceros using the Grasshopper and Kangaroo plug-ins. Model-2 utilised the initial model developed for Model-1, wherein the form was achieved by inwardly pushing the corners of a flat lattice until it attained a curvature enclosing space. As split bamboo is more flexible compared to full-culm bamboo, the apex height for Model-2 was designed to be significantly higher than that of Model-1. During the form finding process, it was anticipated that the apex would reach a height of 2.50 m, and the four corners could be moved inward as far as 1.80 m (Figure 6-10).

A 1:50 scale model was crafted to illustrate the erection process and determine the appropriate method. This scaled model, made from rattan with a diameter of 2 mm, was presented to the workers. In addition to depicting the model, the connectors were also explained. It was deemed crucial to design flexible connectors during the erection phase, which could be fixed once the desired form was achieved. Following discussions, it was decided that the gridshell would be erected by initially constructing flat grids on the ground, then pulling them up using chain blocks and pushing the corners inward until the maximum curvature was reached. Wire was chosen to tie the connectors, allowing them to be fixed at the end of the form finding process.

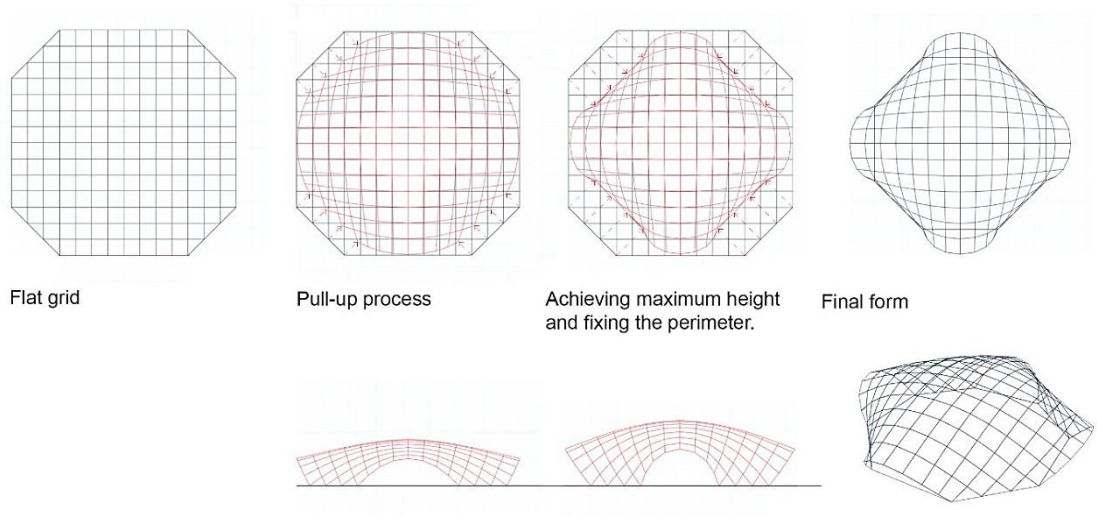


Figure 6-10. Form Finding of Model 2 using split bamboo.

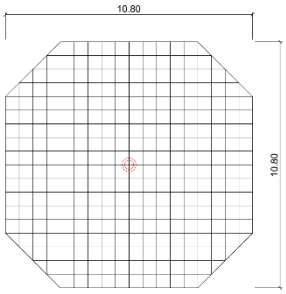
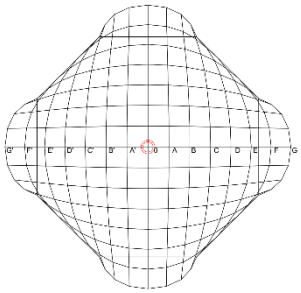
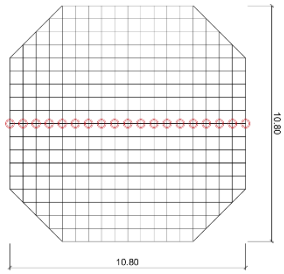
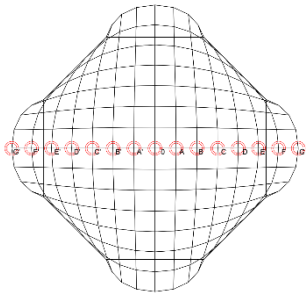
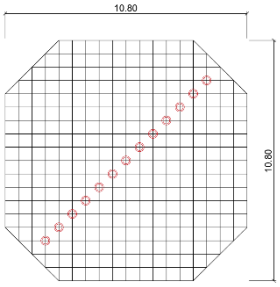
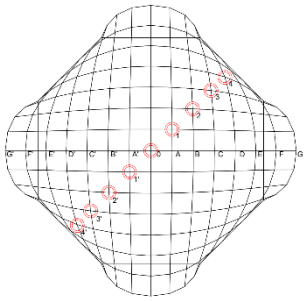
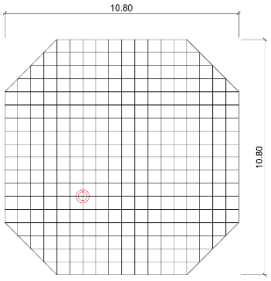
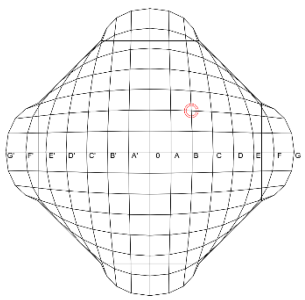
6.2.5. Experimental Set-up for Load Test

Load tests were conducted on the day following the completion of the models, involving the application of loads such as steel plates and concrete bricks. The loads were distributed based on four predefined scenarios: concentrated loads at the centre point, along the centre line, diagonal line, and asymmetric position (Table 6.1). Prior to application, the loads were measured, and deflections were recorded using a meter tape and laser meters.

Originally, it was intended to elevate Model-1 by installing bamboo posts beneath the roof structure and then suspending the loads for testing. However, due to safety concerns, it was decided to conduct the load tests without elevating the structure. Load tests can be unpredictable, and the risk of structural collapse presents a serious safety hazard during testing. Therefore, the loads were directly placed on top of the structure, specifically at the connector points. This approach minimised the risk of injury in the event of structural failure. Load application for Model-2 involved suspending buckets and placing concrete bricks inside them.

Throughout the testing process, safety protocols were strictly adhered to, ensuring that the loads remained within the structural capacity of the models. Testing was promptly halted at the first sign of damage or potential collapse to mitigate any risks.

Table 6-1. Point loads position on the full-scale models.

Model 1: Full-culm bamboo	Model 2: Split bamboo
Scenario 1: Centre point/apex	
	
Scenario 2: Centre line	
	
Scenario 3: Diagonal line	
	
Scenario 4: Asymmetric point	
	

6.3. Results of the Construction Process

6.3.1. Bending Test and Depth of Curvature

Findings from the experiment on the depth of curvature of bamboo culms revealed limitations in bending capabilities. Based on the experiment, the average depth of curvature achievable with G. apus, derived from bending 10 bamboo culms, ranged around 60-65 cm. These results indicated a restricted radius of curvature. Recorded characteristics of failures

during the experiments primarily included buckling, stress concentration, and fibre shrinking.

Buckling-induced failure is evident in (Figure 6-11a), where splitting and visible buckling occurred at the upper part of the culm. This failure stemmed from the bamboo fibre's inability to withstand compression stress, as observed in similar failures during bending parallel to the fibre test and discussed in Section 4.3.4. Buckling in bamboo culms necessitated crucial consideration due to its potential to cause splitting throughout the culm and consequent collapse of the entire structure.

Failure attributed to stress concentration was caused by stress focused on the rope point, where force was applied to bend the bamboo. When the culm was pulled down to create curvature, stresses concentrated at the rope placement position, leading to local buckling or crippling of the culm, resulting in significant failure of the entire beam (Figure 6-11b).

Additionally, failures occurred due to stress induced by thermal or heating effects. Heating softened the bamboo fibre, increasing its flexibility to achieve deeper curvatures. However, upon removal of heat and rapid cooling, fibre shrinkage could result in breakage and splitting (Figure 6-11c). Attempts were made to continuously heat and bend the bamboo on the construction site until significant curvature was achieved, producing deeper curvature than without heating. However, upon cooling, the bamboo culms unexpectedly broke

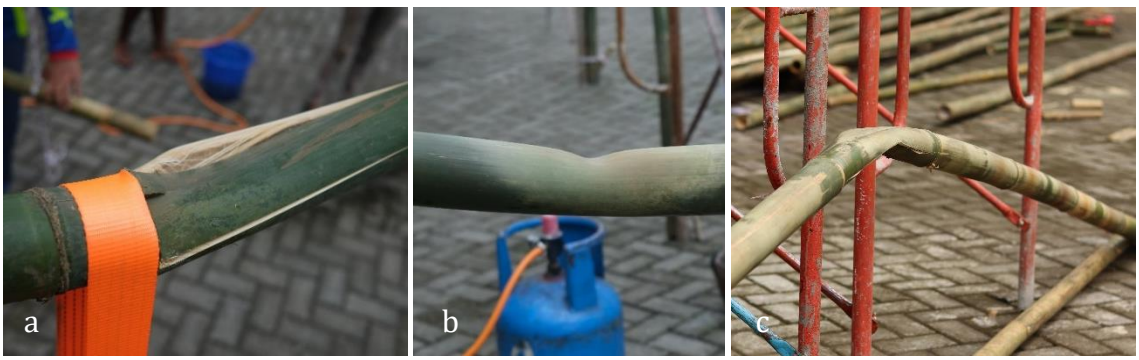


Figure 6-11. The characteristic of failures: a. Buckling, b. Stress concentration, c. Fibre shrinking after heating due to thermal loss.

6.3.2. Construction of Gridshell Structure Model Using Full-culm Bamboo

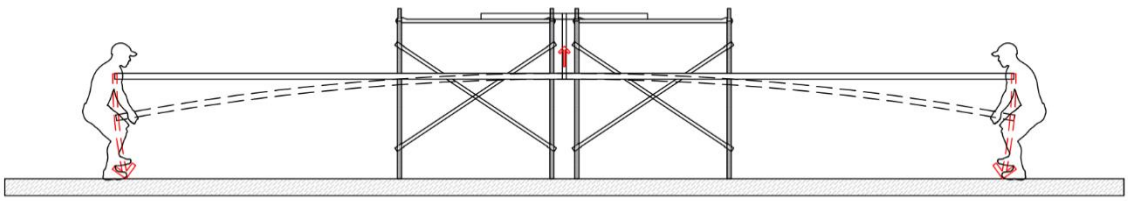
The initial step preceding the construction of Model-1 involved determining the optimal apex height based on empirical findings regarding the depth of curvature. Based on the bending experiment, the average depth of curvature for bamboo species *Gigantochloa apus*, with a length of 6 metres, ranged from 60 to 65 cm. Consequently, to elevate the apex, the span was increased from 8.40 m to 10.80 m, while maintaining a grid size of 0.6 x 0.6 m.

The construction approach for Model-1 required assembling two central arches and subsequently positioning additional members in alignment with the initial arches. Form finding was achieved by individually bending the members, avoiding timber gridshell erection methods such as pull-up, push-up, and ease-down, primarily due to safety considerations and limitations in bamboo culm bending capabilities.

Initially, an arch was crafted by joining two bamboo culms on the ground to form an elongated pole. Two sets of scaffolding were erected closely, and the elongated pole was gradually raised while two workers applied downward pressure on its ends. This process resulted in the construction of an arch reaching approximately 1.20 m in height. To prevent the elongated member from reverting to its original straight shape, the pole was secured to the scaffolding, and an additional bamboo pole was laid on the ground and tethered to the two pole corners (Figure 6-12a&b).

Subsequently, the second arch was erected by placing a long pole atop the first arch. The pole was slowly bent into an arch by gently pulling its tips towards the ground, taking great care to prevent buckling and breakage. Once the tips reached the ground, another pole was laid on the ground, and the tips were secured, forming the second arch (Figure 6-12c). Additional scaffolding sets were assembled to maintain the shape of the second arch.

Upon completion of the two arches, eight additional poles were laid on the ground to delineate the perimeter or boundary of Model-1. These poles served as a mould for the boundary and provided guidance for constructing subsequent arches (Figure 6-12d). Several shorter poles were temporarily installed beneath the arches to preserve their curvature.



a



b



Figure 6-12. a. Illustration of method in bending the bamboo poles; b. The first arch; c. The second arch; d. ground grid as guidelines.

The subsequent step involved assembling four arches at the D, H, 1, and 2 axes to establish the desired shape (Figure 6-13a-b). The process mirrored that of the second arches. Bamboo poles were positioned at the central point directly beneath the first and second arches. Subsequently, the central point was elevated until reaching the first and second arches, while two workers lowered the poles' tips and secured them to the perimeter. All connections employed non-fixed connection types, using ropes solely to maintain the form. Throughout this stage, all scaffolding was dismantled and substituted with short poles serving as temporary supports.

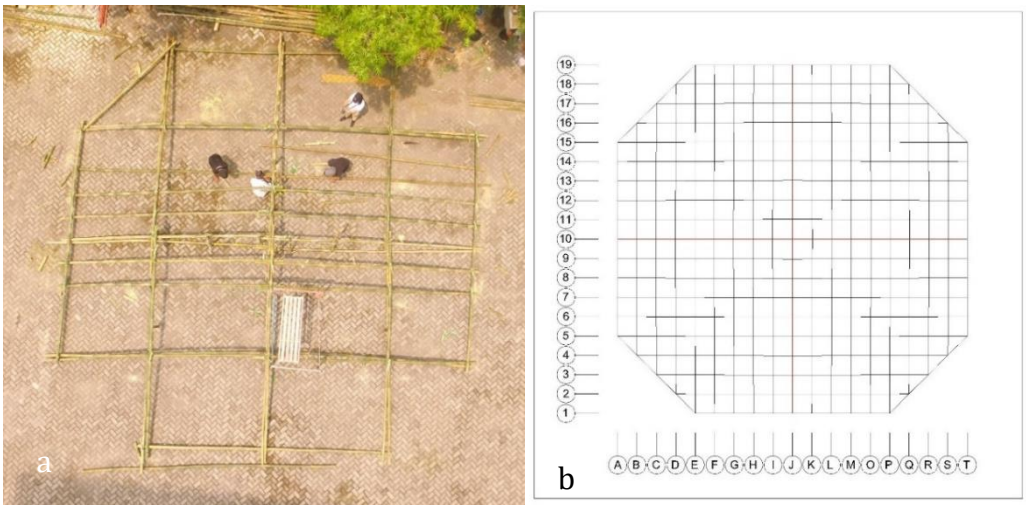


Figure 6-13. a. Early construction stage of Model 1; b. Grids arrangement and axis.

After the initial arches were erected, the remaining arches were assembled using the same method until all grid members were interconnected, forming a lattice structure (Figure 6-14a). All members were manually bent without employing any specific techniques. Consequently, to ascertain the maximum height the structure could attain, the bamboo culms were heated using a torch. The workers continuously applied heat and water to prevent cracking during the heating process (Figure 6-14c). A tripod was then erected, and the lattice was elevated using a chain block to increase its height (Figure 6-14b). Short bamboo poles were swiftly installed beneath the arches to sustain the height and curvature.



Figure 6-14. a. The workers were completing Model-1; b. Raising the height by pulling the gridshell using a chain block; c. Heat application to add the curvature.

During construction, it was necessary to connect two bamboo culms because the length of each member exceeded six metres. To extend the members, an internal union jointing method was used, as depicted in Figure 6-15. This technique is commonly used by bamboo craftsmen in Indonesia. Two bamboo culms were joined by inserting smaller bamboo tubers inside the two bamboo culms, and wires were tied around the tips to tighten the joint.



Figure 6-15. Jointing technique using internal union; a. The smaller bamboo tube was inserted; b. Two bamboo culms were connected; c. Position on other culms.

The second method for lengthening the members involved overlapping two bamboo culms and tying them together (Figure 6-16). The overlap was placed on top of other arches. From the construction process, it was found that the first method produced better curvature compared to the second method. Lengthening the bamboo pole by overlapping two culms resulted in a less smooth curvature and left the tips protruding, which could disrupt the overall curvature. However, the first method was more complicated, requiring more time and a better-skilled worker to produce a good joint.



Figure 6-16. a - b. Lengthen the member by overlapping.

Nodal connections in gridshell structures must allow for rotation and movement during the form-finding and erection processes; however, once the desired form is achieved, the connections should be fixed. In this study, lashing joint was used to assemble bamboo poles in Model-1 (Figure 6-17). The construction team suggested this join when we discussed the requirements needed for connection systems for form-finding purposes. Lashing joint was chosen for their ability to accommodate rotational flexibility and the natural shrinkage of bamboo culms during construction.



Figure 6-17. Nodal connection using lashing join.

The lashing joints proved essential during the form-finding stage, allowing for adjustments in pole positions and angles as the gridshell structure took shape. Construction teams found them straightforward to implement, and based on their experience, these joints provided robust connections under load. Observations during construction revealed minimal instances of slippage or disconnection, demonstrating their reliability in maintaining structural integrity.

The flexibility of the lashing joints also facilitated easy loosening and fastening of connections by simply adjusting the ropes. Despite being made solely from ropes, the connections were sufficiently strong to hold the bamboo members securely in place. This knotting technique, long employed by Indonesian bamboo craftsmen in knock-down structures, showcased its durability and ability to resist movement.

Moreover, these connections effectively accommodated bamboo's natural shrinkage. As the bamboo culms used in Model 1 gradually lost moisture content, causing a reduction in diameter, the lashing joints allowed for adjustments without compromising the structural integrity. Craftsmen could easily tighten the ropes by untwisting and retying the knots as needed

Meanwhile, the connections between grid members and boundary or perimeter beams were secured using nuts and bolts (Figure 6-18a and Figure 6-18bFigure 6-17). During the assembly process, flexibility and adjustability were crucial, hence lashing joints were employed. However, once the gridshell had achieved its intended curvature, the focus shifted to securing these connections permanently. Therefore, nuts and bolts were used at the boundary connections to firmly fix the grid members in place. This fixation was necessary to maintain the structural integrity of the gridshell structure under loads and to prevent any unintended shifting or movement that could compromise its stability.

Observations during construction showed that these fixed connections effectively maintained the shape and withstood the relaxation process typical in gridshell structures. Once all the connections at the boundary were secured, all supports were removed to allow the gridshell to stand independently. The final gridshell achieved a curvature with a total height of 1.12 m, slightly reduced from its height during the form-finding process. The connections were secure, demonstrating their ability to resist initial forces effectively.



Figure 6-18. a. Nuts and bolts connection at the perimeter; b. connection at the boundary; c. failure due to diametric compression; d. failure due to longitudinal splitting.

Although the connections were able to maintain the constructed structures, during the load tests, the fixed connections failed, leading to the collapse of the structure. When the loads were applied, the beam members exerted significant forces on the boundary conditions, causing the bamboo to break. The failure modes observed included crushing due to diametric compression, where the bamboo was crushed under the pressure exerted perpendicular to its grain (Figure 6-18c), and splitting, where the bamboo culms split apart along their length (Figure 6-18d). These failures underscored the challenges in ensuring the robustness and reliability of fixed connections in bamboo gridshell structures, especially under dynamic loading conditions

6.3.3. Construction of Gridshell Structure Model Using Split bamboo

Building a bamboo gridshell using split bamboos was less complicated compared to using full-culm bamboo. The split bamboo was produced by splitting a full-culm bamboo into several long pieces. When bamboo is split into long members, its flexibility increases compared to its full-culm state because the diaphragm no longer limits the wall. However, this process significantly reduces its strength and rigidity.

The section properties of split bamboos were similar to timber laths; however, maintaining dimensional consistency was challenging unless the split bamboos were processed into laminated bamboo. Unprocessed split bamboos retain the characteristics of raw bamboo, with tapering and varying wall thickness—thicker at the bottom and thinner at the top. Given the flexibility of split bamboos, the erection method for Model 2 followed similar techniques used for timber gridshells. The construction stage involved assembling the split bamboos into a flat grid on the ground, pulling the lattice using chain blocks, pushing the four corners inward, and fixing the perimeter.

The first construction stage involved splitting full-culm Dendrocalamus asper bamboo (Figure 6-19). This process was done manually using axes. The method was quick and uncomplicated due to the parallel nature of bamboo fibres, which allowed the culm to be easily split. The bamboo slats were trimmed to ensure width consistency and to remove parts of the diaphragm. Since the available length was only six metres, while the required length was a minimum of 8.40 metres, two bamboo slats were joined to create longer members. The slats were bound at different locations, creating continuous members.



Figure 6-19. a. Splitting methods using axe; b. Trimming the split bamboo.

Before construction, a discussion with the workers was conducted to explain and decide on the construction method and other details. During the discussion, we emphasised the importance of nodal connections, which should allow rotation and movement but be fixed

once the final form is achieved. Consequently, the construction workers proposed using thin wires tied into a crossed shape for the connections, as depicted in Figure. This crossed tie would allow limited translational and rotational movement and could be tightened after achieving the desired form. Therefore, the connections at the grid were tied using thin wire, while the perimeter connections used nuts and bolts to prevent the lattice from loosening.



Figure 6-20. a. Detail connection using thin wire for split bamboo; b. Connection during erection process.

The construction began by laying the slats on the ground, arranging the grid, and measuring the distances. It was important to ensure the mesh size was accurate because, even though the bamboo had been split and trimmed, the dimensions varied. Some members might have wider sections, while others might be slightly bent. Once the grids were consistent and matched the planned dimensions, the nodes were connected using thin wires, with the lead worker frequently checking to ensure the mesh grid's dimensions were consistent. This process continued until all the members were attached, forming a complete lattice (Figure 6-21a and Figure 6-21b).



Figure 6-21. a. Process of laying the members and forming the grids; b. Completion of the lattice.

After the flat lattice was completed on the ground, the workers constructed two tripods on either side of the grid and installed two chain blocks. The chain blocks were connected to two nodal points, and the erection process began by gradually pulling up the chain blocks. As the lattice started to rise, the workers quickly installed the ratchet straps at the four corners, which would act as anchors for the structure. The ratchet straps significantly aided the workers in maintaining the shape, making the process of positioning the four anchors less challenging. Once the ratchet straps were properly installed, the workers continued to gradually raise the lattice. Additional construction workers were positioned at the four anchors to push and hold the positions simultaneously. Solely pulling the anchors inward with the ratchet straps might cause failure due to stress concentration. The process is illustrated in Figure 6-22a to Figure 6-22d.



Figure 6-22. a. Erection process; b. Installation details of the chain blocks to the lattice; c. Shaping the form; d. Additional workers pushed the corner while the rachet strap was shortened.

The form-finding process continued by pulling the lattice and adjusting the corners. Initially, the anchors were to be moved as far as 1.50 metres, and the apex height was

intended to reach between 2.40 and 2.50 metres. However, before achieving the planned position and height, the slats at the perimeter snapped and buckled Figure 6-23a and Figure 6-23b). The buckled members were located in the middle of the perimeter slats, where the curvature was the deepest. Consequently, the workers halted the erection process, and the lead worker measured the distance between each anchor point. The lead worker provided directions for the anchor positions, and the other workers moved to fix the positions accordingly, ensuring each point had the same distance. Then, eight beams were prepared and installed as a boundary to stop further movement and hold the final shape (Figure 6-23c). The erection process of the bamboo gridshell using split bamboos was faster than with full-culm bamboo. Starting from the installation of the chain blocks, the pulling process to completion took approximately two hours.



Figure 6-23. a-b. Buckling at opening members; c. Installing the boundary beams; d. Completed structure.

The final gridshell model reached a maximum height of 2.34 metres, and the anchor points were moved inward by approximately 1.40 metres. It was difficult to accurately identify the movement because the initial position shifted several times when the lattice was pulled. The structure proved to be strong, as evidenced by two workers climbing to the top

to dismantle the chain blocks. After the completion, the chain blocks were removed, but the ratchet straps remained in position. Since the structure was built without a foundation, the ratchet straps helped the boundary maintain the final form and acted as tension members. The workers replaced the snapped slats with new ones the following day.

6.3.4. Load Testing of Gridshell Models

Loads were applied by placing concrete blocks and steel plates on top of Model 1. The concrete blocks were carefully measured and applied one by one, while the workers monitored deflection measurements. However, during the load application based on Scenario 2, the structure suddenly collapsed, and the gridshell lost its height immediately. The cause was identified after investigating the failure. The primary reason was the poor connection at the boundary. The boundary was constructed from eight bamboo poles of the G. apus species and connected using nuts and bolts. When the loads were applied, the members transferred the loads to the boundary and stressed the beams. The connection couldn't withstand the tension force and broke immediately (Figure 6-24a). Additionally, the bamboo tips were crushed at the connection point (Figure 6-24b), and some of the beams were cracking and splitting (Figure 6-24c). Subsequent tests couldn't be conducted due to the collapse of the structure.



Figure 6-24. a. Failure at the joineries between beams (1); b. Failure at joineries between beams (2); c. Cracking and splitting.

The load tests were conducted by hanging buckets on the lattice and using concrete blocks as the loads. Similar to the tests on Model-1, the loads or concrete blocks were carefully measured and placed inside the buckets, after which the workers measured the displacement. The loads were applied three times by adding concrete blocks one by one. Before each load application, the Model was measured to identify the initial height. Figure 6-25 illustrates the initial geometry before loading.

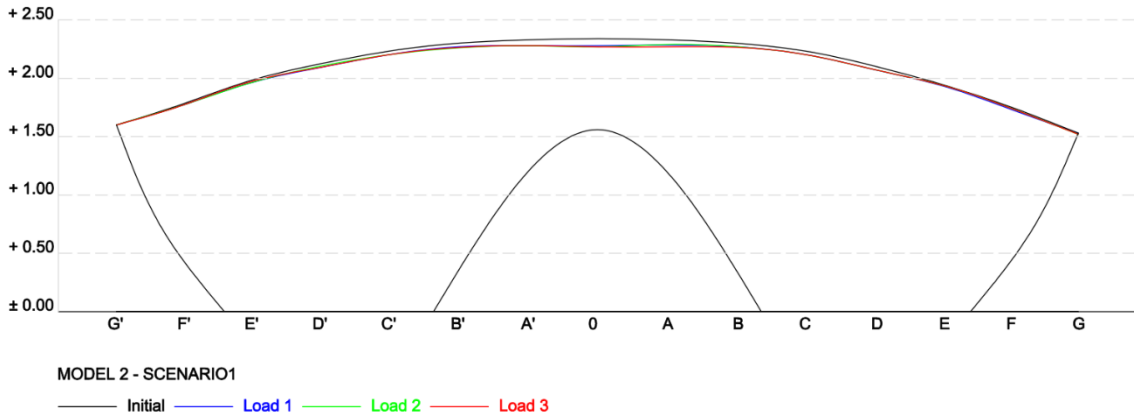


Figure 6-25. Initial gridshell shape before loading.

In scenario 1, the first load application was 4.19 kg, the second was 12.34 kg, and the third was 20.86 kg. The measured displacement was plotted and presented in Figure 2.25, which also illustrates the deformation shape in curvature. The first to third load applications induced maximum displacements of approximately 0.060 m, 0.070 m, and 0.075 m, respectively. The curvature shapes exhibited gradual deformation with a sharp pointed curve at the loading point, indicative of deformation under point load. The displacement range from the first to the second load application was higher, with a difference of around 0.010 m, whereas the difference between the second and third load applications was 0.005 m.

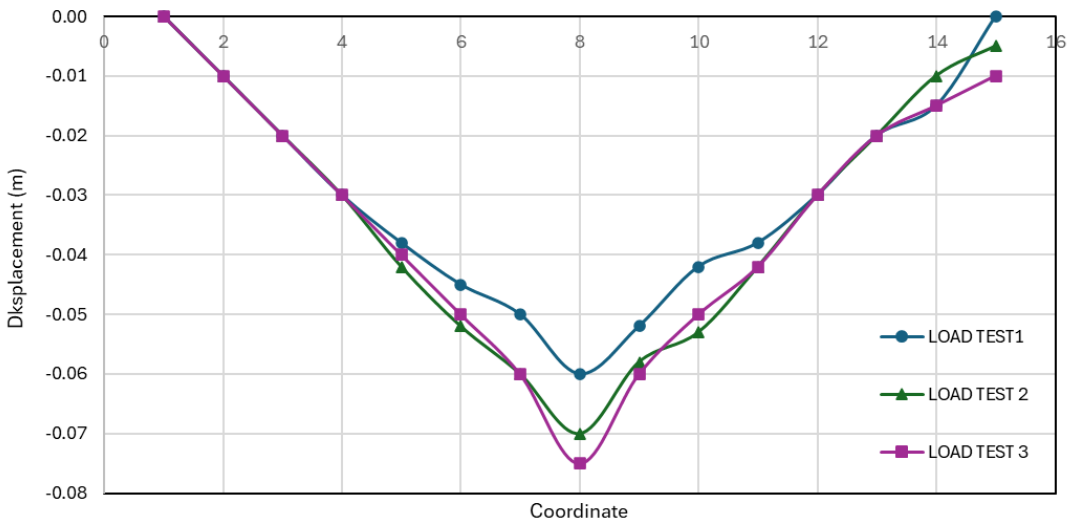


Figure 6-26. Displacement and deformation curve from the Scenario 1 loading applications.

The load application for Scenario 2 can be seen in Figure 6-27 and Table 6-2, while the displacement curve is illustrated in Figure 6-28. The maximum displacements recorded from Scenario 2 for the first to third load applications were 0.038 m, 0.060 m, and 0.083 m, respectively. The curve shape, which illustrated the deformation, showed an uneven profile where the nodal area in the middle was slightly raised while the two nodes adjacent to the centre were slightly lower. This indicated how the gridshell shape deformed under symmetric line loads, reflecting the stress distribution and the response of the gridshell members to the loads.

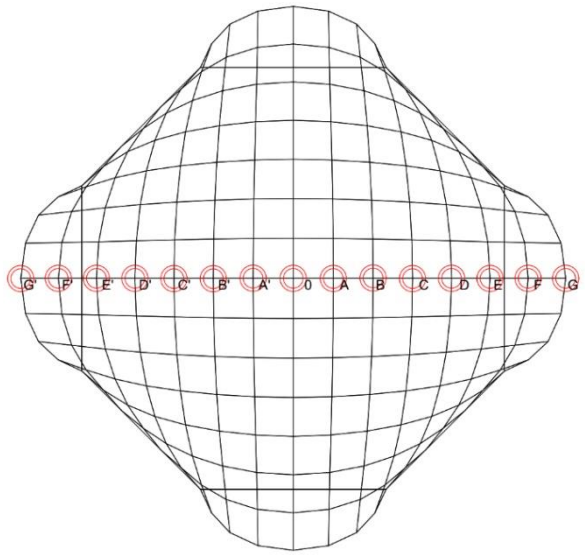


Figure 6-27. Point loads and measurement Scenario 2.

Table 6-2. Loads – Scenario 2 (in kg)

Points	Load 1	Load 2	Load 3
G'	3.91	7.92	11.82
F	3.60	7.90	11.84
E'	4.29	8.40	12.58
D'	4.23	8.33	12.28
C'	4.22	8.30	12.45
B'	4.13	8.20	12.21
A'	4.22	8.20	12.27
0	4.19	8.22	12.34
A	4.09	8.25	12.19
B	4.14	8.24	12.37
C	4.24	8.44	12.53
D	4.06	8.16	12.27
E	4.10	8.14	12.34
F	4.08	8.09	12.96
G	4.10	8.70	11.01

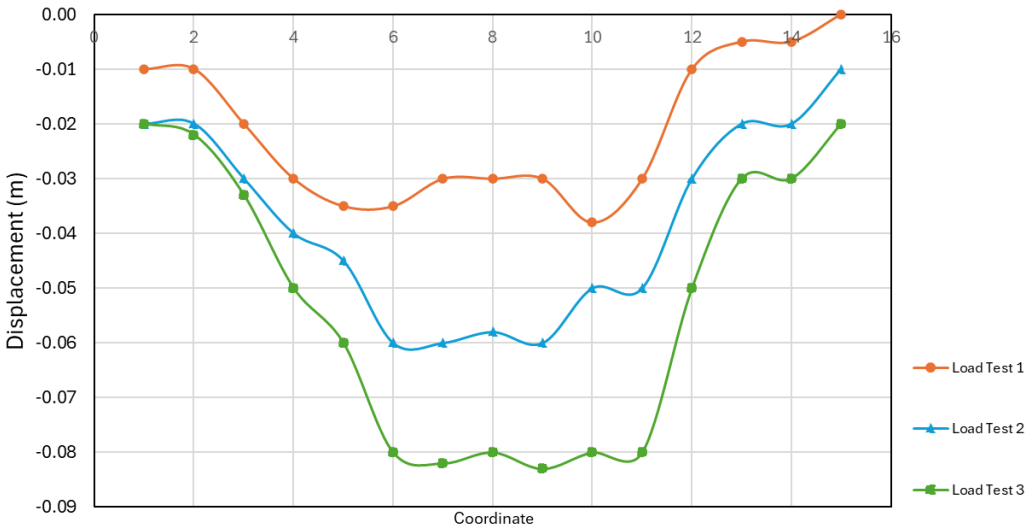


Figure 6-28. Displacement of main curve due to Scenario 2 loading application.

In Scenario 3, loads were applied along the diagonal line. Due to the steep curvature near the anchor, the loads were hung on four points outside the centre point (Figure 6-28 and Table 6-3). The maximum displacement resulting from the first application was 0.080 m, the second was 0.100 m, and the third was 0.110 m. The deformation illustrated in Figure 6-29 showed significant displacement around the middle part, particularly between the C'-B' measurement points. The deformation curve exhibited a different pattern from Scenario 2, where the loads were applied along the centre line. The bumpy curve indicated stress concentration between points C' caused by the diagonal loads. The curve was also asymmetric and uneven with a jagged profile, indicating high-stress concentrations near the loading area.

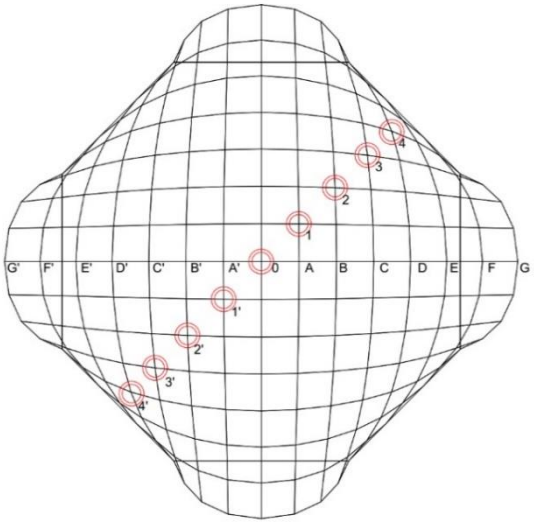


Figure 6-29. Point loads and Measurement Scenario 3.

Table 6-3. Loads - Scenario 3 (in Kg)

Points	Load 1	Load 2	Load 3
4	4.23	8.33	12.28
3	4.22	8.30	12.45
2	4.13	8.20	12.21
1	4.22	8.20	12.27
0	4.19	8.22	12.34
-1	4.09	8.25	12.19
-2	4.14	8.24	12.37
-3	4.24	8.44	12.53
-4	4.06	8.16	12.27

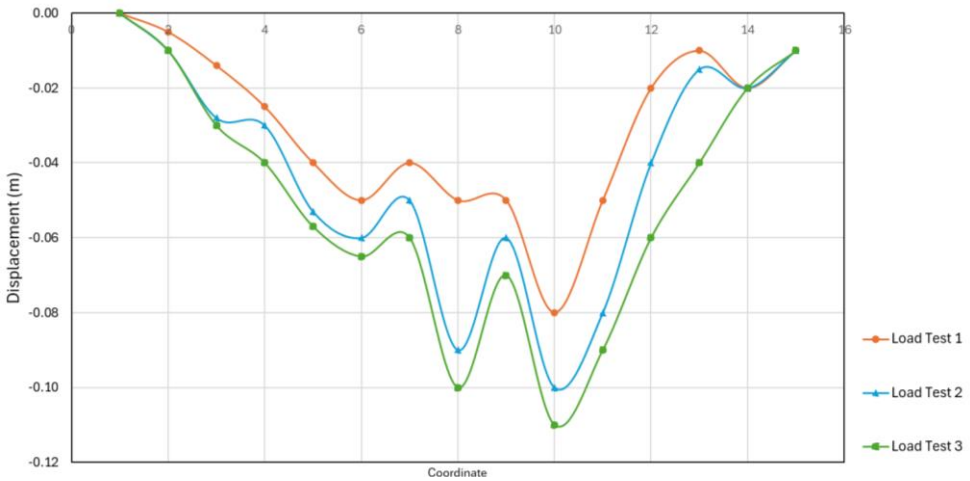


Figure 6-30. Deformation of main curve due to Scenario 3.

In Scenario 4, the load applications used the same weights as in Scenario 1, which were 4.19 kg, 12.34 kg, and 20.86 kg. However, the load was applied at an asymmetrical position (see Table 6-1). The asymmetrical positioning caused uneven deformation, which illustrated in Figure 6-31, with displacement detected primarily on the side near the load point, while the other side showed negligible displacement. The maximum displacements recorded were 0.035 m, 0.042 m, and 0.050 m for the first, second, and third load applications, respectively.

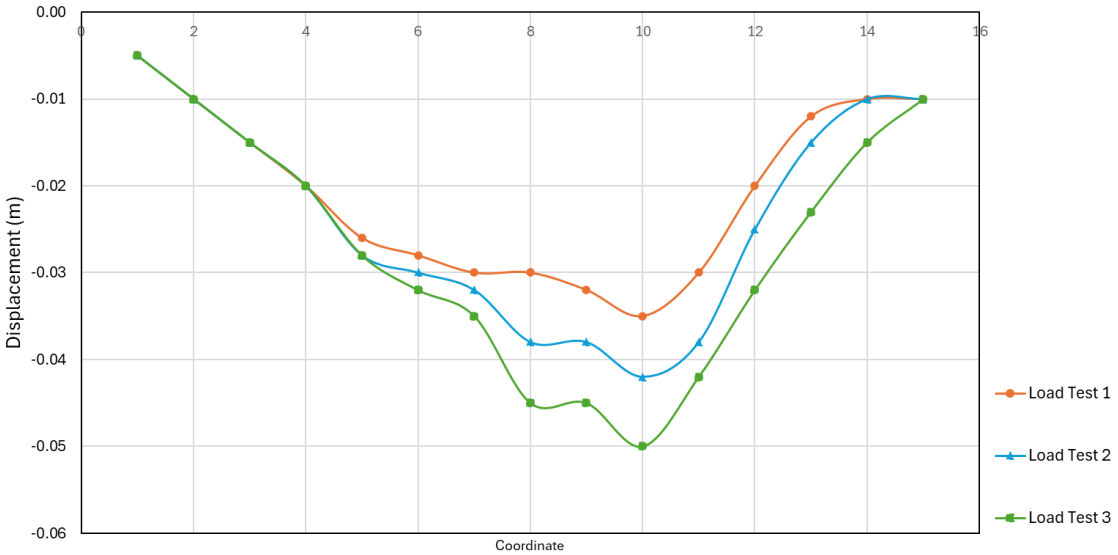


Figure 6-31. Deformation of main curve due to Scenario 4.

The loading applications based on the four scenarios provided valuable insights into the deformation behaviour and structural response of bamboo gridshell models under different loading conditions. Understanding the deformation and stress distribution on full-scale models can inform designers and engineers about critical deformations and displacements that could be crucial for structural integrity. These insights are essential for optimising the design and placement of supports and connections, ensuring better performance and safety in bamboo gridshell structures.

6.4. Discussion

6.4.1. Determining Construction Methods for Full-culm Bamboo Gridshell Structures

In constructing bamboo gridshell structures, selecting appropriate and suitable construction methods is crucial for ensuring structural integrity and performance. Bamboo, as a material for gridshell structures, presents both constraints and opportunities. The distinctive characteristics of bamboo significantly influence the methodology employed in constructing gridshell structures, as evidenced by the construction of two full-scale models.

Common methods used in timber gridshell structures, such as pull-up, push-up, and ease-down, as presented in Section 2.3.16, may not be directly applicable to bamboo. Therefore, this section discusses the challenges involved in determining suitable construction methods for bamboo gridshell structures, arising from the unique combination of material characteristics and structural requirements.

The construction of full-scale models posed significant challenges due to the inherent complexities of working with full-culm bamboo. Previous studies on bamboo gridshell structures have predominantly focused on smaller diameter bamboo, which is more flexible and easier to bend. For instance, Rockwood's experimentation (Rockwood, 2015), illustrated in Figure 6-1 and discussed in Section 6.1, primarily utilised small diameter bamboo, highlighting its advantages in flexibility (as discussed in Section 4.4.2.)

In contrast, Indonesian bamboo typically has larger diameters, which enhance stiffness but complicate the bending process required for gridshell structures. While this stiffness contributes positively to structural performance, achieving the necessary curvature for gridshell geometry becomes more challenging. Additionally, the larger diameter of bamboo contributes to its significant weight, which impacts the entire construction process.

During construction, we encountered difficulties due to the combination of stiffness and weight when attempting to elevate the full-culm bamboo model, as illustrated in Figure 6-14 and Figure 6-32. Despite applying heat to soften the bamboo fibres and using chain blocks to lift the shell, achieving curvature was challenging. The stiffness of the bamboo also prevented workers from adjusting the boundary conditions inward effectively. Furthermore, the natural tendency of bamboo culms to revert to their original form added complexity to the process.



Figure 6-32. Efforts in raising the full-culm gridshell curvature; a. Using chain blocks, b. The workers tried to push up the structure.

Drawing lessons from the construction process of Model-1 in this study, bamboo gridshell structures made from full-culm bamboo are best realised through individually

bending each member and assembling them into the desired curvature. This approach involves temporarily securing the culms to scaffolding, which helps maintain the desired curvature and shape, as depicted in Figure 6-12, thereby preventing the culms from reverting to their original form. The bending process becomes more manageable and allows for individual shaping with minimal disruption to other members. Moreover, this method anticipates potential buckling and member failures that may occur during construction. Should a member break during bending, immediate replacement is feasible, enhancing the resilience and manageability of bamboo construction.

This method shows promise for the implementation on more complex geometries, such as gridshell structures with multiple curvatures. However, further research is necessary, as current applications of full-culm bamboo in gridshell structures have primarily focused on single-curved configurations using small to medium diameters, for example the ZBC pavilion and UNAM pavilion. Multiple-curved gridshells introduce greater complexities in the bending process. Additionally, assembly methods must be conducted meticulously by employing appropriate scaffolding and temporary support systems capable of accommodating varied geometries.

Split bamboo is created by splitting whole culm bamboo, which results in the loss of certain inherent properties. For instance, the absence of the diaphragm significantly reduces stiffness, while simultaneously, increase the capability of bamboo in bending. This change in sectional profile increases flexibility but greatly reduces its stiffness. However, the new profile resembles timber laths, which have been extensively and effectively used in gridshell structures. Therefore, split bamboo has significant potential for gridshell applications.

Given that the cross-sectional area of split bamboo is similar to timber laths, the assembly and erection methods for split bamboo gridshell structures can be based on the techniques used for timber gridshells. This strategy was applied in this study, and it proved effective, as demonstrated by the successful construction of the split bamboo gridshell using similar methods to those used for timber gridshells.

Unlike full-culm bamboo, split bamboo is highly flexible and can be bent easily. As individual members, split bamboo is weaker than full-culm bamboo, as illustrated in Figure 6-33, where split bamboo significantly bent under load. However, when assembled into a grid and bent together, the structure gains strength. The split bamboo acts as a membrane, transferring loads across its surface. Initially perceived as weak, split bamboo proved strong and reliable for gridshell structures. Its flexibility and less complexity of assembly make it comparable to timber laths, allowing it to be erected in a manner similar to timber gridshell structures



Figure 6-33. Testing on split bamboo showing a significant deformation in shape.

Learning from the Arc at Green School, where split bamboo was used in an anticlastic gridshell with negative curvature, the designers aimed to optimise bamboo's tensile strength. Since bamboo excels in tension, using split bamboo in a negative curvature ensures the gridshell primarily bears tensile forces. For positive or synclastic curvature, full-culm bamboo is considered stronger as the forces would predominantly act in compression. The cross-sectional profile of full-culm bamboo is larger, and its compression strength is moderately good, with the test in Section 4.3.1 presenting a Modulus of Rupture (MOR) between 30-40 N/mm^2. In contrast, the significantly smaller cross-sectional profile of split bamboo indicates it is weaker than full-culm bamboo. However, this study demonstrated that split bamboo is sufficiently strong to be formed into synclastic shapes, similar to timber gridshell structures.



Figure 6-34. The utilisation of split bamboo; a. at The Arc, utilised in anticlastic curvature; b. in this study, utilised as synclastic curvature.

In terms of handling and construction, split bamboo gridshell structures can be built quickly. In this study, splitting and preparing the bamboo took only two days, while assembling the grid took place simultaneously. Erecting the gridshell and fixing the boundary conditions required just two hours. This efficiency highlights the advantages of using split bamboo over full-culm bamboo.

One issue to be aware of during construction is the potential for fibre kinking during the form-finding process. As shown in Figure 6-23, perimeter members experienced fibre kinking, leading to buckling. Another problem encountered was layering. It is advisable to use two layers of split bamboo rather than a single layer. The challenge lies in lengthening the members. In timber gridshells, timber laths can be lengthened using finger joints, which have limitations and can break during erection (Harris et al., 2003). However, lengthening split bamboo can be done more simply by overlapping two layers of split bamboo and tying them. Although specific joints for split bamboo are possible, they are time-consuming and complicated due to variations in the shape of split bamboo.

Therefore, while constructing split bamboo gridshell structures is less complex than using full-culm bamboo, issues related to form-finding and detailing must be considered to achieve successful construction. Applying similar methods used in timber gridshells to split bamboo indicates the potential for extensive utilisation of split bamboo as a replacement for timber gridshells. This is particularly relevant in Indonesia, where environmental issues such as forest fires and illegal logging (as highlighted in Introduction, Section 1.1) necessitate alternative materials to timber.

6.4.2. Critical Reflection on the Construction Process

Building two gridshell models provided deeper insights into the construction process of gridshell structures, an area that is less explored and documented, particularly in Indonesia, where construction practices heavily rely on community traditions and apprenticeship. Learning from the construction challenges can offer comprehensive knowledge for future applications. This section discusses the challenges faced during the construction process, which can be categorised into the high variability and the uncertainty of bamboo as a building material.

The challenge arising from bamboo morphology relates to its significant variation in diameter, wall thickness, and straightness. Unlike gridshells made from timber, which can be processed into uniform sections, achieving similar uniformity with bamboo is difficult, both as full-culm and split. Full-culm bamboo is clearly tapered, with varying thickness from

base to tip, and the occurrence of nodes and internodes, all contributing to its variability. Even when split into slats, these characteristics remain.

The construction of the full-culm bamboo models used approximately 120 pieces of green bamboo from the species *Gigantochloa apus*. Although the supplier had sorted the bamboo, the variation was evident, as seen in Figure 6-35. To address the issue of variability, we implemented a meticulous sorting process by matching bamboo culms of similar outer diameters and wall thickness when creating curvature and lengthening the members. However, the process was complicated, frequently requiring extensive sorting and adjustment, which was time-consuming.



Figure 6-35. The non-uniform morphology of bamboo; a. from the longitudinal view, b. from the cross-sectional view.

The high variability of bamboo morphology impacted the assembly process, complicating the connection systems. We relied on lashing techniques, which provided flexibility but required high skill and precision. This lashing connection could be adjusted by tightening the ropes for different diameter bamboo and for potential shrinking. However, the inconsistency in dimensions could potentially affect the structural performance by influencing load distribution and stability.

Another significant issue with bamboo utilisation is its uncertain characteristics as a natural material. The uncertainty was discussed in Chapter 4 and is indicated by the brittle tendency and failure modes in bamboo. This uncertainty makes it difficult to predict performance and ensure the reliability of bamboo for structural applications. For instance, during experimentation on bending and depth of curvature, sudden breakages occurred. Additionally, during the bending and assembling process of full-culm bamboo, audible cracking sounds were often heard, leading to cautiousness in bending the bamboo. Many culms experienced sudden breakage during the bending process, resulting in less efficient

material usage. Furthermore, during the load tests on full-culm bamboo, the structure collapsed suddenly, which could endanger occupants in real structures.

Further problems were related to the connections. When it was necessary to lengthen the members, smaller diameter bamboo had to be inserted into the hollow tube, a complicated task requiring highly skilled construction workers. Additionally, the gridshell's numerous connection points led to mistakes and inconsistencies in tying the lashing joints. Similar problems were reported by Crolla (2017), during the construction of the ZBC pavilion, where issues in coding and identifying connections arose due to the high variability of bamboo morphology.

These phenomena indicate that the high variability in bamboo morphology presents significant challenges in the construction of gridshell structures. While ISO 19624:2018 provides guidance on grading bamboo, the inherent variability of bamboo makes the grading process itself challenging. The timber industry has successfully developed comprehensive grading and coding systems, which could serve as valuable models for the bamboo industry.

Adopting methods from the timber industry could be beneficial for the bamboo sector. For instance, the bamboo industry can implement detailed grading processes that include information such as the source of the culms, harvesting age, position within the culm, diameter, and thickness. This approach could address the challenges posed by bamboo's variability, offering a more standardized and reliable way to classify and use bamboo in construction. By integrating these practices, the bamboo industry can enhance the consistency and quality of bamboo materials, making them more suitable for complex structural applications like gridshells. Such advancements would not only improve the construction process but also promote the wider adoption of bamboo as a sustainable building material.

Learning from these experiences, it became clear that pre-selecting and grading bamboo culms based on detailed specifications could significantly improve efficiency in construction management and structural performance. The unpredictability of bamboo should be meticulously and carefully mitigated. This unpredictability could compromise the safety of structures and occupants. Therefore, these two aspects should be considered in every bamboo utilisation project.

6.5. Summary

The construction of bamboo gridshell was investigated by building two full-scale models representing the different types of bamboo applications: full-culm and split. Investigation

on bamboo gridshell using full-culm bamboo was started by exploring the depth of curvature and the bending method. The erection method suitable for full-culm bamboo was conducted by individually bending and laying the bamboo poles. Meanwhile, the erection method for the split bamboo was relatively uncomplicated and faster and could be done using similar methods to timber gridshell. The main problems found in full-culm bamboo gridshell were the less flexibility of bamboo culm and the connection design. Whilst the split bamboo's main problems were the strength and rigidity.

The construction process has revealed that the most suitable method for constructing full-culm bamboo gridshell structures involves individually assembling members by bending them on-site. This approach effectively mitigates the challenges posed by bamboo's non-uniform morphology and its inherent uncertainties. In cases where bamboo culms break during form-finding, replacements can be installed without compromising the entire structure's integrity. Conversely, for split bamboo, the assembly and erection processes can adopt methods similar to those used for timber gridshell structures. The role of connections in maintaining the gridshell shape and ensuring its safety and durability is crucial. Lessons learned from the failure of Model-1 underscore the importance of carefully designing the connection systems, especially at the boundary, to withstand applied loads effectively.

Publication History:

Part of this chapter has been published in WCTE 2023 conference on 19-22 June 2023 in Oslo, Norway. The paper title is “Bamboo gridshell: from the material to the structure”. Information regarding the conference can be accessed through *https://wcte2023.org/* while the paper can be accessed through *https://www.proceedings.com/069179-0023.html*

CHAPTER 7 | PARAMETRIC MODELLING: FORM-FINDING AND OPTIMISATION OF BAMBOO GRIDSHELL STRUCTURE

7.1. Overview

From the literature review, it is evident that while the research on form-finding and optimisation in various types of gridshell structures is extensive, studies focusing specifically on bamboo gridshells are scarce. Limited sources are available, even though the scope has expanded to include bamboo for bending-active structures in general. Notably, the studies discussed in literature review highlight the limited evolution of gridshell structure research from physical models to computational simulations. However, only a few studies exploring spatial structures using bamboo have integrated bending-active principles into their design and incorporated these processes into form-finding and optimisation.

The limitations observed in bamboo gridshell structures, particularly in terms of form-finding and optimisation, suggest significant potential for further investigation. Form-finding and optimisation are crucial factors in gridshell design, presenting specific challenges when utilising bamboo. Therefore, studies on the geometry and form-finding of bamboo gridshells that accommodate the characteristics of bamboo and account for its limitations need to be extensively examined.

Furthermore, while bamboo is recognised as a lightweight and sustainable material, optimising bamboo gridshell structures is essential to achieve efficiency in material usage and stress distribution. Employing suitable optimisation strategies for bamboo gridshell structures is crucial key in achieving not only safe but also efficient structures. Therefore, study on optimisation methods and strategies suitable for bamboo gridshells is needed. Addressing these gaps will significantly advance the understanding and application of bamboo in gridshell design.

Therefore, the objectives of this chapter are:

- To investigate the form-finding process of gridshell geometries that considers bamboo's limitation in bending.
- To assess the effect of modifications based on optimisation strategies to the structural performance.
- To develop optimised structure for bamboo gridshell.

7.2. Research Methods

7.2.1. Research Design and Material Selection

The research design for this study incorporated a systemic approach combining computational modelling and optimisation methods to investigate the form-finding and optimisation of bamboo gridshell structures. This study was conducted in three stages: initial form-finding using bending-active principles to determine feasible shapes; structural analysis to evaluate the efficacy of various optimisation strategies; and the refinement and optimisation of the gridshell design to enhance structural efficiency and material utilisation.

The entire process was facilitated in the Rhinoceros 3D modelling software, with specialised plug-ins as Grasshopper for parametric design, Kangaroo for the form-finding, and Karamba 3D for structural analysis. The integration of tools enabled an iterative design workflow, which is depicted in Figure 7-1.

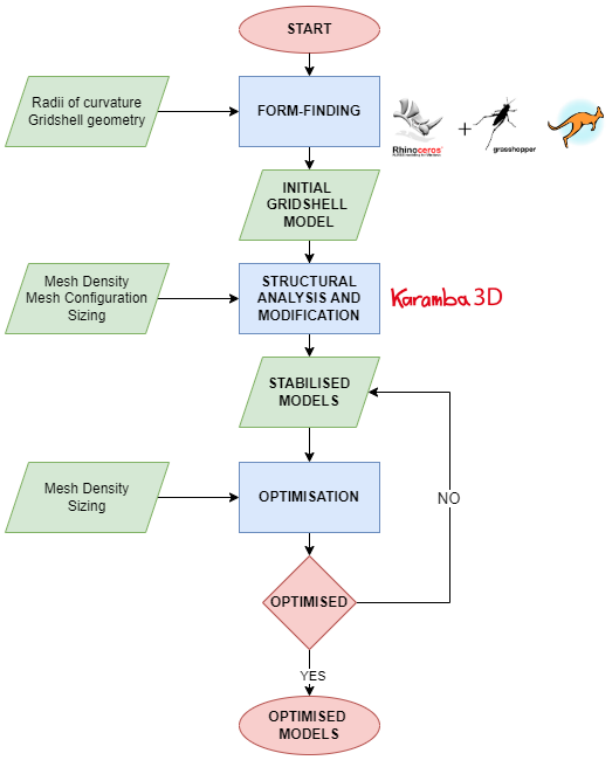


Figure 7-1. Research workflow.

This study utilised three species of bamboo: *Gigantochloa apus, Gigantochloa atter*, *Dendrocalamus asper*. These species were studied in the previous objectives and chosen based on their differing mechanical properties and availability, providing a robust basis for assessing the structural capabilities and limitations of both full-culm and split bamboo. The use of full-culm and split bamboo allowed for a comprehensive analysis of their

morphological characteristics, material properties, and overall suitability for use in gridshell structures. Therefore, adapting the design process to the unique attributes of bamboo as a construction material.

7.2.2. Initial Model Development

The basic geometry selected for this study was a synclastic gridshell supported by four anchors. This geometry was chosen to simplify the structure, allowing the study to focus on the impact of material utilisation and its effect on structural behaviour. This decision aligned with prior studies on similar forms of timber gridshells, such as Woodome gridshell, Toledo gridshell, Portalen Pavilion, and the gridshell pavilion in Trondheim, which have been studied in the literature (Saleh Tabari, Khojastehmehr, & Filz, 2022; Dyvik et al., 2016; Labonnote et al., 2016; D'Amico et al., 2015; Pone et al., 2013). These examples, illustrated in Figure 7-2, provided insights into synclastic gridshell structures and used as form-finding approach of this study.



Figure 7-2. Examples of similar gridshell forms a. Woodome project; b. Toledo gridshell; c. Portalen Pavilion; d. Throndheim gridshell
Source: a., b., c., (Saleh Tabari, Khojastehmehr, & Filz, 2022), d. (Labonnote et al., 2016)

The form-finding process, as described in this chapter, was adapted to accommodate two types of bamboo: full-culm and split bamboo. In Chapter 4 and Chapter 6, it was noted that full-culm bamboo exhibits limitations in bending, which constrains the achievable curvature without compromising the structural integrity. On the other hand, the use of split bamboo allowed for a gridshell with higher degree of curvature, reflecting its greater flexibility. Therefore, form-finding process carefully considered the inherent radii of curvature of each bamboo type to optimally design the geometry of the structure.

7.2.3. Bending-Active Form-Finding

The form-finding stage aimed to create gridshell geometries that respond to the minimum radius of curvature, thereby reflecting the bending-active gridshell principle. To achieve this aim, the displacement data obtained from the bending parallel to the fibre tests were chosen for determining the radius of curvature in this study. These bending tests provided detailed

insight into the mechanical properties of bamboo, such as the Young's modulus (E) and bending strength (f_m), alongside direct measurement of displacement under load. These detailed mechanical properties are crucial for accurately modelling the structural behaviour of bamboo gridshell in computational simulations. Therefore, the data, as analysed and presented in Table 4-18 were utilised to ensure scientific reliability and to facilitate direct application in Karamba 3D. Based on the data, the minimum radii of curvature for full-culm bamboo species G. apus, G. atter, and D. asper were determined to be 12.59 m, 13.87 m, and 27.47 m, respectively.

Table 7-1. Input data of radii of curvature for Model-1

	Gigantochloa apus	**Gigantochloa atter**	**Dendrocalamus asper**
Radius of curvature	12.59 m	13.86 m	27.47 m

In contrast, split bamboo exhibits higher flexibility since the diaphragm and hollow tube no longer constraint the sectional area. Moreover, with significantly smaller sectional profile, the radius of curvature can reach deeper curvature. However, determining the minimum radius of curvature during construction was challenging due to the high flexibility and variability of the sectional profiles. During the form-finding process of Model-2, four bamboo slats at the perimeter snapped, primarily because the joints at the perimeter were fixed, not because the slats exceeded the minimum radius of curvature. The main concern with using split bamboo in gridshell structures is deformation. Load tests showed significant displacement in Model-2, which was predictable given the thin cross-section of split bamboo, resulting in significantly lower stiffness compared to full-culm bamboo. Therefore, the form-finding for split bamboo focused on exploring the correlation between apex height and structural optimisation by adjusting the anchor position.

The initial design for split bamboo utilised Model 2 with spans of 8.40 x 8.40 m, and the anchors were moved 1.40 m inward from their initial positions. This model was selected because, during construction, Model 2 was built using *Dendrocalamus asper* bamboo slats, which have the thickest walls among the three species studied. Additionally, the significant deformation observed during load tests indicated that the effect of smaller bamboo utilisation could be thoroughly explored during the structural analysis process.

7.2.4. Structural Analyses of Optimisation Modification Strategies

Structural analyses were conducted on the initial gridshell models to evaluate the effectiveness of three key modifications: mesh density, mesh configuration, and sizing. As

highlighted in the literature review, optimising gridshell structures involves adjustments in geometry, topology, and sizing. Assessing the impact of each strategy on overall structural performance is crucial. Therefore, this study implemented these modifications to evaluate their outcomes, which will inform the selection of stabilised models as baselines for further optimisation.

The modifications were carried out as follows:

- **Mesh density**

  Mesh density, a component of geometry optimisation, involves refining the mesh of the gridshell shape without altering the fundamental structural topology. This assessment aimed to determine the impact of changing the mesh density on stress distribution and material usage. Simulations were performed on Model-1 and Model-2, varying the mesh density to observe its effects on stress distribution, displacement, and material usage.

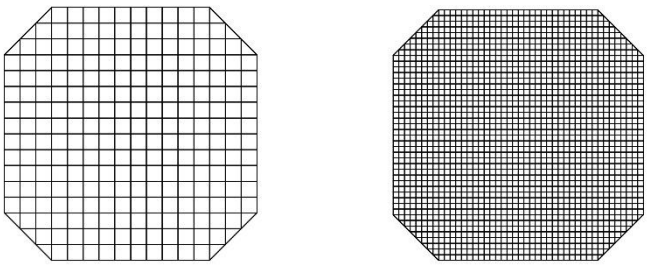
- **Mesh configuration**

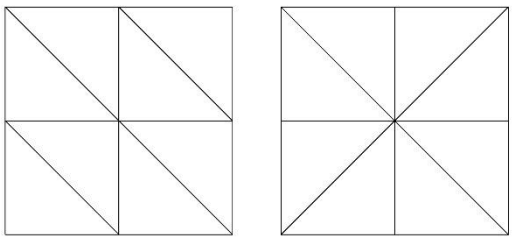
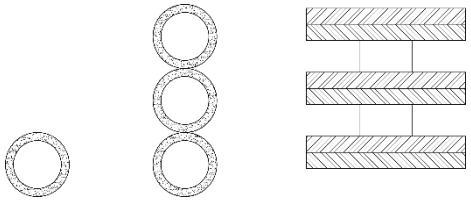
  Mesh configuration involves altering the arrangement or layout of the mesh elements to achieve more efficient stress distribution and material utilisation. This modification aimed to identify the optimal mesh configuration that maximises structural performance under given constraints and loading conditions. This study reconfigured the initial quadrilateral mesh into a triangular pattern or diagrid. The diagrids were arranged in both one-way and two-way triangulations.

- **Sizing**

  Sizing modifications focused on adjusting the size of grid members. Given that each bamboo species has distinctive cross-sectional dimensions and wall thickness, the modifications were implemented by adding layers to the grid members. The assessment aimed to evaluate the impact of these adjustments on stress distribution, displacement, and material usage.

Table 7-2. Modification parameters on initial design.

	Modifications
Mesh Density (MD)	 MODEL-1: From MD16 to MD44 MODEL-2: From MD14 to MD38

Mesh Configuration (MC)	 One-way triangulation Two-way triangulation
Sizing (SZ)	 Adding layers into grids

Simulations were conducted using Karamba 3D with input parameters specified in Section 7.2.6. Sensitivity analysis was conducted to evaluate the impact and effectiveness of each modification. This involved evaluating stress distribution through utilisation factors, which indicate the material's capacity to withstand stresses, maximum displacement, and total mass to gauge material usage efficiency. The results were used to establish the baseline model for structural optimisation.

7.2.5. Optimisation Process

Structural optimisation was conducted using Rhinoceros with plug-ins Grasshopper, Kangaroo, and Karamba 3D. This iterative process aimed to refine the baseline model by adjusting three key parameters, detailed in Table 7-2. Sensitivity analysis was employed to iteratively adjust these parameters and achieve an optimised model that balances optimal utilisation factors, maximum displacement, and total mass. The goal was to enhance structural performance by systematically modifying mesh density, mesh configuration, and sizing of both full-culm and split bamboo gridshell models. This approach allowed for precise evaluation of stress distribution and material efficiency, ensuring the final optimised model met or exceeded performance criteria established during the baseline assessment.

7.2.6. Input Parameters in Computational Simulations

Structural analysis in Karamba3D required input data including elements, supports, loads, cross-sections, material, and joints. Since a gridshell structure is a type of shell structure

composed of grid elements, the grid members were modelled as beams in Karamba3D. Polyline were generated in Grasshopper, and the form-finding was executed using the solver in Kangaroo. Karamba3D then converted these curves into beam elements, consisting of 'element' as beams and 'points' as the joints.

Input material properties for the simulation were based on the material test results reported in Chapter 4. Karamba3D offers two options for material types in the input material properties: isotropic and orthotropic. The orthotropic option would be ideal since bamboo is an anisotropic material with different properties in axial and transverse directions. However, the orthotropic option in Karamba3D is applicable only for the shell element. Thus, when orthotropic properties are applied to beam elements, only the material in the primary direction are considered. This limitation has been noted in other research (Gokul Santhosh, Singh, & Abdul Akbar, 2023; García et al., 2015). Therefore, for form-finding and optimisation, the bamboo was treated as an isotropic material, with input properties adjusted accordingly in Karamba3D.

To ensure the reliability of the simulation, material properties from the material tests were adjusted in strict compliance with ISO 22156:2021. This standard provides guidelines for the structural design and construction of bamboo structures, ensuring the analysis was in accordance with the standards. National standards for bamboo structures are currently not available in Indonesia. Therefore, ISO 22156:2021 was used to ensure the adherence to internationally recognized guidelines for the structural design and construction of bamboo structures.

The Young's modulus (E) was calculated based on the 5th percentile characteristic strength with 75% confidence, considering a service class and load duration factor of 0.55, and safety factor of 2, as detailed in Chapter 5, Equation 5-3. The tensile strength (f_t) and compression strength (f_C) were calculated following equation 7-1. The allowable design strength (f_i) was determined from the 5th percentile of characteristic strength with 75% confidence. The redundancy factor (C_R) was set at 0.90 due to the non-redundant nature of the structural members, and the service class and load duration (C_{DF}) was 0.55, corresponding to service class 2 for permanent and long-term load. The modification factor for service temperature, applicable to structures exposed to heat $T \leq 38$°C and the component safety factor (FS_m) was 2.00. The input material properties are presented in Table 7-3.

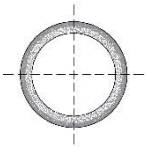
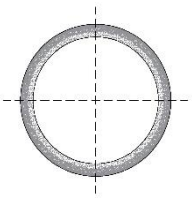
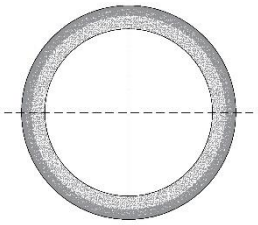
$$f_i = f_{ik} \times C_R \times C_{DF} \times C_T(1/FS_m) \qquad 7\text{-}1$$

Table 7-3. Input material properties.

Material Properties	Units	Gigantochloa apus	Gigantochloa atter	Dendrocalamus asper
Young's modulus	kN/cm²	340.71	396.02	423.77
In-plane shear modulus	kN/cm²	131.04	152.31	162.99
Transverse shear modulus	kN/cm²	5.09	5.16	7.82
Specific weight	kN/m³	6.67	6.13	6.52
Tensile strength	kN/cm²	4.86	3.83	3.95
Compressive strength	kN/cm²	0.76	0.85	0.98

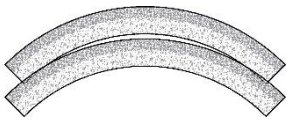
The cross-section dimensions for full-culm bamboo were determined in accordance with ISO 222156:2021. When variations of diameter and wall thickness within the culm were greater than 10%, dimensions were based on the minimum culm diameter and wall thickness. Profile dimensions were derived from material test data and specimen measurements, using the minimum values for diameter and wall thickness.

Table 7-4. Input cross-section dimension for full-culm bamboo.

Input: Dimension	Gigantochloa apus	Gigantochloa atter	Dendrocalamus asper
Cross-section			
Diameter (*D*) in cm	4.87	7.19	10.70
Wall thickness (*δ*) in cm	0.45	0.47	0.78

Profile dimensions of the split bamboo were assumed from the dimensions of full-culm bamboo divided into several slats. Given that bamboo culm taper naturally, with diameter and wall thickness decreasing from base to top, the split bamboo cross-section dimensions varied as well. However, after splitting, the split bamboo could be trimmed, manually or using machine, to achieve a relatively constant width. Wall thickness variations were determined by using the minimum wall thickness, in line with ISO standards. The input profile or cross-section dimensions of split bamboo are shown in Table 7-5.

Table 7-5. Input cross-section dimension for split bamboo.

Input: Dimension	Gigantochloa apus	Gigantochloa atter	Dendrocalamus asper
Cross-section			
Width (*b*) in cm	2.80	4.40	6.00
Height (*h*) in cm	2 x 0.43	2 x 0.47	2 x 0.74

Loads applied to the models included gravity and mesh loads. Karamba3D automatically applied gravity loads to active structural elements when the specific weight was defined. Additional loads, such as those from roofing, wind pressure, and precipitation, were applied as 'MeshLoad' with a value of 1 kN/m^2. The mesh load component converted surface loads into equivalent point loads, distributing them based on the tributary area. Consequently, the loads automatically adjusted based on the mesh size during the optimisation stage.

Connections were configured to release all six degrees of freedom (DOF), thereby creating a pinned connection where elements can rotate freely but cannot translate relative to each other. This principle underlined the hinged connection, which, in bamboo gridshells, represents simple lashing or bolting that less rigidly fixes the members together.

Boundary conditions or supports were established as fixed supports, which restrict both displacement in all directions and rotations. This setup ensures that the gridshell models remained stable and behaved predictably under applied forces.

7.3. Results

7.3.1. Form-Finding of Full-culm Bamboo

Form-finding for gridshell structures can be achieved through the discretisation of the target surface or through the active bending of members. In this study, the design approach was material-led, and the form-finding processes in Grasshopper were conducted by actively bending the members. Since the members were formed through active-bending principle, it was imperative that the curvature did not exceed the minimum radius of curvature. The curvature analysis was performed to ensure that these limits were not surpassed.

The form-finding process commenced with the construction of a flat grid on the ground, followed by the inward movement of the four-line anchor. Although erecting a full-culm bamboo gridshell proved more effective by bending the members individually, during the design stage, the form-finding could proceed similarly to that of Model-2, provided that the minimum depth of curvature was maintained. Additionally, a force was applied at the apex to slightly enhance the curvature at the centre. In practical construction settings, these forces could take the form of scaffolding, simple temporary poles to support the curvature, or by pulling the grids using chain blocks. Following the adjustment of the anchors and the application of forces, the gridshell underwent a relaxation stage until it reached its final shape; the curvature analysis was conducted iteratively until the critical curvatures could accommodate the minimum radius.

This process resulted in three distinct curvatures and heights derived from three bamboo species (see Figure 7-3 and Table 7-6). The initial models, which also served as control models for structural analysis, were designed with a mesh size of 1.00 x 1.00 m. The final geometry of the gridshell using G. apus exhibited the highest curvature, with a total apex height of 1.54 m and an opening height of 0.80 m. Conversely, the model utilising G. atter demonstrated a slightly lower curvature, with an apex height of 1.40 m and an opening height of 0.74 m. Meanwhile, D. asper produced a gridshell with the lowest curvature among the three models, achieving a total height of 0.72 m and an opening height of 0.37 m.

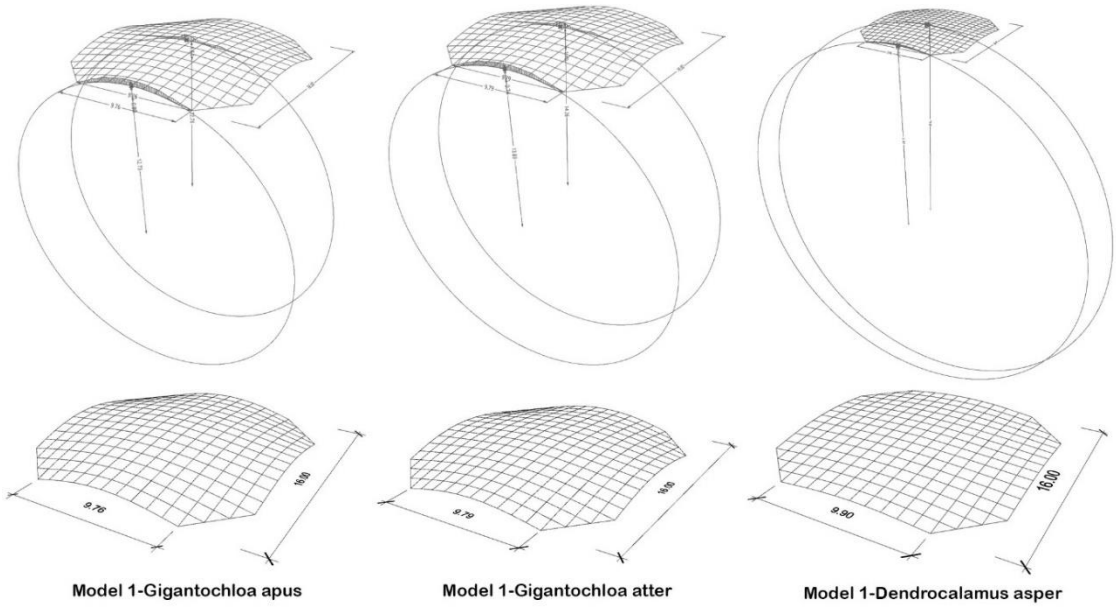


Figure 7-3. Curvature analysis and form-finding of full-culm models.

Table 7-6. Radii of curvature and height resulting from the form-finding process.

	M1-AP (*Gigantochloa apus*)		**M1-AT** (*Gigantochloa atter*)		**M1-AS** (*Dendrocalamus asper*)	
Total height (apex)	1.54	m	1.40	m	0.72	m
Centre curvature radius	12.76	m	14.26	m	29.00	m
Opening height	0.80	m	0.74	m	0.37	m
Opening curvature radius	12.73	m	13.89	m	27.83	m

The bending-active form-finding process underscored the challenges and limitations associated with using full-culm bamboo to achieve deeper curvatures. Despite their inherent flexibility, all three bamboo species demonstrated constraints in attaining significant curvatures suitable for gridshell structures. G. apus emerged as the most adept among the selected species, achieving the highest curvature. Conversely, D. asper exhibited prominent limitations in bending to form suitable gridshell structures, resulting in narrow and nearly

flat geometries. This characteristic poses drawbacks for its application in gridshell construction, as it would necessitate significantly higher compressive forces, resembling more of a beam and slab floor structure rather than a surface gridshell.

This form-finding process underscores the critical importance of selecting the appropriate bamboo species for architectural applications. The aesthetic aspects of gridshell geometries must be carefully considered to achieve desired curvatures. Therefore, choosing the right bamboo species is crucial to ensure that gridshell structures not only meet structural demands but also achieve aesthetically pleasing curvatures.

7.3.2. Effect of Modifications on Structural Performance of Full-Culm Bamboo Gridshell Models

Based on the geometries achieved from the form-finding process, modifications were applied, and structural analysis was performed. Modifications of mesh density were executed by starting with an initial mesh size of 1.00 x 1.00 m and then gradually reducing the mesh size by increasing the density from 16 to 44. The results of the structural analysis for the initial mesh size, depicted in Figure 7-4, indicated unstable structural performance across all models, as evidenced by extremely high utilisation factors and displacement. These results suggested that the initial mesh size could not produce stable structures and that increasing the mesh density alone did not necessarily improve structural stability.

All models presented in Figure 7-4 showed utilisation factors above the threshold of 100%, indicating that the structures operated above safe limits and were likely to fail. The results also demonstrated that increasing mesh density was only effective up to a certain point, beyond which additional mesh did not enhance structural stability. Specifically, models of *G. atter* and *D. asper* showed improved structural performance when the mesh size was decreased from 1.00 x 1.00 m to 0.62 x 0.62 m; however, further increases in mesh density resulted in higher utilisation factors.

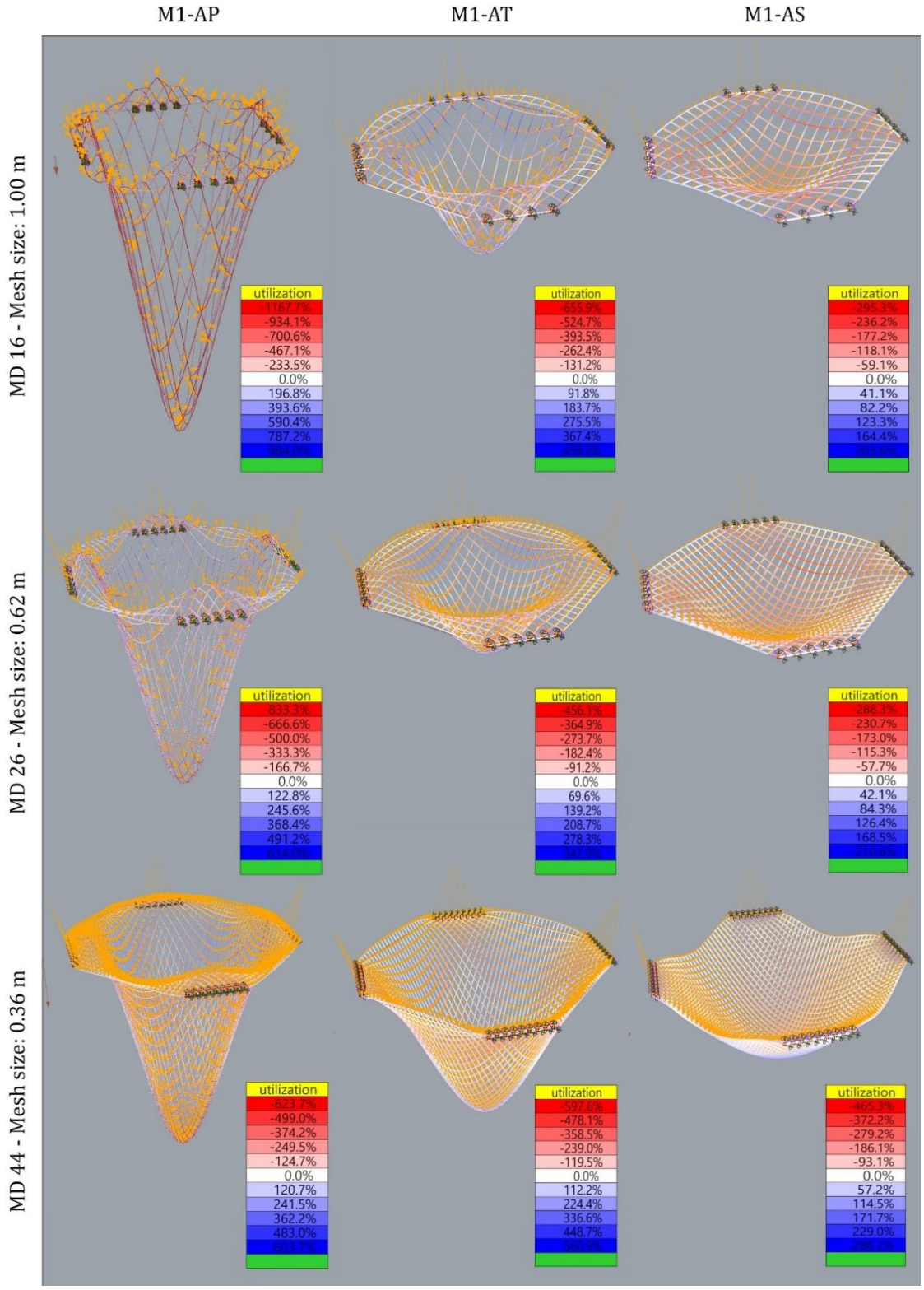


Figure 7-4. Deformed shape due to mesh density modification on Model 1.

An evaluation of mesh density modification and maximum displacement showed similar trends, as depicted in Figure 7-5a. Displacements across all models decreased noticeably when the mesh density increased from 16 to 20, corresponding to a reduction in mesh size

from 1.00 x 1.00 m to 0.80 x 0.80 m. Beyond this point, the behaviour varied across models. Models using *G. apus* exhibited a linear reduction in displacement with increasing mesh density, though the reduction became less significant after a mesh density (MD) of 20. Conversely, models using *G. atter* showed a slight reduction in displacement only until the MD was modified to 32. Beyond an MD of 32, the displacement increased. Similarly, in models using *D. asper*, displacement gradually increased with mesh density after MD 20. These results indicated that the effectiveness of mesh density in stabilising the structure varied among bamboo species, likely due to differences in cross-sectional dimensions and overall weight of the structures.

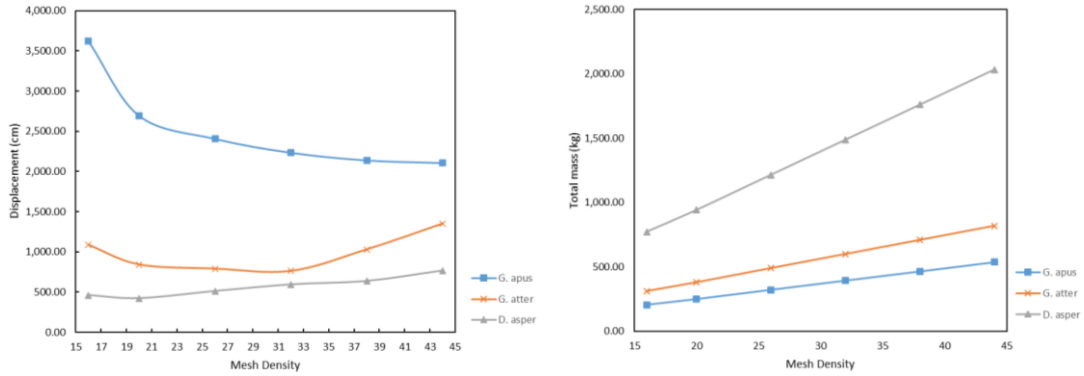


Figure 7-5. Effect of mesh density: a. Mesh density and displacement; b. Mesh density and total mass.

The observed differences in displacement behaviour can be attributed to the total mass of the structures. Increasing the mesh density necessitated the installation of more bamboo culms, consequently increasing the self-weight of the structures. Although bamboo is generally recognised as a lightweight material, variations in diameter, wall thickness, and density among different species significantly influenced the total mass. As illustrated in Figure 7-5b, the total mass of models using *G. apus* bamboo remained comparatively light, with a minimal increase in mass despite higher mesh density. In contrast, the total mass of the models incorporating *G. atter* and *D. asper* increased significantly as the mesh density intensified, thereby adding substantial dead loads to the structures. Consequently, displacement escalated in proportion to the mesh density. While the average densities of the three bamboo species showed minimal variance, the dimensions and wall thickness of *G. atter* and *D. asper* were notably greater than *G. apus*.

The results indicated that beyond a certain threshold, increasing mesh density negatively impacted the structural integrity of the gridshells. Excessively dense meshes can lead to inefficiencies and potential structural vulnerabilities. From a practical standpoint, higher

mesh density complicates the construction process of gridshell structures. The complexity arises from the need to manage and assemble a larger number of bamboo culms, which demands more time and precision during construction. Furthermore, the increased number of members and weight pose challenges in handling and positioning, especially where manual assembly is required. Therefore, while denser meshes may initially seem advantageous for enhancing structural rigidity, their impact on displacement and practicality must be carefully considered. Higher mesh densities may lead to higher labour costs and extended project timelines, thereby affecting overall project feasibility.

Modifying the mesh configuration from quadrilateral to triangular significantly improved the overall structural performance. When comparing the initial model, which exhibited extreme deformation and displacement, a notable reduction can be observed in Figure 7-6. However, the utilisation factors and displacement values remained high, with all utilisation factors exceeding the threshold of 100%. Only the model using *D. asper* with triangulation in two directions fell below the threshold, with utilisation factors of 94.1% in compression and 16.8% in tension. These results indicate that although mesh configuration effectively enhances structural performance, additional modifications are necessary to achieve stable structures.

Mesh triangulation proved effective in minimising displacement, as depicted in Figure 7-7a. In all models, displacement was significantly reduced, with the triangular configuration providing better stability than the quadrilateral one. Consequently, the overall structural performance improved significantly. However, the recorded displacements remained extremely high, particularly for models using G. apus. Despite the two-way triangulation, displacements were recorded as 54.27 cm for G. apus, 25.75 cm for G. atter, and 26.45 cm for D. asper.

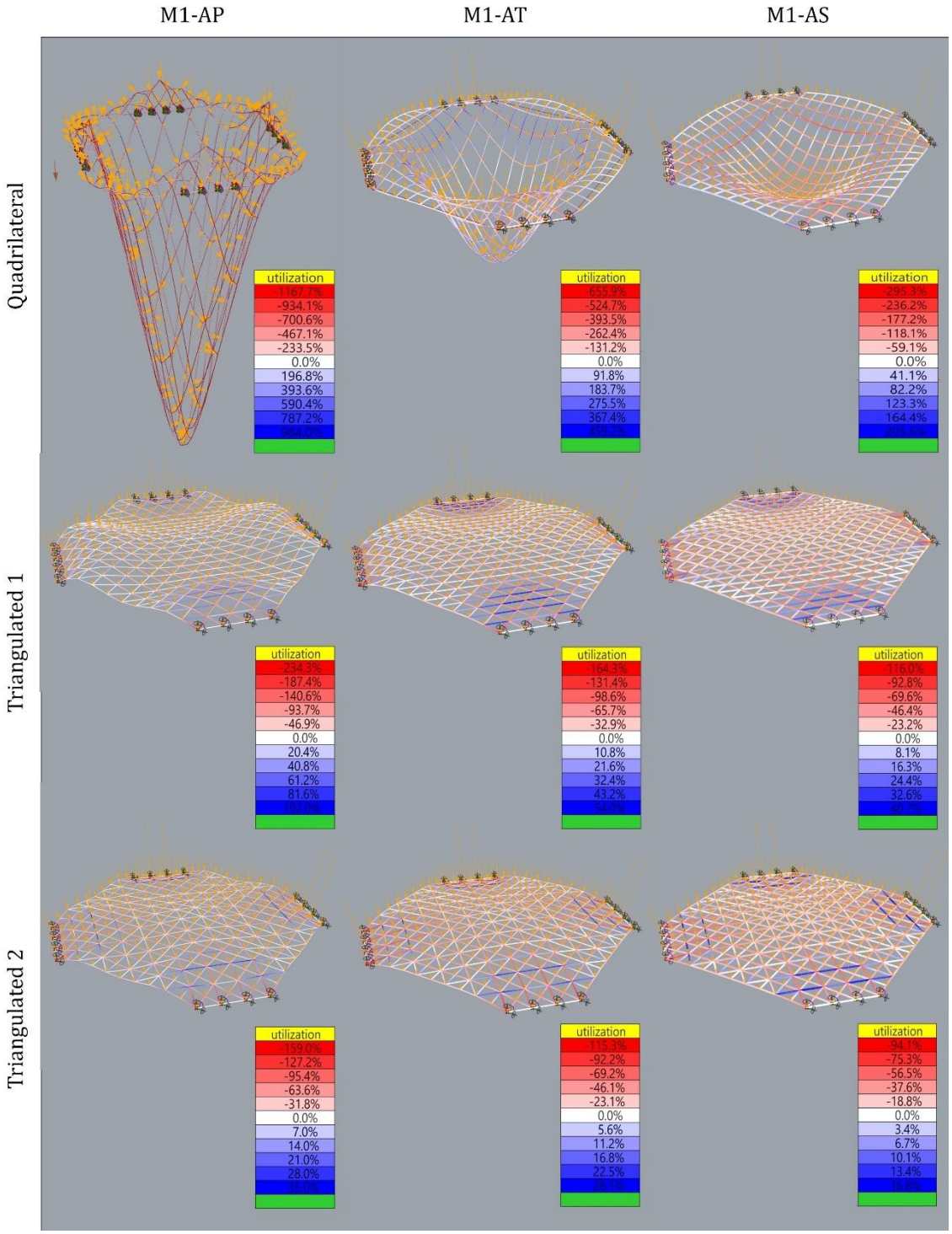


Figure 7-6. Shape deformation resulting from mesh configuration modification.

Two-way triangulation demonstrated better performance compared to one-way triangulation (Figure 7-7a). In terms of material usage, both one-way and two-way triangulation utilised a similar amount of material, resulting in comparable total mass. Therefore, self-weight did not affect structural performance, and the improvement was solely due to the configuration. Two-way triangulation enhanced performance by

approximately 30%-40% compared to one-way triangulation. For example, the maximum utilisation factor in compression for the model using G. apus with one-way triangulation was 234.30%, while two-way triangulation reduced it to 159.00%, a reduction of 32%. This demonstrates the effectiveness of two-way triangulation, as also depicted in Figure 7-7b.

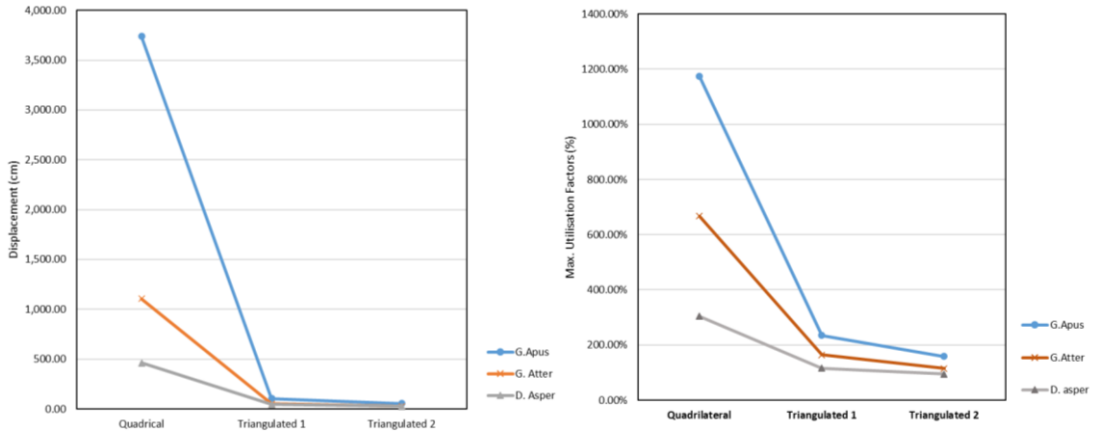


Figure 7-7. a. Effect of mesh configuration modification on utilisation factors; b. Effect of mesh configuration on displacement

These results demonstrate that changing the mesh configuration from quadrilateral to triangular effectively increase the structural performance of full-culm bamboo gridshell models. Two-way triangulation exhibited superior performance in utilisation factors and displacement, showcasing its efficacy in distributing stress and withstanding forces. However, additional modifications are required to achieve fully stabilised structures from the initial model.

Modifying the sizing of gridshell members was undertaken by adding layers to the grids. Constructing bamboo structures with more than one pole is a common practice in bamboo construction, applied to mitigate uncertainty factors and ensure structural safety. Bamboo is susceptible to longitudinal splitting due to changes in moisture content and can suddenly fail under applied loads due to its brittle characteristics. This is known as redundancy in bamboo structures. Given that each bamboo species has unique cross-sectional dimensions, this method was adopted to assess the effect of sizing modification.

Maintaining a consistent mesh size of 1.00 x 1.00 m, layers were incrementally added to each grid line, and the structural performance was analysed. The model structures' curvature was assumed to consist of layers of bamboo culms, ranging from one layer to six layers in each curvature line. Figure 7-8 illustrates significant displacement reduction from the initial models as the layer count increased from one to two. Deformation exhibited

similar patterns to mesh density, with stresses concentrated in the middle part of the geometry, resulting in the greatest deformation and displacement in that region.

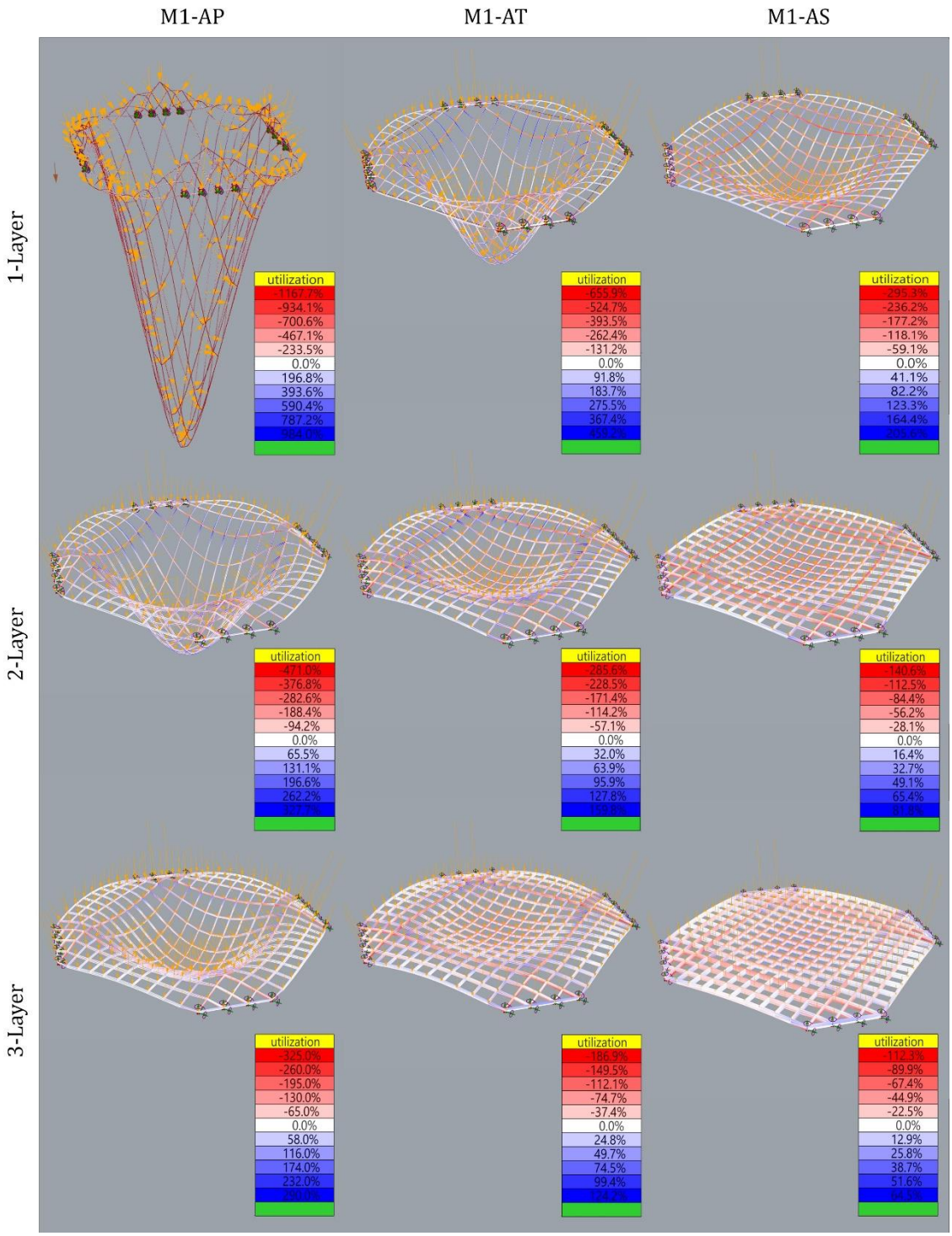


Figure 7-8. Shape deformation due to modification in the number of bamboo grid layers.

Sizing modification showed a similar trend to mesh density in terms of material usage; however, in displacement, sizing modification demonstrated better performance, as

evidenced by the graphs in Figure 7-8 and Figure 7-9. Adding a second layer to the mesh significantly reduced the utilisation factors (Figure 7-8) and also significantly decreased displacement. However, the contribution of adding subsequent layers became gradually less significant (Figure 7-9a). Adding layers to grid members increased flexural stiffness and improved structural performance. Nonetheless, similar to mesh density, incorporating more bamboo culms increased the total mass of the structures. Figure 7-9b shows a significant increase in total mass, especially for *D. asper*.

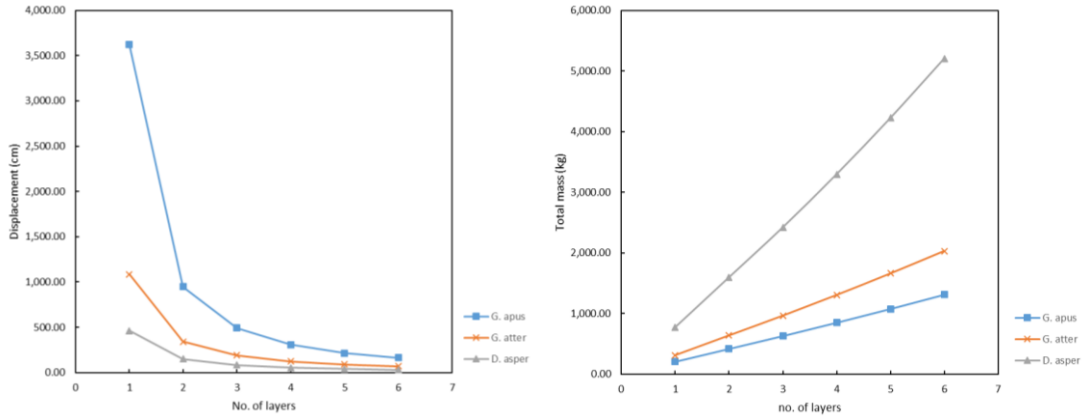


Figure 7-9. Effect of sizing modification: a. on the displacement; b. on the total mass.

These results indicate that sizing modification by adding layers to the grid members should aim to identify the optimal number of layers to achieve the best structural performance while maintaining material usage efficiency. As with mesh density, adding layers could increase the total mass, thereby reducing material efficiency. Furthermore, adding layers could complicate the assembly and erection process of full-culm bamboo gridshell structures. Precise connection systems, boundary conditions, and supports should be carefully designed to ensure structural stability and safety.

7.3.3. Optimisation of Full-Culm Bamboo Gridshell Model

Considering the assessment of the effectiveness of modifications, the baseline structure was determined by evaluating several key factors: aesthetics, material usage, structural efficiency, and ease of construction. From an aesthetic perspective, among the three bamboo species, *G. apus* demonstrated its ability to achieve deeper curvatures, as presented in Figure 7-3 and Table 7-6Table 7-6. Radii of curvature and height resulting from the form-finding process.. In contrast, *D. asper* resulted in almost flat gridshells without significant curvature. Although *G. atter* showed moderate bending performance, its gridshell geometry was less

pronounced than that of *G. apus*. Therefore, from an aesthetic standpoint, *G. apus* is the best selection.

In terms of material usage, *G. apus* offers a balanced approach, indicated by a less significant increase in total mass in all modifications compared to the other species. *D. asper*, with its large outer diameter and thick walls, exhibited a significant increase in total mass, which not only reflects higher material usage but also impacts boundary conditions and supports. *G. atter* showed moderate performance but had similar behaviour to *D. asper* in terms of mesh density, as shown in Figure 7-15, where its material usage increased significantly. This result indicates that the lightness of *G. apus* is beneficial for material efficiency.

Regarding structural efficiency, *G. apus* demonstrated greater versatility. Although initial simulations showed that *D. asper* had the smallest utilisation factors, its performance tended to stagnate or become less significant due to its weight. *G. apus*, on the other hand, could significantly improve its performance with appropriate modifications such as adding layers and adjusting mesh density. This adaptability makes *G. apus* a more efficient choice for achieving an effective structure.

Ease of construction is a critical factor, particularly for large-scale gridshell projects. *G. apus*, with its smaller outer diameter, would be easier to bend and assemble into a gridshell structure. In contrast, bending a culm of *D. asper* could be very challenging. Its outer diameter can reach up to 15-20 cm, and wall thickness can exceed 2 cm. These properties would complicate the bending process and logistics. The smaller, more manageable dimensions of *G. apus* not only simplify the construction process but also enhance safety and reduce labour costs.

Therefore, the baseline model in this study was designed based on the selection of G. apus as the primary material. The baseline model incorporated modifications assessed previously, featuring a mesh size of 1.00 x 1.00 m (MD16), two-way triangulation (MC2), and utilising two layers of bamboo culms (SZ2). Structural analysis of the baseline model revealed utilisation factors of 72.10% in compression and 18.30% in tension, a total mass of 708.63 kg, and a displacement of 22.61 cm. The baseline geometry for Model-1 is illustrated in Figure 7-10.

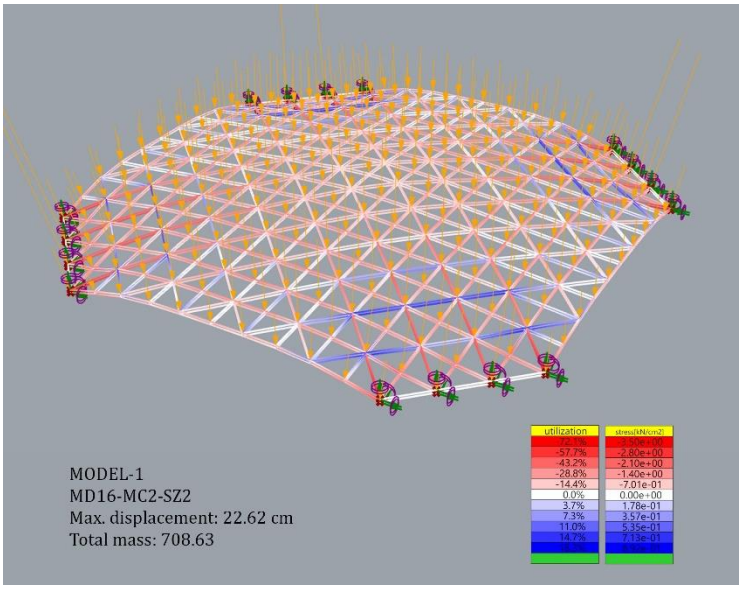


Figure 7-10. Baseline Model-1 for optimisation.

Optimisation was carried out by adjusting the mesh density across a range from MD12 to MD18 and by adding layers from SZ1 to SZ3, as depicted in Figure 7xx. Decreasing the mesh density from MD14 to MD12 resulted in notable increases in displacement and utilisation factors, suggesting that stresses were exceeding the material's capacity limits, leading to significant deformation and potential structural failure. Consequently, the emphasis shifted towards increasing mesh density to enhance structural integrity.

The series of optimisation simulations led to the identification of an effective mesh density for the gridshell model, as depicted in Figure 7-12. The optimal mesh density was found to be MD14, with a mesh size of approximately 1.14 x 1.14 m. At this configuration, both the utilisation factor and displacement were minimized, indicating the ideal mesh size for gridshell models. Increasing the mesh density to MD16 and MD18 resulted in higher utilisation factors and displacement values, consistent with the simulations discussed in Section 7.3.2.

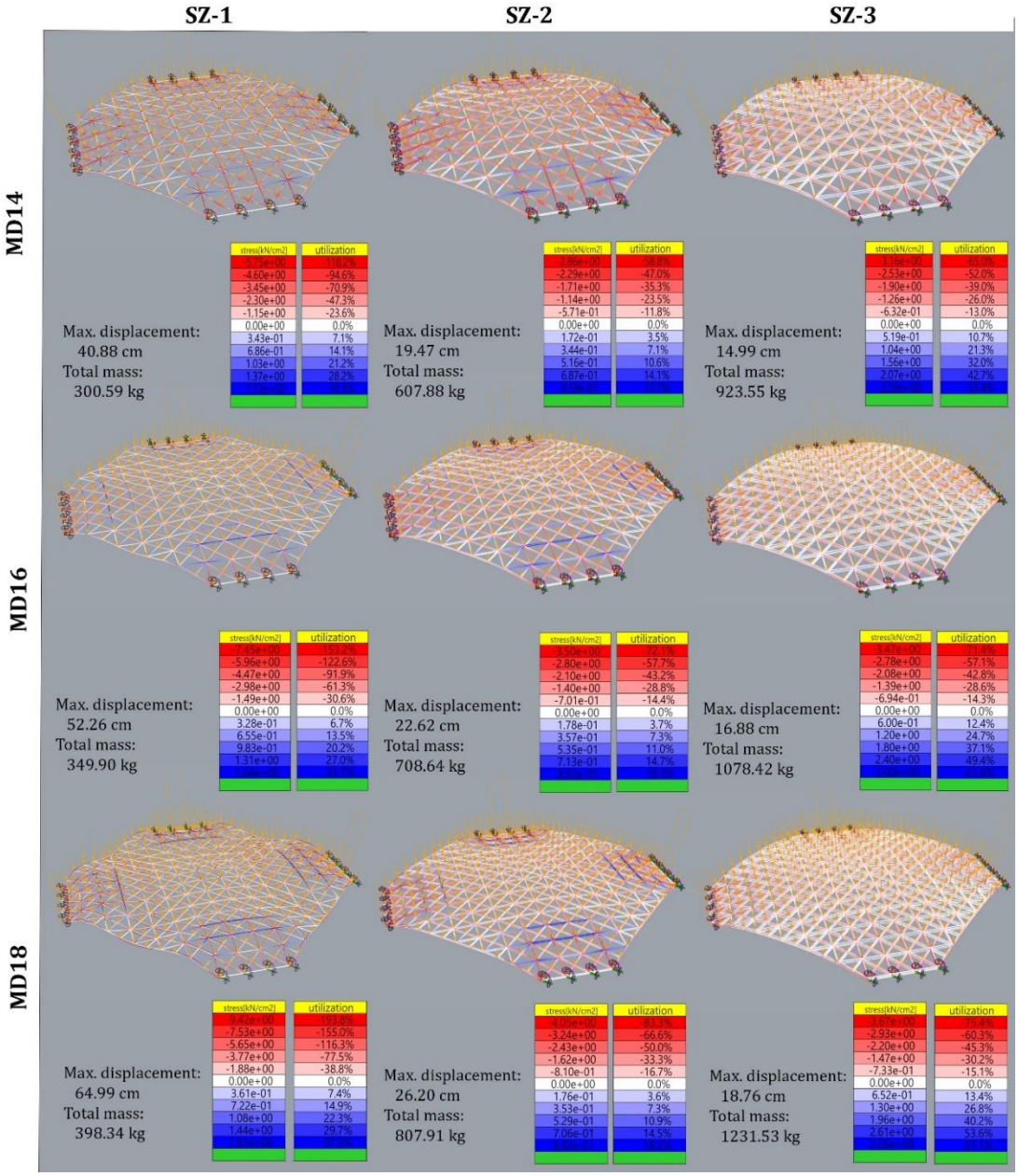


Figure 7-11. Optimisation of Model-1

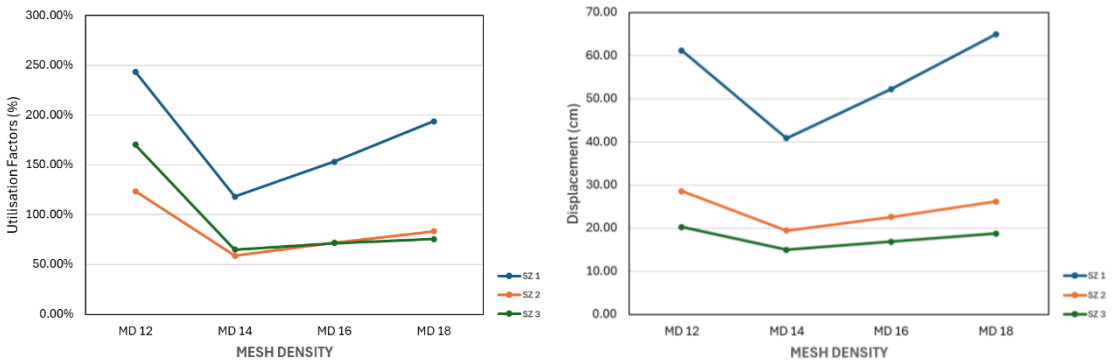


Figure 7-12. a. Effect of mesh density and sizing optimisation on utilisation factors; b. Effect on displacement of Model-1 using full-culm bamboo G. apus.

Adding layers effectively improves the structural performance, as illustrated in Figure 7-12. A single layer of bamboo was unable to withstand the loads, resulting in compromised structural integrity evident from the high utilisation factors and displacement. By adding an additional layer of bamboo, stiffness was increased, thereby enhancing the ability to maintain structural integrity.

Therefore, based on the results, the optimised model was MD14-SC3, indicating a gridshell model with a mesh size of 1.14 x 1.14 m, configured with two-way triangulation, and comprising three layers of bamboo culms. The optimised model successfully reduced displacement to 14.99 cm and utilisation factors to 65% in compression and 53.40% in tension. Despite an increased total mass of 923.55 kg, the significant reduction in displacement, while simultaneously improving the utilisation factors, demonstrates the effectiveness of the optimisation.

7.3.4. Form-Finding of Split Bamboo

The form-finding process for the spilt bamboo gridshell models commenced with the establishment of a flat grid layout on the ground plane. This initial step involved defining the outer boundary or perimeter members of the grid structure. Inside the boundary, a series of points and polylines were plotted to define the grid members. These points and polylines were then interconnected and intertwined to establish the basic framework of gridshell geometry. The process ensured that the grid configuration could mimic the behaviour of bending-active principles during the form-finding process.

To facilitate the form-finding process, adjustable anchor points were placed at the four corner lines. These anchor points were designed to be moveable and adjustable, controlled through sliders that dictated the extent of their movement. These adjustable anchor points allowed for iterative adjustable during form-finding process and mirrored the construction method employed in the form-finding of split bamboo as described in CHAPTER 6 of this study.

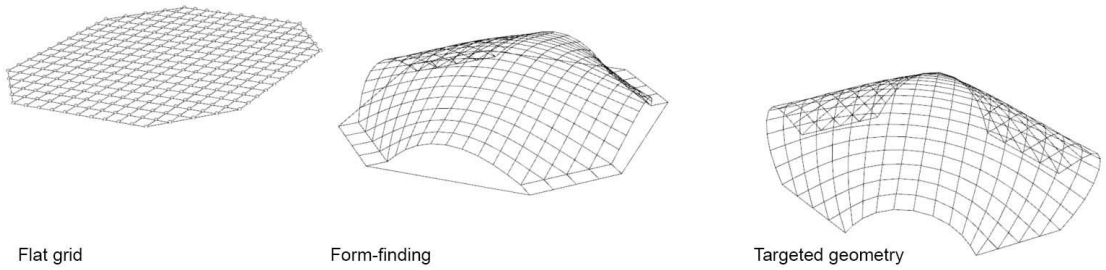


Figure 7-13. Form-finding process of targeted geometry of Model-2.

The elements in Grasshopper were inputted to Kangaroo to generate the gridshell models as illustrate in Figure 7-13. Load factors were applied, and the anchor points were adjusted to achieve the desired curvature. Given the material's nature as split bamboo, achieving deeper curvatures was highly feasible. Consequently, the form-finding process was finalised based on the heights achieved in the full-scale model described in CHAPTER 6

7.3.5. Effect of Modifications on Structural Performance of Split Bamboo Gridshell Models

Using the geometry presented in Figure 7-13, modifications to mesh density (MD) were performed. The mesh density was increased from MD 14, with a mesh size of 0.60 x 0.60 m, to MD 38, with a mesh size of 0.22 x 0.22 m. This increase was feasible for split bamboo due to its lighter weight and flexibility, similar to the weaving system of bamboo baskets. Figure 7-14 illustrates the deformation resulting from the densification of the mesh, showing that the models remained unstable. The utilisation factors of the initial model were extremely high, exceeding the threshold of 100%, indicating that the stresses surpassed the material's capacity, leading to structural collapse. This suggests that simply increasing mesh density could not produce stable structures.

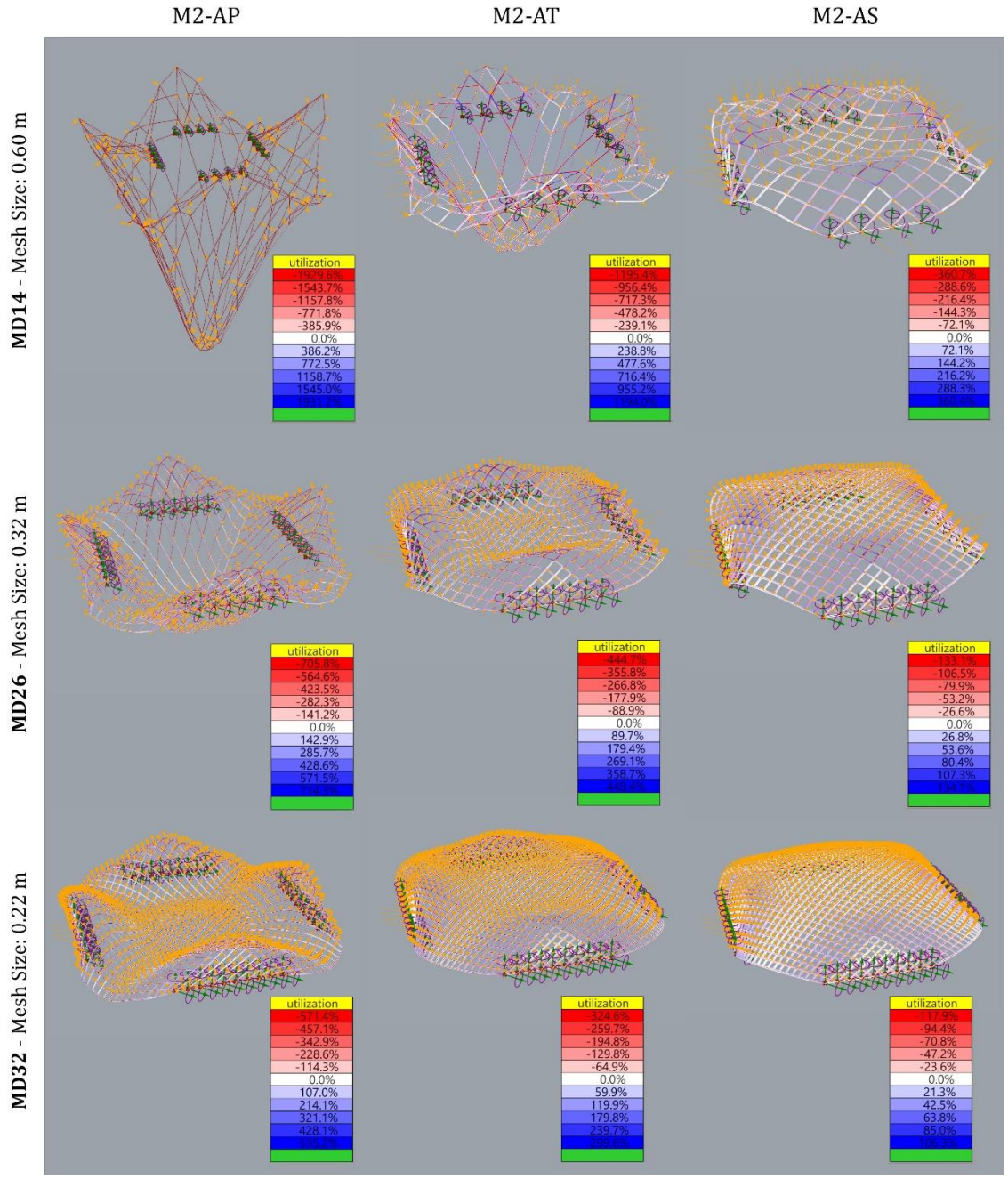


Figure 7-14. Results of mesh density modification on utilisation factors of Model 2.

The effects of mesh density on displacement and total mass are presented in Figure 7-15. Modification on mesh density on Model-2 showed different results to Model-1, particularly with *D. asper*. For models using *G. apus* (M2-AP), modification on mesh density significantly reduced displacements. The displacements were greatly reduced when the mesh density increased, and the grids were denser. A similar pattern was shown in models using *G. atter* (M2-AT); the displacements were reduced along with the increase of mesh density, even though not as significant as M2-AP. Meanwhile, the displacements on models using *D. asper* (M2-AS) were also reduced when the mesh densities were increased. However, the

displacement reduction became less significant when the meshes were getting denser (from MD26 to MD 38).

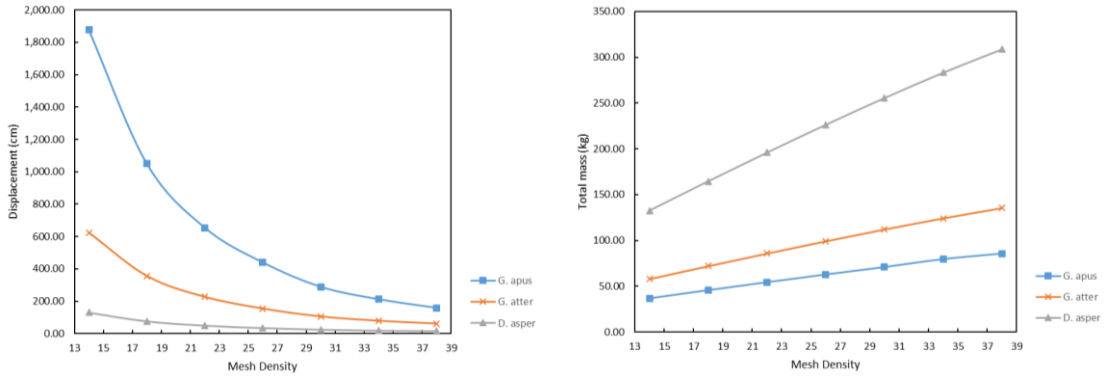


Figure 7-15. Effect of mesh density on Model 2: a. Effect on the maximum displacement; b. Effect on the total mass.

Examining the effect of mesh density on the total mass of the structure in Figure 7-15b, split bamboo was significantly lighter than bamboo culms, and the total mass was lower than bamboo culms. Aside from the density, the total mass was also related to the member's profile dimension of each species. Bambo *G. apus* in the analysis had the highest density; however, since *G. apus* had the smallest outer diameter, the profile of split bamboo was also the smallest compared to the other two species. Therefore, bamboo *D. asper* had the highest total mass since the profile's dimension was the biggest, and weight contributed to the displacement, even though not as substantial as in Model 1. As seen in the graph of *D. asper* in Figure xx. a., the displacements were slightly reduced when the mesh density was increased. The modification of Model 2 showed that increasing mesh density can reduce displacement. However, similar to Model 1, the displacements on all models were extremely high, indicating that modification by only increasing the mesh density did not provide better structural performance.

Changing the mesh configuration from quadrilateral to triangular showed significant improvement across all gridshell models which enhanced the overall structural integrity, as depicted in Figure 7-16. From the utilisation factors presented in the figure, the stress distribution in Model 2 was more balanced with the utilisation factors in compression (negative value) and in tension (positive value) becoming more similar. The higher curvature and triangulated mesh configuration contributed to this balance by providing better stability.

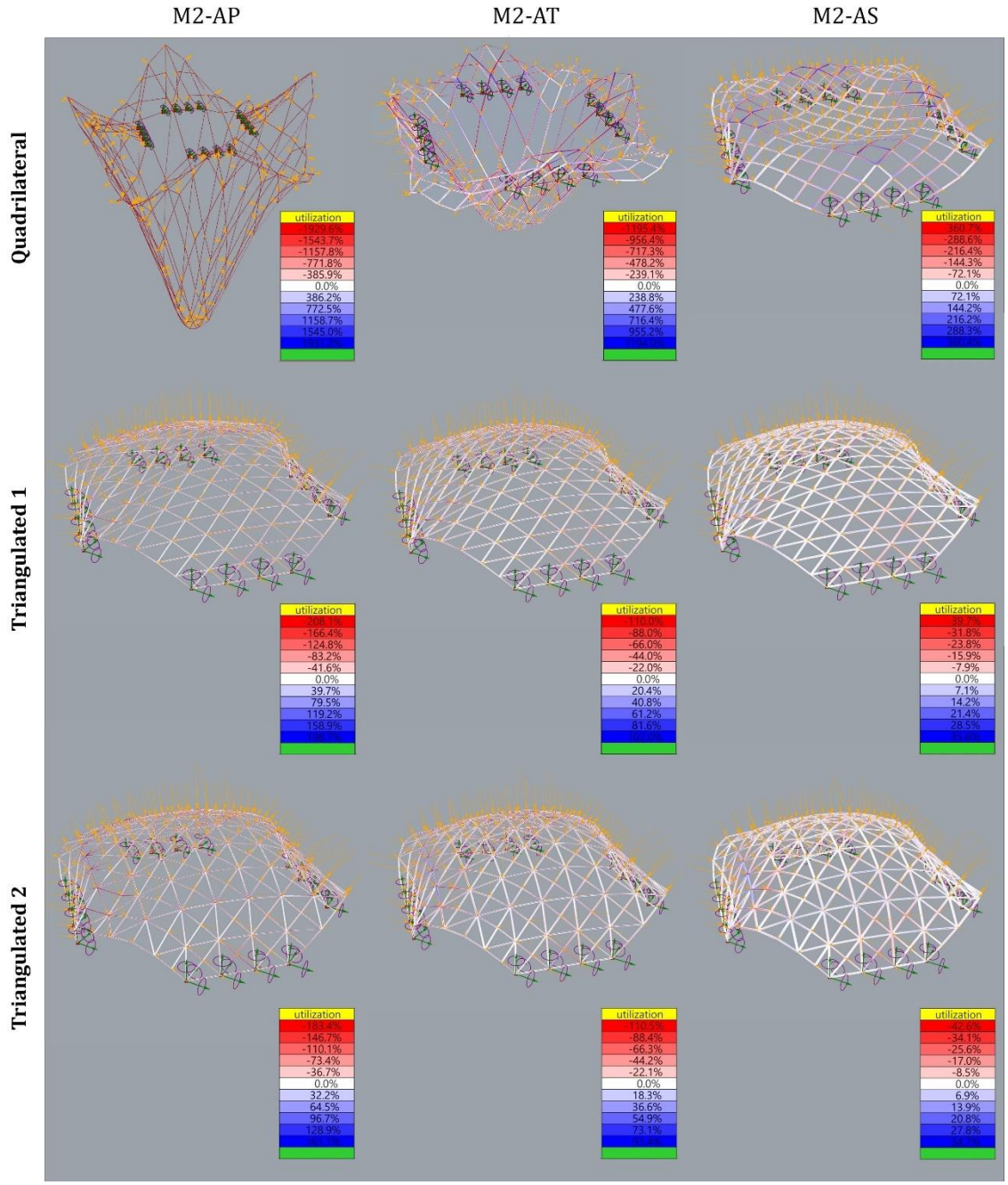


Figure 7-16. Deformed shape and utilisation factors of mesh configuration modification.

However, among all the gridshell models, only the models using D. asper were fully stabilised by the triangulation modification, while other models remained unstable. This discrepancy was influenced by the cross-sectional dimensions of the split bamboo used. G. apus had a small cross-sectional dimension, and G. atter had significantly thin walls, both of which affected the overall profile's height and stability. Consequently, models using these two bamboo species required further modifications to achieve full stabilisation.

Interestingly, the results of one-way and two-way triangulation on Model-2 showed a different trend compared to Model-1, as presented in Figure 7-17. In Model-2, there was no

significant difference between one-way and two-way triangulation. This can be seen from the utilisation factors in the figure, where the one-way triangulation managed to significantly reduce the utilisation factors and displacement. However, modifying to two-way triangulation showed similar results to one-way. This trend differed from Model-1, where two-way triangulation performed better than one-way. This result might be influenced by the higher curvature in Model-2, leading to an even stress distribution within the grids.

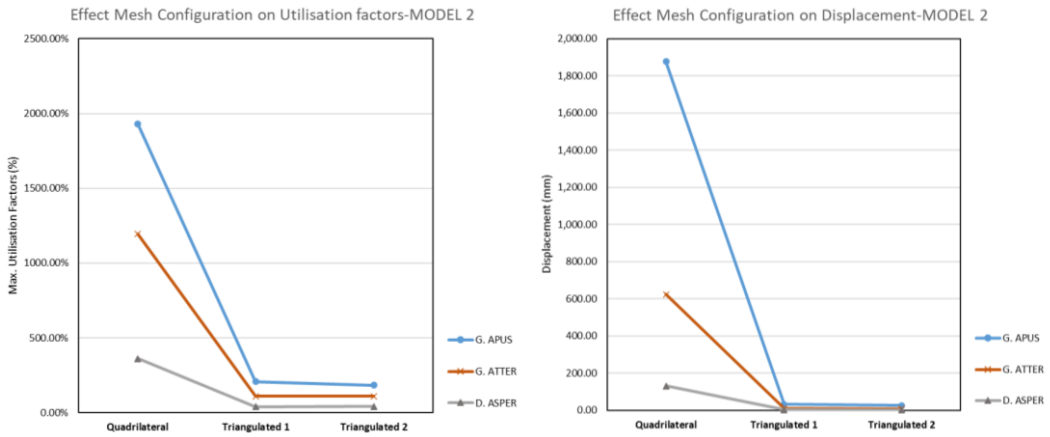


Figure 7-17. a. Effect of mesh configuration modification on utilisation factors; b. Effect on displacement.

Modifying the mesh configuration from quadrilateral to triangular enhanced the structural integrity and stress distribution. For Model-2, both one-way and two-way triangulation showed similar performance in reducing stress distribution, utilisation factors, and displacement, while not significantly increasing the total mass. These results demonstrated the significant role of mesh configuration in stabilising the structures.

Modifying the size of the grid members was performed by adding layers, similar to Model 1. The number of layers in Model 2 was initially set to two and gradually increased to four. As presented in Figure 7-18, the deformed shapes of the modified models showed better structural performance than the initial models. All models exhibited less deformation as the number of layers increased, with significant improvements observed in models using G. apus. These results indicate that the sizing modification effectively stabilised the structure. Increasing the profile height through additional layers consequently increased the structure's stiffness.

The outer diameter of the G. apus culm was the smallest among the three species, resulting in small profile dimensions for the split form, with an assumed width of 2.80 cm

and a thickness of 0.48 cm. In contrast, D. asper had the largest diameter and thickest wall, with profile dimensions assumed to be 6.00 cm in width and 0.74 cm in thickness. Considering these profile dimensions, models using D. asper achieved stabilised structures with fewer layer additions.

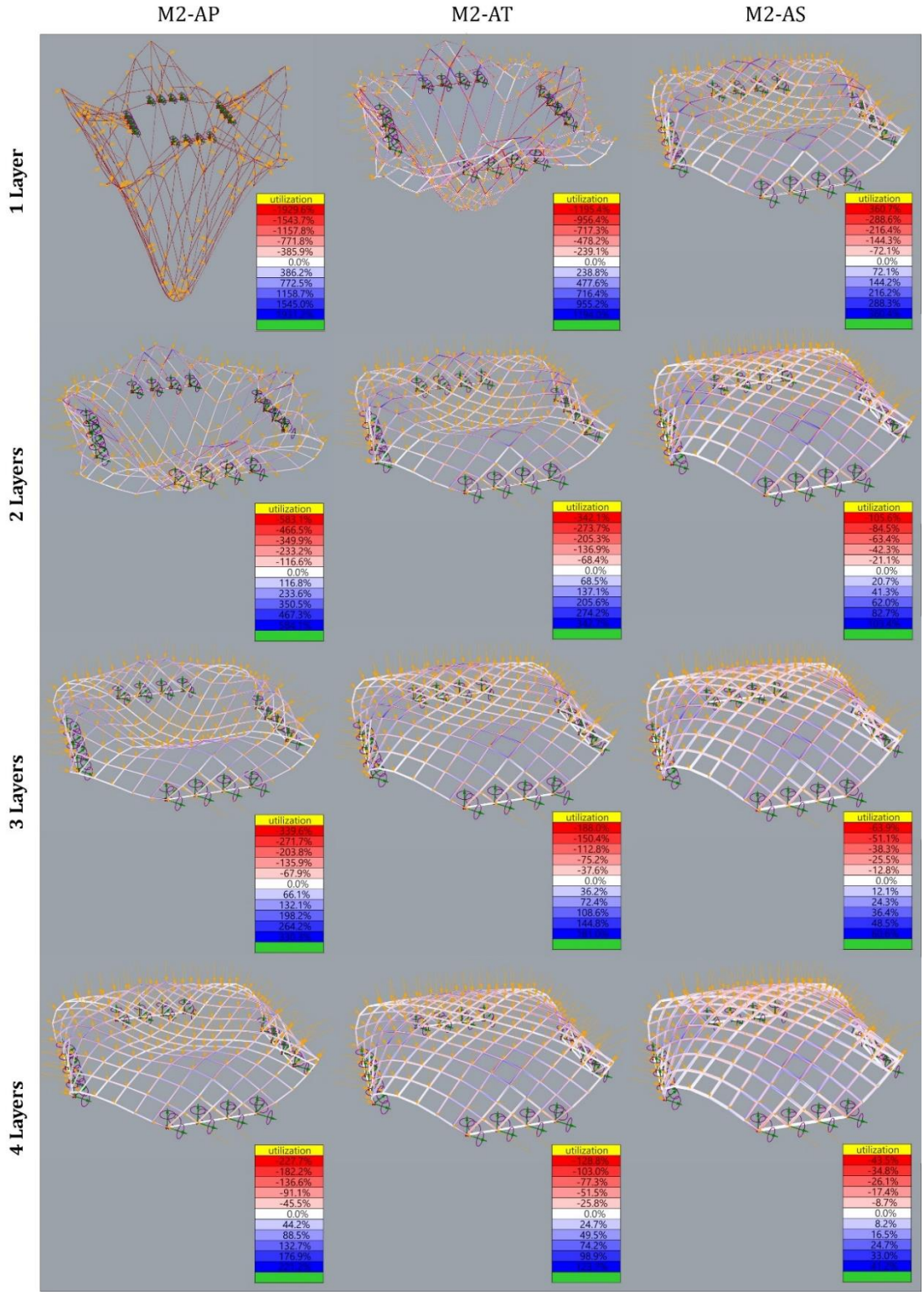


Figure 7-18. Deformed shape and utilisation factors due to sizing modifications

The effect of sizing optimisation on the displacement can be seen in Figure 7-19a, and the graph showed the displacement in model using *G. apus* reduced immediately once one layer was added to the structure. However, although the layers had been increased three times, the structure had not stabilised, and the final displacement was 117.90 cm, which was extremely high, and the structure collapsed. Similarly to models using *G. atter*, the final displacement after the layer increase was 40.19 cm. However, the model using *D. asper* was able to reach minimum displacement, which was only 9.46 cm in the final optimisation iteration.

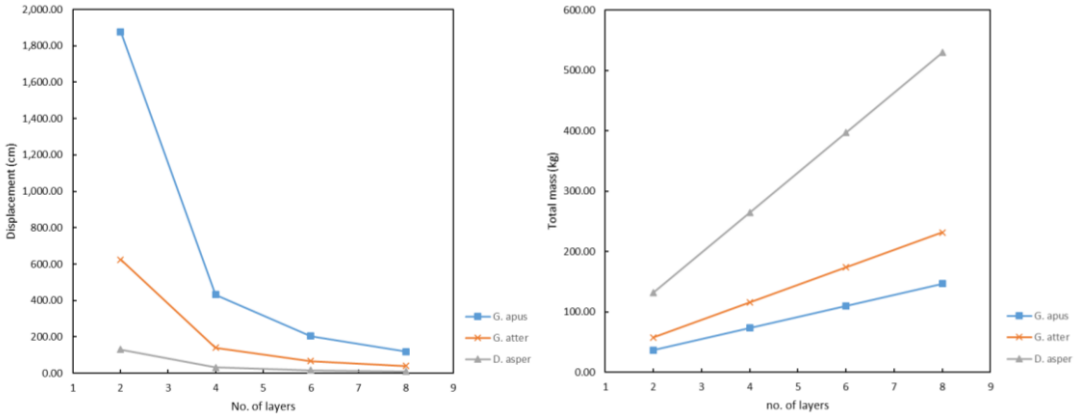


Figure 7-19. a. Effect of sizing modification on displacement; b. Effect on total mass.

The downside of adding more layers was the increase in total mass, which was greater than the increase resulting from modifications of mesh density and mesh configuration. As seen in Figure 7-19b, the total mass of all models increased significantly, with the increment being higher than that observed for mesh density and mesh configuration modifications. However, since split bamboo is considerably lighter than full-culm bamboo, the effect on displacement was less significant. Additionally, as the modification of sizing increased the profile's height, it also increased the structure's stiffness more significantly than modifications of mesh density.

7.3.6. Optimisation of Split Bamboo Gridshell Model

The results from the assessment of optimisation parameters in Section 7.3.5 indicated that all bamboo species, in their split form, showed potential for use in gridshell structures. Consequently, optimisation was conducted on all bamboo species to determine the most suitable structures for each. The baseline models were designed by first stabilising the initial

model. The baseline model used gridshell structures with span dimensions of 8.40 x 8.40 m and a mesh size of 0.60 x 0.60 m (MD14) as the initial geometry from form-finding. To stabilise the structure, the mesh configuration was changed to triangular in two-way direction (MC2), and two layers were added (SZ2). The baseline structure is depicted in Figure 7-20.

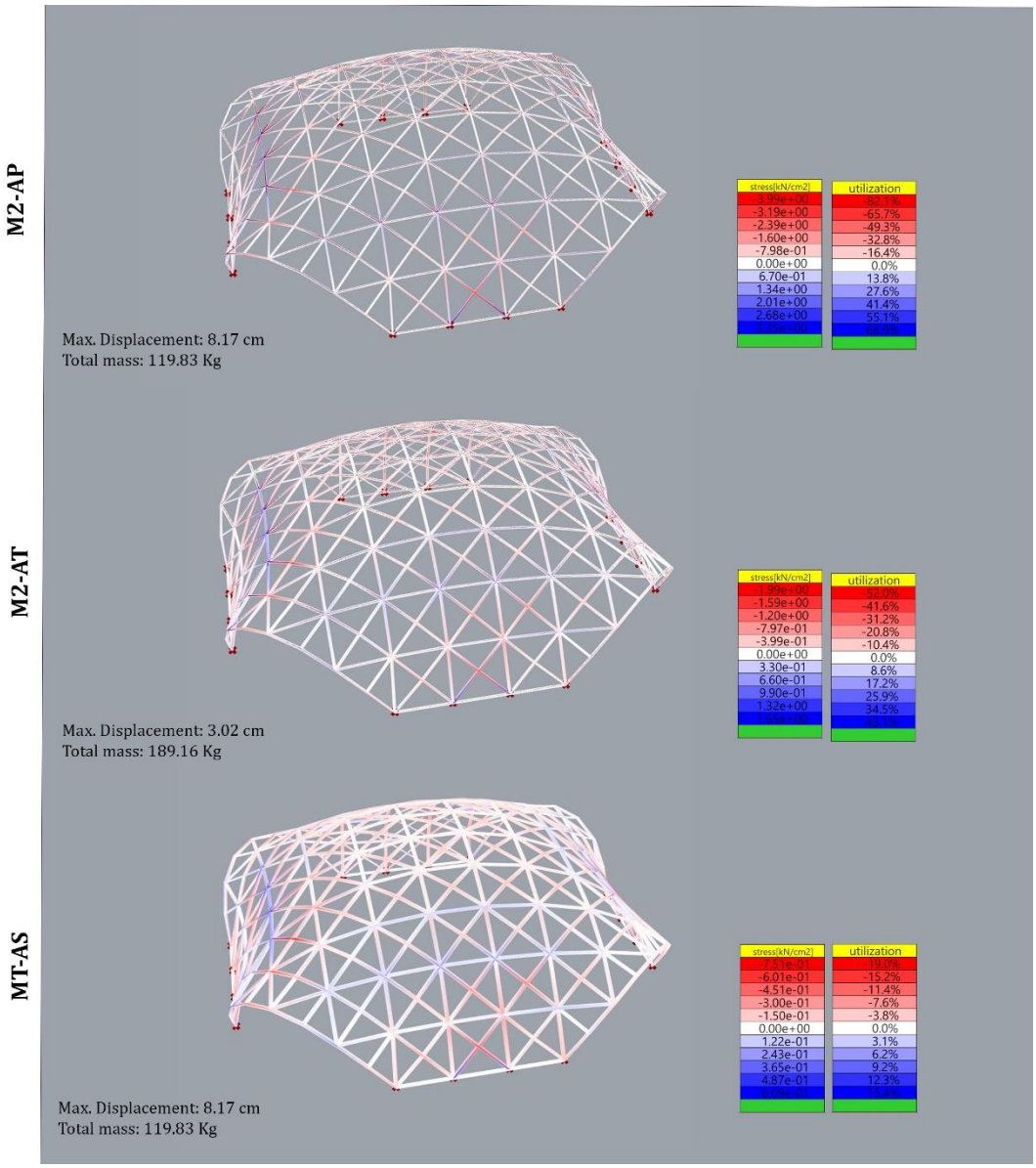


Figure 7-20. Baseline Model-2 for optimisation.

The baseline structures were stabilised, with maximum utilisation factors below the threshold of 100%: 82.10% for G. apus, 52% for G. atter, and 19% for D. asper. Optimisation aimed to enhance structural efficiency and material usage, considering utilisation factors, displacement, and total mass. During optimisation, the mesh configuration was set to two-

way triangulation, while the mesh density was varied between MD12 and MD18, and the sizing was modified from one to three layers.

Optimisation results for Model-2 using G. apus showed that increasing the mesh density significantly reduced utilisation factors and displacement at MD16. However, increasing the mesh density to MD18 led to higher utilisation factors and displacement. Although the utilisation factors of MD18 remained below the threshold, with SZ1 having a utilisation factor of 88.70% in compression and 64.90% in tension, it is crucial to note that increased mesh density also increased the total mass. Furthermore, increasing the mesh density to MD18 significantly increased displacement, particularly for the model with one layer, where displacement rose from 6.57 cm to 18.46 cm. Despite the utilisation factor being below the threshold, indicating the material's capacity to withstand the stresses, the high displacement suggested significant deformation under applied loads.

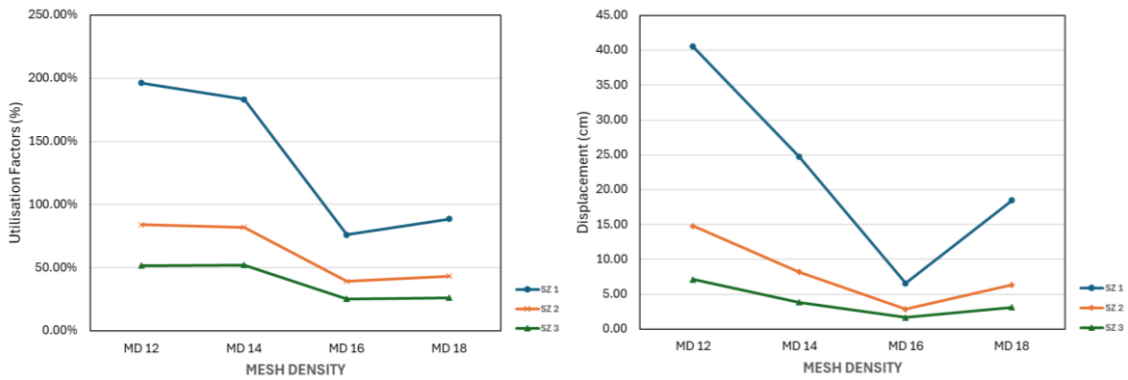


Figure 7-21. a. Effect of optimisation by modifying mesh density and sizing on utilisation factors of Model-2 using Gigantochloa apus; b. Effect on displacement.

Model-2 using *G. atter* exhibited similar performance to *G. apus*, with utilisation factors and displacement increasing when the mesh density was reduced to MD12 and showing optimal performance at MD16 (Figure 7-22). Additionally, both utilisation factors and displacement increased at MD18. However, overall displacement and utilisation factors were lower than those in models using *G. apus*. When utilised as split bamboo, the cross-sectional dimension of *G. atter* was wider than that of *G. apus*, with a similar wall thickness. This sectional profile contributed to the improvement of structural performance.

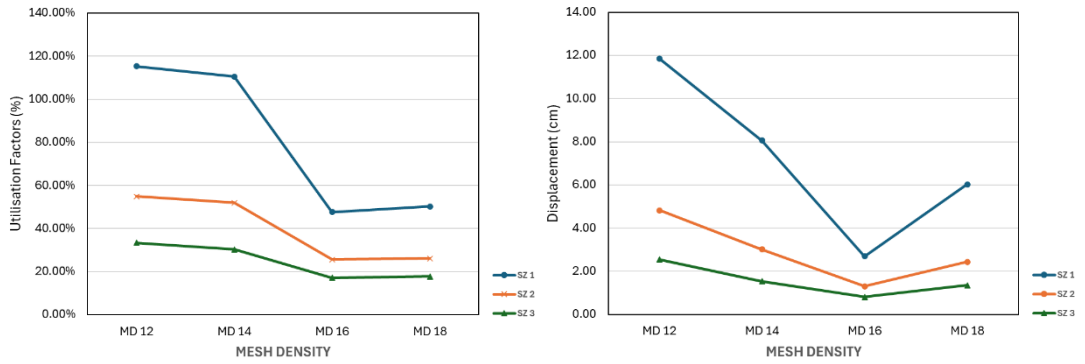


Figure 7-22. a. Effect of optimisation by modifying mesh density and sizing on utilisation factors of Model-2 using Gigantochloa atter; b. Effect on displacement.

Model-2 using *Dendrocalamus asper* also exhibited a similar trend to the other two species. It is important to note that the baseline structure of *D. asper* already demonstrated great performance with a utilisation factor of 19% for compression and 15.40% for tension, a displacement of 0.84 cm, and a total mass of 431.97 kg. Moreover, similar to the other two species, MD16 resulted in lower displacement and utilisation factors. Additionally, all modifications applied to D. asper resulted in utilisation factors and displacement within safety limits.

However, although these values demonstrated that the structure was stable and within safety limits, the low utilisation factors indicated that the material capacity was not fully utilised, suggesting inefficiencies in material usage. This inefficiency implies that there is potential to optimise the design further to make better use of the material's properties while maintaining structural integrity.

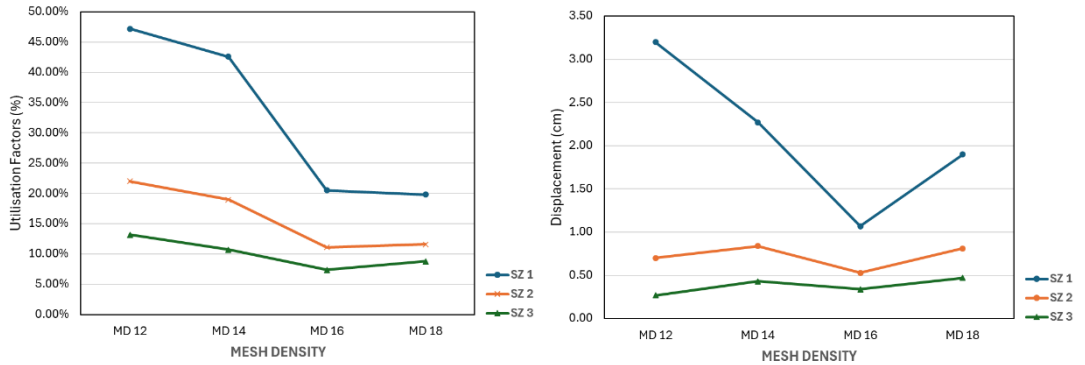


Figure 7-23. a. Effect of optimisation by modifying mesh density and sizing on utilisation factors of Model-2 using Dendrocalamus asper; b. Effect on displacement.

From these analyses, the optimised structures of Model-2 were proposed as illustrated in Figure 7-24. For Model-2 using *G. apus*, optimisation involved increasing the mesh density from MD14 to MD16 while reducing the layers from two to one. This optimisation improved overall performance by significantly reducing the total mass from 119.83 kg to 69.35 kg and

displacement from 8.18 cm to 6.57 cm. The utilisation factor of the optimised structure was 76.20% in compression and 47.10% in tension.

Model-2 using G. atter was similarly optimised by increasing the mesh density from MD14 to MD16 and reducing the layers from SZ-2 to SZ-1. This optimisation reduced the total mass from 189.19 kg to 109.48 kg and displacement from 3.02 cm to 2.70 cm.

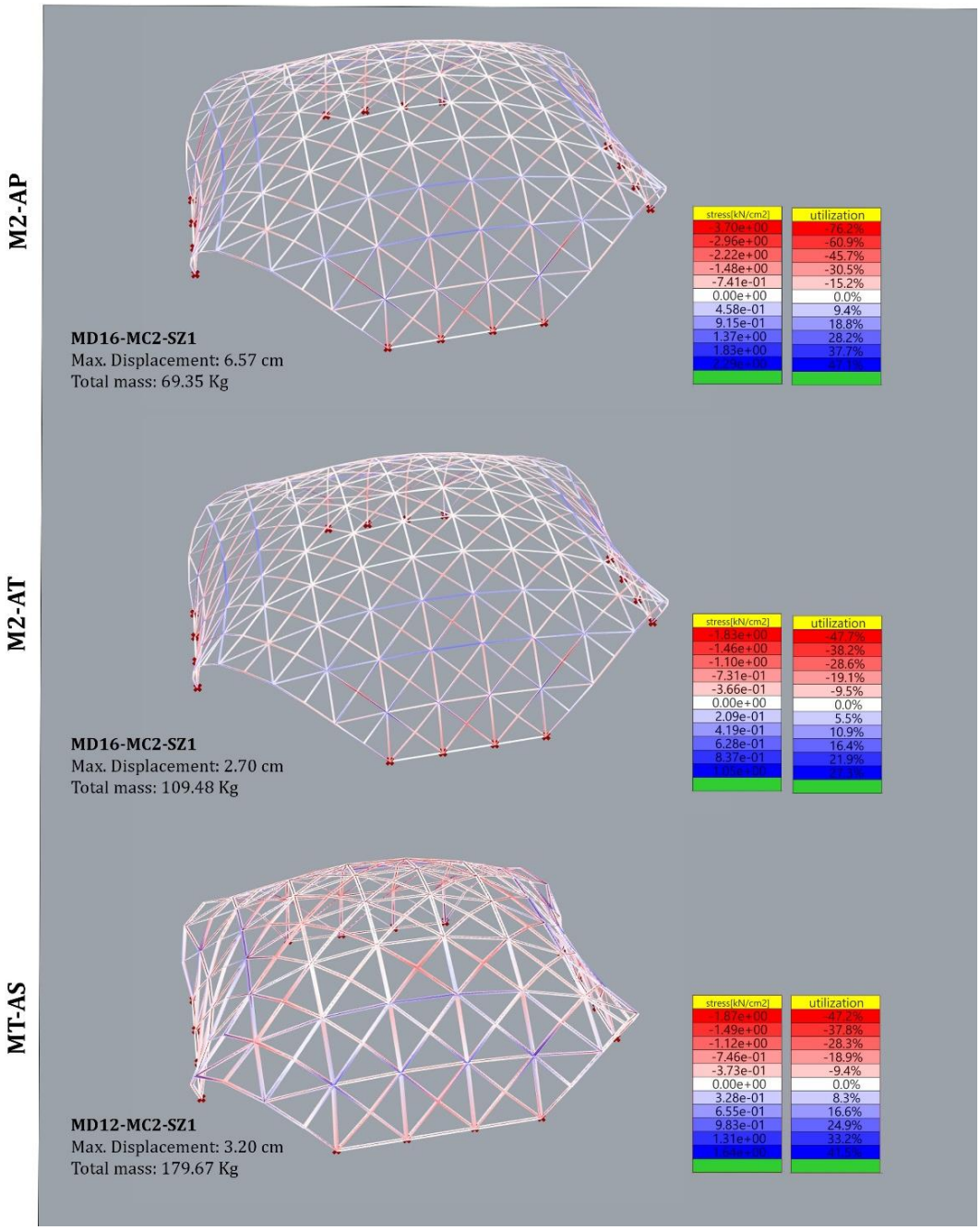


Figure 7-24. Proposed optimised structure for Model-2 using spilt bamboo based on the material selection.

Meanwhile, Model-2 using D. asper was optimised by reducing the mesh density from MD14 to MD12 and reducing the number of layers from SZ-2 to SZ-1. This optimisation increased the utilisation factors from 19% to 47.20% in compression and from 15.40% to 41.50% in tension, remaining within the safety threshold and enhancing the utilisation of material capacity. The optimised structure also reduced the total mass from 431.97 kg to 179.67 kg, while increasing the displacement from 0.84 cm to 3.20 cm. Although the displacement increased, the value remained small and within safe limits.

The optimisation process undertaken in this study underscored the distinctive attributes of bamboo, where each species exhibited unique dimensions and wall thicknesses that directly influenced their cross-sectional profiles. All species considered, including G. apus and G. atter, demonstrated promising potential for use in gridshell structures when employed in their split bamboo form. Notably, D. asper showed its greater potential in increasing the structural performance. Its superior performance attributes were evident across various parameters, confirming its suitability for achieving stable and efficient gridshell structures. These findings underscore the importance of selecting bamboo species carefully based on their inherent physical characteristics to optimise structural outcomes in architectural applications.

7.4. Discussion

7.4.1. Form-finding of Bamboo Gridshell Structures

The form-finding process is a crucial step in the design process of bamboo gridshell structure, as this stage determines the initial geometry and stability of the structure. In the design practice of bamboo architecture in general, the form-finding process often overlooks the unique characteristics of bamboo, including its bending capability. Bamboo is perceived as a flexible material, leading to the common misleading perception among designers that bamboo is easy to bend. However, in reality, bamboo, especially full-culm bamboo, has some extent of limitations in bending.

The form-finding process for gridshell structures using full-culm bamboo clearly revealed significant limitations in achieving deeper curvature. From a material standpoint, this issue was discussed in Chapter 4, where the bending capability was determined by the Young's modulus, bending strength and cross-sectional dimensions (see Section 4.4.2). When incorporating the bending capability of bamboo in the form-finding simulation, the minimum radii of curvature produced significantly narrow curvatures. This outcome is particularly important for architectural designs that requiring expansive and unobstructed

interior spaces. Additionally, this characteristic suggests that bamboo is more suitable for large-span gridshell structures, where the curvature can be designed to be less pronounced. Moreover, expanding the span also provides possibilities to increase the curvature, if desired by the architect.

The suitability of full-culm bamboo utilisation generally depends on the cross-sectional dimensions and the bending capability of the species. As discussed in Chapter 4, bamboo's flexibility and stiffness are critical for gridshell design. Smaller diameter bamboo is more flexible but less stiff and is prone to buckling. Conversely, larger diameter bamboo provides greater stiffness and better resistance to buckling but is significantly less flexible. Finding the suitable diameter, along with the appropriate material properties, is an important task in design practice to achieve effective form and material selection.

Despite resulting in a narrow curvature, this should not hinder the application of full-culm bamboo for gridshell structures. For design implementation, the narrow curvature can be mitigated by erecting the full-culm bamboo gridshell on pedestals; thus, creating space with sufficient height for activities underneath the structures. This design solution was shown in a bamboo gridshell built by UNAM, led by Prof. Oliva Salinas (Lorenzo et al., 2017). The bamboo gridshell was built using full-culm bamboo on top of steel and concrete pedestals (Figure 7-25). Additionally, the ZBC pavilion proved that full-culm bamboo is effective for large-span gridshell structures.



Figure 7-25. a. UNAM pavilion in Mexico (Lorenzo et al., 2017); b. ZBC Pavilion in Hong Kong (Crolla, 2017).

Considering the form-finding results, the curvature produced by *D. asper* was significantly narrow, with its shape almost flattened. Among the three bamboo species studied, *G. apus* was able to produce a significant curvature, resulting in sufficient space underneath for human activities. Therefore, it can be concluded that in terms of material selection, bamboo species such as *D. asper* are not suitable for bending-active gridshells. The

narrow curvature and large diameter make this species less flexible for bending. In contrast, species like *G. apus* are more suitable. Its cross-sectional diameter is neither too small nor too large, providing an ideal combination of stiffness and flexibility for forming gridshell structures.

Split bamboo offers greater flexibility in bending, which is highly advantageous for bending-active systems. The flexibility of split bamboo in bending also has significant potential for utilisation in free-form shapes. Contrary to the full-culm bamboo, split bamboo is less constraint by the radii of curvature, although its stiffness may need to be increased. This enhanced flexibility allows for more complex and varied curvatures, allowing possibilities for intricate architectural designs that are not feasible with full-culm bamboo.

When split into several pieces, *G. apus*, with its smaller diameter and medium wall thickness, produces the smallest width among all the studied species. *G. atter* produces a larger width but the smallest height, whereas *D. asper* produces the largest width and height. Based on the form-finding results, all split bamboo species displayed excellent performance when utilised as split bamboo, indicating its potential for bamboo gridshell structures.

The use of split bamboo can produce material-efficient designs for bamboo gridshell structures, resulting in thinner and lighter structural elements, thereby reducing overall material usage and weight. Additionally, split bamboo structures can be easily modified for other gridshell shapes, offering greater design flexibility.

7.4.2. Optimisation Strategies of Bamboo Gridshell Structures

Implementing optimisation strategies requires comprehensive consideration of overall structural performance. Structural analysis conducted on the initial gridshell models by modifying mesh density, mesh configuration, and sizing revealed that applying only one optimisation strategy to bamboo gridshell models may be less effective and could result in unstable structures. Combining two or more strategies to optimise the structures may prove more effective in achieving balanced stress distribution, displacement, and efficient material usage.

Optimising mesh density involves evaluating the effective mesh size to avoid excessive material usage, which adds unnecessary self-weight to the structures. The common assumption that "more is better" does not apply to gridshell structures, as it can increase displacement and complicate the assembly process. Therefore, determining the optimal mesh size is crucial for enhancing the stability and performance of the structures.

Triangular mesh configuration has proven effective in stabilising gridshell structures. Simulations in Section 7.3.2 and Section 7.3.5 confirmed the effectiveness of triangulation

in stabilising both full-culm and split bamboo gridshell models. However, it is important to note that triangular or diagrid shapes are not the only options for gridshell structures; some bamboo gridshells have successfully used both quadrilateral and triangular configurations. For instance, The Arc of Green School in Bali employs a quadrilateral configuration to cover large span rooms effectively.

Furthermore, structural analysis of split bamboo gridshell models using D. asper demonstrated stable conditions with a quadrilateral configuration when two layers were added. This suggests that while triangular or diagrid configurations effectively stabilise and optimise structures, quadrilateral configurations remain applicable when combined with other optimisation techniques.



Figure 7-26. Grishell mesh at the Arc of Green School, configuring in quadrilateral

Sizing optimisation, which involves adding layers to the grid members, also proved effective in reducing displacement. This method increases stiffness by adding layers, as seen in the simulations. However, similar to mesh density optimisation, adding layers increases the total mass of the structure, particularly for full-culm bamboo. Therefore, determining the optimal number of layers is essential for balancing structural performance with material efficiency.

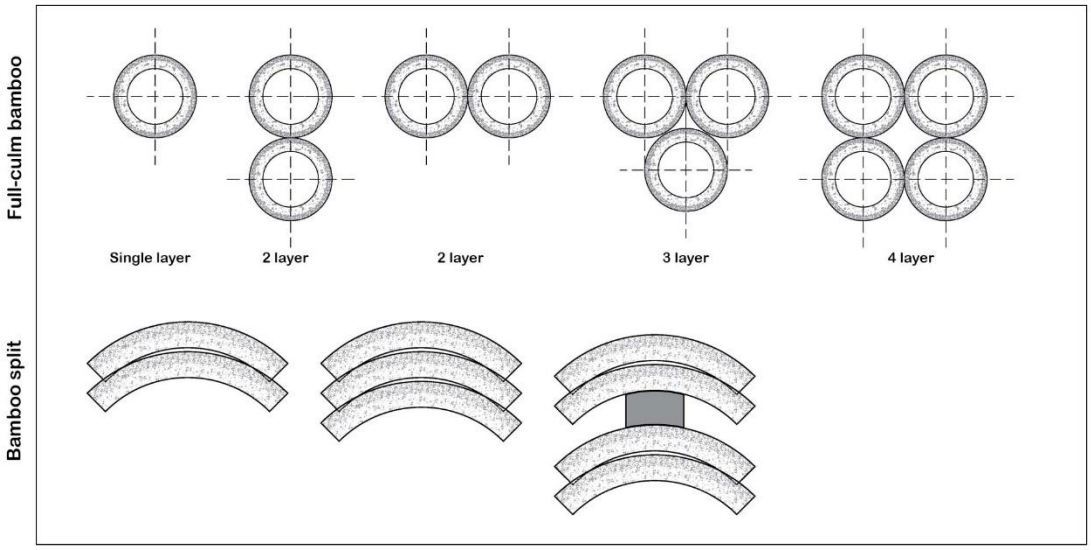


Figure 7-27. Profile section and layering options.

7.4.3. Bamboo Gridshell Structures: Computational Design and Construction Practices

Historically, physical models, validated by full-scale models, were used not only for form-finding and optimisation but also to determine assembly and erection methods, as well as to identify potential issues. Nowadays, computational simulations offer various options and convenient methods for designing gridshell structures. Computer-aided design (CAD) can generate unlimited geometric options for gridshell structures, ranging from regular to free-form shapes using NURBS surfaces. Despite the benefits, there remains a significant gap between computational design and construction practices, which designers and engineers must address and not overlook.

The issues discussed in this section related to the gap between computational design and construction are defined into four main categories: gridshell geometries, material properties and behaviour, and design interpretation and communication. In some cases, these issues are interrelated and connected. Therefore, the discussion aims to gain deeper insight into each issue and seek the underlying reasons.

Issue regarding gridshell geometries includes the consistency and accuracy. Computational-aided design software, with its advanced capabilities, can produce a high variety of shapes and intricate designs. Designing bamboo gridshell structures in CAD software can be performed straightforwardly by creating the shapes and meshing the surface. However, during the process, designers often overlook the characteristics of bamboo and the assembly and erection methods, which play crucial roles in achieving the designated form.

Designers often live under the misconception that bamboo is highly flexible and easy to bend. However, in reality, bending a full-culm bamboo using bending-active principles is challenging. Therefore, as suggested in Section 7.4.1, designers should consider the radii of curvature and perform the curvature analysis during the form-finding process. Furthermore, the selection of suitable species and the determination of cross-sectional forms and dimensions, as discussed in Section 4.4.2, also aid designers during the design stage. These strategies can be employed to produce robust gridshell geometries and ensure their applicability and buildability when utilising bamboo as the grid members.

However, when suitable gridshell geometries have been achieved, challenges related to the assembly and erection methods may necessitate significant changes to the geometries. Learning from the construction process in this study (see Chapter 6), the bending methods, together with the assembly and erection methods, contributed to significant changes from the initial design. Initially, the models were planned to be erected by assembling them on the ground and then bending the members by pulling up the grids and moving the anchors, resulting in four openings, as depicted in Figure 7-29.a.

Gigantochloa apus was chosen for the full-scale model because the species exhibits the smallest cross-section dimension and the best performance in bending compared to other studied species. Moreover, with the plan of using heat by torching the bamboo, it was possible to achieve a higher curvature (see Figure 7-28). However, bending full-culm bamboo was extremely challenging, as described in Section 6.3.1. Many bamboo poles broke and failed during the bending process. Furthermore, during the investigation, rather than the pull-up method, erecting the full-culm bamboo gridshell was more effectively and efficiently achieved by bending the members individually while assembling them into a complete structure.



Figure 7-28. a Experiment in bending bamboo poles, b. Bending bamboo by torching.

Based on these findings, a major change in the gridshell geometry was necessary. Model-1 underwent a redesign process that involved expanding the gridshell dimensions from 8.40 x 8.40 metres to 10.60 x 10.60 metres, modifying the shape to increase the curvature, and altering the boundary conditions (Figure 7-29). This process demonstrated the accuracy of the design approach, which had already considered the bending method, as well as the assembly and erection methods, as crucial. Without a proper plan and prior investigation of the construction process, realising the gridshell geometry produced by computational design would likely fail.

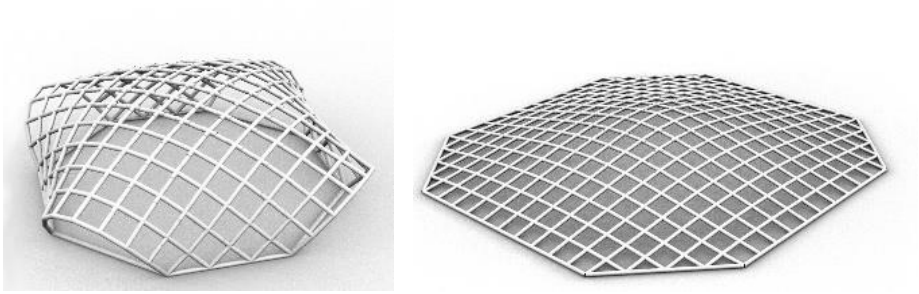


Figure 7-29. a. Expected curvature during design process, b. Final gridshell geometries after investigating the depth of curvature.

Furthermore, we also recorded deviations between the designed geometry and the final shape achieved in construction. As detailed in Section 6.3.2, the most significant deviation was observed in the final height of the gridshell, particularly in Model-1. This model gradually lost height over time, with an immediate reduction occurring once all supports were removed. The primary cause of this issue was the absence of a foundation system. Model-1 was constructed without a proper foundation, relying solely on bamboo poles installed as the boundary condition.

The boundary condition is crucial for maintaining the structural shape and resisting forces such as gravity and load applications, including meridional and hoop stresses. In Model-1, the lack of a foundation system resulted in excessive stress on the boundary conditions. Consequently, during the loading process, Model-1 was unable to withstand the applied loads, leading to its failure. This highlights the importance of an adequate foundation system to support the boundary conditions and ensure the structural integrity of gridshell constructions

These issues indicate that the form-finding process during construction proceeds differently from the same process in computational design. Designing the geometry in CAD software results in a pristine design with clear shapes and controlled parameters. However, discrepancies are inevitable during construction. Constructing the bamboo gridshell structure may result in deviations and less accuracy of final shapes than the designated

geometries. The construction process, which involves craftsmanship, workers' skills, and local technologies, significantly affects the accuracy of the building.

The second issue concerns the material properties and inherent behaviour of bamboo as natural material. Bamboo is anisotropic, meaning its strength, stiffness and elasticity vary in different directions and locations within its culms. Additionally, its morphology and dimensions are challenging to standardise and accurately capture in computational modelling and simulation. Although finite elements analysis (FEA) can accommodate the anisotropic characteristics of bamboo, it has limitations in representing the variation of material properties within the culms, which differ from the base to the top sections. This issue sets a limitation in this study, which further discuss in Section 7.4.4.

Moreover, environmental conditions at the construction site can influence the material properties and often result in discrepancies between computational design and the as-built structures. Changes in moisture content, for instance, can reduce the strength properties of bamboo, leading to deviations from the expected performance predicted by the computational simulations. Being a hygroscopic material, bamboo can absorb and release moisture from the environment, leading to changes in dimensions, forms (due to shrinking), and material properties. Eventually, these behaviours, especially in the long term, affect the overall structural integrity and stability of the as-built structures, which are challenging to predict in computational simulations.

Computational design and simulations often assume ideal and static conditions, whereas the actual environment exhibits dynamic and unpredictable changes. Bamboo absorbs and responds to these changes, ultimately affecting its material properties. Therefore, solely relying on computational design for bamboo gridshell structures, and bamboo structures in general, cannot accommodate the inherent uncertainty in the performance of bamboo. Performing validation through physical models and setting up a monitoring system during the structure’s lifespan would provide a robust assessment of structural performance.

Furthermore, computational modelling often produces less realistic visualization of the material. While seamless members and joineries can be easily produced in a digital environment, achieving neat and precise joineries in physical construction requires high craftsmanship and specialised tools. Despite considerable effort, the results can sometimes be less than satisfactory. In computational design, bamboo is often depicted as sleek, uniform hollow tubes. In reality, bamboo is rough, irregular, and characterised by uneven nodes, and many culms are not perfectly straight. This discrepancy affects the visualisation but also highlights the inherent beauty and unique characteristics of bamboo in the building, which are often difficult to fully display in computational design and modelling.

The third issue discussed in this section was communicating the design to workers and the role of scale models in design and construction. While CAD software can produce detailed drawings, these are often challenging for construction workers to interpret. Bamboo construction in Indonesia relies heavily on craftsmanship and community knowledge, making scaled models more effective for explaining details. Using scaled models is a common practice in Indonesia, with most bamboo buildings constructed with their guidance. Therefore, two scaled models were prepared before constructing the full-scale models (Figure 7-30). These models helped visualise the design, particularly for the assembly and erection processes. The connection and layering of Model-1 were decided after examining the scaled model, while Model-2 was crucial for explaining the assembly of flat grids on the ground and the erection process. Workers gained a better understanding after the demonstration and could erect Model-2 according to plan.

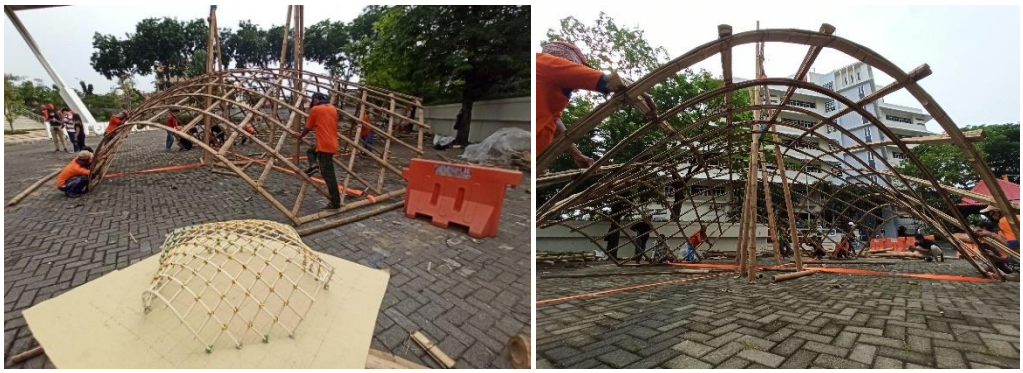


Figure 7-30. a. Role of scale model as guideline for construction workers; b. Erection process of full-scale model.

The described process highlights potential factors that can cause discrepancies between the design and built bamboo gridshells. When designing a bamboo gridshell, the bending capability and methods should be thoroughly explored during the design process, as these determine the geometries. Deviations in the built construction are inevitable due to factors such as the accuracy of construction methods, the natural behaviour of the material, and external influences.

7.4.4. Limitations of the Study and Future Applications

As discussed in Section 7.4.3, the natural characteristics of bamboo are challenging to interpret and capture for use in computational design. This study addresses these limitations. Capturing and incorporating the variation of bamboo into simulations cannot

be achieved simply by using average values. The primary reason is high variability in bamboo properties and its brittle in response to certain stresses.

In a batch of bamboo poles used for construction, there is always a possibility that some poles will exhibit significantly lower or higher strength properties Despite undergoing a grading process, the presence of poles with lower strength within the batch cannot be completely ruled out. Using average values for simulations poses a high risk, as these values may not account for the weakest materials. Furthermore, as evidenced by the material tests in Chapter 4, the brittle nature of bamboo can lead to sudden structural collapse.

To address this issue in simulations, this study set up the material properties in accordance with ISO 22156:2021, which recommends adjusting material properties by considering factors such as safety, utilisation, and load factors. The brittleness and variability of bamboo potentially introduce a degree of uncertainty that should not be eliminated from computational methods. This issue underscores the importance of incorporating safety factors in bamboo structures to mitigate potential inconsistencies in materials.

Despite the limitations, the methods used in this study can be implemented in the design process of bamboo gridshell structures in general. Moreover, although the focus of this study is on Indonesian bamboo, the same processes and methods can be applied to other bamboo species. The key parameters to consider include the selection of bamboo species based on their bending capabilities – such as diameter, Young's modulus, and bending strength – and the specific requirements of the gridshell design, including span, designated geometry, and loads.

The entire process outlined in this chapter, including form-finding, structural analysis, and optimisation, can serve as a model or reference for architects and engineers engaged in the design of bamboo gridshell structures. This study offers a framework for navigating the complexities inherent in working with bamboo by incorporating and considering its characteristics at each stage. This approach ensures that the inherent properties and behaviours of bamboo are effectively integrated into the design process, thereby enhancing the structural integrity of the structures.

7.5. Summary

This chapter has focused on the form-finding and optimisation of bamboo gridshell structures using full-culm and split bamboo. The form-finding process revealed limitations in bending full-culm bamboo, particularly those with larger outer diameters, which could only produce very narrow and almost flat curvatures. Conversely, split bamboo

demonstrated versatility in achieving deeper curvatures. Selecting the appropriate bamboo species and forms (full-culm and split) is crucial in the design process of bamboo gridshells, considering both structural performance and the aesthetic resulting from the curvature.

The optimisation process was conducted by modifying mesh density, mesh configuration, and sizing parameters using computational tools such as Rhinoceros and the plug-ins Grasshopper, Kangaroo, and Karamba 3D. Structural analysis revealed that employing multiple optimisation strategies concurrently was more effective than singular approaches, as it balanced stress distribution, reduced displacement, and optimised material usage. This integrated approach ensured the stability and efficiency of the gridshell structures.

This chapter emphasises the importance of selecting appropriate bamboo species and employing effective optimisation strategies to achieve stable and efficient gridshell structures. The findings underscore the nuanced relationship between bamboo's physical properties, mesh configurations, and the overall performance of gridshell designs, providing valuable insights for future architectural applications and structural designs involving natural materials like bamboo

Publication history:

Part of this chapter has been published in eCAADe 2023 conference on 20-22 September 2023 in Graz, Austria. The paper title is "Form Finding and Optimisation of Bamboo Gridshell Structures". Information regarding the conference can be accessed through *https://ecaade2023.tugraz.at/* while the paper can be accessed through *http://ecaade.org/publications/downloads/* eCAADe 2023 Digital Design Reconsidered Volume 1 page 579-588.

CHAPTER 8 | CONCLUSION: UNDERSTANDING BAMBOO GRIDSHELL STRUCTURES

8.1. Recapitulation of Research Objectives and Key Findings

A comprehensive understanding of the utilisation of Indonesian bamboo for gridshell structures was the general objective of this study, developing from the primary research question. To achieve this general objective, four particular objectives were formulated to gain a thorough understanding of the four parameters involved in the design process, as explained in Section 1.4. The four parameters were material, form and forces, and construction, with the fourth parameter being form-finding and optimisation, which necessitates the combination of the previous three. Although the four objectives were investigated through separate experimentation and simulation methods, these parameters are interdependent, as explained in CHAPTER 3 Section 3.2.

This section summarises the objectives and highlights the key findings of this study.

8.1.1. Material Properties of Indonesian Bamboo Species

Studies on the material properties of Indonesian bamboo were performed in Objective I of this thesis. The goals were set to obtain mechanical properties data, examine material characteristics and behaviour, and determine bending capabilities. The key findings of the material tests performed on selected Indonesian bamboo species - *Gigantochloa apus*, *Gigantochloa atter*, and *Dendrocalamus asper* - are described as follows:

- **Material properties data set**

  The material tests produced data sets of the physical and mechanical properties of selected Indonesian bamboo species. The results confirmed and highlighted the anisotropic nature of bamboo, with relatively excellent strength properties parallel to the fibre, such as compression (f_C), tension (f_t), and bending (f_m); low strength in shear parallel to the fibre (f_V) and bending perpendicular to the fibre ($f_{m,90}$); and exceptionally low strength in tension perpendicular to the fibre ($f_{t,90}$). The findings suggest that bamboo applications for structural design should consider the limitation of material properties, which might affect structural integrity and details, such as connection systems. These data sets are beneficial for the calculation and assessment of bamboo applications in general structures and gridshell structures. However, problems in

identifying the appropriate sections within the culms (base/bottom – middle – upper) can influence the accuracy of the data. Consequently, proper identification and coding systems in the bamboo industry are proposed for more accurate data and bamboo application in the future.

- **Susceptible behaviour of bamboo to certain loads**

  Based on the failure modes, bamboo behaves differently depending on the type of load it bears. The investigation on the stress-strain curve showed that bamboo exhibits ductile characteristic under compression parallel to the fibre (f_C), whereas under other types of loads such as tension (f_t), shear (f_V), and bending parallel to the fibre (f_m), and tension ($f_{t,90}$) and bending perpendicular to the fibre ($f_{m,90}$), it showed brittle behaviour. These characteristics suggest that bamboo is susceptible to certain loads and may collapse unexpectedly. This finding underscores the uncertainty associated with using bamboo as a building material and highlights the importance of incorporating these behaviours into considerations during the structural analysis stage to ensure structural integrity and safety.

- **Bending capabilities**

  Studies on the bending capabilities in Section 4.4.2 suggest an applicable method for evaluating and determining the radii of curvature of bamboo, which can be obtained through its cross-sectional dimension (D), Young's modulus (E_m), bending strength (f_m), and displacement data (Δ). Analysis of the bending capabilities revealed that cross-sectional dimensions are crucial in determining the stiffness and flexibility of bamboo. Elastic gridshell structures require materials that are flexible enough to be bent but sufficiently stiff to bear loads. Therefore, methods for determining the radii of curvature can provide preliminary data for designing bamboo gridshell geometries and for the form-finding process, while at the same time, analysing the stiffness and strength needed for the structures.

- **Bamboo species selection**

  The analysis and assessment in Section 4.4.3 indicated that *G. apus* – as full-culm bamboo – showed excellent performance for elastic gridshell structures. Its relatively smaller cross-sectional dimensions, combined with excellent Young's modulus and bending strength, provide higher flexibility and smaller radii of curvature, while at the same time exhibiting the stiffness needed to withstand loads. Conversely, *D. asper* showed unfavourable performance due to its larger cross-sectional dimensions and thick wall. These findings underline the importance of selecting suitable bamboo

species for gridshell structures, taking into account the outer dimensions of the bamboo culms and assessing their bending capabilities.

Although this study focused on Indonesian bamboo species and only investigated three selected species, the methods could be applied to all bamboo species. Moreover, the data set and analysis produced in CHAPTER 4 contribute to the database of material properties of Indonesian bamboo species, especially for the application on bending-active structure systems. The data set can now be utilised for structural analysis of bamboo structure with a broader scope. Therefore, despite its limitation on material selection, the contribution of this study is significant.

However, as discussed in Section 4.4.1, the high variability of bamboo properties within its culms can cause a less accurate determination of material properties. Moreover, guidance on harvesting and selecting bamboo plants at the optimal age and season, as practised traditionally in Indonesia, can increase and maintain bamboo quality. It is advisable for the government to construct and set up a national standard (SNI/*Standar Nasional Indonesia*) for grading bamboo quality in accordance with the climate and local knowledge. Additionally, as in the timber industry, imposing standards such as labelling and coding for source, age, and section position within the whole culm can mitigate the non-uniformity and high variability of bamboo as a building material.

8.1.2. Structural Performance of Bamboo Gridshell Structures

Structural analysis aimed to evaluate the structural behaviour of bamboo gridshell structures through Finite Element Analysis (FEA) and to perform a comparative study of FEA results with load tests on a full-scale model. The key findings are:

- **Bamboo gridshell behaviour under load applications**
  FEA simulations depicted the deformed shape, displacement, and stress distribution of gridshell models under four scenarios of load applications. The results identified critical areas and displacement under various types of loads. By pinpointing high-stress areas and significant displacements, designers can plan appropriate reinforcements to ensure structural integrity.
- **Discrepancies between FEA and real-world load tests.**
  A comparative study between FEA results and load tests on full-scale models revealed similarities in the pattern of deformation shapes. However, overall results showed that the displacements recorded in load tests were generally smaller than those predicted by FEA. Despite this, one scenario indicated a relatively higher maximum

displacement. This suggests that although FEA is a robust tool for simulating structural performance, empirical validation is essential to ensure the safety of bamboo gridshell structures.

8.1.3. Construction Methods and the Process of Erecting Gridshell Structures

Objective III of this study aimed to assess and investigate suitable construction methods for bamboo gridshell structures. This investigation involved constructing two full-scale gridshell models using full-culm and split bamboo, reflecting common utilisation methods in bamboo structures. Load tests were conducted to evaluate structural behaviour under four different load scenarios. The key findings are summarised as follows:

- **Bending limitations of full-culm bamboo**

  Full-culm bamboo exhibited limitations in bending. Despite efforts to increase the curvature, many poles broke due to bending. Although applying heat to soften the fibres can slightly raise the curvature, it is crucial to prevent potential splitting due to thermal loss during the cooling stage, as detailed in Section 6.3.1. Additionally, bamboo tends to revert to its original form during bending. These findings suggest that considering the minimum radius of curvature is essential to reduce breakage during the bending process.

- **Construction method for full-culm bamboo**

  The construction process outlined in Section 6.2.3 proposed CHAPTER 6 an effective method for erecting full-culm bamboo structures by individually bending and assembling members one by one. This approach potentially reduces complexity caused by bamboo stiffness, allowing each culm to be bent individually without being overly heavy or impacting other members. Furthermore, this method offers a practical solution for replacing broken bamboo culms without compromising the entire grid system.

- **Construction challenges of full-culm bamboo**

  The construction process revealed that the non-uniform morphology of bamboo culms increase the complexity of the assembling stage, especially when lengthening members and establishing connections. This suggests the necessity of a thorough selection and grading process for bamboo culms. Additionally, it highlights the need to improve quality control standards from bamboo suppliers and industries in Indonesia, as discussed in Section 8.1.1.

- **Construction and performance of split bamboo**

Constructing the Model-2 demonstrated that split bamboo performs well in gridshell structures, with a less complicated and quicker erection process, using methods similar to those employed for timber gridshells. Lengthening members by overlapping split bamboo, as described in Section 6.3.3, proved to be a less complex method than was the case with the full-culm bamboo. Split bamboo offers greater flexibility, suggesting its suitability for more complex shapes, such as multiple curvatures or free-form geometries.

- **Boundary condition and connection systems**
  Failures observed in Model-1 during the load test highlighted weaknesses in the connection systems and boundary conditions. The investigation revealed that the connections at the boundaries failed to resist axial and circumferential forces, leading to splitting and structural collapse. These findings underscore the importance of robust boundary conditions and well-calculated connection systems, especially for full-culm bamboo, to ensure they can withstand applied forces.

In addition to the key findings, this study highlights the contribution of construction workers' skills to the quality of the structures. Bamboo construction practices in Indonesia are heavily dependent on local craftsmanship and community knowledge, typically acquired through apprenticeship. Consequently, the quality of constructed structures can vary significantly in accordance with the workers' skill levels. Furthermore, the lack of a national standard or building codes dedicated to bamboo structures contributes to inconsistencies in building quality. These phenomena can lead to increased risk and safety issues in bamboo construction in Indonesia. Therefore, it is recommended to develop a national standard and codes (SNI) to provide a comprehensive framework for bamboo construction practices.

8.1.4. Form-Finding and Optimisation Strategies

The purposes of Objective IV include form-finding, structural analysis of optimisation strategies, and the proposed optimisation plan. Investigations into the form-finding process was performed by incorporating the bending capabilities of bamboo. The aim of the structural analysis was to investigate the optimisation strategies, while the optimisation proposed the selection of optimised bamboo gridshell structures. The key findings are:

- **Effective form-finding strategies**
  Incorporating the radii of curvature by conducting curvature analysis in Grasshopper demonstrated an effective method for designing gridshell geometries using full-culm bamboo. The geometries designed through this method were able to accommodate the

bending limitations and prevent curvatures beyond the bamboo's bending capabilities. Methods described in Section 4.4.2. could be employed to determine the radii of curvature of bamboo culms, while workflow in Section7.3.1 could be applicable during the design stage. These findings led to a proposed workflow for the design process of bamboo gridshell structures. Applying these methods offers logical and safe application of full-culm bamboo for various geometric options, without neglecting its limitations in bending.

- **Impact and implications of optimisation strategies**

  Structural analysis of the optimisation strategies revealed that optimisation for bamboo gridshell structures should consider factors such as utilisation, material usage, and stress distribution. When performing optimisation analysis, it is important to account for the high variation in material properties and the unpredictability of bamboo performance. Therefore, a robust standard reference is needed to ensure that calculations accommodate these limitations, as stated in Section 7.2.4. Regarding bamboo gridshell design, all optimisation strategies, including topology, geometry, and sizing, should be carefully assessed and calculated through sensitivity analysis to achieve an optimised formula. This formula should inform the optimal geometry, mesh density, mesh configuration, and the number of layers needed for optimal structures.

- **Gaps between computational design and construction practices**

  A critical issue discussed in Section 7.4.3 addressed the gap between computational design and construction practices. The discussion suggested that these gaps are influenced by factors such as the ability of computational tools to capture the high variability of bamboo, the relaxation process after construction and its creep behaviour, and the influence of environmental conditions on the structures. Discrepancies between computational designed and actual structures are expected. This gap underscores the need for more sophisticated modelling techniques that can simulate the long-term behaviour of bamboo under varying environmental conditions. Incorporating factors such as moisture variation, temperature changes, and biological degradation into computational simulations can provide a more accurate prediction of the bamboo structure's performance, thereby reducing the discrepancy between design and reality.

8.2. Recommendations for Future Research

Reflecting on the entire research process and considering the key findings, several gaps have been identified that present opportunities for future research. This section outlines potential research topics that could significantly contribute to the further development and understanding of bamboo gridshell structures. Potential future work are suggested in the following areas:

- **Advanced and robust material testing**

  Since bamboo is a natural material with hundreds of species and significant variation in properties, advancements in material science and testing technologies could offer more precise and comprehensive data. Although the current test reference for obtaining material properties, such as ISO 22157:2019, has been extensively used for bamboo, more reliable testing protocols employing the latest technologies provide an opportunity to refine existing methods. Future research could conduct further exploration on non-destructive testing (NDT) methods and advanced computational modelling. Additionally, processing the data using artificial intelligence (AI) technologies could improve the identification and determination of bamboo's material properties, bringing the results closer to real-world conditions. Future research that can capture the high variation of properties within the culm, or map and visualise these variations graphically, could also become an intriguing area of study.
- **Innovation on the construction methods**

  This area offers significant opportunities, given that only a few bamboo gridshell structures have been built, most of which are non-permanent. This study has highlighted the challenges in constructing full-scale bamboo structures due to the inherent properties, characteristics, and behaviours of bamboo. Future research could focus on developing suitable, more effective and efficient, and less time-consuming assembly and erection methods for full-culm bamboo. Such research should accommodate the material's limitations, uncertainties, and weaknesses; thus, potentially proposing concrete and applicable results.
- **Developing connection systems**

  Critical failures in the connection systems of full-culm bamboo underscore the necessity for robust connection designs in bamboo gridshell structures. The inherent uncertainties of bamboo as a building material demand meticulously engineered connection systems. Currently, knowledge of bamboo joineries and connection systems is predominantly derived from traditional, locally developed craftsmanship

methods. Moreover, there are only a few comprehensive studies on bamboo joineries and connections that examine their strength and capabilities or provide precise measurements of their ultimate strength. Consequently, this research area holds significant potential for exploration, applicable to general bamboo structures or specifically to dedicated connection systems for bamboo gridshell structures.

- **The durability of bamboo gridshell structures**

  A phenomenon observed in this study was that during the relaxation stage of form-finding, gridshell structures lose height until they stabilise. However, this study did not investigate the deformation and displacement of the structures caused by creep. Future research dedicated to investigating the influence of bamboo's creep behaviour on the structural integrity and final geometries of bamboo gridshell structures is needed. Such work would produce results, not only for gridshell structures but also for other bending-active structures using bamboo.

- **Future development for computational design**

  A major challenge for the computational design of bamboo structures lies in capturing the high variability of bamboo properties and integrating them into computational models. Current finite element method (FEM) software attempts to address the anisotropic characteristics of bamboo but often falls short in accommodating other factors such as the tapering shape of bamboo culms, variability in connections, and the distribution of properties within the culms. As a result, discrepancies and gaps frequently arise, posing critical challenges in the design and its implementation, particularly for gridshell structures. The complexity of using bamboo in gridshell structures requires advanced calculations. Developing algorithms and software that can accurately represent the natural behaviour and inherent uncertainties of bamboo would be a challenging yet highly beneficial future endeavour for the advancement of bamboo construction.

- **National standards, building codes, and regulations**

  A critical issue in bamboo construction practices and industries in Indonesia is the lack of comprehensive formal building codes and standard specifically for bamboo structures. Therefore, developing suitable codes and standards that reflect the characteristics and context of Indonesia is recommended for future work. Bamboo industries and practices have a high degree of potential, and Indonesia possesses extensive local knowledge regarding bamboo, from cultivation to construction. Documenting this local wisdom and knowledge, while simultaneously developing robust and reliable methods and building codes, could be a significant area of

research. The results could produce building codes for bamboo structures in Indonesia that meet international standards, promote the safe use of bamboo, and preserve the cultural richness of bamboo craftsmanship practices.

- **Sustainable environmental impact**: Lastly, in line with sustainable development goals, the primary aim of utilising bamboo in building is to contribute to sustainable development efforts. Therefore, future research could analyse the environmental impact of using bamboo in gridshell structures. This could include investigating material usage, construction waste, life-cycle analysis, and other related issues.

.

REFERENCES

Adriaenssens, S., Block, P., Veenendaal, D. & Williams, C. (Eds.). (2014). *Shell Structures for Architecture: Form Finding and Optimization*. London ; New York: Routledge/ Taylor & Francis Group.

Akinbade, Y., Nettleship, I., Papadopoulos, C. & Harries, K. A. (2021). Modelling Full-Culm Bamboo as a Naturally Varying Functionally Graded Material. *Wood Science and Technology*, 55(1), 155–179.

Amada, S., Munekata, T., Nagase, Y., Ichikawa, Y., Kirigai, A. & Zhifei, Y. (1996). The Mechanical Structures of Bamboos in Viewpoint of Functionally Gradient and Composite Materials. *Journal of Composite Materials*, 30(7), 800–819.

Anokye, R., Kalong, R. M., Bakar, E. S., Ratnasingam, J., Jawaid, M. & Awang, K. (2014). Variations in Moisture Content Affect the Shrinkage of Gigantochloa Scortechinii and Bambusa Vulgaris at Different Heights of the Bamboo Culm. *BioResources*, 9(4), 7484–7493.

Arce-Villalobos, O. O. (1993). Fundamentals of the Design of Bamboo Structures. Retrieved May 17, 2022, from https://research.tue.nl/en/publications/fundamentals-of-the-design-of-bamboo-structures(9808cdbc-df77-47ed-aaba-2490de9ae96b).html

Ashby, M. F. (1999). *Materials Selection in Mechanical Design*. Oxford, OX ; Boston, MA: Butterworth-Heinemann.

Awalluddin, D., Mohd Ariffin, M. A., Osman, M. H., Hussin, M. W., A. Ismail, M., Lee, H.-S. & Abdul Shukor Lim, N. H. (2017). Mechanical Properties of Different Bamboo Species (J.-W. Park, H. Ay Lie, H. Hardjasaputra, and P. Thayaalan, Eds.). *MATEC Web of Conferences*, 138, 01024.

Banik, R. L. (2015). Morphology and Growth, in: Liese, W. and Köhl, M. (Eds.), *Bamboo*, (pp. 43–89). Tropical Forestry. Cham: Springer International Publishing. Retrieved August 11, 2021, from http://link.springer.com/10.1007/978-3-319-14133-6_3

Bystriakova, N., Kapos, V., Stapleton, C. & Lysenko, I. (2003). *Bamboo Biodiversity: Information for Planning Conservation and Management in the Asia-Pacific Region*. UNEP-WCMC/INBAR 2003.

Chang, F.-C., Chen, K.-S., Yang, P.-Y. & Ko, C.-H. (2018). Environmental Benefit of Utilizing Bamboo Material Based on Life Cycle Assessment. *Journal of Cleaner Production*, 204, 60–69.

Chilton, J. & Tang, G. (2017). *Timber Gridshells: Architecture, Structure and Craft*. London ; New York: Routledge.

Christensen, P. W., Gladwell, G. M. L. & Klarbring, A. (2009). *An Introduction to Structural Optimization*. Dordrecht: Springer Netherlands Springer e-books.

Clark, L. G., Londoño, X. & Ruiz-Sanchez, E. (2015). Bamboo Taxonomy and Habitat, in: Liese, W. and Köhl, M. (Eds.), *Bamboo*, (pp. 1–30). Tropical Forestry. Cham: Springer International Publishing. Retrieved October 11, 2022, from http://link.springer.com/10.1007/978-3-319-14133-6_1

Collins, M. & Cosgrove, T. (2016). A Review of the State of the Art of Timber Gridshell Design and Construction

Correal, J. F. (2016). Bamboo Design and Construction, in: *Nonconventional and Vernacular Construction Materials*, (pp. 393–431). Elsevier. Retrieved September 9, 2022, from https://linkinghub.elsevier.com/retrieve/pii/B9780081000380000147

Crolla, K. (2017). Building Indeterminacy Modelling – the 'ZCB Bamboo Pavilion' as a Case Study on Nonstandard Construction from Natural Materials. *Visualization in Engineering*, 5(1), 15.

Crolla, K. (2018). Bending Bamboo Rules: Beyond Century-Old Typologies. *Journal of Architectural Education*, 72(1), 135–145.

Crolla, K. & Fingrut, A. (2016). Protocol of Error: The Design and Construction of A Bending-Active Gridshell from Natural Bamboo, in: *Living Systems and Micro-Utopias: Towards Continuous Designing*, (pp. 415–424). Melbourne: CAADRIA.

Crotty, M. (1998). *The Foundations of Social Research: Meaning and Perspective in the Research Process*. London ; Thousand Oaks, Calif: Sage Publications.

Damayanto, I. P. G. P. & Fefirenta, A. D. (2021). Pola persebaran marga bambu di Indonesia. *Prosiding Seminar Nasional Biologi*, 7(1), 24–41.

D'Amico, B., Kermani, A., Zhang, H., Pugnale, A., Colabella, S. & Pone, S. (2015). Timber Gridshells: Numerical Simulation, Design and Construction of a Full Scale Structure. *Structures*, 3, 227–235.

Douthe, C, Baverel, O. & Caron, J. F. (2006). Form-Finding of a Gridshell in Composite Materials. *JOURNAL OF THE INTERNATIONAL ASSOCIATION FOR SHELL AND SPATIAL STRUCTURES*, 47(150), 10.

Douthe, C., Baverel, O. & Caron, J.-F. (2006). Form-Finding of a Grid Shell in Composite Materials. *Journal of the International Association for Shell and Spatial Structures*, 47(1), 53–62.

Douthe, C., Caron, J. F. & Baverel, O. (2010). Gridshell Structures in Glass Fibre Reinforced Polymers. *Construction and Building Materials*, 24(9), 1580–1589.

Dyvik, S. H., Manum, B. & Rønnquist, A. (2021). Gridshells in Recent Research—A Systematic Mapping Study. *Applied Sciences*, 11(24), 11731.

Dyvik, S. H., Mork, J. H., Nilsen, M. & Luczkowski, M. (2016). Modular Kinematic Timber Gridshell; a Simple Scheme for Constructing Advanced Shapes. *Proceedings of IASS Annual Symposia*, 2016(19), 1–10.

Edemskaya, E. & Agkathidis, A. (2016). Rethinking Complexity: Vladimir Shukhov's Steel Lattice Structures. *Journal of the International Association for Shell and Spatial Structures*, 57(3), 201–208.

Elnagar, O. (2017). Gridshell Structures in Laminated Bamboo. Retrieved January 11, 2023, from http://rgdoi.net/10.13140/RG.2.2.14388.55688

Ervianti, D., Widjaja, E. A. & Sedayu, A. (2018). Bamboo Diversity of Sulawesi, Indonesia. *Biodiversitas Journal of Biological Diversity*, 20(1), 91–109.

Gangwar, T. & Schillinger, D. (2019). Microimaging-Informed Continuum Micromechanics Accurately Predicts Macroscopic Stiffness and Strength Properties of Hierarchical Plant Culm Materials. *Mechanics of Materials*, 130, 39–57.

García, B. O. F., Morelos, R. E. P., Oliva, J. G. S. & Zetina, C. G. (2015). Parametric Design and Structural Analysis of Sustainable Bamboo Grid Shells in Mexico. *Proceedings of IASS Annual Symposia*, 2015(25), 1–10.

Goh, Y., Yap, S. P. & Tong, T. Y. (2020). Bamboo: The Emerging Renewable Material for Sustainable Construction, in: *Encyclopedia of Renewable and Sustainable Materials*, (pp. 365–376). Elsevier. Retrieved January 22, 2020, from https://linkinghub.elsevier.com/retrieve/pii/B9780128035818107489

Gokul Santhosh, S., Singh, A. P. & Abdul Akbar, M. (2023). Parametric Studies and Optimization of Grid Shell Structures Using Genetic Algorithm, in: Sil, A., N. Kontoni, D.-P., and Pancharathi, R. K. (Eds.), *Recent Trends in Civil Engineering*, (pp. 109–122). Lecture Notes in Civil Engineering. Singapore: Springer Nature Singapore. Retrieved July 24, 2023, from https://link.springer.com/10.1007/978-981-19-4055-2_10

Grosser, D. & Liese, W. (1971). On the Anatomy of Asian Bamboos, with Special Reference to Their Vascular Bundles. *Wood Science and Technology*, 5(4), 290–312.

Handana, M. A. P., Surbakti, B., Harisdani, D. D., Karolina, R. & Rizki, T. F. (2020). Compressive and Tensile Strength of Bamboo Species. *IOP Conference Series. Earth and Environmental Science*, 519(1). Retrieved August 2, 2023, from https://www.proquest.com/docview/2555968039/abstract/9D20686C53034326PQ/1

Harries, K. A., Bumstead, J., Richard, M. & Trujillo, D. (2017). Geometric and Material Effects on Bamboo Buckling Behaviour. *Proceedings of the Institution of Civil Engineers - Structures and Buildings*, 170(4), 236–249.

Harris, R. (2011). Design of Timber Gridded Shell Structures. *Proceedings of the Institution of Civil Engineers - Structures and Buildings*, 164(2), 105–116.

Harris, R., Dickson, M., Kelly, O. & Roynon, J. (2004). The Use of Timber Gridshells for Long Span Structures, in: Lahti, Finland.

Harris, R., Romer, J., Kelly, O. & Johnson, S. (2003). Design and Construction of the Downland Gridshell. *Building Research & Information*, 31(6), 427–454.

Harris, R. & Roynon, J. (2008). The Savill Garden Gridshell Design and Construction: 10th World Conference of Timber Engineering, in: Miyasaki, Japan. Retrieved December 17, 2022, from http://www.ewpa.com/mag/ewpa_pastConference.php

Hernández, E. L. (2015). Design and Optimisation of Elastic Gridshells. Retrieved January 10, 2023, from https://opus4.kobv.de/opus4-udk/frontdoor/index/index/docId/994

Hernández, E. L., Baverel, O. & Gengnagel, C. (2013). On the Design and Construction of Elastic Gridshells with Irregular Meshes. *International Journal of Space Structures*, 28(3–4), 161–174.

Huang, J. M. & Zhou, Y. (2018). Computational Bamboo Grid-Shell: An Exploration of Digital Design with Traditional Craftsmanship. *Proceedings of IASS Annual Symposia*, 2018(20), 1–4.

Huang, Z., Sun, Y. & Musso, F. (2017). Assessment on Bamboo Scrimber as a Substitute for Timber in Building Envelope in Tropical and Humid Subtropical Climate Zones - Part 2 Performance in Building Envelope. *IOP Conference Series: Materials Science and Engineering*, 264, 012007.

Husain, H., Hill, C., Ashaari, Z., Uyup, M. K. A., Abd, M., Latif, A, A., Mohmod, A., & Kandungan. (2007). Equilibrium Moisture Content and Volumetric Changes of Gigantochloa Scortechinii. *Journal of Tropical Forest Science*, 19, 18–24.

INBAR. (2005). *Global Forest Resources Assessment 2005, Indonesia: Country Report on Bamboo Resources*. Forestry Department FAO of the UN.

Janssen, J. J. A. (1981). *Bamboo in Building Structures*. Eindhoven: Technische Hogeschool Eindhoven.

Javadian, A., Smith, I. F. C., Saeidi, N. & Hebel, D. E. (2019). Mechanical Properties of Bamboo Through Measurement of Culm Physical Properties for Composite Fabrication of Structural Concrete Reinforcement. *Frontiers in Materials*, 6, 15.

Kis-Jovak, J. I. (Ed.). (1988). *Banua Toraja: Changing Patterns in Architecture and Symbolism among the Sa'dan Toraja, Sulawesi, Indonesia*. The Netherlands: Royal Tropical Institute.

Kotelnikova-Weiler, N., Douthe, C., Hernandez, E. L., Baverel, O., Gengnagel, C. & Caron, J.-F. (2013). Materials for Actively-Bent Structures. *International Journal of Space Structures*, 28(3–4), 229–240.

Kromoser, B. & Huber, P. (2016). Pneumatic Formwork Systems in Structural Engineering. *Advances in Materials Science and Engineering*, 2016, e4724036.

Labonnote, N., Mork, J. H., Dyvik, S. H., Nilsen, M., Rønnquist, A. & Manum, B. (2016). Experimental and Numerical Study of the Structural Performance of a Timber Gridhsell, in: Vienna.

Li, J., Yuan, Y. & Guan, X. (2016). Assessing the Environmental Impacts of Glued-Laminated Bamboo Based on a Life Cycle Assessment. *BioResources*, 11(1), 1941–1950.

Li, Q. (2018). *Form Follows Force: A Theoretical Framework for Structural Morphology, and Form-Finding Research on Shell Structures*. A+BE | Architecture and the Built Environment.

Lianto, F., Trisno, R., Husin, D. & Teh, S. W. (2019). Changing the Face of Modern Architecture: Bamboo as a Construction Material. Case Study: Green School, Bali – Indonesia. *IOP Conference Series: Materials Science and Engineering*, 508, 012023.

Liddell, I. (2015). Frei Otto and the Development of Gridshells. *Case Studies in Structural Engineering*, 4, 39–49.

Lienhard, J., Alpermann, H., Gengnagel, C. & Knippers, J. (2013). Active Bending, a Review on Structures Where Bending Is Used as a Self-Formation Process. *International Journal of Space Structures*, 28(3–4), 187–196.

Lienhard, J. & Knippers, J. (2013). Considerations on the Scaling of Bending-Active Structures. *International Journal of Space Structures*, 28(3–4), 137–148.

Liese, W. & Tang, T. K. H. (2015). Properties of the Bamboo Culm, in: Liese, W. and Köhl, M. (Eds.), *Bamboo*, (pp. 227–256). Tropical Forestry. Cham: Springer International Publishing. Retrieved August 11, 2021, from http://link.springer.com/10.1007/978-3-319-14133-6_8

Liuti, A. & Pugnale, A. (2015). Erection of Post-Formed Gridshells by Means of Inflatable Membrane Technology, in: *Living and Learning: Research for a Better Built Environment*, (pp. 678–687). Melbourne: The Architectural Science Association and The University of Melbourne. Retrieved January 10, 2023, from http://rgdoi.net/10.13140/RG.2.2.20637.31202

Lo, T. Y., Cui, H.Z & Leung, H. C. (2004). The Effect of Fiber Density on Strength Capacity of Bamboo. *Materials Letters*, 58(21), 2595–2598.

Lo, T. Y., Cui, H. Z & Leung, H. C. (2004). The Effect of Fiber Density on Strength Capacity of Bamboo. *Materials Letters*, 58(21), 2595–2598.

Lobovikov, M., Schoene, D. & Yping, L. (2012). Bamboo in Climate Change and Rural Livelihoods. *Mitigation and Adaptation Strategies for Global Change*, 17(3), 261–276.

Lorenzo, R., Lee, C., Oliva-Salinas, J. G. & Ontiveros-Hernandez, M. J. (2017). BIM Bamboo: A Digital Design Framework for Bamboo Culms. *Proceedings of the Institution of Civil Engineers - Structures and Buildings*, 170(4), 295–302.

van der Lugt, P., van den Dobbelsteen, A. A. J. F. & Janssen, J. J. A. (2006). An Environmental, Economic and Practical Assessment of Bamboo as a Building Material for Supporting Structures. *Construction and Building Materials*, 20(9), 648–656.

Lukman, M. Y. (2015). A STUDY ON THE GATHERING STYLES OF INDONESIAN CULTURE Case Study of Tudang Sipulung and Bale-Bale in Makassar Islands. Retrieved March 1, 2024, from https://doi.org/10.18910/53973

Macdonald, A. (2001). *Structure and Architecture*. Oxford: Architectural Press.

Minke, G. (2016). *Building with Bamboo: Design and Technology of a Sustainable Architecture* (J. K. Henderson, Tran.). Basel: Birkhäuser.

Mitch, D. (2009). Splitting Capacity Characterization of Bamboo Culms. Retrieved from http://d-scholarship.pitt.edu/6704/1/Derek_Mitch_Thesis_March_2009.pdf

Muhsin, A., Febriany, L. M., Hidayati, H. N. & Purwanti, Y. D. (2015). Material Bambu sebagai Konstruksi pada Great Hall Eco Campus Outward Bound Indonesia. *Reka Karsa: Jurnal Arsitektur*, 3(3). Retrieved January 17, 2023, from https://ejurnal.itenas.ac.id/index.php/rekakarsa/article/view/719

Naicu, D., Harris, R. & Williams, C. (2014). Timber Gridshells: World Conference on Timber Engineering (WCTE) 2014 Retrieved December 16, 2022, from http://www.wcte2014.ca/

Nath, A. J., Lal, R. & Das, A. K. (2015). Managing Woody Bamboos for Carbon Farming and Carbon Trading. *Global Ecology and Conservation*, 3, 654–663.

Nordahlia, A., Anwar, U., Hamdan, H., Zaidon, A., Paridah, M. & Razak, O. A. (2012). Effects of Age and Height on Selected Properties of Malaysian Bamboo (Gigantochloa Levis). *Journal of Tropical Forest Science*, 24(1), 102–109.

Nurdiah, E. A. (2016). The Potential of Bamboo as Building Material in Organic Shaped Buildings. *Procedia - Social and Behavioral Sciences*, 216, 30–38.

Nurdiah, E. A., Asri, A. & Hariyanto, A. D. (2015). GENDERED SPACE IN WEST SUMBA TRADITIONAL HOUSES. *DIMENSI (Journal of Architecture and Built Environment)*, 42(2), 69–76.

Nurmadina, Nugroho, N. & Bahtiar, E. T. (2017). Structural Grading of Gigantochloa Apus Bamboo Based on Its Flexural Properties. *Construction and Building Materials*, 157, 1173–1189.

Oliva Salinas, J. G., Mendoza, M. & Meza, E. G. (2018). Reflections on Frei Otto as Mentor and Promoter of Sustainable Architecture and His Collaboration with Kenzo Tange and Ove Arup in 1969. *Journal of the International Association for Shell and Spatial Structures*, 59(1), 87–100.

Patil, S. & Mutkekar, S. (2014). Bamboo as a Cost Effective Building Material for Rural Construction. *Journal of Civil Engineering and Environmental Technology*, 1(6), 35–40.

Peloux, L. D. (2017). Modeling of Bending-Torsion Couplings in Active-Bending Structures. Application to the Design of Elastic Gridshells. Retrieved January 10, 2023, from https://theses.hal.science/tel-01757782

Pone, S., Colabella, S., D'Amico, B., Fiore, A., Lancia, D. & Parenti, B. (2013). Timber Post-Formed Gridshell: Digital Form-Finding / Drawing and Building Tool.

Prijotomo, J. (2008). *Pasang Surut Arsitektur Indonesia*. Surabaya: CV Arjun.

Quinn, G. C., Gengnagel, C. & Williams, C. J. (2015). Comparison of Erection Methods for Long-Span Strained Grid Shells. *Proceedings of IASS Annual Symposia*, 2015(8), 1–12.

Quinn, G. & Gengnagel, C. (2014). A Review of Elastic Grid Shells, Their Erection Methods and the Potential Use of Pneumatic Formwork, in: (pp. 129–143). Ostend, Belgium. Retrieved January 10, 2023, from http://library.witpress.com/viewpaper.asp?pcode=MAR14-011-1

Quinn, G. & Gengnagel, C. (2018). Full Scale Prototype for the Pneumatic Erection of Elastic Gridshells. *Proceedings of IASS Annual Symposia*, 2018(15), 1–8.

Quinn, G., Gengnagel, C. & Bletzinger, K.-U. (2016). Simulating Pneumatic Erection of Strained Grid Shells via Dynamic Relaxation. *Proceedings of IASS Annual Symposia*, 2016(16), 1–10.

Rockwood, D. (2015). *Bamboo Gridshells*. London; New York: Routledge, Taylor & Francis Group.

Rombouts, J., Lombaert, G., De Laet, L. & Schevenels, M. (2019). A Novel Shape Optimization Approach for Strained Gridshells: Design and Construction of a Simply Supported Gridshell. *Engineering Structures*, 192, 166–180.

Rombouts, J., Schevenels, M., De Laet, L. & Lombaert, G. (2019). Optimal Design of Gridshells. Retrieved January 10, 2023, from https://kuleuven.limo.libis.be/discovery/fulldisplay/lirias2812207/32KUL_KUL:Lirias

Saleh Tabari, M. H., Khojastehmehr, F. & Filz, G. H. (2022). Parametric Thinking for Decision-Making in Elastic Gridshell Design. *Proceedings of IASS Annual Symposia*, 2022(14), 1–14.

Schefold, R., Nas, P. & Domenig, G. (Eds.). (2004). *Indonesian Houses*. Singapore: Singapore University Press.

Scurlock, J. M. O., Dayton, D. C. & Hames, B. (2000). Bamboo: An Overlooked Biomass Resource? *Biomass and Bioenergy*, 19(4), 229–244.

Seifi, H. (2019). Topology Optimisation and Additive Manufacturing of Structural Nodes of Gridshell Structures - RMIT University. Retrieved from https://researchrepository.rmit.edu.au/esploro/outputs/doctoral/Topology-optimisation-and-additive-manufacturing-of-structural-nodes-of-gridshell-structures/9921863834901341

Seixas, M., Bina, J., Stoffel, P., Ripper, J. L., Moreira, L. E. & Ghavami, K. (2017). Active Bending and Tensile Pantographic Bamboo Hybrid Amphitheater Structure. *Journal of the International Association for Shell and Spatial Structures*, 58(3), 239–252.

Seixas, M., Eustáquio Moreira, L., Stoffel, P. & Bina, J. (2021). Form Finding and Analysis of an Active Bending-Pantographic Bamboo Space Structure. *Journal of the International Association for Shell and Spatial Structures*, 62(3), 206–222.

Sharma, B., Gatoo, A., Bock, M., Mulligan, H. & Ramage, M. (2015). Engineered Bamboo: State of the Art. *Proceedings of the Institution of Civil Engineers - Construction Materials*, 168(2), 57–67.

Sharma, B., Harries, K. A. & Ghavami, K. (2013). Methods of Determining Transverse Mechanical Properties of Full-Culm Bamboo. *Construction and Building Materials*, 38, 627–637.

Sharma, R., Wahono, J. & Baral, H. (2018). Bamboo as an Alternative Bioenergy Crop and Powerful Ally for Land Restoration in Indonesia. *Sustainability*, 10(12), 4367.

Suzuki, S., Slabbinck, E. L. M. & Knippers, J. (2020). Computational Bamboo: Digital and Vernacular Design Principles for the Construction of a Temporary Bending-Active Structure, in: Gengnagel, C., Baverel, O., Burry, J., Ramsgaard Thomsen, M., and Weinzierl, S. (Eds.), *Impact: Design With All Senses*, (pp. 224–236). Cham: Springer International Publishing.

Tan, T., Rahbar, N., Allameh, S. M., Kwofie, S., Dissmore, D., Ghavami, K. & Soboyejo, W. O. (2011). Mechanical Properties of Functionally Graded Hierarchical Bamboo Structures. *Acta Biomaterialia*, 7(10), 3796–3803.

Tang, G. (2013). Timber Gridshells: Beyond the Drawing Board. *Proceedings of the Institution of Civil Engineers - Construction Materials*, 166(6), 390–402.

Tang, G. (2015). An Overview of Historical and Contemporary Concrete Shells, Their Construction and Factors in Their General Disappearance. *International Journal of Space Structures*, 30(1), 1–12.

Terpenny, J., Nnaji, B. & Bøhn, J. H. (1998). Blending Top-Down and Bottom-Up Approaches in Conceptual Design.

Trujillo, D., Jangra, S. & Gibson, J. M. (2017). Flexural Properties as a Basis for Bamboo Strength Grading. *Proceedings of the Institution of Civil Engineers - Structures and Buildings*, 170(4), 284–294.

UN-Habitat. (2013). *53 UN-Habitat Model Project 2013/2014: Time to Think Urban*. Nairobi: UN-Habitat.

Widjaja, E. A. (2000). Bamboo Diversity and Its Future Prospect in Indonesia, in: *Proceeding of the Third International Wood Science Symposium*, (pp. 235–240). Kyoto, Japan: JSPS-LIPI. Retrieved from

https://www.researchgate.net/publication/280571859_Bamboo_Diversity_and_its_future_prospect_in_Indonesia

Widyowijatnoko, A., Trautz, M. & Baier, B. (2012). *Traditional and Innovative Joints in Bamboo Construction*. Aachen: Mainz.

Yang, X. & Xu, W. (2021). A Tool for Searching Active Bending Bamboo Strips in Construction via Deep Learning, in: (pp. 463–472). Hong Kong. Retrieved March 3, 2023, from http://papers.cumincad.org/cgi-bin/works/paper/caadria2021_080

Zea Escamilla, E., Habert, G. & Wohlmuth, E. (2016). When CO2 Counts: Sustainability Assessment of Industrialized Bamboo as an Alternative for Social Housing Programs in the Philippines. *Building and Environment*, 103, 44–53.